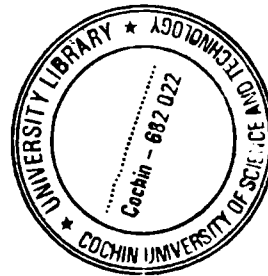


G8968

Mixed Layer Characteristics and Hydrography off the West and East Coasts of India

**Thesis submitted to the
Cochin University of Science and Technology
In partial fulfilment of the degree of
DOCTOR OF PHILOSOPHY IN MARINE SCIENCE**

**Under the
FACULTY OF MARINE SCIENCES**



**by
P.A. MAHESWARAN. M.Sc.**

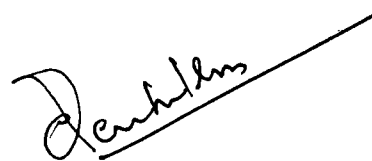
**NATIONAL INSTITUTE OF OCEANOGRAPHY
Regional Centre - 682018**

August 2004

Certificate

I hereby certify that the thesis titled as “**Mixed layer characteristics and hydrography off the west and east coasts of India**” submitted by P.A. Maheswaran, Research scholar (Reg.No.2147), National Institute of Oceanography, Regional Centre, Kochi-18, is an authentic record of research carried out by him under my supervision, in partial fulfilment of the requirement for the Ph.D degree of Cochin University of Science and Technology in Marine Science and that no part of thereof has previously formed the basis for the award of any degree, diploma or associateship in any university.

Kochi-18
02.08.2004



Dr.C.Revichandran
Supervising Guide, Scientist
National Institute of Oceanography
Regional Centre,
Kochi-18, Kerala, India

Preface

The study of mixed layer dynamics has an important bearing on the exchange of heat, carbon dioxide, freshwater and other related properties between the atmosphere and ocean surface. The absorption of energy from the sun within this layer is the major source of energy for all oceanic processes. Because of the sharp temperature and density gradients below the mixed layer, its variation affects the acoustic propagation limiting the horizontal range. It also influences the transport of nutrients, phytoplankton and zooplankton abundance, thereby influencing the fisheries. Mixed layer also influences cyclogenesis - generation of cyclones.

The Arabian Sea and Bay of Bengal are land locked at the north and forced by seasonally reversing monsoon winds. Accordingly, the surface circulation of both the basins undergoes seasonal reversal. The coastal currents along the west and east coasts of India and the fast moving coastally trapped Kelvin waves provide a link between the Arabian Sea and Bay of Bengal. However, the basins show large contrasts in hydrographical conditions, mostly caused by the salinity structure in the upper layers. The resultant variations in stratification in the Arabian Sea and in the Bay of Bengal affect the vertical mixing. For example, during winter monsoon, the cold dry continental winds blows over both the Arabian Sea and the Bay of Bengal resulting in appreciable cooling and evaporation of surface waters. In the northern Arabian Sea, this cooling together with the ambient high surface saline waters leads to the densification of surface waters, which in turn triggers convective overturning down to a depth of about 100m, resulting in substantial fertilization with nutrients, enhancing the biological production. On the contrary, in the Bay of Bengal, the surface cooling does not lead to densification. The convective mixing is resisted by the stable condition provided by the freshwater lens; cold water in the surface layer stay stagnant, below which the temperature increases with the depth resulting in strong thermal inversion. Coastal upwelling, wind driven mixing, lateral advection and winter cooling makes the Arabian Sea a

region of high biological productivity. In contrast, the Bay of Bengal is traditionally considered to be a region of less biological productivity. Along the east coast of India, weak upwelling does occur, but the upwelled water does not make it to the surface. The ecosystems of the Arabian Sea and Bay of Bengal are very much influenced by the climate, mixed layer and thermohaline processes in the region. The differential response to the atmospheric forcing on the sea surface in the Arabian Sea and Bay of Bengal, gives different mixed layer characteristics. Therefore, the region off the west and east coasts of India have been chosen for present study – to understand the mixed layer characteristics and general hydrography.

Earlier, there was a scarcity of simultaneous data sets in respect of physical, chemical and biological parameters from the waters off the west and east coast of India. But the ongoing Marine Research – Living Resources (MR-LR) programme of the DOD, New Delhi concentrates on the Indian waters of the EEZ. It is designed to assess and evaluate the environmental parameters and the marine living resources of the EEZ of India by the simultaneous collection of physical, chemical and biological parameters using the various sophisticated instruments onboard *FORV Sagar Sampada*. The present study mainly concentrates on the processes occurring in the upper 300m layer off the west and east coasts of India, using high quality MR-LR data sets. The study is of paramount importance for understanding the physical forcings on biological production in the eastern Arabian Sea and the western Bay of Bengal.

The thesis is divided into six chapters. Chapter 1 give an introduction to the mixed layer, which includes the importance, factors affecting the mixed layer and the literature review on the mixed layer. The general hydrography off the west and east coasts of India and the main objectives of the present study are also presented in this Chapter. Materials and methods of the present study are covered in Chapter 2. Detailed description of MR-LR programme and other data sets (NIO hydro – CD and climatological) used in the study as well as the processing techniques are also provided in this chapter. In Chapter 3, the

monthly evolution of mixed layer depths and the barrier layer thickness together with other surface met-ocean parameters like sea surface temperature, surface salinity, wind speed, short wave radiation, net heat flux and evaporation minus precipitation in each grid are discussed. Comparison between the coastal and open ocean region in the two basins are also addressed in this chapter.

Chapter 4 explains the general hydrography off the west coast of India. The physical forcings on the biological production in the context of upwelling, winter cooling and the intrusion of low saline waters from the Bay of Bengal are highlighted in this chapter. In Chapter 5, the general hydrography of the Bay of Bengal is covered. The physical forcings such as the fresh water influx induced stratification, eddies, coastal upwelling and winter cooling are linked to the biological production. The differential responses of Arabian Sea and Bay of Bengal to the atmospheric forcings are also highlighted in this chapter. In Chapter 6, summary of the present study and recommendations for future studies are provided.

LIST OF ACRONYMS

AS	Arabian Sea
ARGO	Global Array of observations
ASHSW	Arabian Sea High Salinity Watermass
AVHRR	Advanced Very High Resolution Radiometer
BOB	Bay of Bengal
BOBPS	Bay of Bengal Process Studies
COADS	Comprehensive Ocean Atmospheric Data Set
CTD	Conductivity - Temperature – Depth
DOD	Department of Ocean Development
E	East
e.g.	exempli gratia (Latin word meaning ‘for the sake of example’)
EEZ	Exclusive Economic Zone of India
EICC	East India Coastal Current
E-P	Evaporation - Precipitation
et al.	et alii (Latin word meaning ‘and others’)
etc	et cetera (Latin word meaning ‘and other similar things; and so on’)
FORV	Fishery & Oceanographic Research Vessel
FORV	Fisheries Oceanographic Research Vessel
FSU	Florida State University
GF/F	Glass Fibre/Filter
GW	Great whirl
HOAPS	Hamburg Ocean Atmosphere Parameters and flux from Satellite
IIOE	International Indian Ocean Expedition
ILD	Isothermal Layer Depth
ILD	Isothermal Layer Depth
IMC	Indian Monsoon Current
IODC	Indian Oceanographic Data Centre
JGOFS	Joint Global Ocean Flux Studies
LH	Lakshadweep High (Laccadive High)

MLD	Mixed Layer Depth
MONEX	Monsoon Experiment
MR-LR	Marine Research Living Resources
N	North
NE	Northeast
NEC	North Equatorial Current
NIO	National Institute of oceanography
OGCM	Ocean General Circulation Models
ORV	Oceanographic Research Vessel
P-E	Precipitation – Evaporation
PGW	Persian Gulf Watermass
PP	Primary Productivity
psu	Practical Salinity Unit
RSW	Red Sea Watermass
RV	Research Vessel
SE	Socotra Eddy
SEC	South Equatorial Current
SMC	Southwest Monsoon Current
SSM/I	Special Sensor Microwave/Imager
SSS	Sea Surface Salinity
SST	Sea Surface Temperature
SW	Southwest
SWR	Short Wave Radiation
T/P	Topex/Poseidon
TKE	Turbulent Kinetic Energy
TTS	Typical Tropical Structure
UNESCO	United Nations Education, Scientific and Cultural Organisation
viz	videlicet (Latin word meaning ‘namely’)
WICC	West India Coastal Current
WMC	Winter Monsoon Current

CONTENTS

	Page No.
Chapter 1 Introduction	1
1.1. Surface mixed layer	
1.2. Barrier layer	
1.3. Factors controlling the mixed layer	
1.4. Geographic location of the study area	
1.5. Oceanography of the study area	
1.6. Previous work	
1.7. Present study	
Chapter 2 Materials and Methods	21
2.1. Study area	
2.2. Data Source and Processing	
2.3. Methods	
Chapter 3 Mixed Layer Characteristics	48
3.1. Arabian Sea	
3.2. Bay of Bengal	
3.3. Discussion	
Chapter 4 Hydrography off the eastern Arabian Sea	102
4.1. Spring intermonsoon	
4.2. Summer monsoon	
4.3. Fall intermonsoon	
4.4. Winter monsoon	
4.5. Summary	
4.6. Hydrological structure	

Chapter 5	Hydrography off the western Bay of Bengal	140
5.1	Spring intermonsoon	
5.2	Summer monsoon	
5.3	Winter monsoon	
5.4	Hydrological structure	
5.5	Differential response of Arabian Sea and Bay of Bengal	
Chapter 6	Summary and Conclusion	179
References		187

Chapter 1

INTRODUCTION

1.1. Surface mixed layer

Oceanographers refer to the upper layers of the ocean with nearly uniform hydrographic properties as the surface mixed layer, which usually extends up to a depth of 25 to 200m in the tropical regions (Pickard & Emery, 1982). This layer gains heat through solar radiation continually and suffers heat loss due to outgoing long wave radiation and evaporation. In addition, vertical mixing, wave induced turbulence, convergence, divergence, internal waves controls the characteristics of the mixed layer. Below this layer, there is a zone of rapid transition, where properties change rapidly with time. Further down, is a steady zone where the properties gradually change. Considering the vast expanse of oceans, the surface mixed layer that represents only of 'skin deep'. Surprisingly it is this surface layer, which mainly dictates and regulates the entire bio-resources and also balances the global climate change. They protect the marine life by insulating them from abrupt changes in the atmosphere, as well as the changes due to the deep oceans. Over large parts of the ocean, the mixed layer thickness varies seasonally and diurnally. It usually reaches much deeper in winter when cooling at the sea surface caused by release of heat stored in the ocean to the atmosphere. During spring and summer the mixed layer absorbs heat, moderating the earth's seasonal temperature extremes.

Oceanographers have given a great deal of importance to study the dynamics of the upper layer of the ocean, because mixed layer plays an important role in the exchange of heat, moisture and momentum between the atmosphere and bulk of underlying ocean. The absorption of energy from the sun within this layer is the major source of energy for all oceanic processes. The thickness of the upper ocean determines both thermal and mechanical inertia of the layer that is in direct

contact with the atmosphere. On the global scale, the upper ocean is one of the most important factors in determining climate of the earth system (Kraus, 1977). Understanding the processes responsible for the mixed layer variation gives an insight into conditions at the sea surface, air-sea interactions and other environmental settings of the region. Many biological and chemical parameters have strong gradients in the upper 100m; hence oscillations in the depth of mixing can be a major forcing function for vertical exchange in surface waters. Species with high surface concentrations (phytoplankton, particles, aggregates) are mixed or pumped downward, while species whose concentrations increase with depth (nutrients, CO₂) are pumped upward. The upward mixing of nutrients enhances the production. Banse (1987) pointed out that the seasonal variations in mixed layer dynamics and upwelling is also an important determinant of the annual cycle of primary productivity in the Arabian Sea. In warmer, low wind environments, water is shallowly mixed and surface phytoplankton quickly consumes available nutrients. In cooler, high wind environments water is mixed down to the base of seasonal thermocline, increasing the supply of nutrients to the euphotic zone enhancing the productivity.

1.2. Barrier layer

Over large part of the world ocean, upper ocean density stratification is controlled primarily by temperature. However, in regions of positive water balance such as western equatorial Pacific (Lukas and Lindstorm, 1991) and Bay of Bengal (Sprintall and Tomczak, 1992; Vinayachandran *et al.*, 2002; Rao and Sivakumar, 2003), surface stratification defining the base of the mixed layer, is often controlled by salinity. The mixed layer can then be significantly shallower than would be expected based upon the temperature stratification (Cronin and McPhaden, 2003). The salinity stratified isothermal layer between the base of the mixed layer and top of the thermocline is often referred to as the 'barrier layer' (Godfrey and Lindstorm, 1989), since it acts as a barrier to turbulent entrainment

of cold water into the surface mixed layer.

Occurrence of the barrier layer exerts an important influence on mixed layer dynamics. The term barrier layer is indicative of its effect on the mixed layer heat budget. Presence of the barrier layer means that any water entrained from the isothermal layer into the mixed layer has the same temperature as the water in the mixed layer. No heat is therefore transferred through the bottom of the mixed layer. Thus, the heat input at the surface will perpetually raise the temperature of the upper ocean if it is not horizontally advected away from the region.

1.3. Factors controlling MLD

Factors controlling MLD are described in detail in the following section. The turbulence, which may result in the mixed layer deepening or stratifying, requires an energy input that may be generated by kinetic energy and/or by potential energy at the sea surface. Kinetic energy, from the transfer of the wind momentum to the sea, results in mixing processes such as wave action, entrainment and horizontal advection by currents. Potential energy is measured by buoyancy flux that reflects change of density due to heat and freshwater fluxes. A schematic mixed layer is shown in Figure 1, which summarizes the processes that affect the mixed layer.

1.3.1. Radiative heat fluxes

The solar heating is the principal source of oceanic heat and circulation (Pond and Pickard, 1983). The absorption of solar radiation within the water column and the exchanges of heat and fresh water across the sea surface alter the stratification of the layer. This may either stabilize or destabilize the water column. The kinetic energy generated from the turbulence (Turbulent Kinetic Energy - TKE) always works to reduce the stratification in the water column.

During a heating season or when energy is received by the top layer of the ocean exceeds the loss due to sensible heat flux and evaporation, a stable stratification is established. The positive heat balance at sea surface increases the

upward buoyancy flux, which always act to oppose the vertical motion and remove the TKE. As a result the surface layer retreat to shallower depth within which the TKE is exactly sufficient for the complete mixing.

When the sensible and latent heat fluxes dominate over the heat budget terms, especially during winter and night, the heat and fresh water loss to the atmosphere increases the surface density and leads to instability. This instability increases the kinetic energy from the turbulence, which is sufficient to dissolve the stratification by the buoyancy input. The excess energy will be used to entrain water across the base of the mixed layer, resulting in deepening of the mixed layer.

1.3.2. Winds

Wind blowing over the ocean transfers momentum to the ocean surface. The wind blowing over the sea surface initiates the turbulence, which leads to mixing. The increase in wind speed increases the TKE, which always work against the stratification and giving increase in potential energy. The mixed layer will deepen through entrainment owing to the excess energy.

1.3.3. Salinity

Salinity plays an important role in controlling near surface vertical mixing. The major processes determining the surface layer salinity distribution in the ocean are evaporation E , precipitation P and river runoff. In regions, where $P-E > 0$ and salinity is low, such as the central and eastern equatorial ocean and the Bay of Bengal, the mixed layer shallows because of decreased entrainment (Han *et al.*, 2001). Conversely, in region where $P-E < 0$ and salinity is high such as northern Arabian Sea and a broad region of the southern tropical ocean, mixed layer deepens because of increased entrainment.

1.3.4. Waves

The waves generated by surface winds also initiate mixing in the oceans, by particle movement of wave action and by the turbulence caused by breaking

waves. The depth of the mixing by waves depends on the stability of the thermocline (Laevastu and Hela, 1970). The energy transfer from the wind to the water in the form of waves is balanced by the dissipation of mechanical energy by the turbulence generated by breaking waves (Philips, 1958). The wave height of the ocean depends mainly on the wind speed. Higher the wind speed, higher the wave height resulting in deepening the mixed layer.

1.3.5. Currents

Surface currents in the ocean are significant in the mixed layer variability. Warm currents usually head away from the equator bringing low saline waters and therefore shallowing the mixed layer due to the increase in stratification. Conversely, cold currents usually flow towards the equator, bringing high saline surface waters causing the mixed layer to deepen due to the densification of surface waters. The different circulation patterns evolve eddies and gyres in the ocean basins. In the northern hemisphere, usually cyclonic eddies push subsurface cold waters upward and ensuing thin mixed layer. On the contrary, warm core eddies resulting in convergence of surface waters, which cause the mixed layer deepening.

1.3.6. Vertical motion – Upwelling / Sinking

Wind stress at the sea surface not only causes horizontal movement of water, it also leads to vertical motion (Brown *et al*, 1995). When the wind stress leads to a divergence of surface water, deeper water rises (upwelling). Consequently, the sea surface is lowered, the thermocline raised and therefore the mixed layer reduced. Conversely, when there is a convergence of the surface water, sinking occurs and causes the sea surface to rise and thermocline to deepen. Upwelling of subsurface water and sinking of surface water occur all through the coastal boundaries of north Indian Ocean and in the equatorial Indian Ocean. Thus the vertical motion is an important factor for determining the MLD off the Indian coasts.

1.3.7. Internal waves

The internal waves occurring at the surface between the density layers within the sea, also affect the mixed layer depth. Particular surfaces are in the thermocline in oceanic waters, where the density difference is mainly due to temperature difference or at the halocline in coastal waters where the density difference is mainly due to salinity difference (Pond and Pickard, 1983). As the internal waves travel along, the mixed layer alternately gets thicker and thinner. Convergence may cause the bands of irregular ripples on the sea surface above them and leads to the mixed layer deepening, while divergence results the mixed layer to reduce (shallow).

1.4. Geographic location of the study area

The Arabian Sea (AS) and Bay of Bengal (BOB) are unique among the low latitude seas because they are terminated in the north by Asian landmasses and have marked continental influence. They experience seasonal reversal of atmospheric forcings, consequently the upper layers exhibit different oceanographic characteristics during different seasons. The west coast of India forms the eastern boundary of the AS basin and east coast of India forms the western boundary of the BOB basin. The ecosystems of the two regions are very much influenced by the seasonal winds, mixed layer processes, thermohaline circulation processes and the remote forces. The enhanced evaporation in the eastern Arabian Sea and the substantial amount of freshwater influx in the western Bay of Bengal provides diverse surface stratification in the two regions. Hence, the response of the atmospheric forcings on the sea surface in the AS and BOB was observed to be paradoxical. Therefore, west and east coasts of India have been chosen for present study area.

1.5. Oceanography of the Study Area

The Northern Indian Ocean is considered to be the most complex and

oceanographically least understood. It is bounded at northern, eastern and western sides; such a geographical situation causes asymmetry in its structure and circulation pattern compared to the Pacific and Atlantic Ocean. The coastline is surrounded by the largest landmass, which enhances the differential heating. The land has a lower capacity to maintain heat than that of the water. Therefore, a strong land-ocean thermal gradient develops in this region, causing monsoons.

During the summer months high solar insolation causes the landmass to heat up which give rise to low pressure. The low pressure drives southwesterly moist winds, which eventually brings heavy rainfall to India from June to September. During winter, air over the Siberia Plateau becomes cooler than air over the surrounding seas, producing a large anticyclone with winds circulating clockwise, causing cool north – easterly winds to blow over the Indian Ocean. This northeasterly wind brings rainfall to the south east coast of India and is known as northeast monsoon, which is active till December. The periodic reversals in the winds drive corresponding changes in the upper ocean currents as well (Fig. 1.2c & 1.2d).

1.5.1. Arabian Sea

The monsoonal winds over the AS forces spectacular seasonal variations, particularly in the reversal of boundary currents and seasonal upwelling. During SW monsoon, the winds over the western Arabian Sea are jet like in structure known as the Findlater jet (Findlater, 1969) and extend from the African coast to India (Gujarat) [Fig.1.2c]. Seaward of the wind jet, the wind speed decreases cause negative wind-stress curl, which drives strong Ekman pumping that deepens the mixed layer considerably. Ekman convergence is dominated to the southeast of the Findlater jet, causing a deep mixed layer (Rao *et al.*, 1989) while the Ekman divergence in the northeast leads to upwelling (Bauer *et al.*, 1991). With the onset of southwest monsoon, boundary currents along the AS basin changes its direction. An oceanic gyre, the monsoonal gyre, does occur in the AS basin

(Schott, 1983). Two anticyclonic eddies, the Great whirl (GW) and the Socotra Eddy (SE) develops during this period. The north equatorial current (NEC) is replaced by much stronger eastward flowing Indian monsoon current (IMC) during summer. Upwelling in the Arabian Sea is synchronized with one season, southwest monsoon, which is in contrast to the other major upwelling areas, where it is an annual phenomenon. Intense upwelling takes place along the coasts off Somalia, Arabia and along the southwest coast of India. Open ocean upwelling was also reported along the central Arabian Sea (Bauer *et al.*, 1991; Muraleedharan & Prasanna Kumar, 1996; Mohan and Ali, 1995). Even though the overall direction of winds during the SW monsoon over the north Indian Ocean is from the southwest, along the west coast of India, the direction of winds varies roughly west-southwest in the north to approximately west-northwest in the south (Fig. 1.2c). Shetye and Shenoi (1988) compared the annual cycles of long shore components of wind stress and ship drift data along the west coast and found that during SW monsoon, the local winds drives the surface circulation. The surface current during the SW monsoon along the west coast of India is towards the equator and the thermocline shallows near the coast (Shetye *et al.*, 1990).

During the northeast monsoon (November – February), the winds in the coastal region off western India are generally northerlies (Fig. 1.2a). But the coastal current flows poleward along the west coast of India, which is peculiar, because most other eastern boundary currents flow with the wind (Mittelstaedt, 1986). Westward flowing north equatorial current (NEC) bifurcates at the southeastern tip of India with a branch flowing northward as the West India Coastal Current (WICC), [Wyrтки, 1973; Shetye *et al.*, 1991]. The northeasterly winds drive a southward boundary current along the coast of Somalia. In the northern Arabian Sea, cool and dry continental air brought by prevailing northeast trade winds intensifies the evaporation leading to surface cooling. This combined with reduced incoming solar radiation and high ambient salinity (>36 psu) drives

convective mixing in the northern AS that lead to the injection of nutrients up into the surface layers from the thermocline (Madhupratap *et al.*, 1996). This enhances the biological production and is roughly of the same magnitude as the production due to upwelling in the south (Banse 1987, Madhupratap *et al.*, 1996). Hence, the Arabian Sea is considered as one of the most biologically productive ocean regions (Ryther *et al.*, 1965) mainly due to the upwelling during summer monsoon and winter cooling during winter monsoon. However, during spring and fall transition periods, weak winds and surface layer heating produces strong stratification and shallow mixed layers, which limit the primary production.

In the AS evaporation exceeds precipitation on an annual scale. The evaporative cooling and convection leads to the formation of Arabian Sea High Salinity Watermass (ASHSW) during winter in the northern Arabian Sea. Apart from the ASHSW, the Arabian Sea receives the high saline waters from the Persian Gulf and Red Sea that make the Arabian Sea high saline.

1.5.2. Bay of Bengal

The BOB is a unique semi-enclosed basin experiencing seasonally reversing monsoons, depression and severe cyclonic storms. It also receives a large amount of rainfall and river runoff. On an average, the annual rainfall over the Bay is in excess of 2m (Gill, 1982). In addition, the annual discharge from bordering rivers exceeds $1.5 \times 10^{12} \text{ m}^3$ (UNESCO, 1988). Most of the freshwater influx to the Bay occurs during the southwest monsoon (June-September). The freshwater input induces estuarine characteristics with reduced surface salinity over most of the Bay, which in turn hampers exchange processes between the atmosphere, surface and deep waters and consequently affects the biological and biogeochemical processes. The continental shelf along the east coast of India is very narrow in the south and gradually widens towards north with an average width of about 40km. The coastline itself has interesting geomorphologic features such as a northeast orientation from the southern end of the peninsula to 10°N that

abruptly turns to east-west and then orients in rather a north-south direction from 10°N to 13.5°N. Beyond it, rather abruptly, the coastline orientation changes to southwest-northeast direction. This feature presumably plays a critical role in the circulation along the east coast of India as evident from the selective upwelling zones, northward coastal current and variable offshore Ekman transport along the northern Bay during the southwest monsoon period (Shetye, *et al.*, 1993).

The winds during SW monsoon over the BOB are generally from southwest and are favourable to upwelling along the east coast of India. While during winter monsoon, northeasterly winds blow over the western BOB (Hastenrath and Lamb, 1979). The hydrography and circulation of the Bay is rather complex with the river discharge and seasonal reversal of currents. Recently the western boundary current in the Bay of Bengal has been named as the East India Coastal Current (EICC). Characteristics of this current have been investigated from analyses of satellite infrared imageries (Legeckis, 1987), shipboard surveys (Shetye *et al.*, 1991b; 1993; 1996, Sanilkumar *et al.*, 1997; Shankar, 2000) and T/P altimetry (Vinayachandran and Yamagata, 1998; Eigenheer and Quadfasel, 2000). The current along the east coast of India, EICC, reverses seasonally (Fig. 1.2b, 1.2d). Its poleward phase starts in February and is best developed in March – April, forming a western boundary current of a basin wide anticyclonic gyre. During SW monsoon, the EICC is weak and is poleward in the south, but is equatorward in the north. As the SW monsoon withdraws, flow along the south east coast reverses and the EICC is equatorward all along the coast till January (Shankar *et al.*, 1996; McCreary *et al.*, 1996). Rather than the local winds, remote forcings from the equator would have an important effect in the BOB circulation (Yu *et al.*, 1991; Potemra *et al.*, 1991). In this mechanism, equatorial Kelvin waves reflect off the eastern boundary of the Indian ocean, partly as a packet of coastal Kelvin waves that propagate around the perimeter of the Bay and partly as a packet of Rossby waves that radiate westward back into its interior. According to Potemra *et al*

(1991) the seasonal circulation in the Bay of Bengal is propagated by a large anticyclonic gyre across the whole Bay during December to March followed by two counter rotating flows, anticyclonic on the western side and cyclonic on the eastern side producing northward currents along both coasts and southward flow down the middle. This pattern persists until early summer (April – June), when the anticyclonic flow extends across the whole Bay and in the SW monsoon months (July and August) is characterized by counter clockwise flow and finally in the autumn, two rotating flows develop again with southward current along both coasts and northward flow in the centre.

Though the upwelling is not intense in BOB as in AS, there have been reports of upwelling along the east coast of India during SW monsoon (La Fond 1957; Murty and Varadhachary, 1968; Gopalakrishna and Sastry, 1985; Sanilkumar *et al.*, 1988, Shetye *et al.*, 1991b). A freshwater water plume detached from the coast by a 40km wide upwelling band was observed during the SW monsoon season (Shetye *et al.*, 1991b). The seasonal reversal of coastal currents and circulation pattern induces cyclonic and anticyclonic eddies. During spring intermonsoon, a basin wide anticyclonic gyre forms in the BOB while cyclonic eddies develops in the near shore region of the poleward flowing EICC (Shetye *et al.*, 1993; Murty *et al.*, 1993; Sanilkumar *et al.*, 1997). Cyclonic eddies were also reported during summer monsoon (Babu *et al.*, 1991, Madhupratap *et al.*, 2003).

BOB is traditionally considered to sustain low biological production compared to its western counterpart, the AS. Recent measurements using clean C^{14} uptake techniques also corroborate this fact (Madhupratap *et al.*, 2003; Jyothibabu *et al.*,). The narrow continental shelf, heavy cloud cover and the enormous river discharge into the sea may be the possible reasons for the observed poor production (Radhakrishna *et al.*, 1978). The river discharge brings in large quantities of suspended material, which lower the transparency of waters, thus limiting the photosynthesis. The greater degree of stratification and stability due

to the low saline waters hamper the vertical mixing and thereby restricting any possible introduction of nutrients to surface layer. However, nature itself triggers some mechanism to bring up the nutrients to the surface, like occurrence of cyclones. Though cyclones are disastrous in land, it makes the bay – highly productive (Madhu *et al.*, 2001). The cyclones, which occur mainly during April/ May and October/November tend to churn up the area, injecting nutrients to the euphotic zone, enhancing production in the upper layers.

1.5.3. Interaction of the AS and BOB

The coastal currents along the west and east coasts of India provide a link between AS and BOB. Two basins exchange fresh/salt water and heat through these currents flowing into each other. The branches of the SMC and WMC that flow around the Lakshadweep high and low in the southeastern Arabian Sea (McCreary *et al.*, 1993; Bruce *et al.*, 1994; Shankar & Shetye, 1997) link up the circulations in the Arabian Sea and Bay of Bengal in the surface layers. The SMC flows eastwards south of Sri Lanka and enter into the Bay. It is fed by a flow from the southwest near the equator and by the flow around the Lakshadweep low. East of Sri Lanka, the SMC flows northeastwards into the Bay of Bengal. The SMC transports high-salinity water (Arabian Sea High Salinity Water) into the Bay (Wyrтки, 1971; Murty *et al.*, 1992; Gopalakrishna *et al.*, 1996; Han & McCreary, 2001). The WMC flows westward south of Sri Lanka, where it divides into two branches, one flowing westward into the southern Arabian Sea, the other flowing around the Lakshadweep high into the WICC. The WMC transports low salinity water (Bay of Bengal water) into the eastern Arabian Sea, where it is entrained into the Lakshadweep high and spread along the west coast of India by the WICC (Wyrтки, 1971, Bruce *et al.*, 1994, Han, 1999; Shenoi *et al.*, 1999; Shankar & Shetye, 1997; Han & McCreary, 2001). The Lakshadweep high resulting from the incoming Rossby waves during November/December is believed to be the starting stage for the formation of mini warm pool (>30.8°C; Joseph, 1990) in the

southeastern Arabian Sea during spring intermonsoon. In general, during spring intermonsoon, due to clear skies and weak winds the heat is accumulated in the upper layer of Arabian Sea. In addition, the low saline waters from the BOB along the southeast coast of India, produces more stratification, hence more heat accumulates in the shallow mixed layer and leads to the formation of mini warm pool (Sengupta *et al.*, 2002; Sanilkumar *et al.*, 2004).

1.6. Previous Work

1.6.1. Mixed layer studies

A number of investigators have made attempts to study the mixed layer dynamics based on both observations as well as models. Munk and Anderson (1948) developed the first realistic model of the mixed layer with stratification. Later, Kraus and Turner (1967) extended this approach and developed a 1-D numerical model to examine the seasonal thermocline changes based on energy argument. Denman (1973) modified the work of Kraus and Turner (1967) by including routinely used meteorological data as input and simulated the time dependent behaviour of the surface mixed layer. Later several authors extended Kraus and Turner (1967) work by integrating the heat and energy conservation equations over the mixed layer (Niiler and Kraus, 1977; Garwood, 1977; Gaspar, 1988).

Several climatologies of the MLDs exist for the tropical Indian Ocean (Colborn, 1975; Robinson *et al.*, 1979; Hastenrath and Greisher, 1989; Rao *et al.*, 1989, 1991; Levitus, 1982). They found the deepest MLDs during summer and winter monsoon and shallowest in April-May in the AS and BOB. Rao *et al.* (1989) generated the monthly mean climatology of MLD, sea surface temperature and surface current of the tropical Indian Ocean. Gopalakrishna *et al.* (1988) examined the influence of wind on the variability of the mixed layer in the northern Indian Ocean during different phases of summer monsoon, based on the time series data collected during MONSOON-77 and MONEX-79. Prasad and

Bahuleyan (1995) used Levitus data to prepare MLD and thermocline climatology of the western Indian Ocean. McCreary *et al* (1993) used a numerical model to study the dynamics of mixed layer in the Indian Ocean. The model estimated the entrainment and detrainment in the mixed layer from the wind stirring and surface cooling and simulated the observed SST pattern reasonably well with error less than 0.5-1.0°C. They pointed out the importance of physical processes like advection, remote forcing, etc on the variability of MLD climatology in different regions.

A common difficulty is encountered in relating the mixed layer depth (MLD) from the vertical profiles of temperature and salinity. Most of the climatologies of MLD in the northern Indian Ocean are based on temperature criterion. However, very few climatological atlases are available on the density criterion (Levitus *et al*, 1982; Rao and Sivakumar, 2003). The main disadvantage of the MLD based on temperature gradient is that, it would not represent the actual MLD in the regions where the freshwater influx dominates. The freshwater influx into the Bay of Bengal maintains a barrier layer, which has a thickness of 25m during SW monsoon (Sprintall and Tomczak, 1992). Using the time series observations in the northern BOB, Vinayachandran *et al* (2002) reported a 30m thick barrier layer formation in the SW monsoon. They examined the fresh water affects on the sea surface temperature and ocean – atmosphere coupling through the dependence of the MLD on salinity. Based on the subset of the recently published salinity database of the global oceans, Rao and Sivakumar (2003) examined the influence of sea surface salinity of the north Indian Ocean on the seasonal evolution of the MLD. They found that the incorporation of salinity effect reduces the thickness of the near surface mixed layer and this reduction is most pronounced in the Bay of Bengal. Han *et al*. (2001) studied the influence of precipitation minus evaporation (P-E) and river runoff in the Bay of Bengal on the dynamics, thermodynamics and mixed layer physics in the upper Indian Ocean.

They showed that in the regions where precipitation exceeds evaporation ($P-E>0$) the mixed layer was found to be thin because of decreased entrainment and increased barrier layer. Shenoi *et al.* (2002) compared the TKE available for mixing the stratified water column to a constant depth of 50m in the AS and BOB. It is shown that the energy available for mixing in AS is almost an order of magnitudes greater than that seen in the BOB during summer monsoon. The energy required for mixing in the BOB is about three times greater than that in the AS. They concluded that the shallow MLD in the BOB is primarily driven by a combination of weaker winds and strong near surface stratification due to the low saline surface waters. But Prasad (2004) found that the salinity stratification difference between the two basins plays virtually no role in the depth of MLD and SST. Comparatively shallow MLD in the BOB during the summer monsoon results from the weaker kinetic energy driven vertical mixing owing to weaker winds. During winter, the main reason for the difference in MLD in the AS and BOB is the asymmetry in the net heat flux field, which is caused by a difference in latent flux, a consequence of the difference in humidity. However, no previous information is available dealing the influence of mixed layer and barrier layer on the biological production in the two systems, AS and BOB.

1.6.2. Hydrography off the west and east coasts of India

After the International Indian Ocean Expedition (1960-1965), IIOE, many comprehensive studies to understand the hydrography have been made along the west coast (Banse, 1968; Johannessen *et al.*, 1981; Shetye *et al.*, 1990; 1991; Muraleedharan *et al.*, 1995, JGOFS (Joint Global Ocean Flux Studies)-India). Many studies have reported the upwelling along the west coast of India during SW monsoon season (Banse, 1959, 1968; Ramasatry and Myrland, 1959; Sharma, 1966; 1978; Johannessen *et al.*, 1981; Shetye *et al.*, 1990; Muraleedharan *et al.*, 1995; Sanilkumar *et al.*, 2004). Darbyshire (1967) observed cold waters near the coast during SW monsoon, but denied the role of wind-induced upwelling. Banse

(1968) observed that cool, upwelled water was present along the entire shelf off the west coast of India during SW monsoon. Bauer *et al* (1989) studied the oceanic surface properties in the central Arabian Sea during the SW and NE monsoon. They linked the effect of mixed layer to the phytoplankton distribution. In recent years, under the aegis of the Arabian Sea-Joint Global Ocean Flux Studies (JGOFS), substantial amount of information is available on the physical forcings and biological production in the AS (Barber *et al*, 2001; Madhupratap *et al*, 1996; Smith 1998; 1999; 2000; 2001; Prasanna Kumar *et al.*, 2001a; 2001b). Using a three dimensional physical-biological model, McCreary *et al* (2001) noted that the diurnal and intraseasonal forcing is a potentially important aspect of AS biological and mixed layer dynamics. They found that the biological activity is primarily determined by the MLD and the biological response is one-dimensional. Studies using the satellite derived chlorophyll concentration and mixed layer models found a significant correlation indicating strong influence of SST on biological production in AS (Shetye 1986; Sathyendranath *et al.*, 1991; Nakamoto *et al.*, 2000).

Similarly, after the IIOE, many hydrographic surveys were carried out to understand the physical characteristics off the east coast of India (La Fond, 1957; Suryanarayana *et al*, 1991; Murty *et al.*, 1992a; 1992b; Shetye *et al.*, 1991b; 1993; 1996; Gopalakrishna *et al.*, 2002; Sarma *et al.*, 1999; Babu *et al.*, 2003). However, very few workers have attempted to address the physical forcings on biological production. Gomes *et al* (2000) examined the influence of physical processes and freshwater discharge on the seasonal bloom of phytoplankton in the BOB, using shipboard data as well as ocean colour imagery from OCTS and Seawifs. They found that heavy freshwater influx resulted in strong vertical stratification, which impeded the vertical transfer of nutrients leading to low biological production. Murty *et al.* (2000) related the subsurface chlorophyll maxima to the vertical stability of the water column in BOB. The recent Bay of Bengal Process Studies

(BOBPS) conducted by the National Institute of Oceanography, Goa, documented the less productive nature of the bay using simultaneously measured data on physical, chemical and biological parameters during the SW monsoon (Madhupratap *et al.*, 2003; Prasanna Kumar *et al.*, 2002). They found that strong stratification caused by the low salinity upper regime prevented the surfacing of nutrients and thereby reducing the productivity.

Most of the programmes (for *e.g.* JGOFS, BOBPS) limited their survey into a single basin, either AS or BOB and mainly concentrated in the open ocean region. The major limitations of the previous surveys are the lack of seasonal coverage along the coastal regions (west and east coast) and most of the data were collected by hydro casts at standard depths. No previous attempts to compare the hydrography of EEZ of India along the AS and BOB with collocated sampling using the same methodology.

1.7. Present study

The present study aims an exhaustive study of the MLD characteristics and hydrography of the EEZ of India, using the recent data. The main objectives are as given below

- 1) To bring out an optimal definition of the MLD, which can be applicable for the coastal regions off the west and east coast of India, using the recently collected Conductivity – Temperature – Depth profiles of Marine Research – Living Resources (MR-LR) programme
- 2) To investigate the mixed layer processes and the formation of the barrier layer in the two basins - AS and BOB and to compare and contrast the coastal and open ocean variability of mixed layer in the two basins
- 3) To study the upper layer hydrography off the west and east coasts of India and its influence on biological production.

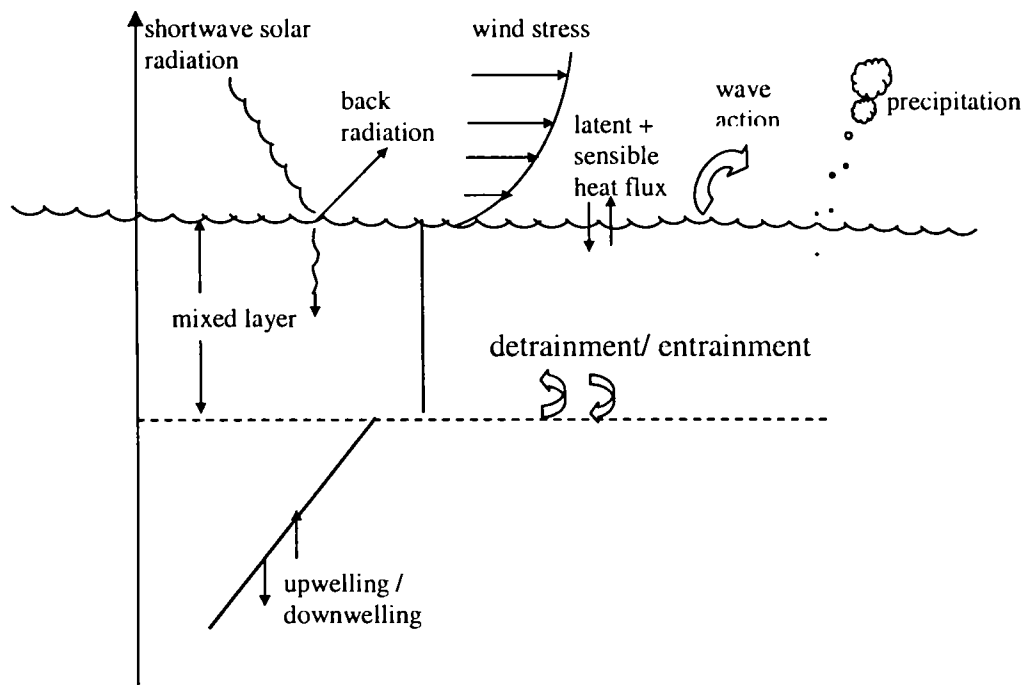


Figure 1.1. Schematic diagram showing mixed layer processes

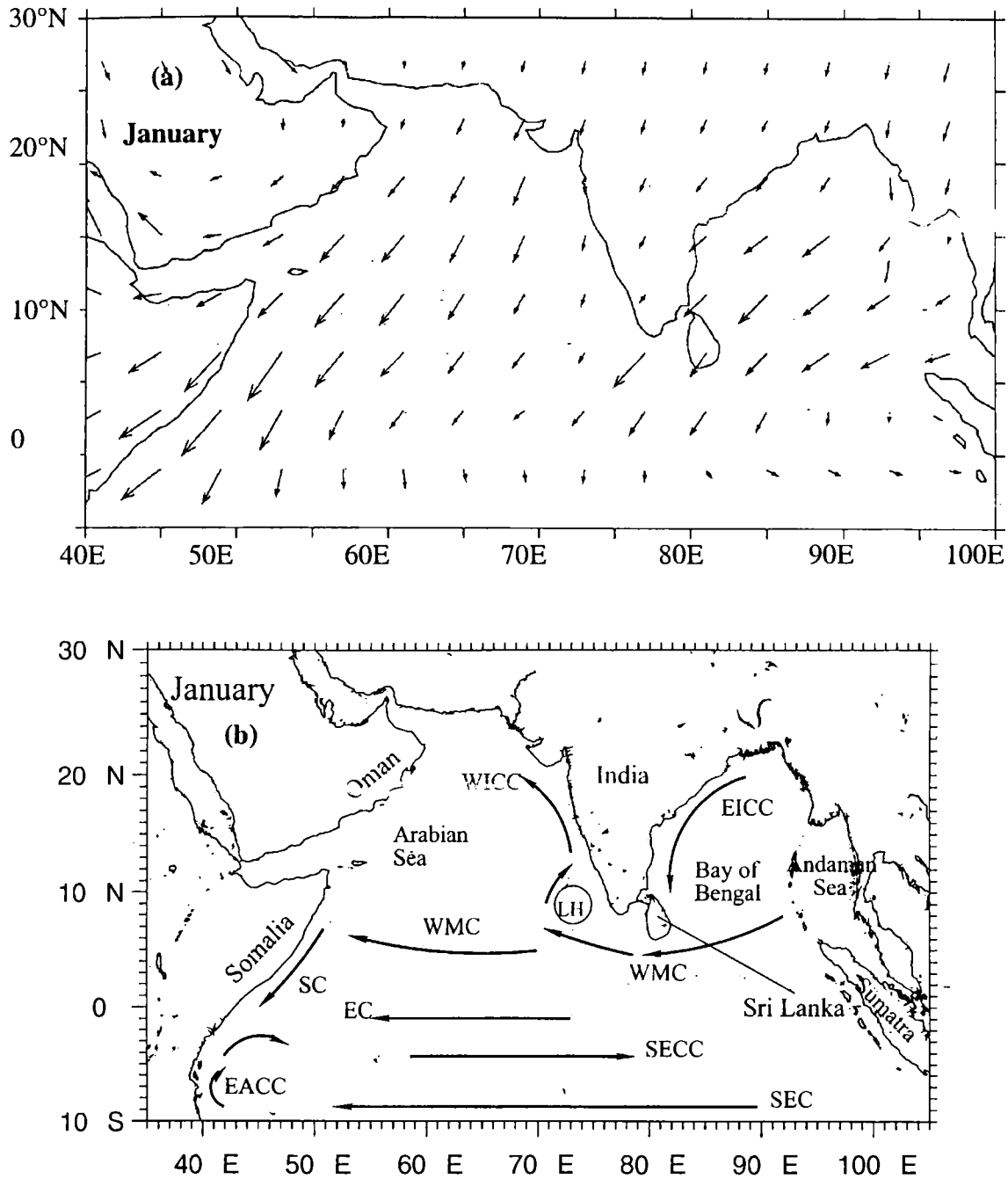


Figure 1.2. Surface wind stress (a & c) and schematic representation of the circulation (b & d) during January (a & b) and July (c & d) in the northern Indian Ocean. Wind stress is reproduced from climatology (Hellerman & Rosenstein, 1983), while circulation schematics from Shankar, *et al.* (2002)

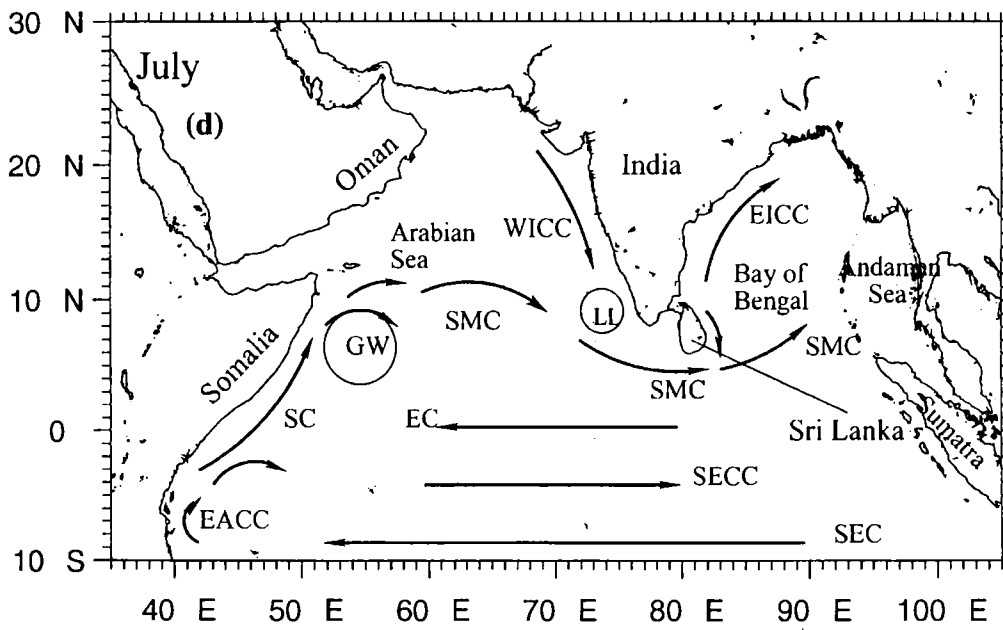
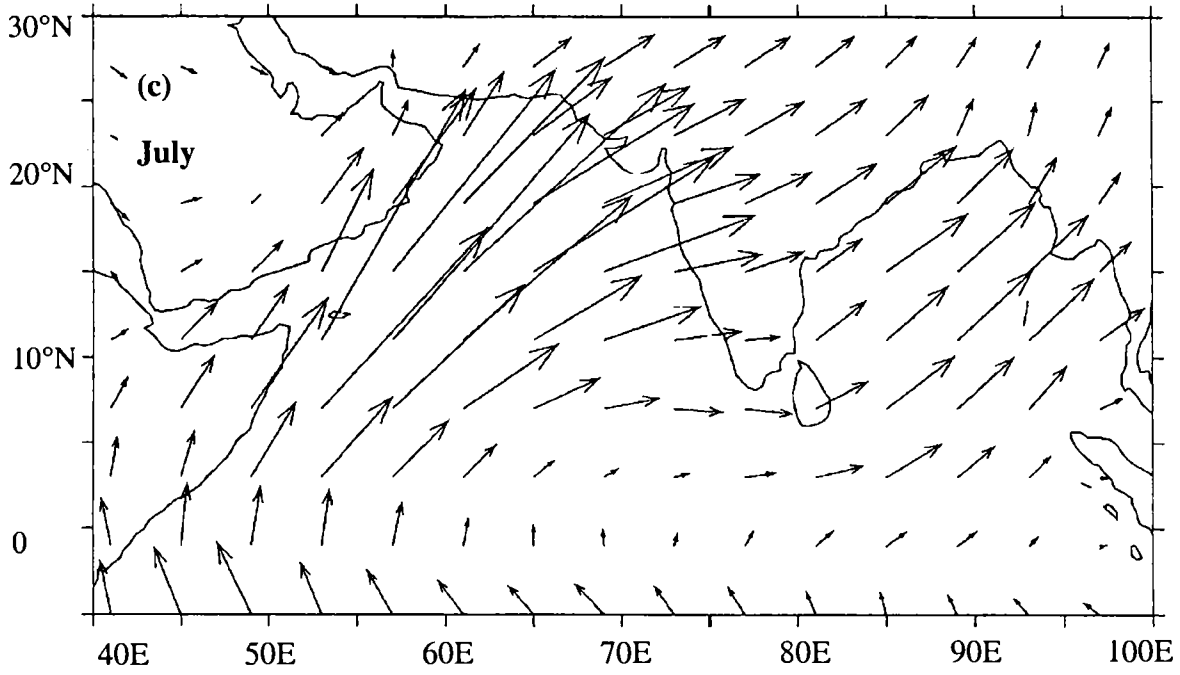


Figure 1.2 (continued)

Chapter 2

Materials and Methods

2.1. Study area

Region of the study covers the AS and BOB, the two basins located in the west and east coast off Indian subcontinent, in the northern Indian Ocean. The major data utilized for this study are collected from the eastern AS and the western BOB, during the ongoing MRLR programme of the DOD and published climatological data sets.

In the third chapter, an attempt is made to understand the MLD characteristics pertaining to open ocean and coastal grids, in the AS and BOB. For the sake of brevity and comparison, not the whole of the AS and BOB have been examined. Attention is restricted to two meridional transects, stretching 8°N to 22°N in the AS and 8°N to 20°N in the BOB, one along the central basin and another along the coastal regime (Fig. 2.1). The meridional strip along the central Arabian Sea is centred at 65°E and that in the central BOB centered at 91°E, have been divided in to grids of 2° longitude and 2° latitude. A similar scheme was adopted by Naidu *et al.* (1999), for studying upwelling in the AS and BOB. Grids north of 20°N in the BOB have not examined, because the region is much influenced by coastal processes and river discharge. Stations having depth less than 200m near the shore is considered as the coastal station. The area under the MR-LR programme in AS and BOB is the chosen domain of the hydrographic study for Chapter 4 and 5 (Fig. 2.2).

2.2. Data Source and Processing

2.2.1 Marine Research - Living Resources (MR-LR) Programme

This is an ongoing multi-disciplinary programme, since 1998 May, with extensive and systematic coverage in the EEZ of India, and is funded by the Department of Ocean Development, Government of India. The International

examined and outliers were discarded manually. This quality-controlled data on temperature and salinity were used in the present study. Dynamic computations were carried out with reference to 500db surface (Pond and Pickard, 1983). For shallow stations, the method suggested by Fomin (1964) was adopted. Water samples were collected using Rosette sampler fitted with Niskin water bottles (Fig. 2.3) from 14 standard depths (viz. 0,10, 20, 30, 50, 75, 100, 150, 200, 250, 300, 500, 750 and 1000m) and analysed for nitrate with a SKALAR auto-analyzer. For measuring chlorophyll *a* water samples were collected from 7 discrete depths up to a depth of 1% light illumination as compared to the surface. Two litres of water from each depth was filtered through GF/F filters (nominal pore size $0.7\mu\text{m}$) and analysed spectrophotometrically (Perkin-Elmer UV/Vis) using 10 ml of 90% acetone for extraction. Column chlorophyll *a* (mg m^{-2}) was calculated by integrating the values obtained at discrete depths. Nitracline is defined as the depth at which the nitrate concentration is $1\mu\text{M}$ (Gomes *et al.*, 2000) and the depth at which dissolved oxygen is 2.8 mg/l is taken as the depth of the 1st level of under saturation in oxygen.

2.2.2. Hydrographic data

To study the monthly evolution of MLD, besides MR-LR programme, the hydrography data were taken mainly from NIO-hydro CD, distributed by the Indian Oceanographic Data Centre (IODC) of the National Institute of Oceanography (NIO), Goa, India. The hydro CD contains temperature and salinity data from hydro casts as well as CTD casts, collected by the onboard RV Gaveshani and ORV Sagar Kanya during the period 1976 – 1996. In addition, data were taken from world ocean database 1998 CD (Levitus *et al.*, 1998) and JGOFS India programme. The Indian JGOFS programme conducted 7 surveys in the AS onboard ORV Sagar Kanya during 1992 – 1997.

2.2.2.1. Data Processing

The data are processed in the following manner. The data sets of the open

Indian Ocean Expedition (1960-1965), conducted four decades back was an international effort to understand the characteristics of the Indian Ocean, but the west and east coasts of India were not covered extensively as the MR-LR programme.

The MR-LR programme is designed to assess and evaluate the environmental parameters and the marine living resource of the EEZ of India by the simultaneous collection of physical, chemical and biological oceanographic parameters from the seas around India including Arabian Sea, Bay of Bengal and the Andaman Sea. The seasons during which the data have been collected are divided in to four - spring intermonsoon (March-May), summer (southwest) monsoon (June-September), fall intermonsoon (October) and winter (northeast) monsoon (November-February). This classification of the seasons is in accordance with other studies in the JGOFS for AS and BOBPS for BOB (Madhupratap *et al.*, 2003).

The hydrographic surveys were conducted in the AS and BOB, since May 1998, during different seasons and the stations were occupied onboard FORV *Sagar Sampada*. Samplings were done at one degree interval of longitude along 7 transects in AS viz. 8°N, 10°N, 13°N, 15°N, 17°N, 19°N and 21°N and 6 transects in BOB viz., 11°N, 13°N, 15°N, 17°N, 19°N and 20.5°N transects (Fig.2.2). The total number of stations covered for the AS was 41 and 29 for BOB.

2.2.1.1. Data collection and processing

Surface winds were monitored using the automated weather station on board the ship. Sea surface temperature (SST) was measured using a bucket thermometer. CTD (Sea Bird Electronics, Inc., USA, model: SBE-911 plus) was used to collect temperature – salinity profiles and the accuracy and resolution are given in the Table 2.1. Salinity values from CTD were corrected using the values obtained from the Autosal (Guildline, model 8400A) onboard. The data on temperature and salinity available at 1m depth intervals at each station were

ocean transects in AS and BOB were identified and then the profiles with depths less than 100m were discarded, since the MLD in the AS sometimes exceeds 100m (Wyrтки, 1971; Rao *et al.*, 1991). The data for stations having a maximum depth range of 100 to 200m, in the desired grid was extracted for the coastal stations (west and east coast). Sigma-t values were calculated for each depth of the selected individual profiles (UNESCO, 1981). MLD, Isothermal Layer Depth (ILD) and barrier layer thickness were derived from the individual profiles using the methods mentioned in the foregoing section (2.3.1.2). MLD, barrier layer thickness and SSS were then averaged onto 2°x 2° grids for the open and coastal transects. When sufficient number of data existed in each grid, the mean and standard deviation were computed. Individual values outside the limit (mean \pm 2 standard deviation) were removed and the mean was once again determined.

2.2.3. Atmospheric data

Atmospheric data sets used in the study were obtained from three climatologies, viz., i) FSU (Florida State University), ii) Oberhuber and iii) HOAPS (Hamburg Ocean Atmosphere Parameters and Flux from Satellite). SST and wind speed used in the study were obtained from the FSU climatology. These mean monthly data sets are available in 2°x 2° grids over the Indian Ocean for the period of January 1960 – December 1989. The shortwave radiation and net surface heat flux was obtained from the Oberhuber climatology. This climatology derives the heat and radiative flux over the global ocean, based on the COADS (Comprehensive Ocean Atmospheric Data Set) for the period 1950 – 1979. All data are given on a 2° x 2° grid. The evaporation and precipitation data were obtained from the satellite derived climatological atlas of HOAPS CD-ROM (Grassl *et al.*, 2000). The instruments used are AVHRR (Advanced Very High Resolution Radiometer) and SSM/I (Special Sensor Microwave/ Imager). SST was derived from AVHRR data whereas the evaporation and precipitation were computed from the measurements of SSM/I. HOAPS provides the monthly mean

data sets on a $1^\circ \times 1^\circ$ grid for the period July, 1987 to December, 1998. The atmospheric parameters were derived from the climatologies for the same grid points as that of the mean monthly hydrographic data.

2.3. Methods

A balance between the destabilizing effects of mechanical mixing and the stabilizing effects of the buoyancy flux ultimately determines the MLD. In the modeling studies such as ocean general circulation models (OGCM), a common difficulty encountered is relating the MLD predicted by the models to the observed MLD. The reason for this is that the depth of turbulent mixing is sensitive to the thermal and density stratification at the base of the mixed layer and, thereby, to the criteria chosen to define MLD (Kara *et al.*, 2000). Hence the MLD definition should seek to represent turbulent mixing. The benefits of such an optimal selection of MLD have been used to investigate a variety of properties. These include investigating where penetrative solar radiant heat flux affect ocean mixed layer heating (Ohlmann *et al.*, 1996), determining the regions of barrier layers where salinity effects hamper vertical heat flux out of the base of the mixed layer (Sprintall and Tomczak, 1992) and using MLD climatologies as part of constraints or inputs for an OGCM in various heat flux, sea surface temperature and circulation studies (Spall, 1991; Huang and Russel, 1994). Moreover, having such valuable MLD information would help modelers to couple atmosphere and ocean models realistically and to understand the seasonal variations in the productivity of ocean ecosystems (Obata *et al.*, 1996), but more importantly the mixed layer thickness determines the volume or mass over which the net surface heat flux comes to be distributed (Chen *et al.*, 1994).

2.3.1. Estimation of the mixed layer

In view of the importance of MLD in the ocean, many investigators have developed different techniques to determine MLD. It is not always easy to agree on the MLD or even whether a mixed layer exists, as there is not always an

depth of isoproperty layer by visual inspection. Thomson and Fine (2003) developed a split and merge method to obtain the mixed layer depth from the vertical profiles of density. They verified their result with the visually estimated MLD. The distribution of physical properties within the upper layers of the region determines what criteria should be followed to define MLD. Since the AS and BOB undergo seasonal changes in the surface forcing, the temporal and spatial distribution of properties needs to be examined. Visual inspection of temperature, salinity and density profiles indicate that the isothermal, isohaline and isopycnal layers coincide in the upper ocean in the AS. This was observed irrespective of the season or spatial location with few exceptions at certain stations especially near the southwest coast during winter (Fig. 2.4.). While in BOB, usually the isothermal layer was not coinciding with the isohaline and isopycnal layers (Rao and Sivakumar, 1999), and was observed to be deeper than the latter two layers (Fig. 2.5). In this chapter, the aim is to obtain a unique MLD selection criterion, which is equally applicable to AS and BOB.

2.3.1.1 Comparison of various MLD selection criteria

To obtain an optimal definition of MLD, 275 CTD profiles pertaining to different seasons in the AS and BOB, collected under MR-LR programme, are used. Analyses of all the individual profiles of temperature, salinity and density and the visual determination of actual MLD is time consuming and a tedious effort. It is, therefore, desirable to use a standard technique to calculate MLD while dealing with large databases. With that in mind, a comparison has been made between MLD obtained from the profiles (visual) and the one obtained by all the above-mentioned methods, however, the most significant ones are only discussed. The temperature and density at 5m depth is chosen as the reference value for determining the MLD. This depth is chosen to eliminate any possible bias in the profile data due to 'skin effects' at the ocean surface (Fairall *et al.*, 1996). Majority of the profiles in the present study

depth of isopycnal layer by visual inspection. Thomson and Fine (2003) developed a split and merge method to obtain the mixed layer depth from the vertical profiles of density. They verified their result with the visually estimated MLD. The distribution of physical properties within the upper layers of the region determines what criteria should be followed to define MLD. Since the AS and BOB undergo seasonal changes in the surface forcing, the temporal and spatial distribution of properties needs to be examined. Visual inspection of temperature, salinity and density profiles indicate that the isothermal, isohaline and isopycnal layers coincide in the upper ocean in the AS. This was observed irrespective of the season or spatial location with few exceptions at certain stations especially near the southwest coast during winter (Fig. 2.4.). While in BOB, usually the isothermal layer was not coinciding with the isohaline and isopycnal layers (Rao and Sivakumar, 1999), and was observed to be deeper than the latter two layers (Fig. 2.5). In this chapter, the aim is to obtain a unique MLD selection criterion, which is equally applicable to AS and BOB.

2.3.1.1 Comparison of various MLD selection criteria

To obtain an optimal definition of MLD, 275 CTD profiles pertaining to different seasons in the AS and BOB, collected under MR-LR programme, are used. Analyses of all the individual profiles of temperature, salinity and density and the visual determination of actual MLD is time consuming and a tedious effort. It is, therefore, desirable to use a standard technique to calculate MLD while dealing with large databases. With that in mind, a comparison has been made between MLD obtained from the profiles (visual) and the one obtained by all the above-mentioned methods, however, the most significant ones are only discussed. The temperature and density at 5m depth is chosen as the reference value for determining the MLD. This depth is chosen to eliminate any possible bias in the profile data due to 'skin effects' at the ocean surface (Fairall *et al.*, 1996). Majority of the profiles in the present study

showed that the properties at 5m are very close to the surface value.

Figs. 2.6 – 2.16 show the scatter plots of MLD obtained from the temperature and density criteria against the observed MLD (visually determined) in AS and BOB. The panels to the left in the figures are based on temperature criteria and those to the right are based on density criteria. The MLDs obtained from the 0.2, 0.5 and 1.0°C drops from the temperature at 5m are separately plotted against the observed MLD. Hereinafter, the MLDs obtained from the 0.2, 0.5 and 1.0°C drop from the reference temperature will be referred to as ht1, ht2 and ht3, respectively. The MLDs obtained from 0.05, 0.125 and 0.2 unit rise from the 5m depth value against observed MLD. Hereinafter, the MLDs obtained from the 0.05, 0.125 and 0.2 unit rise from the reference value are referred to as hd1, hd2 and hd3, respectively. Figs. 2.6-2.9 display the scatter plots during spring intermonsoon, summer monsoon, fall intermonsoon and winter monsoon seasons in the AS and similarly Figs. 2.10-2.13 display the scatter plots for the respective seasons in the BOB. Figs 2.14 & 2.15 are the respective scatter plots of AS and BOB, in which all the data for the various seasons are pooled together. The seasonal data pertaining to the AS and BOB are pooled together and plotted against the observed MLD (Fig. 2.16). From the above analysis (Figs. 2.6-2.16), it was found that the MLDs based on density criteria have a more significant relationship with the observed MLDs than that based on temperature criteria. The vertical profiles of temperature, salinity and density shows that these isoproperty layers are concurrent at the upper layers in the AS. The MLDs obtained from the density criteria, however, shows much significant correlation than that obtained from the temperature criteria with actual MLDs. In BOB, the temperature based criteria was always unsuccessful and did not show any relation to the actual MLD. For the AS, ht1, ht2 and ht3 have the correlation coefficient squared (r^2) of 0.48, 0.61 and 0.48 ($p=0.95$) significant to the observed MLD in each case. Where as hd1, hd2 and hd3 have the respective correlation coefficients of 0.57, 0.8 and 0.87

and shows 99% significant to the actual MLD in each case. Similarly along BOB, the respective values of r^2 are 0.09, 0.08 and 0.06, showing insignificance of temperature criteria in the MLD computation. Whereas the density criteria (hd1, hd2 and hd3) showed 99% significance to the actual MLD with corresponding r^2 of 0.64, 0.82 and 0.88. As a whole the correlation between actual MLD with ht1, ht2 and ht3 shows a positive correlation with respective r^2 of 0.25, 0.3 and 0.25. But the corresponding values for the density criteria are 0.63, 0.83 and 0.89 with 99% significance. In general ht1 and ht2 are always overestimate the MLD. Hence, for the AS and BOB, the density based criteria for MLD could be taken as proxy for the observed MLD. It was found that MLDs defined by the density difference of 0.2 units from the 5m depth corresponded most closely to the MLD obtained from the profiles.

2.3.1.2. An optimal definition of MLD

In this study, MLD is defined as the depth at which density rises by 0.2 units from the 5m depth value. Since, in the BOB thermal inversions usually exceeds 1°C , the isothermal layer can be redefined as the first depth at which $|T_{\text{ref}} - T_d| > 1^\circ\text{C}$, where T_{ref} is the temperature at 5m depth and T_d is the *in situ* temperature. The difference between MLD and isothermal layer depth (ILD) can be defined as the barrier layer. Shetye *et al.* (1996) and BOBPS programme (Madhupratap *et al.*, 2003) used the same density difference criteria (0.2 kg/m^{-3}) to define the MLD, in their hydrographic surveys. However, it should be noted that 0.2 sigma-t criteria would not be applicable to the whole ocean. For example, at a salinity of 35 psu, and the temperature range $6^\circ\text{C} - 10^\circ\text{C}$, the 0.5°C temperature change corresponds to a sigma-t change of approximately 0.075 magnitude, while that for $24^\circ\text{C} - 26^\circ\text{C}$ temperature range, the sigma-t changes approximately by 0.15 magnitude (Levitus, 1982). In view of the importance of salinity, few MLD definitions based on the variable sigma-t is used for the global oceans (Sprintall and Tomczak, 1992; Rao and Sivakumar, 2003). In this method, the coefficient of expansion is

calculated using surface values of temperature and salinity and determines the variable sigma-t difference required to obtain a particular temperature difference (0.5°C or 1.0°C). Since the present study is concentrated in the northern Indian Ocean, the procedure of incorporating the coefficient of thermal expansion for variable sigma-t criterion is beyond the scope and can be seen that, if salinity is constant, the 1.0°C change in temperature is equivalent 0.2 units in sigma-t change.

Table 2.1. CTD sensors and specifications

Sensor	Range	Accuracy	Resolution
Temperature	-5 to 35°C	0.001°C	0.0002°C
Conductivity	0 to 7 S/m (0 to 70 mmho/cm)	0.0003 S/m	0.00004 S/m
Pressure	Up to 10500m	0.015 % of full scale range	0.001 % of full scale range

Table 2.2. Commonly used MLD criteria

Temperature based criteria		Density based criterion	
Source	Definition	Source	Definition
Ostapoff and Worthem (1974); Wyrki (1971); Colborn (1975); Rao <i>et al.</i> (1981); Wagner (1996); Rao <i>et al.</i> (1983)	$\Delta T = 1.0^{\circ}\text{C}$	Levitus (1982) Miller (1976) Lewis <i>et al.</i> (1990)	$\sigma_t = 0.125 \text{ kg/m}^{-3}$ $\sigma_t = 0.13 \text{ kg/m}^{-3}$ $\sigma_t = 0.2 \text{ kg/m}^{-3}$
Monterey and Levitus (1997)	$\Delta T = 0.5^{\circ}\text{C}$	Shetye <i>et al.</i> (1996)	
Thomson (1976); Rao and Rao (1986)	$\Delta T = 0.2^{\circ}\text{C}$	Kara <i>et al.</i> (2000)	$\sigma_t = \sigma_t(T + \Delta T, S, P) - \sigma_t(T, S, P)$, where S & T at 10m and P=0 $\Delta T = 0.8^{\circ}\text{C}$
Martin (1985)	$\Delta T = 0.1^{\circ}\text{C}$	Sprintall and Tomczak (1992) Monterey and Levitus (1997)	Same as Kara <i>et al.</i> with $\Delta T = 0.5^{\circ}\text{C}$
Price <i>et al.</i> (1986)	Trapping depth = $\Delta T \int_{z_1}^{z_2} T dz$	Brainerd and Gegg (1995) Vinayachandran <i>et al.</i> (2002)	$\sigma_t / \sigma_z = 0.0005 - 0.05 \text{ kg/m}^4$ $\sigma_t / \sigma_z > 0.05 \text{ kg/m}^4$

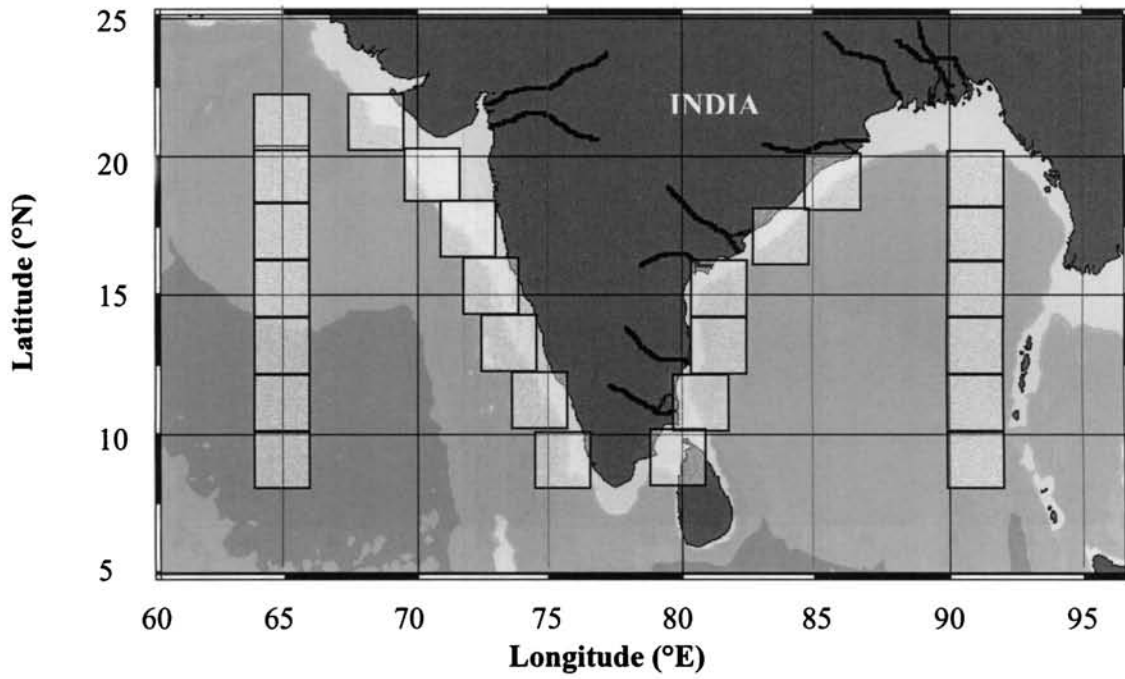


Figure 2.1. Location map and grids used to study the mixed layer characteristics in the Arabian Sea and Bay of Bengal

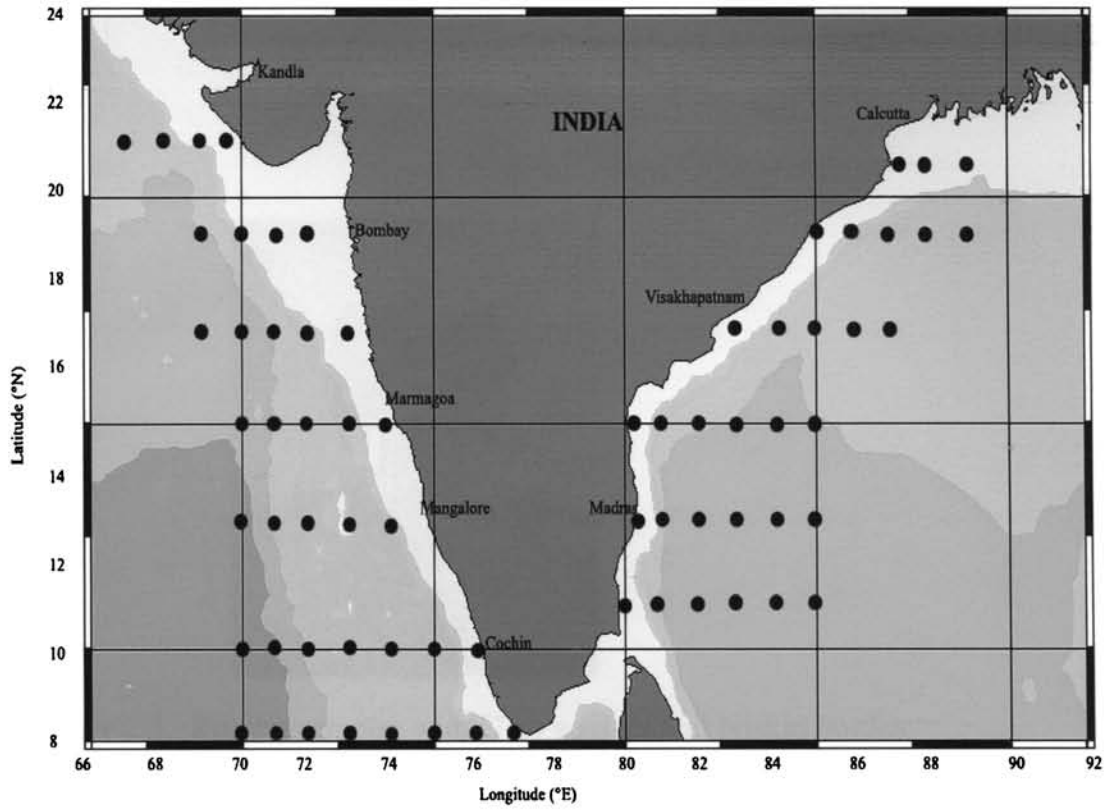


Figure 2.2. Location map of the hydrography under MR-LR programme along the west and east coasts of India

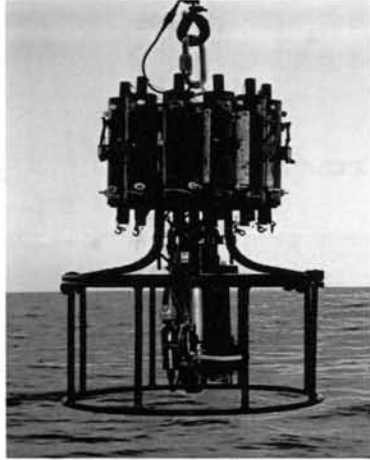


Figure 2.3. Rosette sampler with CTD sensors and Niskin bottles

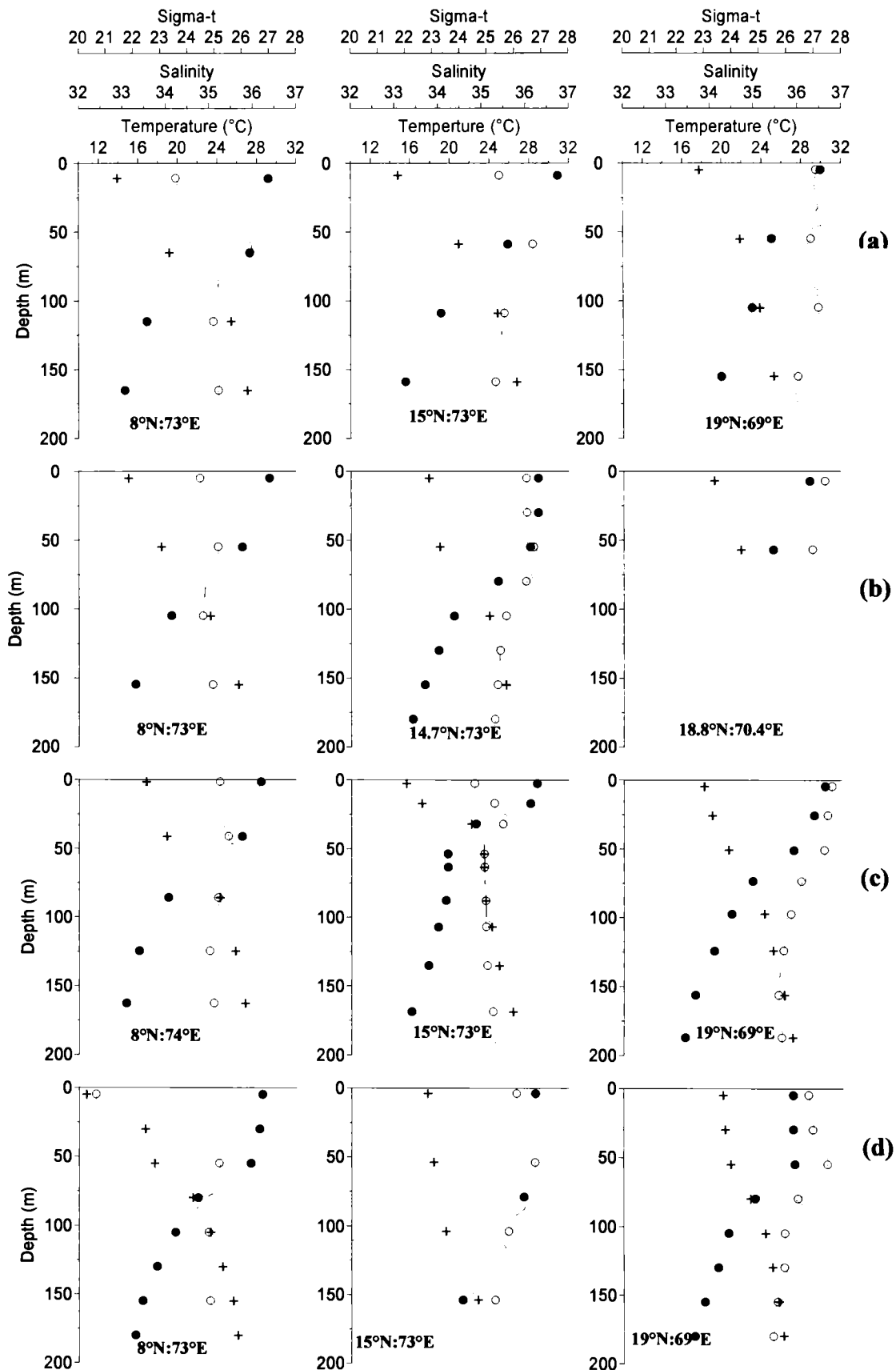


Figure 2.4. Vertical profiles of temperature, salinity and density at selected stations in the Arabian Sea during a) spring, b) summer c) fall and d) winter monsoon seasons

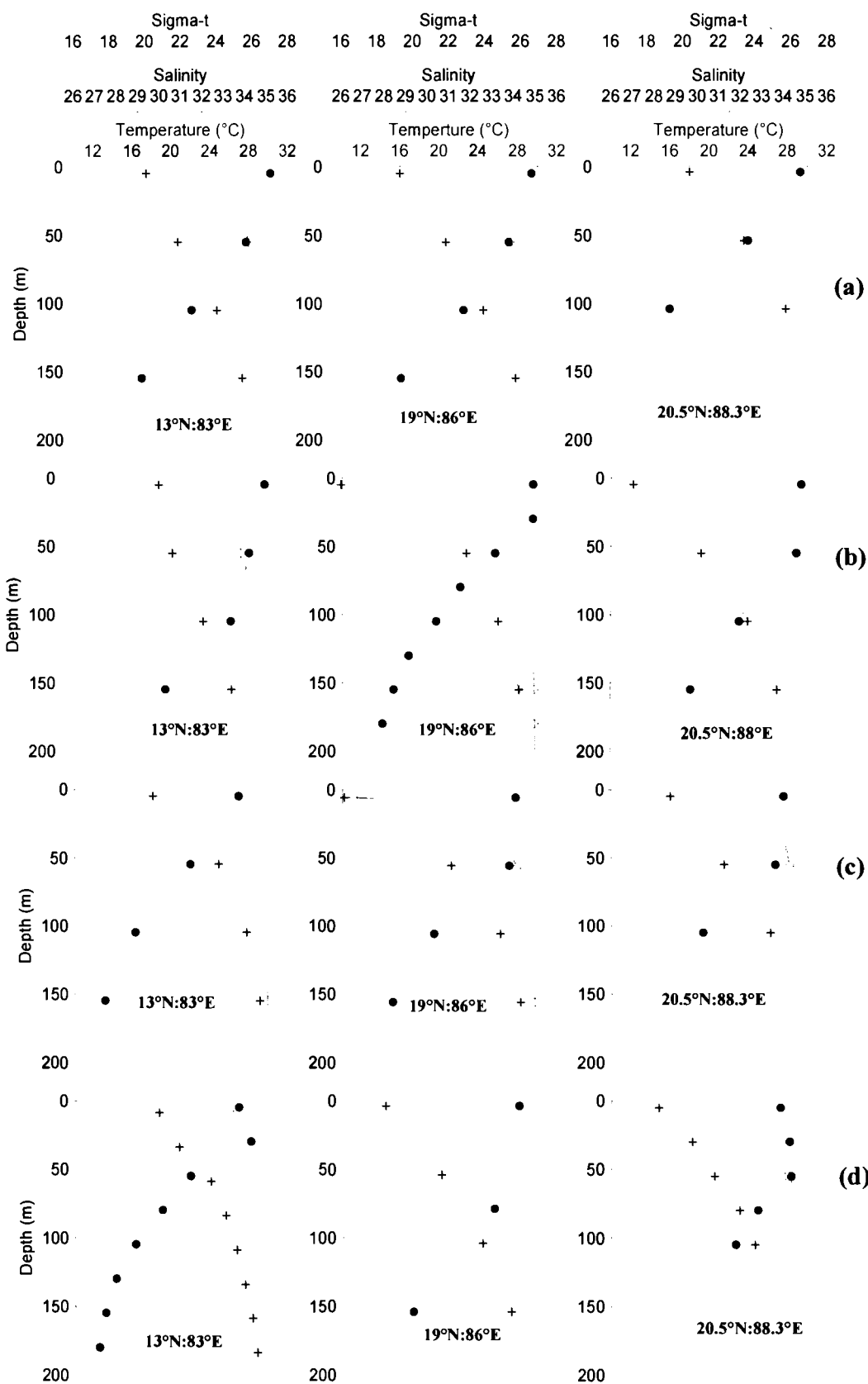


Figure 2.5. Vertical profiles of temperature, salinity and density at selected stations in Bay of Bengal during a) spring b) summer c) fall and d) winter monsoon seasons

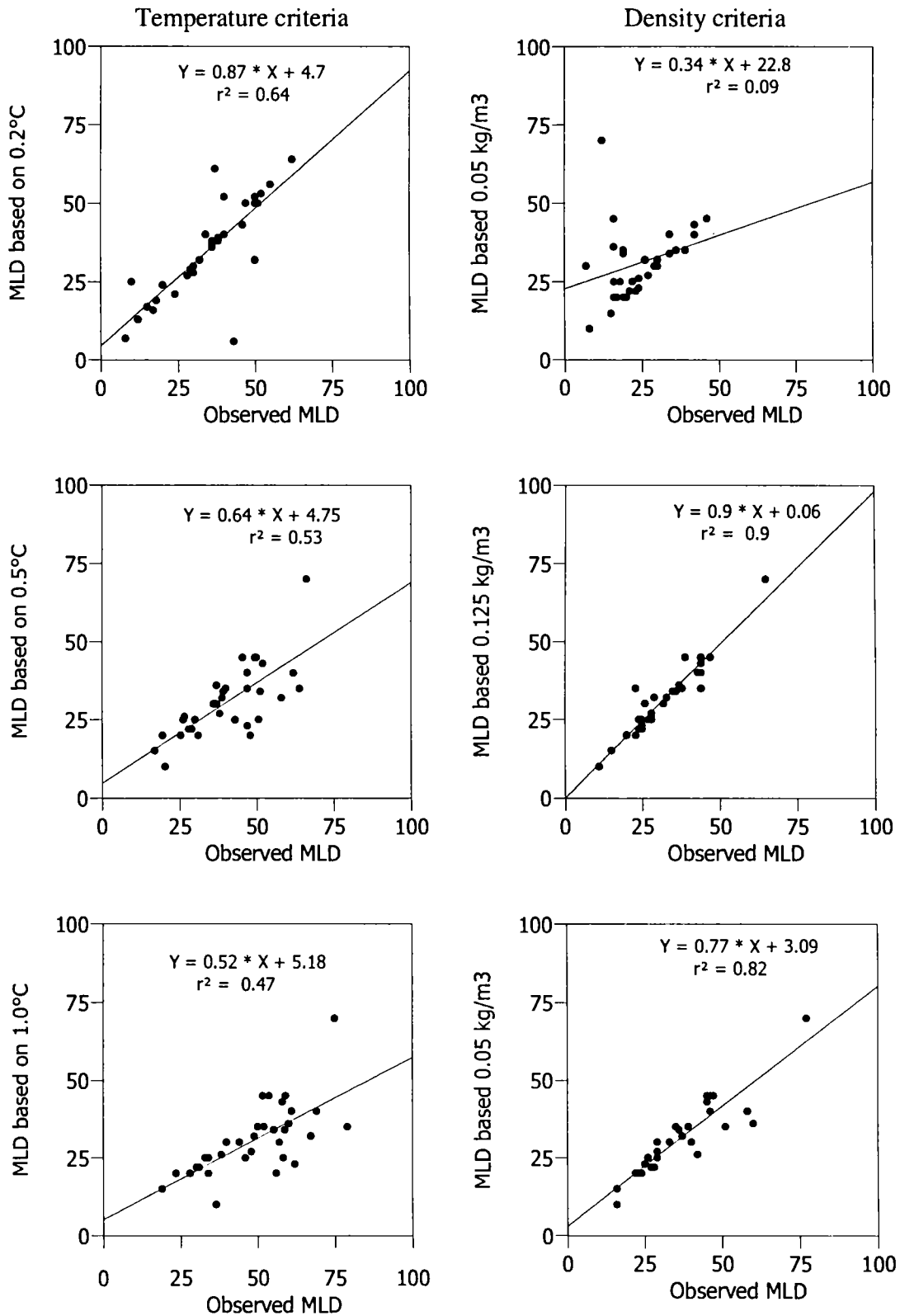


Figure 2.6. Correlation between observed MLD and MLD based on various criteria in the Arabian Sea during spring intermonsoon. Total no. of observations, n=33

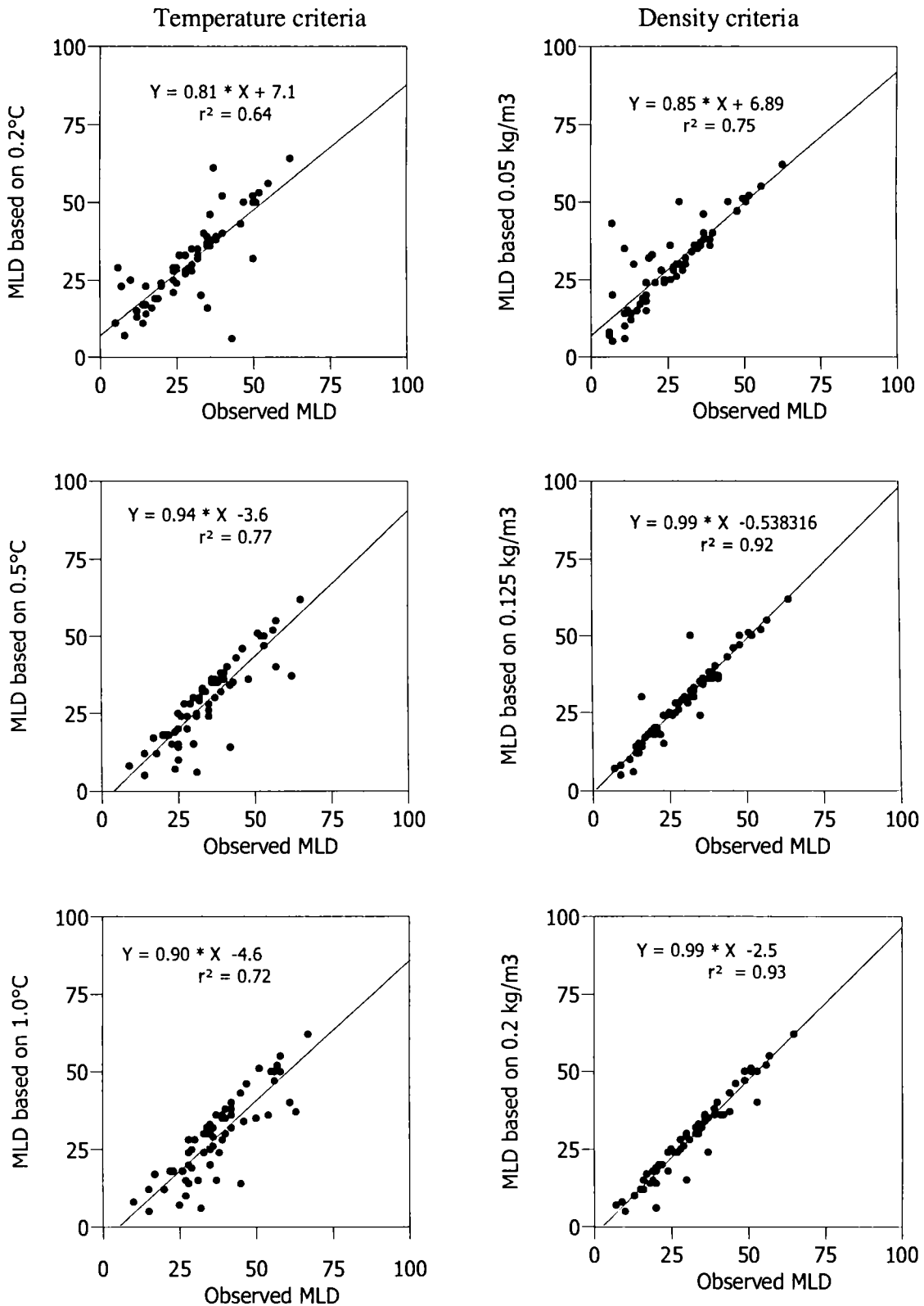


Figure 2.7. Correlation between observed MLD and MLD based on various criteria in the Arabian Sea during summer monsoon. Total no.of observations, n=64

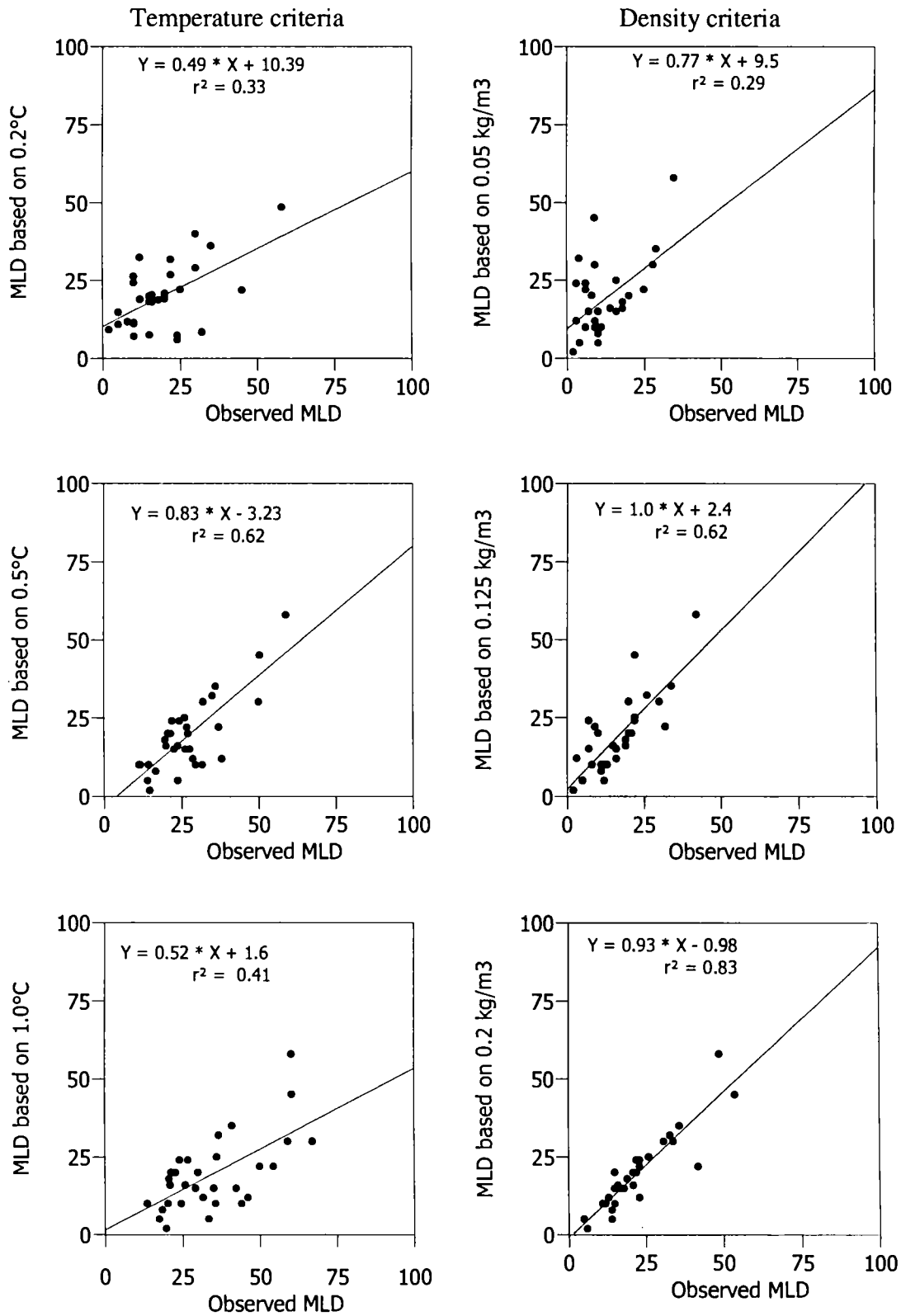


Figure 2.8. Correlation between observed MLD and MLD based on various criteria in the Arabian Sea during fall intermonsoon. Total no. of observations, n=32

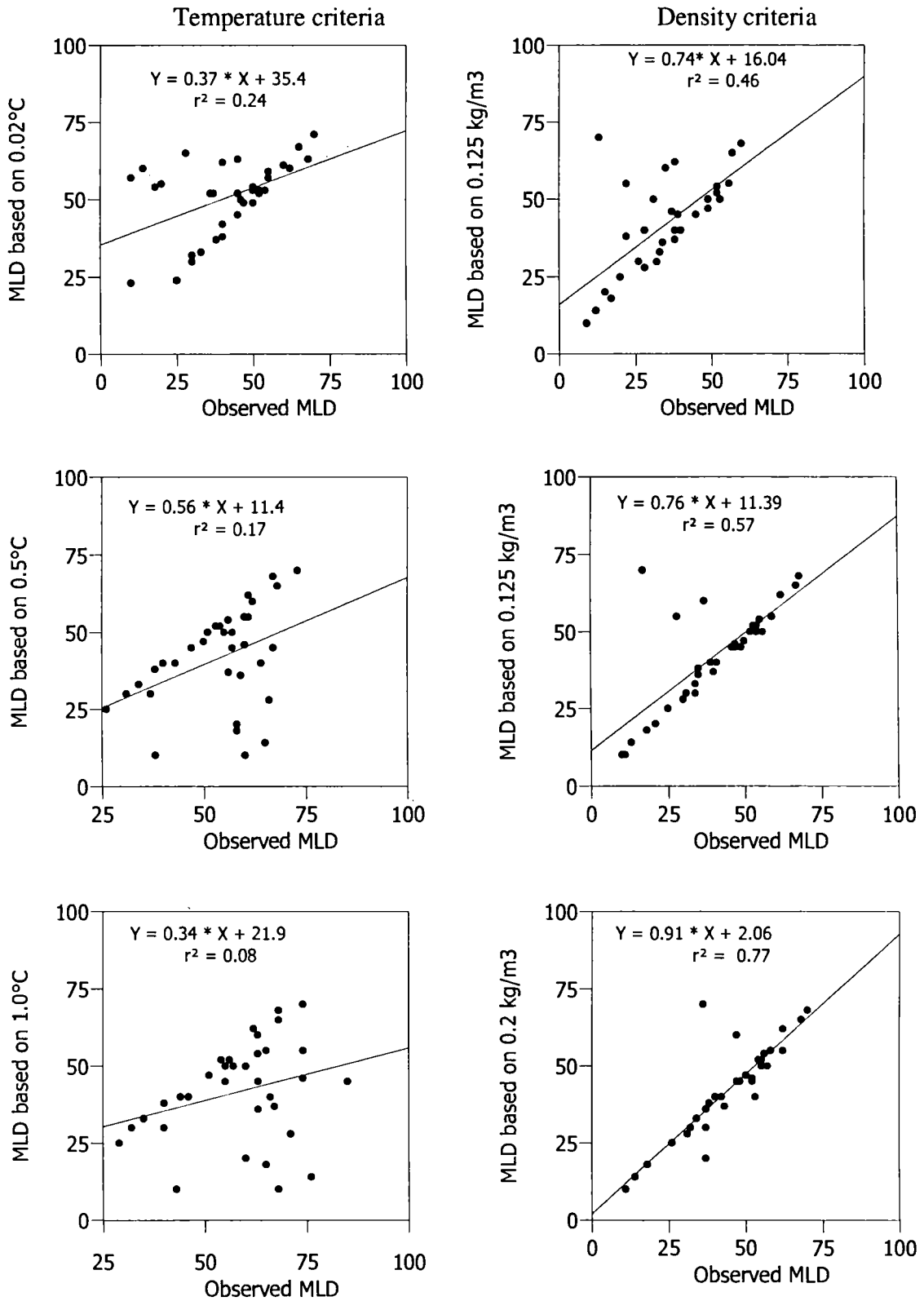


Figure 2.9. Correlation between observed MLD and MLD based on various criteria in the Arabian Sea during winter monsoon. Total no. of observations, $n = 34$.

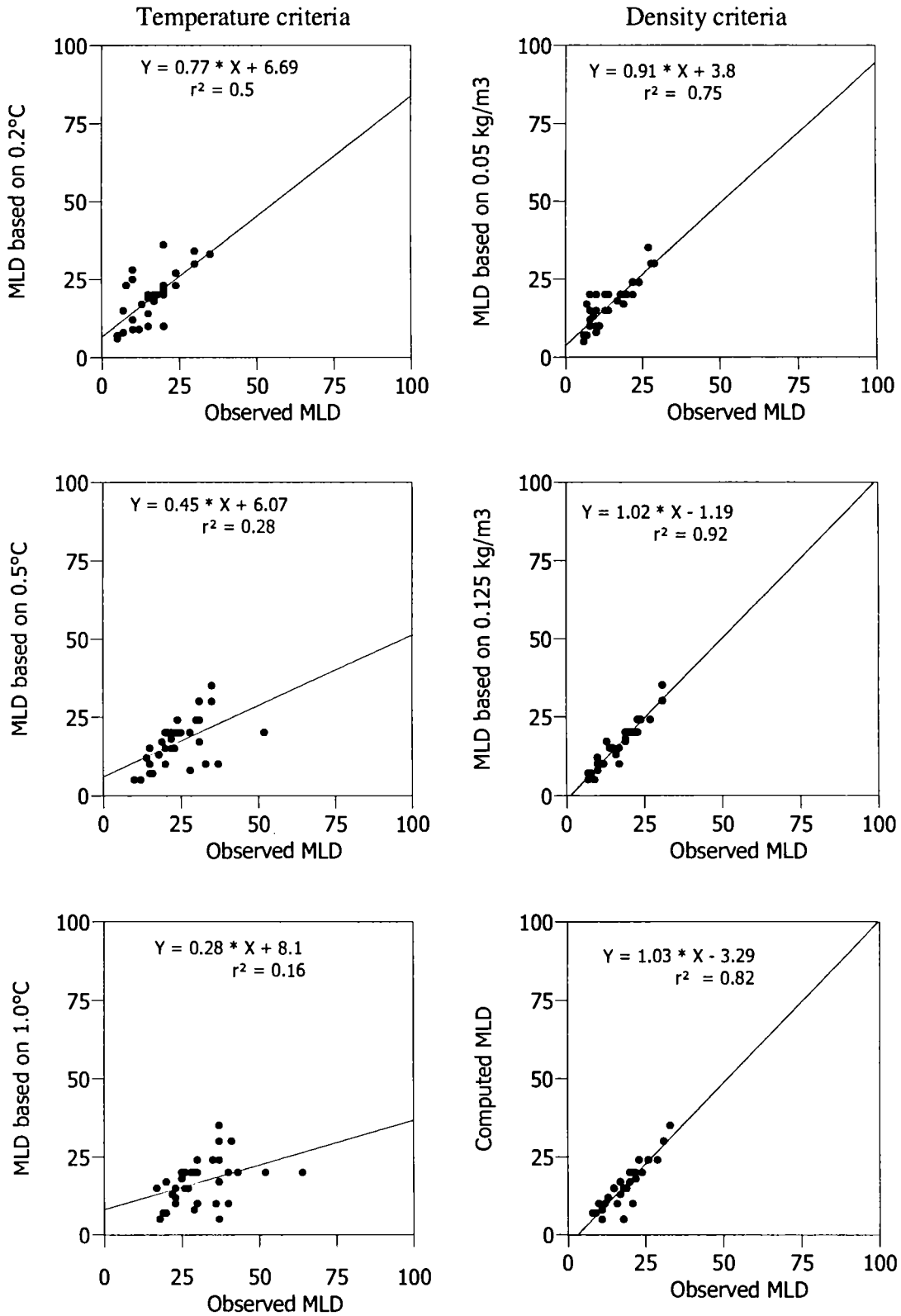


Figure 2.10. Correlation between observed MLD and MLD based on various criteria in the Bay of Bengal during spring intermonsoon. Total no. of observations, n = 34.

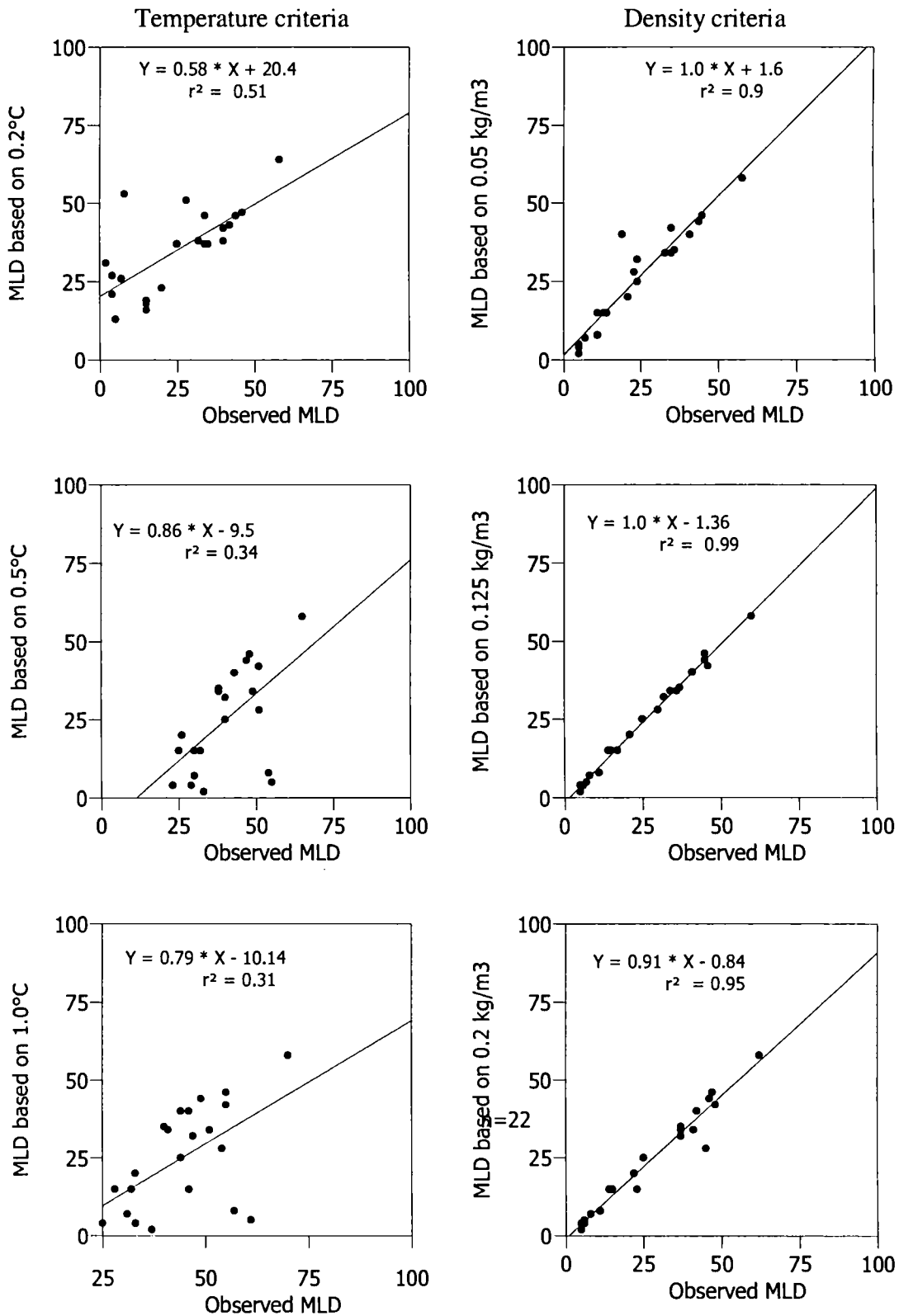


Figure 2.11. Correlation between observed MLD and MLD based on various criteria in the Bay of Bengal during summer monsoon. Total no. of observations, $n = 22$.

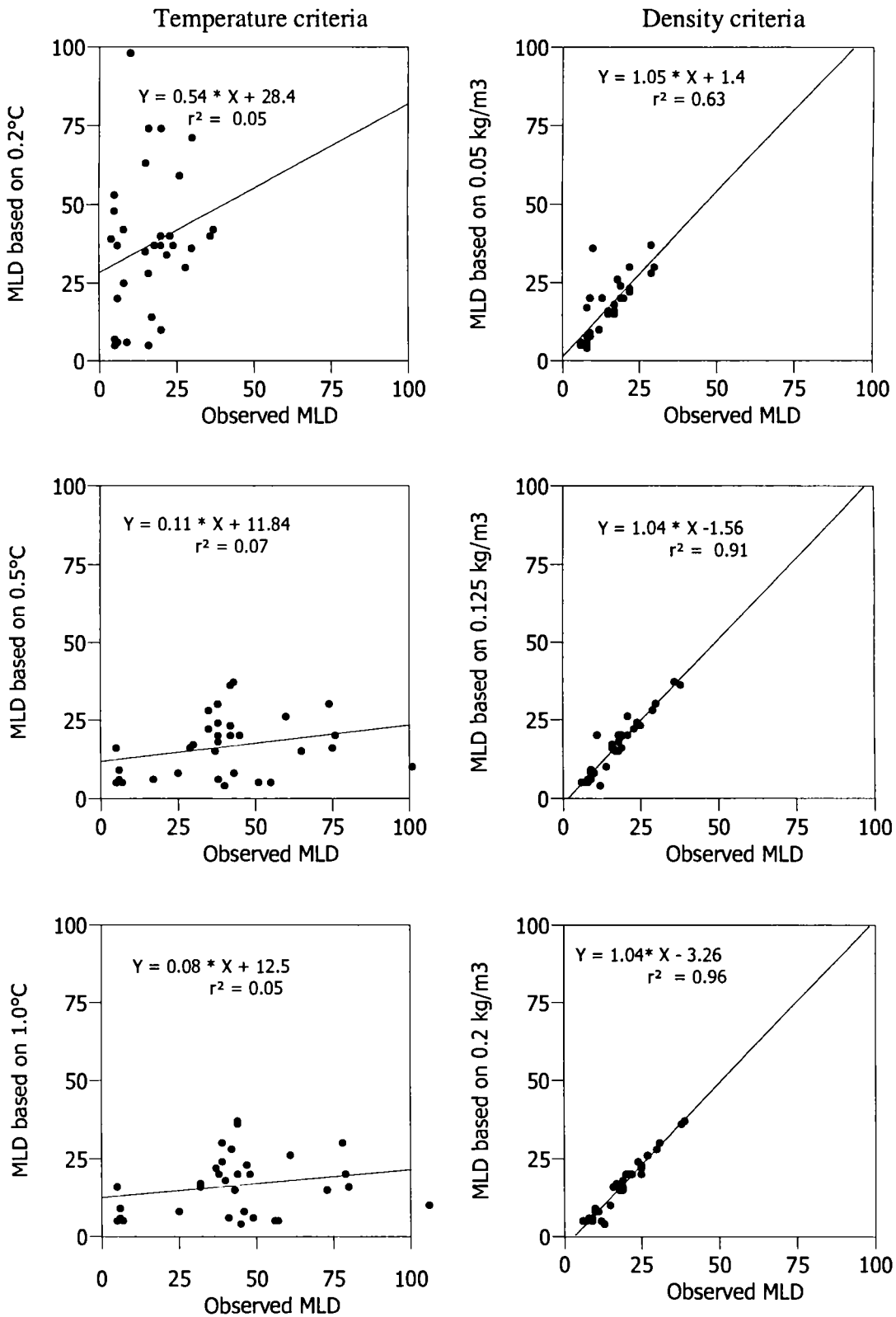


Figure 2.12. Correlation between observed MLD and MLD based on various criteria in the Bay of Bengal during fall intermonsoon. Total no. of observations, n = 32.

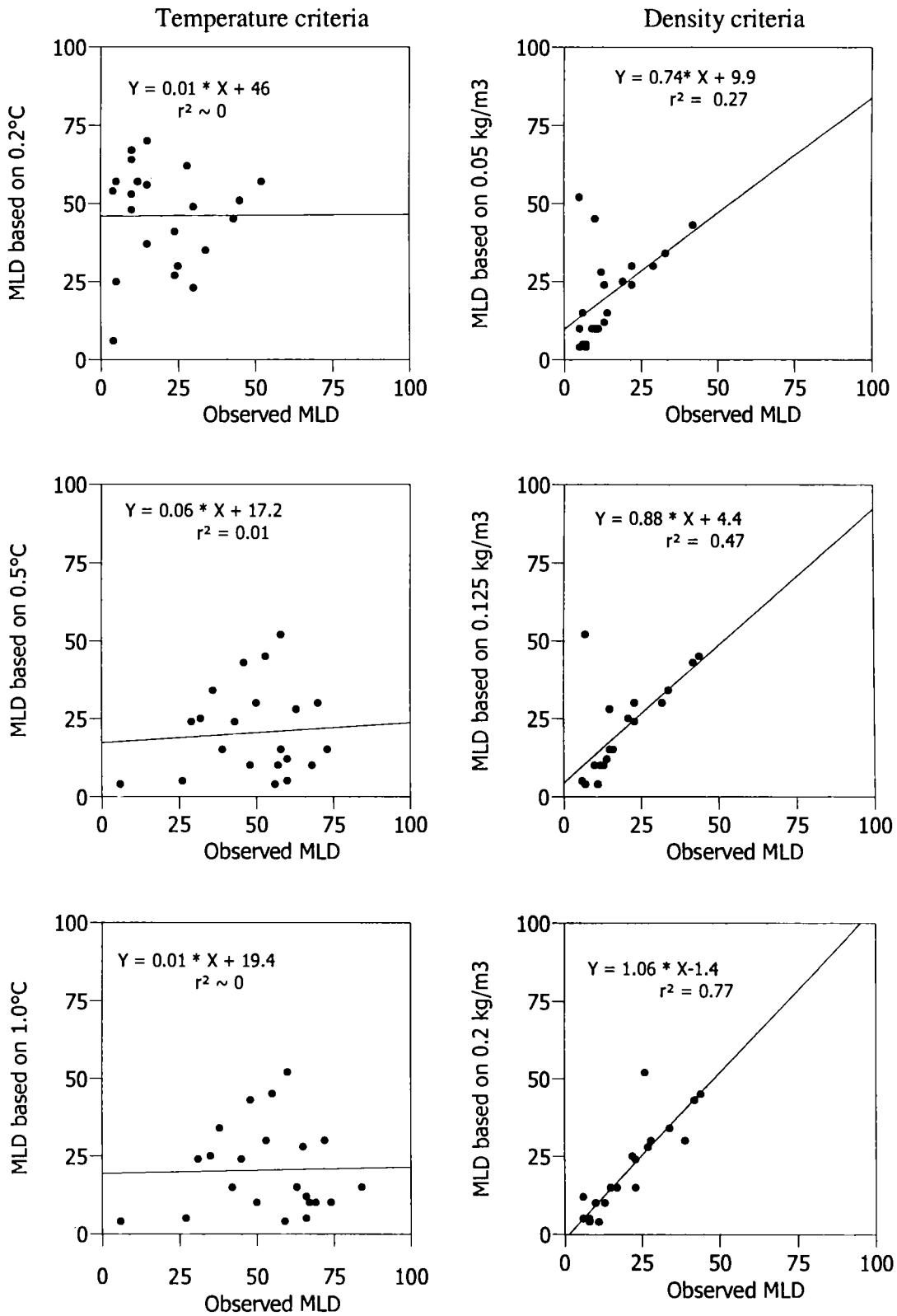


Figure 2.13. Correlation between observed MLD and MLD based on various criteria in the Bay of Bengal during winter monsoon. Total no. of observations, $n = 22$.

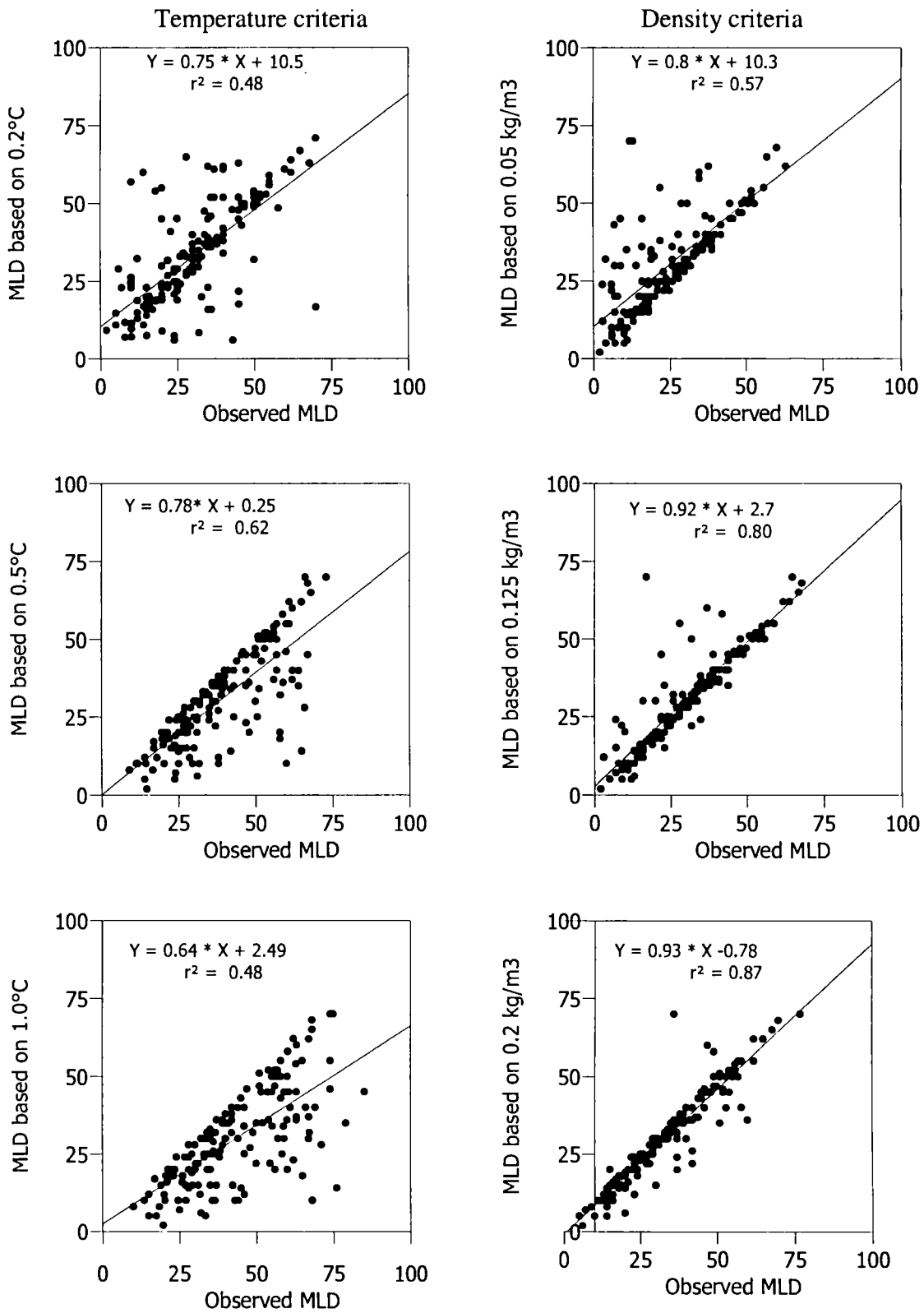


Figure 2.14. Correlation between observed MLD and MLD based on various criteria in the Arabian Sea. Total no. of observations, n = 163.

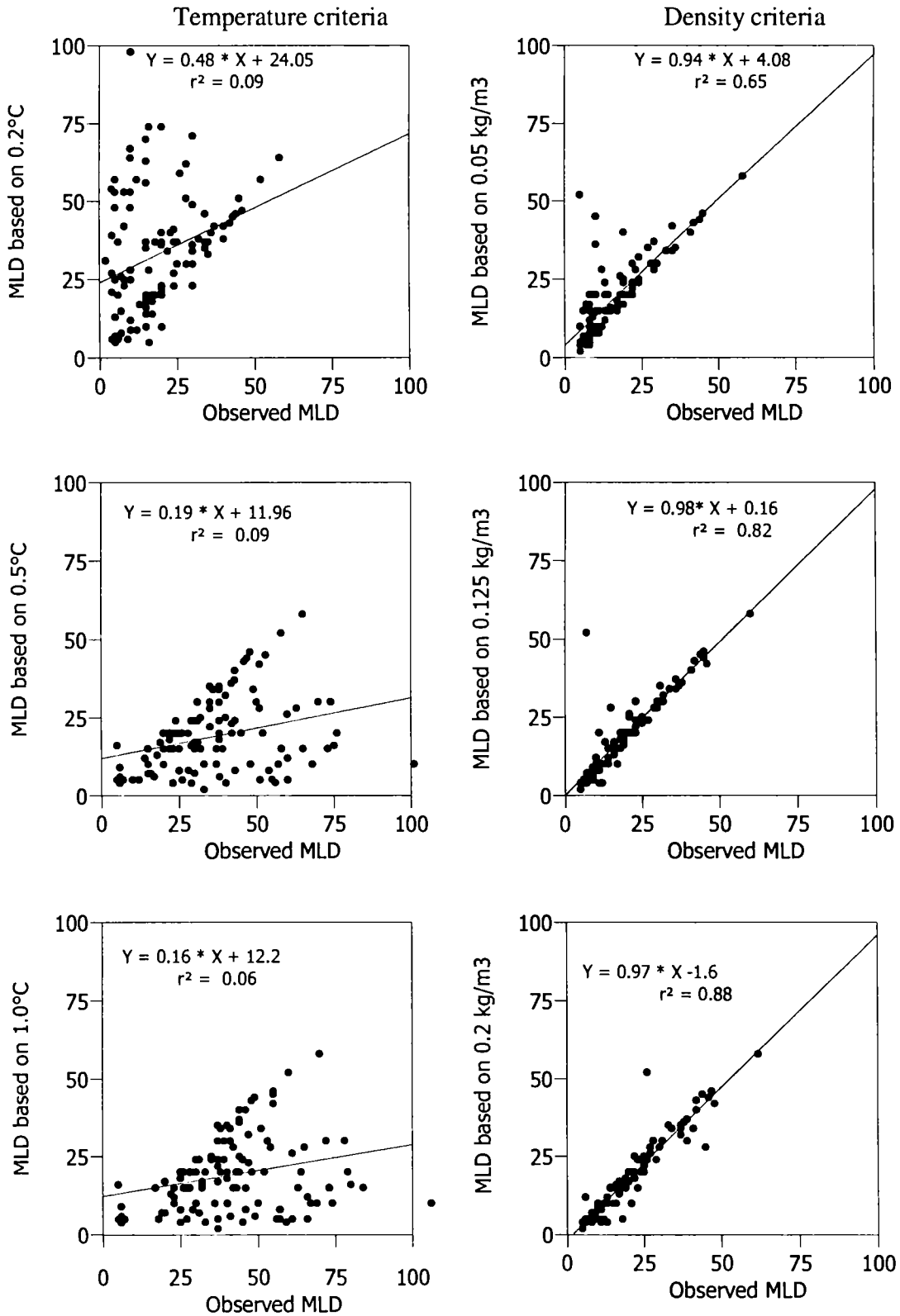


Figure 2.15. Correlation between observed MLD and MLD based on various criteria in the Bay of Bengal. Total no. of observations, $n = 110$.

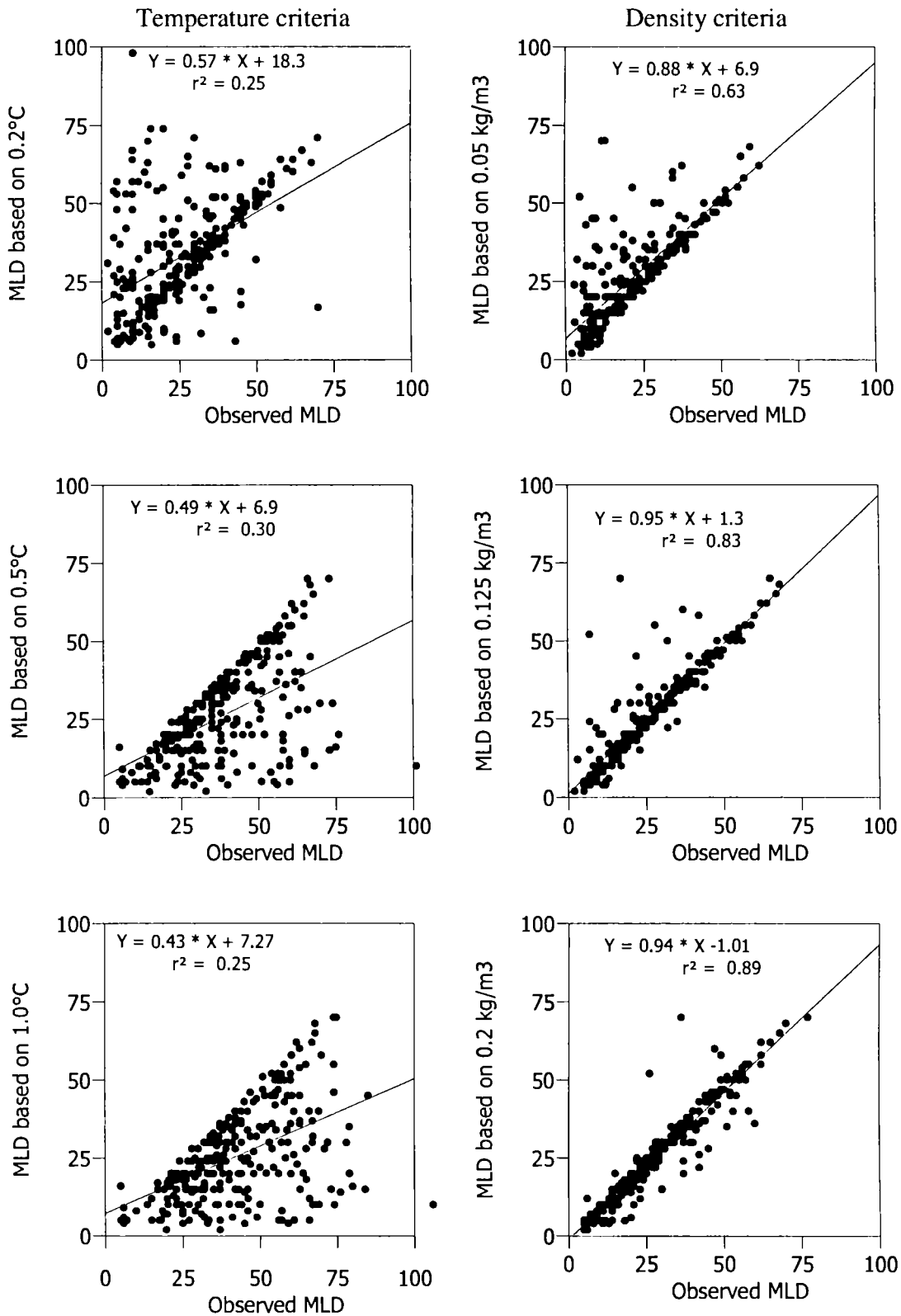


Figure 2.16. Correlation between observed MLD and MLD based on various criteria in the Arabian Sea and Bay of Bengal. Total no. of observations, n = 273.

Chapter 3

Mixed Layer Characteristics

Temporal and spatial variability of the mixed layer depth (MLD), sea surface temperature (SST), sea surface salinity (SSS) and the barrier layer, in each 2°X2° latitude-longitude grid in the AS and BOB are presented in this chapter. The variability of the above four parameters was studied in relation to the atmospheric forcing by analyzing the monthly wind speed, short wave radiation, net surface heat flux, and evaporation – precipitation data in the same grid. In addition, a comparative study of the same parameters in a coastal grid in the same latitude band was also done.

3.1. Arabian Sea

3.1.1. 8°-10°N (Fig. 3.1)

3.1.1.1. Results

SST showed a bimodal distribution in the open ocean as well as in the coastal region. In the open ocean, SST was 27.6°C in January and thereafter it increased to 30.1°C in May. From June to September, SST showed a decreasing phase to 28.4°C and remained almost same till December. In the coastal region, SST increased from 27°C in January to 29°C in April, thereafter the sea surface cooled abruptly and reached a minimum of 25.8°C in August. From August onwards, it showed a steady increase to 26.8°C in November. Differences in SST between the open and coastal ocean showed a maximum during southwest monsoon. During spring intermonsoon (February – April), the open and coastal ocean regimes showed more or less same temperature.

In the open ocean region, a decrease of 1 psu in SSS was seen in January (from 36.5psu) to February and then increased to 36.4 psu in March and thereafter it decreased sharply to 34.5 psu in June. From June onwards, SSS showed an increasing trend and reached 36.6 psu in August and remained almost the same till

December. SSS in the coastal region was 33.9 psu in January and then increased steadily to 35.2 psu in June and decreased to 34.1 psu in July. From July, it showed an increasing trend to 34.8 psu in September and thereafter it decreased gently to 33.4 psu in December. In general, SSS was relatively small in the coastal region and ranged from 33.5 – 35 psu, as compared to the open ocean.

Winds also showed a bimodal distribution in the open ocean as well as the coastal ocean. The two weak periods were observed during March – April and September – November, when wind speed was relatively small (<4m/s). The wind speed peaks up in southwest monsoon in the open ocean as well as in the coastal regions. However, the open - coastal ocean variability of wind speed showed a maximum during the southwest monsoon period. The open ocean showed a wind speed of greater than 8m/s, while the coastal region showed a speed of ~5m/s during the southwest monsoon seasons. During March-May and September-October, the winds in the open and coastal ocean showed a minimum variability.

Short wave radiation (SWR) showed a bimodal distribution, the two peaks occur in March/April and September, respectively. In the open ocean (coastal) region, SWR showed an increase from 180 w/m² (188 w/m²) in January to 230 w/m² (220 w/m²) in April (March) and then decreased to 180 w/m² (160 w/m²) in June. From June to August (September) it once again increased to 220 w/m² (185 w/m²) and then showed a decrease till December. The open ocean values were always high except during December – February when the coastal values were slightly higher than the open ocean values.

Net surface heat flux showed a bimodal distribution, as seen in the SWR distribution. Coastal region showed relatively higher surface heat flux than that seen in the open ocean region. The differences between open and coastal ocean values were observed to be a minimum during the two periods of April-May and September-October. Open Ocean (coastal) region showed a steady increase of net surface heat flux from 10 w/m² (45 w/m²) to 110 w/m² (130 w/m²), from January to April (March). It decreased to -10 w/m² (40 w/m²) in June and again increased

to 90 w/m^2 (92 w/m^2) in September and thereafter it showed a decreasing trend till December.

In general, E-P showed a positive water balance in the coastal region and a negative water balance in the open ocean region. The values in the open ocean showed an increase from 90 mm/month in January to 140 mm/month in February and then decreased to -1 mm/month in June, showing a decrease in evaporation. From June to December, it passed through a cycle of high (July-August) and low (October-November), showing a net evaporation. E-P along the coastal region showed a sudden decrease from 65 mm/month in January to -230 mm/month in June and then increased gradually. However, the precipitation dominated over the evaporation from June to December.

MLD in the open ocean region was around 80 m in January, thereafter it decreased to a depth of 25 m in May and then showed a drastic increase to a depth of 90 m in August. From August, it shoaled suddenly to 45 m in September and thereafter increased steadily during the winter monsoon. In the coastal region shallow MLDs ($<40 \text{ m}$) were observed during all the seasons and very shallow MLDs ($<20 \text{ m}$) were observed during March - October, except in September.

Barrier layer thickness in the open ocean region showed small values ($<20 \text{ m}$) except in June and October, when it was 25 m and 30 m , respectively. In the coastal region, barrier layer thickness was 50 m in January, and remained thicker (40 m) in February and then decreased to 8 m in May and remained almost same till October. From October onwards the barrier layer thickness showed a rapid increase to a maximum of 70 m in December.

3.1.1.2. Discussion

The open and coastal ocean variability of the MLD showed a minimum in March-April as well as in October. The probable reason is that during the periods, the atmospheric conditions are fairly same in both the regions. High net heat flux during the periods produces enough upward buoyancy flux in the surface layer, which is sufficient to oppose the vertical turbulence caused by the weak winds and

causes the MLD to thin. The observed deepening of MLD and cooling of SST during southwest monsoon in the open ocean regions could be due to the increased wind speeds and reduced insolation due to clouds. The strong winds and fairly high rate of evaporation and reduced solar insolation produces strong turbulence at the sea surface, which is sufficient to erode the buoyancy flux, the excess energy is used to entrain the waters below the base of the MLD. Further, large scale Ekman convergence due to negative wind stress curl and associated Ekman pumping in the central AS also contributed to the deepening of mixed layer (Hastenrath and Lamb, 1979; Rao *et al.*, 1991; Schott *et al.*, 2001). However, it was found that the wind driven mixing is stronger than the Ekman pumping and the horizontal advection during summer monsoon (Lee *et al.*, 2000). It is well known that the wind system along the southwest coast of India favours coastal upwelling (Shetye, 1984; Shetye and Shenoi, 1988; Shetye *et al.*, 1989, Muraleedharan *et al.*, 1995, Maheswaran *et al.*, 2000). Strong stratification at the sea surface due to upward pushing of thermocline by the upwelling causes the mixed layer thinning. E-P values along the coastal region indicate high freshwater influx during summer than the northeast monsoon. However, the SSS pattern showed relatively high values in summer monsoon than in the winter. Hence, in winter SSS must be driven by the advection of low saline waters from the equatorial and BOB region. More over, the Ekman transport during southwest monsoon pushes the low saline waters near the coast towards offshore and is replaced by the relatively high saline subsurface waters. While during northeast monsoon, a branch of westward flowing north equatorial current, carrying low saline waters from the BOB through EICC turns north and flows along the west coast of India (Wyrski, 1973; Darbyshire, 1967; Shetye *et al.*, 1991a; Shankar, 2000). During northeast monsoon, relatively strong winds and high rate of evaporation demands fairly deep MLD in the coastal region. But the low saline waters from the Bay of Bengal provide strong stratification in the upper layer and thereby shallowing the MLD in the coastal region and form the barrier layer with significant thickness. Recent studies (Rao

and Sivakumar, 2003; Shenoi *et al.*, 2004) documented the barrier layer distribution along the southwest coast of India. The formation and decaying of barrier layer in the coastal regime is in well accordance with the observations of Shenoi *et al.* (2004). In the open ocean regime, the strong northeast monsoonal winds, reduced solar insolation and high evaporation contribute the secondary maxima of MLD during northeast monsoon.

It can be seen that, in the open ocean regime, atmospheric forcing such as wind speed and surface heat flux contributes to the MLD variability. In the coastal regime, processes such as coastal upwelling and the transport of low saline waters from the BOB, controls the mixed layer.

3.1.2. 10 -12°N (Fig. 3.2)

3.1.2.1. Results

The march of SST resembled that seen in the previous grid, but the coastal and open ocean variability was relatively less in this grid. Variability was its maximum in southwest monsoon and minimum in spring intermonsoon, as seen in the previous grid. In the open ocean, SST decreased from 27°C in January to 26.8°C in February, increased abruptly to 31°C in May and then decreased to 28.5°C, in August-September. From September, SST increased and reached a secondary maximum of 29°C in November, there after it decreased. The corresponding peak values for the coastal region are 29.4°C in May and 27.5 °C in November and low values are 26.8°C in February and 26.5°C in August.

The open ocean SSS showed a decreasing trend from 36.4 psu in January to 35.5 psu in April, and then increased gradually to 36.4 psu in June, thereafter it remained almost same for the rest of the year. In the coastal region, SSS always remained below 35 psu and the minima were observed in the period of January – April (~34.3 psu) and in August (33.8 psu).

Wind speed in the open ocean region showed a decreasing trend from 6.5m/s in January to 4m/s in May, then increased abruptly with the progress of the southwest monsoon and showed a peak value of 11m/s. From September, it

decreased again to 4m/s in October, there after it increased steadily. The coastal stations also followed the same pattern but difference in magnitude. In the coastal region, the wind speed was maximum in southwest monsoon (~6.5m/s). Coastal as well as open ocean values remained same during the intermonsoon seasons (spring & fall), and the maximum variability was observed during southwest monsoon periods.

SWR in the open ocean (coastal) region showed an increase from 176 w/m² (191 w/m²) in January to 250 w/m² (225 w/m²) in April (March) and then decreased to 190w/m² (162 w/m²) in July. The secondary peak value of 212 w/m² (184 w/m²) was observed in August (September) and then decreased gradually till December.

The net heat flux distribution showed that the coastal region received more heat than the open ocean region. The net heat flux also showed a bimodal pattern with two peaks, one in April and another in September and the two minima were in June and in December/January. The corresponding peak values for the open ocean (coastal) region are 125 w/m² (127 w/m²) and 99 w/m² (101 w/m²) and that for the two minima are 0.2 w/m² (38 w/m²) and -6 w/m² (45 w/m²), respectively.

In the open ocean region, E-P showed a net evaporation and displayed almost the same pattern as in the previous grid. E-P in the coastal region showed an initial increase from 68 mm/month in January to 75 mm/month in February and then decreased gradually to -45 mm/month till May, followed by an abrupt decrease to -300 mm/month in June/July. From July onwards, it showed an increasing trend till December. In general, E-P along the coastal region always showed a net precipitation from June to November.

The open ocean region showed a bimodal distribution of MLD with maxima during southwest and northeast monsoon. MLD in the open ocean region showed a decreasing trend from 75m in January to 18m in April – May, then increased rapidly to 95m in August. From August, the MLD decreased steadily and reached secondary minima of 40m in November, there after it increased with

the progress of the winter monsoon. But in the coastal regime, MLD was fairly shallow in all the seasons and showed weak temporal variation and ranged from 10m – 40m.

Barrier layer thickness distribution did not show any significant feature in the open ocean region and ranged from 0 – 20m. During January, the barrier layer along the coastal region showed 30m thickness, remained same till March and then decreased to 5m in June and remains unchanged till November. Subsequently, the barrier layer showed considerable thickness and the maximum thickness of 70m was observed in December.

3.1.2.2. Discussion

As observed in the previous grid, the increase in wind speed, decrease in solar radiation as well as surface heat flux under monsoonal clouds increases the turbulence and results in to a deep MLD in the open ocean regime during summer monsoon. In addition, the peculiarity of the wind pattern in the AS (negative windstress curl) makes the large-scale convergence and Ekman pumping in the central AS which deepens the mixed layer. Similarly, during northeast monsoon, the reduced solar radiation and relatively high rate of evaporation and the secondary wind maxima sustained the deep MLD in January. The observed shoaling of MLD during January to May and October to November appears to be driven by decreasing wind speed and increasing surface heat flux. In the coastal regime, during southwest monsoon, the upwelling process produced a strong stratification, which is sufficient to erode the vertical turbulence caused by the strong monsoonal winds, causing the MLD to thin. During the northeast monsoon, low saline waters from the BOB produces strong stratification at the surface layers, which is able to overwhelm the turbulence due to the wind stirring and surface cooling over the coastal region and consequently forms a barrier layer of significant thickness (>25m). The SST variation was observed to be in phase with the incoming solar radiation with warmer SST during increased incoming solar radiation and colder SST during reduced insolation. The observed maximum

difference of SST between the coastal and open ocean during southwest monsoon season, were associated with the strong upwelling process. Very high rate of precipitation (~300 mm/month) during southwest monsoon demands distinct low saline waters in the coastal region, but the upwelled water sustained moderate saline waters (~33.8 psu).

3.1.3. 12-14°N (Fig. 3.3)

3.1.3.1. Results

Compared to the previous two grids, the variability between the coastal and open ocean appeared to be very less (<0.5°C). SST was 27.2°C in January and remained same in February and showed a steady increase up to 29.5°C in May. From June onwards, SST decreased and reached a secondary low of 27°C in August, there after SST increased to 28.2 in October and then showed a decreasing phase during the northeast monsoon. The distribution of SST in the coastal regime resembled exactly that of the open ocean region. From January to May, the SST in the coastal region showed slightly higher values than that in the open ocean region, for the rest of the year, open ocean values remained high.

SSS along the open ocean region was 36.7 psu in February and decreased to 34.5 psu in March, then increased steadily to 36.5 psu in July and remained same till January. Whereas in the coastal region, SSS was 35.2 psu in January and remained constant till May and showed a sudden decrease to 33.5 psu in September and then increased rapidly to 35.5 psu in October and remained 35.2 psu till December.

Wind speed distribution in the coastal and open ocean regimes showed a bimodal pattern, as seen in the previous grids. In the open ocean, wind speed decreased from 6.0 m/s in January to 4.1m/s in April and remained same in May, then increased rapidly and peaking to 12m/s in August. From August, it showed a steady decrease to 4.5m/s in October, there after it increased gently in northeast monsoon. Similar wind pattern is observed in the coastal region with peak value

of 8.5m/s in July. During the intermonsoon periods (spring & fall), the coastal and open ocean showed less variability.

Incoming solar radiation along the open ocean (coastal) region showed an increasing trend from 178 w/m² (190 w/m²) to 257 w/m² (242 w/m²), from January to April (March) and then showed a decreasing phase to 183 w/m² (161 w/m²) in July. From July to September, it increased to 202 (180 w/m²) and again decreased till December.

The net heat flux at the surface along the open ocean (coastal) region showed an increasing phase from -11 w/m² (49 w/m²) in January to 141 w/m² (135 w/m²) in April and then decreased to -4 w/m² (45 w/m²) in June. From June to September, it showed an increasing trend to 91 w/m² (97 w/m²) and thereafter it decreased.

E-P showed a net evaporation in all the seasons in the open ocean region, whereas in the coastal region, a net precipitation was observed during June to October. E-P in the open ocean showed a value of 150 mm/month in January, which decreased to -8mm/month in June and then increased to 50 mm/month in July/August and remained constant in October and then increased gradually till December. Similarly, in the coastal region, E-P showed a decreasing trend from February (105 mm/month) to June (-302 mm/month) and then increased and remained negative till October and increased further till December.

In the open ocean region, the MLD shallowed abruptly from 80m in January to 20m in March, continued to shallow till June and then increased steadily to 110m in August. From August, it showed a sudden decrease to 50m in November and thereafter it deepened steadily. But relatively shallow MLDs were observed in the coastal region. MLD in the coastal region showed an increase from 25m in January to 45m in February, and then it decreased to 25m during March – June, and thereafter it shallowed (~15m) till November and then showed the deepest MLD in December (60m).

In the open ocean region, the formation of barrier layer is limited to a few meters (<20m) throughout the year except in March (30m). From January to March the layer thickness showed relatively high values (>40m) in the coastal region and for the rest of the year, barrier layer showed insignificant layer thickness (<10m).

3.1.3.2. Discussion

As seen in the previous grids, during southwest monsoon, the strong monsoonal winds, reduced solar insolation and high rate of heat loss due to evaporation triggers deeper MLD (deeper than that seen in the previous grids) in the open ocean region, while in the coastal region, strong upwelling and relatively low saline waters resulted in a thin MLD. The observed shoaling of MLD from February to May and October to November appears to be driven by decreasing wind speed and increasing surface heat flux. The coupling of wind speed, reduced solar radiation and net heat flux resulted in the secondary maxima in MLD during northeast monsoon. Sudden change in MLD with in a month from February-March is associated with the rapid response of open ocean waters to the atmospheric forcings as compared to the coastal region. The reduction in SSS during September in the coastal region must be contributed by the monsoonal rainfall and associated river discharge. The low saline waters from the BOB in the coastal region caused the formation of barrier layer during January to March. As in the previous grids, MLD in the open waters are directly driven by atmospheric forcings, whereas in coastal areas, apart from the atmospheric conditions, upwelling and low saline waters contribute to the MLD variability.

3.1.4. 14-16°N (Fig. 3.4)

3.1.4.1. Results

The SST in the coastal and open ocean displayed bimodal distribution and displayed a similar march, with minimum spatial variability. The two warming phases observed are from February to May and August to October in both regions. Compared to the open ocean, the coastal region was having warmer sea surface

during January to April, and for the rest of the season it was slightly cooler. SST in the open ocean ranged from 25.8°C to 30°C and in the coastal region, from 26.2°C to 29.0°C.

Throughout the year, the SSS were observed to be almost constant (~36.5 psu) in the open ocean region. However, in the coastal region, SSS showed a gradual increase from 35.4 psu in January to 35.8 psu in June, then decreased to 34.5 psu in July and again increased to 35.9 psu in August. From August onwards SSS decreased further to 34.4 psu in November and increased thereafter.

The variability of the wind speed also resembled that seen in the previous grid. The coastal – open ocean variability in the wind field was minimum during intermonsoon period (spring and fall) and maximum in southwest monsoon. Wind speed peaks up to 12m/s in August in the open ocean, while along the coastal region wind speed showed a maximum of 9m/s in July. Relatively weak winds (~4m/s) were observed off the coastal and open ocean regions during intermonsoon seasons.

Incoming solar radiation showed two peaks of heating, one in April and another in October. In the open ocean (coastal) region, SWR showed an increase from 163 w/m² (188w/m²) in January to 264 w/m² (247 w/m²) in April and then decreased to 174 w/m² (165 w/m²), in July. From July onwards it increased and reached the secondary peak of 201 w/m² (180 w/m²) in October and decreased thereafter.

Net surface heat flux in the coastal as well as open ocean region showed two warming and two cooling phases. The open ocean (coastal) region showed a sharp increase from -19w/m² (18 w/m²) in January to 155 w/m² (138 w/m²) in April and then decrease to 12 w/m² (50 w/m²) in June. From June onwards, net heat flux increases drastically till October when it reached a value of 87 w/m² (109 w/m²) followed by a decrease.

In the open ocean region, E-P showed a decreasing trend from January (122 mm/month) to June (11mm/month) and then an increasing trend till December

(149 mm/month). Coastal region also showed similar decreasing trend from January (97 mm/month) to July (-260 mm/month) and then a gradual increase till December (102 mm/month). In general, the open ocean region showed a net evaporative regime except in June. Net precipitation over evaporation was observed during June to October in the coastal region, whereas during the rest of the year the coastal region showed net evaporation.

The MLD also showed bimodal pattern in the open ocean region. In the open ocean region, during January the MLD was around 80m, which increased to 90m in February, and then decreased rapidly to 25m in April, and thereafter remained shallow till June. From June onwards the MLD increased, reached the deeper value of 80m in August, then shoaled to 20m in September and increased thereafter. In the coastal region, MLD was 55m in January, and increased to 60m in February, there after it decreased to 25m in April and then increased further to 40m in August. From August, it shallowed to 25m in September and increased slightly during October-November followed by a sudden increase of 60m in December.

Barrier layer distribution in this grid showed negligible thickness (<20m) in the open ocean region. However, in the coastal region, the barrier layer has significant thickness during November – February (~30m). During the rest of the year, the barrier layer remained thin.

3.1.4.2. Discussion

The initial decrease of MLD, in the open ocean, from February to May was associated with the decrease in wind speed and high solar insolation in this period. The shallow MLD in June cannot be attributed to the wind speed and surface heat flux, as both demand a deeper MLD. The observed deepening of MLD during the southwest monsoon period (July – August) was associated with the typical southwest monsoonal conditions (high winds, increased rate of evaporation, reduced solar insolation). The shoaling of MLD from August to November can be related to the weak winds (~4 m/s) and increased surface heat flux. The

deepening of MLD during northeast monsoon can be associated with the relatively high wind speed (~6m/s) and latent heat flux, both contribute strong turbulence at the sea surface and is sufficient to erode the upward buoyancy heat flux. The high salinity of the surface waters in the open ocean can be attributed to the net evaporation. However, in the coastal region, MLD distribution did not show any direct influence of atmospheric forcings, except in the northeast monsoon. During winter, the observed deeper MLD can be related to the downwelling of surface waters (Shetye *et al.*, 1991). Though the barrier layer was shallower than the previous grids, significant thickness (~30m) during November – February indicates the presence of low saline waters near the coast, in this grid.

3.1.5. 16-18°N (Fig. 3.5)

3.1.5.1. Results

SST showed a bimodal distribution as in the previous grids. The coastal and open ocean regions showed two peaks, one in May and the other in October. SST in the open ocean (coastal) region showed a gentle rise from 25.6°C (25.8°C) in January to 29.5°C (28.8°C) in May and then decreased to 27°C (26.5°C) in August. From August to October, SST rose to 28.2°C (27°C) and then decreased till December.

SSS in the open ocean region showed weak temporal variation, ranging from 36.3 to 36.6 psu. From January to August, SSS in the coastal region remained in a narrow range (35.8–36.2 psu). During September, SSS was 36.7 psu and then decreased to 34.8 psu in October, followed by an increase till December.

Compared to the previous grids, wind speed in the coastal and open ocean regime showed less spatial variability. In the open ocean, wind speed decreased from 5.5 m/s in January to 3.5 m/s in March, then it increased suddenly to a value of 12 m/s in June and remained high (>10m/s) till August. From August, it showed a rapid decrease till October (4.5 m/s) and increased thereafter. The coastal region also showed a bimodal pattern with a decreasing phase from

January (5m/s) to May (4.5m/s), and increasing phase till July (8.5m/s). The secondary minima was observed in October (4m/s), followed by an increasing phase thereafter.

Incoming solar radiation showed two peaks of heating, as in the previous grids. The differences in SWR between the coastal and open ocean were observed to be very small. In the open ocean (coastal) region SWR increased from 171 w/m^2 (166 w/m^2) in January to 233 w/m^2 (232 w/m^2) in April and then decreased to 165 w/m^2 (168 w/m^2) in August. From August to October, it increased to 204 w/m^2 (188 w/m^2) and thereafter it decreased.

Net surface heat flux in the open ocean (coastal) region showed an increasing trend from -29 w/m^2 (1 w/m^2) in January to 160 w/m^2 (154 w/m^2) in March and then decreased to 31 w/m^2 (52 w/m^2) in July. From July to October, it increased to 93 w/m^2 (98 w/m^2) followed by a decrease till December.

E-P in the open ocean was 153 mm/month in January and decreased gradually (with a small rise in May) till August (38 mm/month), followed by a steady increase till December. Similarly, in the coastal region, E-P showed a decreasing trend from 168 mm/month in February to -158 mm/month in June and remained negative till September (-35 mm/month) and the increasing trend continued for the rest of the year.

MLD in the open ocean region was around 80 m in January, which increased to 105 m in February and then showed a sudden decrease in April (10 m) after that it gradually increased to 65 m in August. From August to October, the mixed layer shoaled to 25 m and then deepened during northeast monsoon. Unlike the previous grids, the coastal region also followed the same pattern of variability as the open ocean region. MLD in the coastal region increased from 58 m in January to 65 m in February then decreased to a depth of 20 m in May and thereafter it increased to 40 m in July. From July onwards MLD distribution showed a gradual decrease to 15 m in November followed by a rapid increase in December (70 m).

Very thin barrier layer (<20m) was formed in the coastal as well as in open ocean region.

3.1.5.2. Discussion

MLD during the southwest monsoon appeared to be shallower than the previous grids, while the MLD during winter was relatively deeper than that of the previous grids. The deeper MLDs encountered during northeast monsoon could be linked to moderate wind speed and reduced solar insolation as well as net heat flux. Sudden shoaling (about 100m) of MLD from February to May in the open ocean could be due to its quick response to the atmospheric forcing (wind speed, SWR and net heat flux). Even though the atmospheric conditions during February – May are almost same in both regions, the open ocean responded quickly. Shallow MLD appeared in the spring intermonsoon in the coastal as well as open ocean region, which could be related to low winds and high solar insolation. Unlike the previous grids, the MLDs in the coastal region showed fairly good relation to the atmospheric forcings and the MLD showed two peaks, one in southwest monsoon and another in northeast monsoon. During winter, advection of low saline BOB waters was not evident in the coastal region.

3.1.6. 18 -20°N (Fig. 3.6)

3.1.6.1. Results

In the open ocean regime, SST was 25°C in January and remained same till February and then rose up to 29.5°C in May. From May, it decreased to 27.4°C in August, thereafter it increased till October (28.4°C) and showed a decreasing trend subsequently. The coastal region also showed a similar trend. From January to April and in August, the SST was the same as the open ocean values. For the rest of the seasons, SST in the coastal region showed slightly lower values than that in the open ocean.

SSS pattern did not show any strong seasonality in both regions, as compared to the previous grids. SSS in the open ocean region varied in a narrow

range from 36.2 – 36.7 psu, while in the coastal region, SSS ranged from 35.8 – 36.5 psu.

Wind speed distribution in the coastal as well as open ocean region showed the same trend and nearly same magnitudes. In January, in the open ocean region, wind speed was 5.2m/s, which decreased to 4m/s in March and remained same till April, then showed a sudden increase up to 10m/s in June. From July to October, wind speed decreased to 4.2m/s and then increased till January. The coastal region also followed the same pattern with little variation in magnitude.

SWR distribution in the coastal and open ocean regions showed the same pattern with almost same values. From January to April, it showed an increase from 172 w/m² to 262 w/m² and then decreased to 164 w/m² in August. From August to October, SWR again increased to 195 w/m², followed by a decreasing trend till December.

Net surface heat flux in this grid showed little spatial variation. It showed two peaks of heating, one in April and another in September. The net heat flux in the open ocean (coastal) region was around -39 w/m² (-31 w/m²) in January and it increased steadily to 161 w/m² (158 w/m²) in April and then showed a decrease of up to -51 w/m² (10 w/m²) in December.

High values of E-P were observed in the open ocean region, indicating net high evaporation, and the values ranged from 50 – 150 mm/month. In the coastal region, E-P showed a decreasing trend from 113 mm/month in January to -167 mm/month in August. From August onwards, it gradually increased and attained a value of 94 mm/month in December. In general, E-P in the coastal region showed higher precipitation than evaporation during June to September. Rest of the year, it showed a net evaporative regime.

MLD in the open ocean region showed an increase in depth from 70m in January to 90m in February and then it shoaled suddenly to 20m in May. Thereafter it increased up to 60m in July and remained same in August, then shallowed to 35m in October and subsequently showed a gradual increase. In the

coastal region, MLD showed an increase from 55m (January) to 65m (March) and shoaled there after to 40m (May), then it increased gradually to 50m in July. From July onwards, the MLD shoaled steadily to 20m in October followed by an increasing phase.

Barrier layer distribution showed very low values in the coastal and open ocean regions, which indicate that both isothermal and isopycnal layers are concurrent in this grid.

3.1.6.2. Discussion

The observed deepening of MLD from November to February in the open ocean region was due to the winter cooling process over the region. The SST pattern and MLD suggest that winter cooling peaks up in February. It can be clearly seen that the open ocean region responded quickly to the atmospheric conditions, resulting in a decrease in the MLD abruptly from February to March. However, during March the coastal region is still under the grip of winter cooling process. When the wind speed was high during June and July, the mixed layer was relatively deeper in both coastal and open ocean regions. But the MLDs in the open ocean region were relatively smaller than the previous grids. The probable reason is that, during southwest monsoon, the region northeast of the Findlater Jet was driven by cyclonic wind stress curl (Hastenrath and Lamb, 1979; Halpern and Woiceshyn, 1999) and consequently an upward Ekman pumping, shallows the MLD (Luther, 1987; Bauer *et al.*, 1991; Brock *et al.*, 1991; Brock and McClain, 1992; McCreary *et al.*, 1996). It can be seen that this open ocean grid is roughly north of the mean axis of the Findlater jet (Fig. 1.2). The MLDs in the coastal region are relatively higher than that seen in the previous grids. The warm sea surface and weak wind during October triggers shallow MLD in both coastal and open ocean regimes. Even though the atmospheric conditions such as SST, wind speed, surface heat flux and the SSS are nearly same in both coastal and open ocean regimes during northeast monsoon, MLD showed significant

variation between the two regimes. This suggests the differential response of surface layer of coastal and open ocean to the atmospheric forces.

3.1.7. 20-22°N (Fig. 3.7)

3.1.7.1. Results

The SST, wind speed and SWR showed distribution patterns which were very similar to that of previous grid. SSS along the open ocean region showed a weak temporal variation and ranged from 36.4 to 36.8 psu. In the coastal region, SSS showed a decrease from 36.5 psu in January to 35.7 psu in February and thereafter it increased gradually to 36.4 psu in December except in July, when it showed a minimum of 35.1 psu.

Net heat flux distribution showed very similar pattern as well as values in both the open ocean and coastal regions. In January, it showed a value of -52 w/m^2 in the open ocean and -80 w/m^2 in the coastal region, then it increased to 160 w/m^2 in May and decreased to 60 w/m^2 in July and again showed an increasing trend till October (94 w/m^2) followed by a steady decrease till December.

E-P also showed similar distribution pattern of the previous grid. MLD in the open ocean showed a decrease from 108m in January to 86m in February followed by an abrupt decrease of 30m in March and then increased gradually to 58m in August. From August to September, MLD showed a decrease of 35m and then increased till December (55m). In the coastal region, MLD was observed to be 60m in January and deepened to 125m in February. Then onwards it decreased steadily up to a depth of 15m in May followed by an increase of 45m in June. From June onwards MLD goes on decreasing to 25m in August and remained almost the same till October and then increased further till December.

Barrier layer in the coastal as well as open ocean was observed to be negligible throughout the year, except in the coastal region during January, where the barrier layer thickness was 45m.

3.1.7.2. Discussion

The open ocean region showed the deepest mixed layer in January, whereas the deepest mixed layer in the coastal region was observed in February. This was a clear indication of the differential response of both regions to the prevailing atmospheric conditions. Even though both regions experience almost similar atmospheric conditions, the coastal regions showed one-month lag in response. Moreover, the MLD in the open ocean showed abrupt change from February to March whereas that for the coastal region was gradual. This also could be linked as the open ocean responded faster than the coastal region. The increased wind speed during the southwest monsoon did not result in any noticeable increase in the MLD. This can be linked to the effect of Findlater jet as was seen in the previous grid. It can also be seen that the net evaporation in the open ocean regime sustained high surface salinity.

3.2. Bay of Bengal

3.2.1. 8-10°N (Fig. 3.8)

3.2.1.1. Results

SST pattern showed minimum coastal – open ocean variability in April – May and the variability increased steadily till December. SST in the open ocean decreased from 27.8°C in January to 29.8°C in April and remained same till May and decreased to 28.5 in July - August and remained more or less same till November and decreased thereafter. In the coastal region, SST showed an initial increase of 2.4°C in April from its January value of 25.8°C and remained same till May. From May till December, SST decreased gradually except for almost constant values in September and October.

SSS in the open ocean was 33.3 psu in January, which remained constant till February and decreased to 32.5 psu in May. From May onwards, SSS increased till September when it reached a value of 33.8 psu and thereafter decreased to 32.2 psu in November, followed by a sudden increase of 34.0 psu in December. The coastal region always showed higher values than the open ocean values. In the coastal region, SSS showed a series of ups and downs and ranged

from 32.6 – 35 psu and relatively high values were observed during southwest monsoon and lower values in northeast monsoon.

During January, wind speed was 6m/s in the open ocean, which decreased to 3m/s in April and then increased steadily to 9m/s in June and remained high till August. From August to October, it decreased to 4.5m/s and then increased gradually till January. The coastal region also followed the same magnitudes of wind speed from October to May. Thereafter it increased to 7m/s in June and remained same till August and then decreased till October.

SWR along the open ocean (coastal) region showed an increasing trend from 166 w/m² (175w/m²) to 215 w/m² (221 w/m²) from January to March and then decreased to 161 (174) w/m² in June. It again increased gradually to 174 w/m² (193) in August and then showed a decrease of 150 (158) w/m² in December. In general, the coastal region received more incoming solar radiation than the open ocean region.

The net heat flux distribution showed high spatial variation during the period from April to October, for rest of the year the coastal and open ocean showed more or less same values in the respective months. The net heat flux in the open ocean (coastal) region showed a sudden increase from 16(-5) w/m² in January to 127(128) w/m² in April and then decreased to 3 (56) w/m² in June. From June to October (August), it again increased to 77 (112) w/m² and then decreased to 8(-4) w/m², in December.

E-P in the open ocean showed a value of 108 mm/month in January, decreased thereafter and showed positive values till March indicating excess evaporation over precipitation. From March onwards, it passed through a cycle of highs and lows and showed negative values till November indicating net precipitation. While in the coastal region, E-P showed positive values from January to September and negative values in the remaining months. In this grid, coastal region seemed to display a more evaporative regime than the open ocean region.

MLD in the open ocean showed a decreasing trend from 40m in January to 20m in February, remained shallow (<30m) till April, then increased to 40m in July, more or less same values till November and thereafter increased to 60m in December. In the coastal region, deepest MLD of 55m was observed in March, which decreased steadily to 15m in May and increased to 50m in June. During the rest of the year, MLD was observed to be shallow (<30m).

During January, the barrier layer showed a thickness of 26m in the open ocean region and it deepened to 50m in February and remained shallow (<20m) to about December. Whereas in the coastal region, the barrier layer was found to be significant during December-February and thereafter the barrier layer thinned.

3.2.1.2. Discussion

The observed shoaling of MLD from January to April is driven by the weak winds. Even though the winds along the western BOB are comparable to the Arabian Sea, it could not develop deeper MLD during southwest monsoon as that seen in the AS. The probable reason is that the relatively warm sea surface and low salinity (<33.4psu) in the open ocean produces a strong upward buoyancy flux, which opposes the wind driven turbulence. The deeper MLD in December is driven by the comparatively strong wind speed and reduced solar insolation and net heat flux. The relatively low saline waters and thick barrier layer in the coastal region during winter can be linked to the equatorward EICC, which carries low saline waters from the head Bay. Rest of the region, the net evaporation along the coastal region appeared to maintain high SSS.

3.2.2. 10-12°N (Fig. 3.9)

3.2.2.1. Results

In the open ocean region, SST increased from 27.5°C in January to 29.8°C in May, and then it decreased sharply to 28.5°C in July thereafter it decreased gradually till January. Where as in the coastal region, SST showed an increase of 3.0°C by May from 25.8°C in January, and then decreased to 27°C in August and

thereafter it showed more or less same values till October. Subsequently, the SST showed a steady decrease till January.

SSS in the open ocean regime showed a steady decrease from 34.2 psu in January to 32.8 psu in May, and then it increased gradually to 33.1 psu in September. From October onwards, SSS again decreased to 32.5 psu in November and then increased in December. SSS in the coastal region showed an increase from 32.6 psu in January to 34.3 psu in May. From May till October, SSS oscillated through a cycle of highs and lows in a range of 33.5 – 34.6 psu. In November, the coastal region showed its minimum value of 30.5 psu and remained low till December (~32 psu). From March to September, the coastal region showed relatively high surface salinity than the open ocean.

The pattern of wind speed variability resembled that seen in the previous grid. The coastal and open ocean showed fairly same values in the respective months from October – May. Wind speed showed a decrease from 6m/s in January to 3m/s in April, which then increased to 9m/s in June in the open ocean region and remained the same till August. Thereafter, it decreased to 4.5m/s in October followed by an increase till January. The peak value of wind speed in the coastal region was 7m/s in June and it decreased slightly in July and August, and suddenly decreased to 4.6m/s in October, there after it followed the trend seen in the open ocean.

The pattern of SWR variability also resembled that seen in the previous grid. SWR in the open ocean (coastal) region was 167(159) w/m^2 in January, then showed an increasing trend till March to a value of 228(220) w/m^2 and remained almost same in May. From May onwards, SWR showed a decreasing trend till June (July) and reached a value of 160(174) w/m^2 . Thereafter, it increased to 173(189) w/m^2 in August, followed by a decrease till December.

Net heat flux in the open ocean (coastal) region showed an increase from 19 (-1) w/m^2 to 141 (142) w/m^2 , from January to April, and then decreased to 8 (24)

w/m^2 in June. From June onwards, it again increased till September to a value of 83(105) w/m^2 and decreased thereafter.

Both the coastal and open ocean regions showed the highest value of E-P in January, followed by a decreasing trend. In the open ocean, E-P showed negative values in March – November, indicating the dominance of precipitation over evaporation. Similarly, in the coastal region, the net precipitation was observed during October – December. During the rest of the year, the region appeared to be a net evaporative one.

In the open ocean regime, MLD was 40m in January and then decreased gradually and varied in a narrow range of 25-30m till June. From June onwards, MLD increased till September when it showed a value of 55m and again decreased to 10m in November, followed by an increase to 55m in December. In the coastal region, MLD decreased from 40m in February to 15m in April, which then increased to 45m in July and then showed a drastic decrease in August (15m) and remained shallow till November.

In the open ocean region, the barrier layer showed significant thickness (>20m) during January - February as well as in August. During the rest of the year, the thickness appeared to be very shallow. In the coastal region, the barrier layer always showed shallow thickness (<20m) and the thickness showed an increasing trend from September to January.

3.2.2.2. Discussion

The general shoaling trend of MLD in the open ocean during January to March appears to be driven by the decreasing wind speed and salinity. During June, both wind speed and relatively low values of net heat flux warrants deeper mixed layer, but the low saline waters and warm sea surface overwhelms the deepening process of MLD. The increased wind speed in July-October leads to a relatively deeper MLD during that time. Observed shoaling of MLD in November is due to the low saline waters and light wind conditions. Deeper MLD in December is driven by the relatively strong wind speed and reduced solar

insolation and net heat flux. Deeper MLD during July in the coastal area could be linked to the strong winds. The shoaling of MLD in October- November is related to the very low saline waters in the region mainly due to the rainfall and advection of low saline waters from the head Bay through EICC. For the rest of the year, MLD did not show any direct influence with atmospheric conditions. Observed surface salinity difference between the coastal and open ocean appeared to be induced by the E- P pattern in the respective regions.

3.2.3. 12-14°N (Fig. 3.10)

3.2.3.1. Results

SST showed a bimodal pattern in the coastal and open ocean regions. The initial warming phase was observed from February to May and the respective SSTs in the open ocean are 27°C and 29.5°C and that in the coastal region are 26°C and 29°C. SST decreased gradually till September and reached a value of 28°C in the open ocean and 27°C in the coastal region. The SST thereafter increased till October (open ocean - 28.5°C and coastal region - 27°C), followed by a gentle decrease till January.

SSS in the open ocean showed a value of 33.2 psu in January as well as February and then decreased to 31.1 psu in March. From March till September, it increased gradually to 33.1 and then decreased to 32.0 psu in December. In the coastal region, the SSS also showed a gradual increase from 33.0 psu in January/February to 34.1 psu in May and then oscillated in a narrow range of 33.3-34.0 psu till September, thereafter it showed a drastic decrease to a minimum of 29.5 psu in November.

In the open ocean, the wind speed showed a steady decrease of 5.5 m/s in January to 3m/s in April, which then increased to 8.5m/s in June and remained high till August. From August, it again decreased to 4m/s in October and increased thereafter. The coastal region also followed the same pattern. Wind speed decreased from January to March (4m/s), then it increased rapidly and showed a peak value of 7m/s in June and remained almost same till August.

August onwards the wind speed decreased to 4.5m/s in October and increased thereafter.

SWR showed weak spatial variation during October – April. Both coastal and open ocean regions showed more or less same values in the respective months. SWR showed an increasing phase from 168w/m² in January to 234 w/m² in April. From April to June (July) SWR decreased 160(177) w/m² in the open (coastal) regime, then increased to 172(190) w/m² in September, followed by a decrease till December.

Net heat flux along the open ocean (coastal) region showed an increasing pattern from 24 (4) w/m² in January to 150 (156) w/m² in March (May) and then showed a steady decrease up to 20(64) w/m² in June. From June to September, it again increased to 93(103) w/m² and then showed a decrease upto December, reaching a value of 2(-23) w/m².

E-P in the open ocean was 161 mm/month in January and then decreased gradually to -170 mm/month in September, followed by an increase up to 106 mm/month in December. From May to November, E-P showed negative values indicating high precipitation. In the coastal region, E-P showed an initial increase from 68 mm/month in January to 120 mm/month in April, thereafter it decreased to -144 mm/month in November and in December it showed a high value of 54 mm/month. Negative values of E-P, from August-November, indicate the dominance of precipitation over the evaporation.

MLD in the open ocean showed a steady decrease from 45m in January to 5m in May and remained shallow (<10m) till June. During July, it showed a maximum of 55m and increased little in August, and thereafter it shallowed to 40m in October and then increased till January. Whereas in the coastal region, MLD increased from 20m in January to 60m in February, then decreased in March to 20m and increased further to 30m in May and remained more or less same till June. During July, the coastal region showed a MLD of 55m and then decreased till December (15m).

Relatively thicker barrier layer (>25m) was formed in the open ocean during December to March and with a maximum in February. For the rest of the year, the thickness oscillated in a narrow range 12-17m. Similarly, the coastal region showed thicker barrier layer (>20m) in December and January, and thereafter the thickness was observed to be very shallow (<20m).

3.2.3.2. Discussion

The low saline waters (<33.5 psu) present in the region throughout the year, triggers strong stratification in the surface, which sustained fairly shallow MLD. However, the relatively deeper MLDs in July to September, in the open ocean and in July in the coastal regions appeared to be driven by the strong wind. Relatively deeper MLD (>40m) in the open ocean in the northeast monsoon is triggered by the fairly high wind speed and low net heat flux. But in the coastal region, during northeast monsoon, the TKE resulting from high wind speed and reduced net heat flux is not sufficient to erode stratification produced by the low saline waters (<30 psu). The weak winds and low saline waters (<32 psu) and high surface heat flux in the open ocean region during May - June produces a strongly stratified surface layer and causes the mixed layer to thin. The observed deeper MLD (60m) in February, in the coastal region could not be explained by the prevailing atmospheric conditions.

3.2.4. 14-16°N (Fig. 3.11)

3.2.4.1. Results

In the open ocean region, SST increased from 25.8°C in January to 29.5°C in May, and decreased to 28.1°C in July and remained more or less same till September, and thereafter it showed a slight increase to 28.2°C in November, followed by a sharp decrease in December (27°C). Whereas in the coastal region, SST showed an increase of 4.0°C in May from 25.2°C in January, and then decreased rapidly to 26.8°C in August, and thereafter increased to 27.3°C in October, and steadily decreased till December.

SSS in the open ocean region showed a value of 32 psu in January and remained almost same till April and then increased to 33.3 psu in July. During August the open region showed the lowest value (29.6 psu), afterwards it increased gradually till December. In the coastal region, SSS remained higher during January to October than the open ocean region and then decreased rapidly to 30 psu in December.

Wind speed in the open and coastal region showed a close resemblance in the distribution pattern and magnitude. Little variation was observed during March – May and in July –August, for the rest of the season, coastal and open ocean regions showed almost same values. In the open ocean, wind speed showed a steady decrease from January (5.2m/s) to 3 m/s in March, remained same till April, and then it increased rapidly to 8m/s in June and remained high till August. From August onwards, it decreased to 4m/s in October followed by an increase till January. Unlike in the open ocean, the wind speed in the coastal region showed minimum in March and maximum in June and the corresponding winds were 4m/s and 7m/s.

Variability of SWR showed a close resemblance to that in the previous grid and showed negligible spatial variation during October – April. An increase from 169w/m² in January to 235 w/m² in April was seen in the SWR distribution and a subsequent decrease till June to a value of 159w/m² in the open ocean and to 180 w/m² in the coastal region. From June to September, SWR increased gradually and reached a value of 173w/m² in the open ocean region and 188 w/m² in the coastal region and thereafter it decreased to 144w/m² in December.

Net heat flux in the open ocean showed a sudden increase from 33w/m² in January to 148 w/m² in March, then decreased to 120 w/m² in April and remained more or less steady till May and thereafter showed a sudden decrease till June (25 w/m²). From June onwards, the net heat flux showed a steady increase to 91 w/m² in September and decrease to 7 w/m² in December. The coastal region showed an initial rapid increase from 35 w/m² in January to March, further gradual increase

to 175 w/m^2 in May, followed by a sudden decrease in June (69 w/m^2). From June to October, the net heat flux increased to a value of 87 w/m^2 , followed by a rapid decrease of -24 w/m^2 in December.

In the open ocean, a steady decreasing trend of E-P was seen from January (154 mm/month) to June (-277 mm/month) followed by a gentle increase up to 127 mm/month in December. Negative values observed during May-November indicated net precipitation over evaporation. Similarly, in the coastal region, E-P showed an increasing trend from January (68 mm/month) to April (120 mm/month) and then decreased to -158 mm/month in October, followed by an increase to 73 mm/month in December. In the coastal region, net precipitation was observed during the period July to November.

In the open ocean, MLD decreased from 20 m in January to 10 m in March and then remained shallow ($<20 \text{ m}$) till May. During June, the open ocean showed the deepest MLD (55 m) of the year, and then decreased to 20 m in September and remained more or less same in October and thereafter showed the shallowest MLD (5 m) in December. In the coastal region, MLD showed a sudden increase from 10 m in January to 40 m in March, decreased to 15 m in April and then increased gradually to 35 m in July. From July onwards, it showed a weak temporal variation and ranged from $20\text{-}30 \text{ m}$.

Barrier layer in the open ocean showed a significant thickness ($>30 \text{ m}$) during the period December – March and August – September. Similarly, in the coastal region relatively thicker layer was formed during December – April. Rest of the year, barrier layer formation was insignificant ($<10 \text{ m}$).

3.2.4.2. Discussion

The low saline waters in the region dominated the mixed layer variability over the atmospheric forcings. The observed deeper MLDs in the coastal region during March appears to be driven by relatively high salinity (34 psu) and cool sea surface (26.3°C), where as in July, the strong wind (7 m/s) and high surface salinity (34.5 psu) drives a deeper MLD. In the open ocean regime, relatively low saline

waters (32.2 psu) and weak winds (3 m/s) in March sustain shallow MLD, whereas strong winds (8m/s) drive deeper MLD in June – July. The weak winds and high surface heat flux also produce shallow MLD in October, but the shallowest MLD in December, in both regions can be attributed to the formation of the barrier layer during northeast monsoon. In the coastal region, the equatorward flowing EICC (Cutler and Swallow, 1984; Shetye *et al.*, 1996; Shankar, 2000; Vinayachandran *et al.*, 1996) in northeast monsoon carries low saline waters from northwestern Bay and makes the region less saline, which eventually forms the barrier layer with significant thickness and causes the mixed layer thinning.

3.2.5. 16-18°N (Fig. 3.12)

3.2.5.1. Results

The SST showed minimum differences between the coastal and open ocean, and the variability increased during October - December. SST in the open ocean showed a steady value of 25.4°C in January and February, and then increased sharply to 29.3°C in May, and decreased suddenly to 27.8°C in August and remained almost same till October, followed by a rapid decrease till December (26.5°C). In the coastal region, SST from February to June followed more or less same values as the open ocean. It showed a relatively rapid decrease than that of the open ocean till December, when the observed SST is 25.2°C.

SSS in the open ocean region showed a value of 32.3 psu in January and remained almost same till April and then decreased suddenly to 28.6 psu in June. From June to December, the SSS oscillated in the range 30.1-33 psu. Whereas in the coastal region, SSS showed 32.5 psu in January and remained more or less same till February and then increased gradually to 34 psu in May. From May to July, SSS remained almost constant, thereafter it showed a decrease of ~11 psu in August- September (22.5 psu) and then increased gradually to 30.8 psu in December.

Wind speed in the open ocean showed a decrease of 5m/s in January to 3.5 m/s in March, and then increased to 8m/s in August thereafter it decreased to 5m/s in October, followed by a gradual increase till January. The coastal region also followed the same pattern with nearly same magnitudes. The difference in wind speed between coastal and open ocean region showed maximum (<1m/s) during April to June, for the rest of the year, it showed less variability (<0.4m/s).

The coastal and open ocean regions showed more or less same values of SWR during October – April. SWR showed an increasing trend from 170 w/m² in January to 234 w/m² in April. Thereafter the coastal and open ocean showed variation of SWR. SWR in the open ocean (coastal) region was 206(220) w/m² in May, then decreased to 166(182) w/m² in June and remained nearly same till September, after which SWR showed small spatial variation and decreased to 146 w/m² in December.

Net heat flux in the open ocean region showed rapid increase from 16w/m² to 128 w/m², from January to March and then showed a minor decrease in April and again increase to 112 w/m² in May. From May to June, net heat flux showed a decrease of 80 w/m² and thereafter it increased gradually till October and reached a value of 85 w/m², followed by a decrease till December. The coastal region also showed similar pattern of distribution. Net heat flux in the coastal region was 35 w/m² in January and increased steadily to 130 w/m² in March then remained more or less steady, followed by an abrupt increase in May (175 w/m²). A decrease of 106 w/m² was observed within a month period May-June, thereafter the net flux oscillated till October within the range of 70 - 120 w/m². From October till December, the net heat flux again showed a decrease from 90 w/m² to -50 w/m².

E-P in the open ocean showed two phases, an increasing phase and a decreasing phase. A steady decreasing trend of E-P was seen from January (140 mm/month) to June (-320 mm/month), followed by a gradual increase (except in August) up to 138 mm/month in December. During May-November, E-P showed negative values indicating the net precipitation over the evaporation. Similarly, in

the coastal region, E-P showed an increasing trend from January (98mm/month) to April (120 mm/month) and then decreased to -158 mm/month in October, followed by an increase to 73 mm/month in December. In the coastal region, net precipitation was observed during the period from July to November.

MLD in the open ocean showed a decreasing trend from 34m in January to 6m in April and then remained shallow till June (<10m). During July, the open ocean showed deeper MLD of 60m, thereafter it decreased to 10m in October followed by an increasing trend till December (55m). Throughout the year, in the coastal region, the MLD was observed to be shallow and it varied in a narrow range (10-25m).

From June to October and in January, the barrier layer in the open ocean showed considerable thickness (>25m) and for the rest of the year, thickness was found to be negligible. Similarly, in the coastal region, barrier layer showed significant thickness in the months of January to March and in September.

3.2.5.2. Discussion

The observed deep MLD in July, in the open ocean region appears to be driven by the strong winds and relatively small net heat flux (40w/m^2). Warm sea surface, weak winds and low saline waters in the open ocean region produce a thin MLD during spring and fall intermonsoon seasons. The observed shallow mixed layer during southwest monsoon (June–August) in the coastal region could not be explained by the atmospheric parameters. The strong winds, relatively high SSS and net evaporation in the coastal region warrants deeper MLD in southwest monsoon. Earlier studies suggest that in this grid, coastal upwelling is significant during the southwest monsoon (Murthy and Varadhachary, 1968; Rao *et al.*, 1986; Shetye, *et al.*, 1991; Rao, 2002). Moreover, during the season, frequent cyclonic eddies are observed in this grid and is a quasi-permanent feature along the western BOB in summer (Babu *et al.*, 1991). Both the processes shallows the mixed layer and this could be the reason for the observed thinning of MLD.

3.2.6. 18-20°N (Fig. 3.13)

3.2.6.1. Results

From December to May, both coastal and open ocean regimes showed more or less same SSTs, in the respective months. SST showed an increasing trend from 24.6°C in January to 29°C in May. Thereafter, in the open ocean region, it decreased to 28°C in August and remained constant till October and again decreased suddenly till January. In the coastal region, SST showed a decreasing trend to 27.5°C in August and remained almost constant till October and then decreased rapidly till January.

SSS in the open ocean oscillated in the narrow range of 30-32 psu with minimum in December and maximum in September. In the coastal region, SSS showed a decrease from 32.7 psu in January to 30.6 psu in February, and an increase to 33.1 psu in March and more or less constant till May and thereafter it decreased sharply to 23 psu in August, followed by an increase to 30.3 psu in December.

Wind speed in the open ocean showed a decrease of 1m/s from January to March (3.5 m/s), increase to 7.5m/s in July and continued till September, and decreased thereafter to 4.2m/s in October followed by a gradual increase till January. The Coastal region also followed the same pattern with more or less same values.

The seasonal march of SWR in the coastal and open ocean regions was similar. In general, SWR showed an increasing trend from 165 w/m² in January to 229 w/m² in April and then decreased to 185 w/m² in June. From June to December, it showed weak temporal variation and ranged 145 – 185 w/m².

Net heat flux in the open ocean showed a sudden increase from 9.7w/m² in January to 113 w/m² in March and then showed slight decrease till May, followed by a sudden decrease in June (51 w/m²). From June to October, it showed an increasing trend to 90 w/m² and then decreased rapidly to a value of 1 w/m² in November and remained constant till December. Similarly, the coastal region

showed an increasing trend from 34 w/m^2 to 113 w/m^2 during January to March and then decreased little in April, and again increased, peaking at 138 w/m^2 in May. During June, net flux showed a decrease of 88 w/m^2 from the peak value, then increased till August to a value of 103 w/m^2 and thereafter the net surface flux decreased rapidly to -44 w/m^2 in December.

In general, the coastal and open ocean regions followed similar pattern of seasonal march of E-P. The E-P in the open ocean showed two phases, an increasing phase and a decreasing phase, while the coastal region showed two increasing phases and one decreasing phase. In the open ocean, E-P showed a decreasing phase from January (143 mm/month) to June (-283 mm/month) followed by an increasing phase till December (39 mm/month). The coastal region showed a gradual increasing phase from 59 mm/month in January to 136 mm/month in April, then showed a steady decreasing phase till August (-182 mm/month) followed by a gradual increasing phase to 118 mm/month in December. Negative values of E-P during June – October in the coastal region and from May – October in the open ocean region indicated the dominance of precipitation over evaporation.

Through out the year, MLD in the open ocean region was observed to be shallow ($<25 \text{ m}$). Similarly, in the coastal region, the MLD was very shallow ($<20 \text{ m}$) in all seasons, except in January and April, when MLDs were 25 and 30 m respectively.

The coastal and open ocean regions showed relatively thicker ($>20 \text{ m}$) barrier layer during May – October. For the rest of the year, barrier layer was thin, indicating the coexistence of the surface isothermal and isopycnal layers.

3.2.6.2. Discussion

The observed shallow MLD could be linked to the low saline waters in the region. The low saline water in the region virtually provides the stratification at the surface, and is sufficient to oppose the turbulence produced by the atmospheric forcings.

3.3. Discussion

3.3.1. Arabian Sea

The coastal and open ocean regions showed a bimodal distribution pattern in respect of SST, solar radiation, net heat flux and wind speed. The spatial variability was maximum during southwest monsoon and the variability decreased towards north, during the same season. Along the central AS, the MLD distribution presented here showed considerable agreement with the previous MLD climatologies (Wyrki, 1971; Colborn, 1975; Rao *et al.*, 1991) with two peaks during - summer and winter, as well as shallow MLDs during spring and fall intermonsoon. During southwest monsoon, a notable feature seen along the central AS, north and south of 16°N was the diverse pattern of MLD. South of 16°N, the deepest mixed layer was observed during southwest monsoon (>100m) and the secondary peak of MLD was observed in the northeast monsoon (~80m) and the MLD increased towards north, in both the seasons. While north of 16°N, peak values of MLD observed during northeast monsoon (>100m) were deeper than that seen during southwest monsoon. Moreover, the mixed layer was seen to deepen towards north during northeast monsoon and decrease during southwest monsoon. The reason must be the differential response to the Findlater jet in southwest monsoon and the cooling processes in the northeast monsoon. It is a well-known fact that the north and east of the Jet's axis, the wind shear drives cyclonic curl (Hastenrath and Lamb, 1979; Halpern and Woiceshyn, 1999), leading to divergence, which shallows the mixed layer (Luther, 1987; Bauer *et al.*, 1991; Brock *et al.*, 1991; Brock and McClain, 1992; McCreary *et al.*, 1996). While in northeast monsoon, the cold continental air brought by the prevailing northeast trade winds intensifies the evaporation and leading the sea surface to cool. This combined with reduced incoming solar radiation and high ambient salinity drive convective overturning, resulting in the mixed layer deepening (Madhupratap *et al.*, 1996; Prasanna Kumar and Prasad, 1996; Jyothibabu *et al.*).

Both these processes are responsible for the observed difference in the climatology of the MLD between the north central AS and south central AS.

The processes responsible for the evolution of mixed layer, in the coastal and open ocean regions are entirely different. In the central AS, mixed layer is chiefly controlled by heating and cooling and also by wind stirring. While along the coastal regions, the vertical motions - upwelling and downwelling; and horizontal motions - advection of low saline waters from the BOB seemed to be more important. It is a well-known fact that the west coast of India is a region of intense upwelling during southwest monsoon (Banse, 1959, 1968; Johannessen, *et al.*, 1981; Shetye *et al.*, 1990; Muraleedharan *et al.*, 1995) and is a region of sinking during northeast monsoon (Darbyshire, 1967; Banse, 1968; Shetye, *et al.*, 1991). The upwelling of thermocline waters leads to strong stratification near the surface and causes the mixed layer to thin. The summer cooling in the AS is a well studied feature (Rao, 1984; 1986; Shetye, 1986), which was also discernible in the present study. The increased mixing due to the summer monsoonal winds under the monsoonal clouds (Hasternath and Lamb, 1979) tends to cool the sea surface in the open ocean region. While in the coastal regions, in addition to the above two parameters, the upwelling cools the SST. Even though, the summer time is a cooling phase in the AS, the coastal and open ocean showed maximum differences in SST. This must be due to the strong upwelling that takes place along the SW coast of India. Naidu *et al.* (1999) used the SST anomaly between the coastal and open ocean to delineate the coastal upwelling. The anomaly of SST between the coastal and open ocean region decreased towards north, indicating that the intensity of upwelling decreases towards north (Banse, 1968; Shetye *et al.*, 1990; Muraleedharan and Prasanna Kumar, 1996; Maheswaran *et al.*, 2000). On the other hand, the downwelling of surface waters produce deeper mixed layers during northeast monsoon near the coast. Along the SW coast of India, the low saline BOB waters advected during northeast monsoon through the EICC (Wyrcki, 1973; Darbyshire, 1967; Hareesh Kumar and Basil Mathew, 1997) forms a shallow

halocline in the surface isothermal layer. This reduction in salinity reduces the surface buoyancy and limits the surface mixing to a shallow halocline, creating a significant barrier layer (>30m) between the mixed layer and the top of thermocline. Relatively thicker barrier layer was formed during December – February and the thickness decreases thereafter. This result is in good agreement with that of a recent study (Shenoi *et al.*, 2004). The thickness of the barrier layer decreases towards north and showed insignificant thickness along the coastal region north of 16°N. This indicates that the intrusion of BOB waters in the coastal waters off the west coast is limited only to the southwest coast of India (Hareeshkumar and Basil Mathew, 1997). The absence of BOB waters off the northwest coast, keeps the mixed layer deeper due to the downwelling process. But the deepening of the mixed layer in northeast monsoon along the northwest coast of India is mainly due to the convective mixing, while in the central (14°N-18°N) west coast, the deepening of mixed layer seems to be the convergence of surface waters associated with the downwelling of surface waters. An examination of the monthly evolution of MLD along the coastal and open ocean regions revealed that the coastal region lags the open ocean, in response to the atmospheric conditions. This lag is clearly discernible in the northern grids during northeast monsoon season. Though the surface parameters showed similar conditions in both coastal and open ocean regions, coastal region showed nearly one-month lag in responding. In general, the open ocean regions showed deepest MLD during January-February, whereas coastal regions showed the maximum in February-March. In the open ocean, the decrease of MLDs from deep to shallow, during the retreat of northeast monsoon is much faster than that seen in the coastal region, implying that the open ocean responds rapidly to the atmospheric conditions.

3.3.2. Bay of Bengal

The seasonal march of SST in the western BOB showed distinct warmer waters during March – May and thereafter SST decreases gradually and remained

more or less constant, till the winter conditions sets in north. Like in the AS, the summer cooling is not conspicuous in the BOB, as compared to the AS. The probable reason must be the low saline waters in the BOB, which produces strong stratification and inhibits any possible mixing. The low saline waters in the BOB is an area of interest and recently many have been studied its role in the BOB processes (Howden and Murtugudde, 2001; Han *et al.*, 2001; Rao and Sivakumar, 2003; Prasanna Kumar, *et al.*, 2002). The evolution of the SSS can be related to the river runoff and the internal dynamics such as advection and circulation. The salinity structure along the coastal regions showed the flow characteristics of the EICC (Fig. 14a). Relatively high saline waters were observed along the SE coast of India throughout the year, except in winter. Three distinct features of the EICC can be discernible in the SSS distribution. The intrusion of relatively high saline waters towards north during the spring intermonsoon can be linked to the poleward flowing EICC (Cutler and Swallow, 1984; Shetye *et al.*, 1993; Sanilkumar *et al.*, 1997), which advects relatively high saline waters from south. During southwest monsoon, very low saline waters (< 28 psu) were observed in the coastal regions of the northwestern Bay (north of 16°N) and the salinity gradients increased towards north, while relatively high saline waters were observed in the southeast coast of India. The reduction in SSS towards the north is mainly due to the enormous freshwater influx from the bordering rivers (Rao and Sivakumar, 2003). This freshwater influx results in a sea level high in the northern Bay, which drives an equatorward EICC along the northwestern Bay (Shankar, 2000; Babu *et al.*, 1991) and is well discernible in the salinity distribution as the intrusion of low saline waters towards south along the western BOB (Fig. 14a). The relatively high saline waters in the south of 15°N can be associated to the least river discharge and poleward EICC. During winter monsoon, low saline waters exist along the east coast of India. Considerable reduction of freshwater influx from summer to winter (Rao and Sivakumar, 2003) was not reflected in the SSS distribution during winter (Fig. 14a). This suggests

that the advection of low saline waters maintains the SSS along the east coast of India. The intrusion of low saline waters towards south along the east coast of India during winter indicates the advection of low saline waters from the head Bay through the equatorward EICC.

In general, the central BOB showed relatively low saline waters (<33 psu) throughout the year and the SSS decreases towards north (Fig. 14b). Very low SSS and the maximum gradient in salinity were observed during summer along the northern regions. The low saline waters in the open ocean are mainly due to the offshore advection of river outflows.

The reduction in surface salinity increases the surface buoyancy and controls the surface mixing. Moreover, considerable reduction in the SSS results in a shallow halocline in the isothermal layer and creates a significant barrier layer. Along the SE coast of India, pronounced barrier layer (>30m) was formed during winter monsoon, while along the northeast coast of India and in the central BOB, thick barrier layer was formed in summer monsoon also. Notable formation of the barrier layer in the open ocean region during November – April could not be linked either to salinity or to E-P. However, during winter, the northwestern BOB does not show any distinct barrier layer formation. This is in contradiction to the observation of Rao and Sivakumar (2003). The probable reason could be the large amplitude of thermal inversion, which causes the isothermal layer to thin. During winter, the cold dry continental northeasterly winds cause excessive evaporation, leading to surface cooling (Suryanarayana *et al.*, 1991; Jyothibabu *et al.*). This cold freshwater in the surface layers stay stagnated, below which the temperature increased with depth and the static stability loss by the thermal inversion was compensated by the low saline waters and the amplitude of inversion increases towards north (Shetye *et al.*, 1996; Han *et al.*, 2001; Pankajakshan *et al.*, 2002 Jyothibabu *et al.*).

MLD in the AS and BOB are strikingly different in the open ocean region; mainly during summer and winter monsoon season. Winds over the AS (~11m/s)

during summer monsoon are stronger than that seen in the BOB (~8m/s). The stronger winds over the AS are the consequence of the highlands of East Africa on its west, which serves as the western boundary for the low level atmospheric flow. The resulting low level (Findlater) jet makes the strong winds over the AS (Findlater, 1969). The absence of a similar western boundary effect and the large frictional convergence over the Indian landmass weakens the winds over the BOB (Prasad, 2004). Moreover, the low saline surface waters in the BOB provided strong surface layer stratification, hence required more energy for mixing in the BOB, which is about three times greater than that require in the AS (Shenoi *et al.*, 2002). During the northeast monsoon the prevailing atmospheric conditions over both AS and BOB are comparable. The relatively weak northeasterly winds, which carry dry continental air from the north, enhances the evaporation in the northern AS and BOB. In the AS, heat loss due to the increased evaporation together with the ambient surface salinity initiates the convective mixing, which eventually leads to deeper MLD and cooler SST. But in the BOB, the enhanced evaporation could not lead into the densification of surface waters. Because, the presence of low saline surface waters prevents the further densification due to surface cooling and inhibits the convective mixing, instead it leads to the strong thermal inversion. The differential response of winter cooling between the AS and BOB are further explained in chapter 5.

A comparison of the MLD climatology generated in the present study to the previous climatologies (Wyrтки, 1971; Colborn, 1975; Rao *et al.*, 1991), however showed discrepancies in the BOB and the southeastern AS during winter monsoon. This indicates that the incorporation of salinity in the MLD definition reduces the MLD. It can thus be seen that salinity is an important physical property of seawater in the BOB, which controls the dynamics of the mixed layer. While in the central AS, in general, the atmospheric forcings such as wind speed and surface heat flux controls the MLD evolution, whereas in the coastal regions, horizontal advection and vertical motion dominates. Along the northwest coast of

India, the coastal and open ocean regions showed a time lag in response to the atmospheric conditions. Keeping these in mind, the hydrography of the west and east coasts of India has been subjected to a detailed study using recently collected data, and the results are presented in the subsequent chapters.

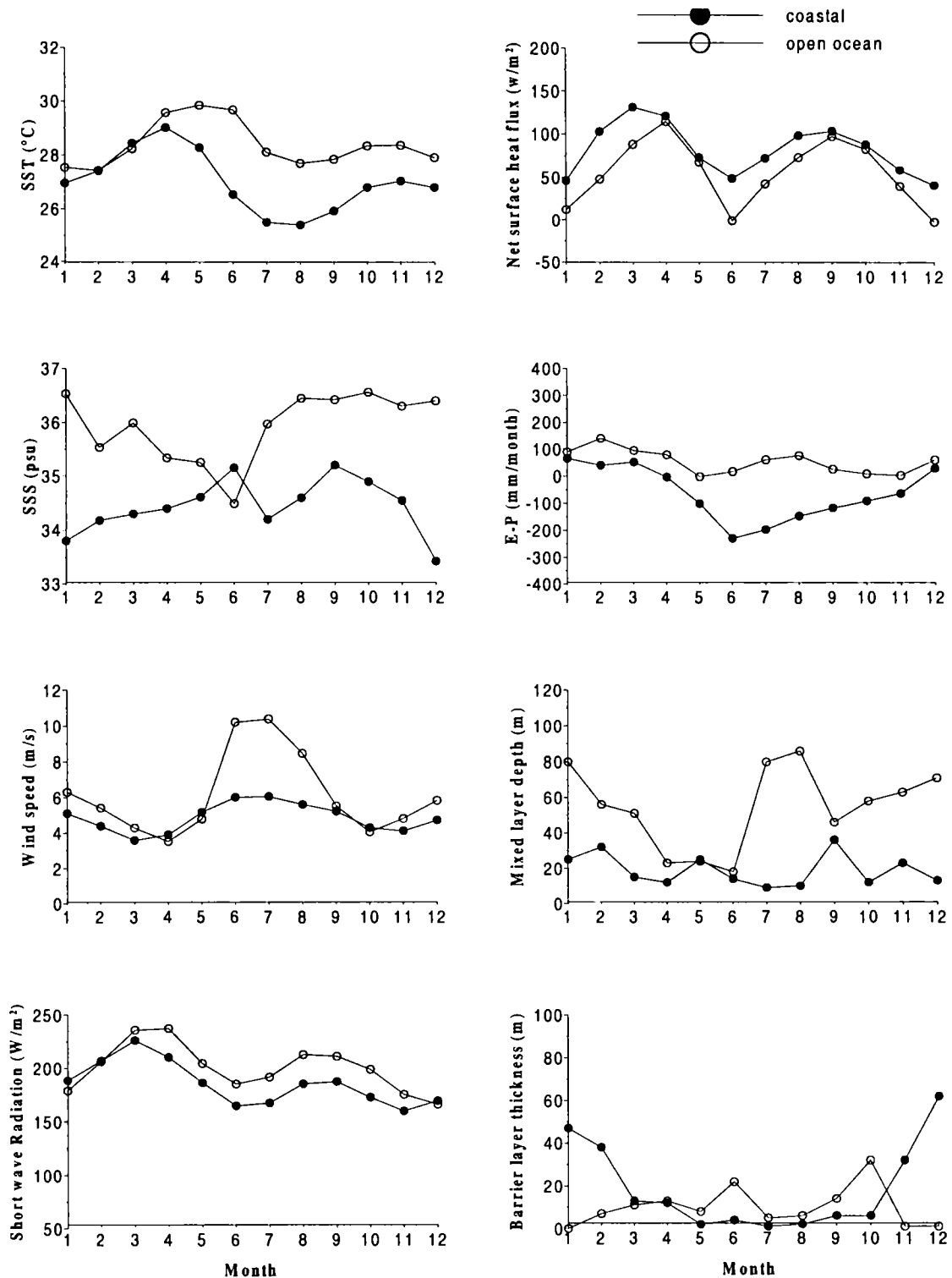


Figure 3.1. Monthly distribution of surface atmospheric and oceanographic parameters in Arabian Sea (8-10°N)

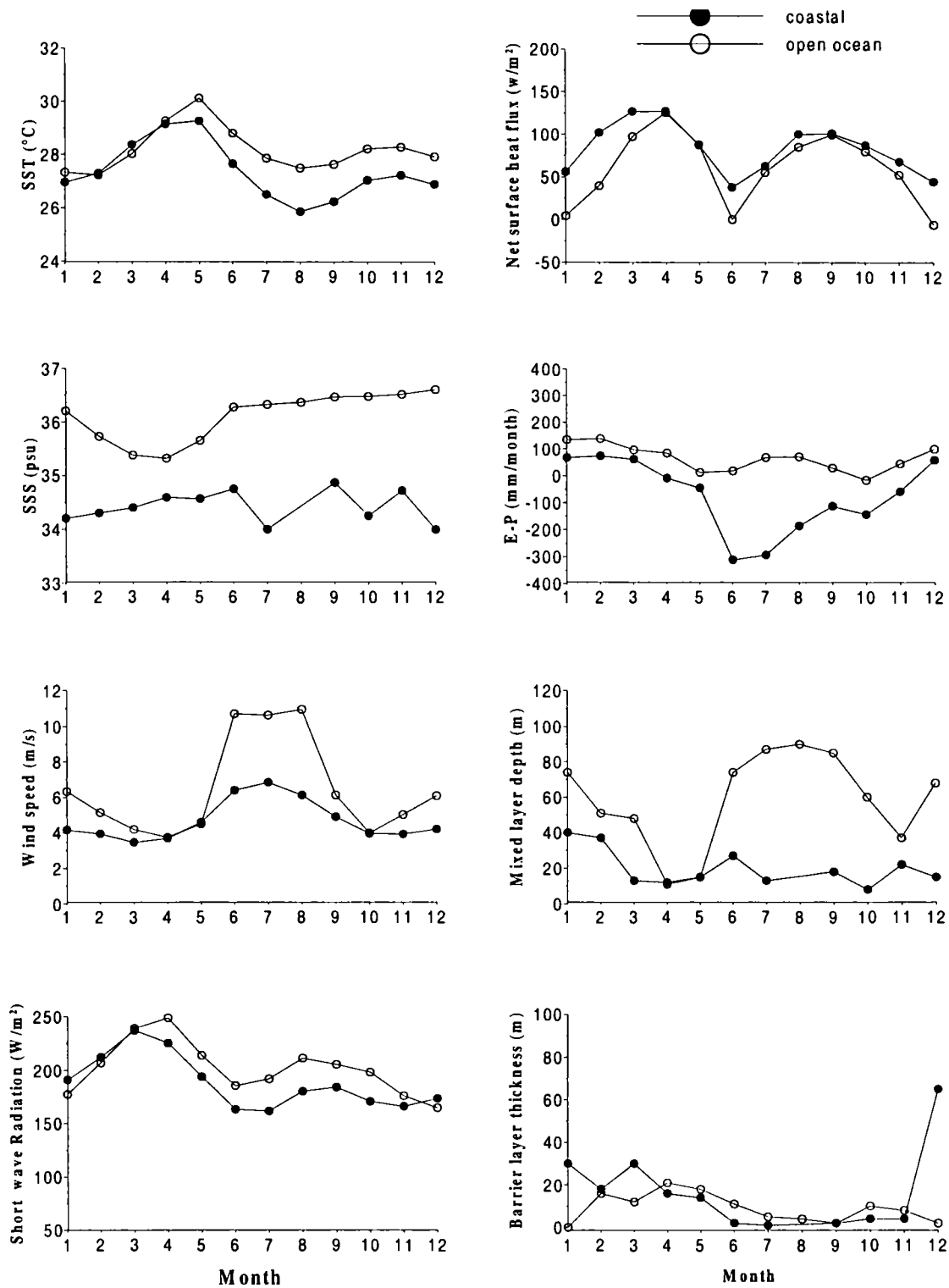


Figure 3.2. Monthly distribution of surface atmospheric and oceanographic parameters in Arabian Sea (10-12°N)

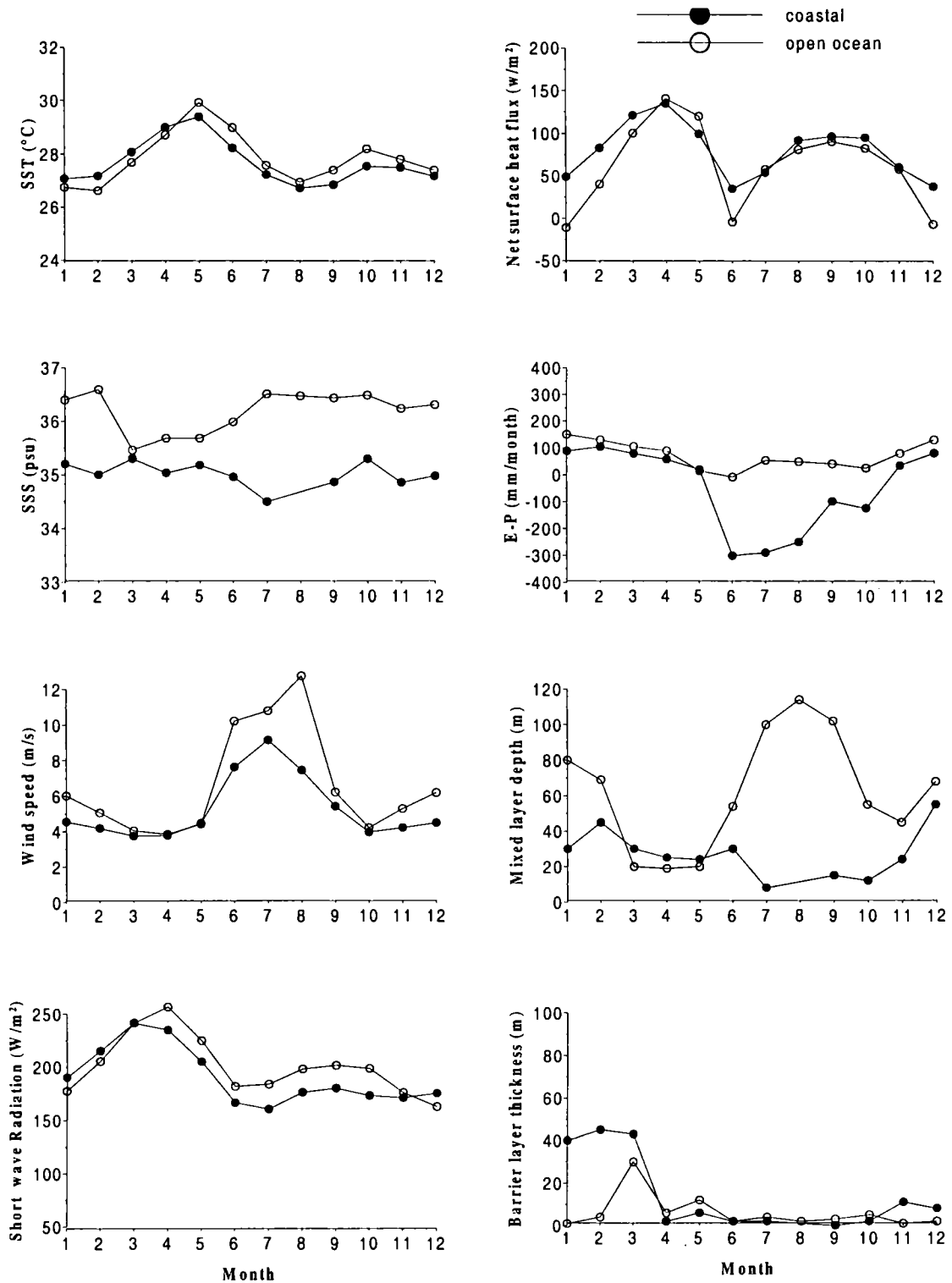


Figure 3.3. Monthly distribution of surface atmospheric and oceanographic parameters in Arabian Sea (12-14°N)

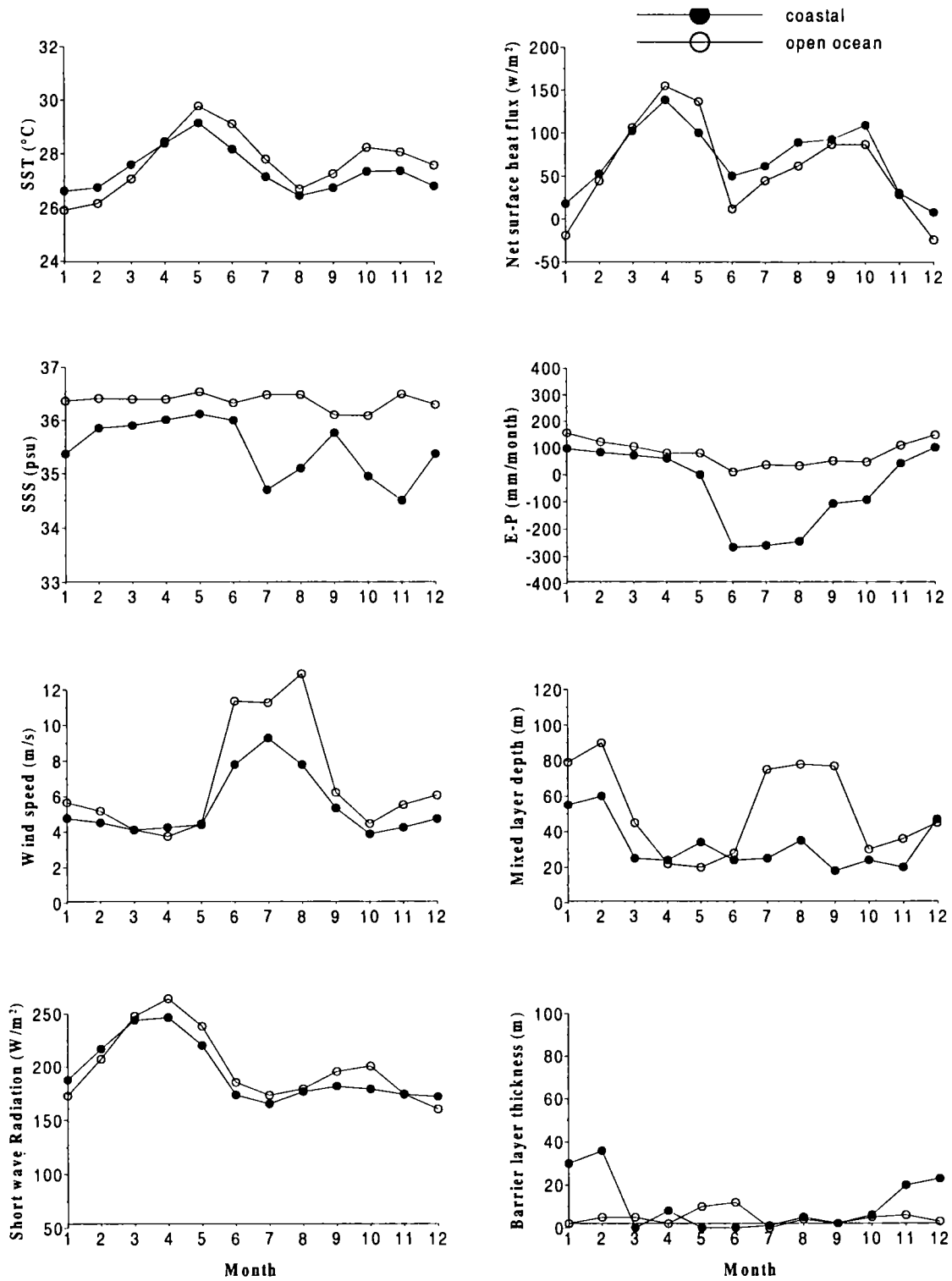


Figure 3.4. Monthly distribution of surface atmospheric and oceanographic parameters in Arabian Sea (14 -16°N)

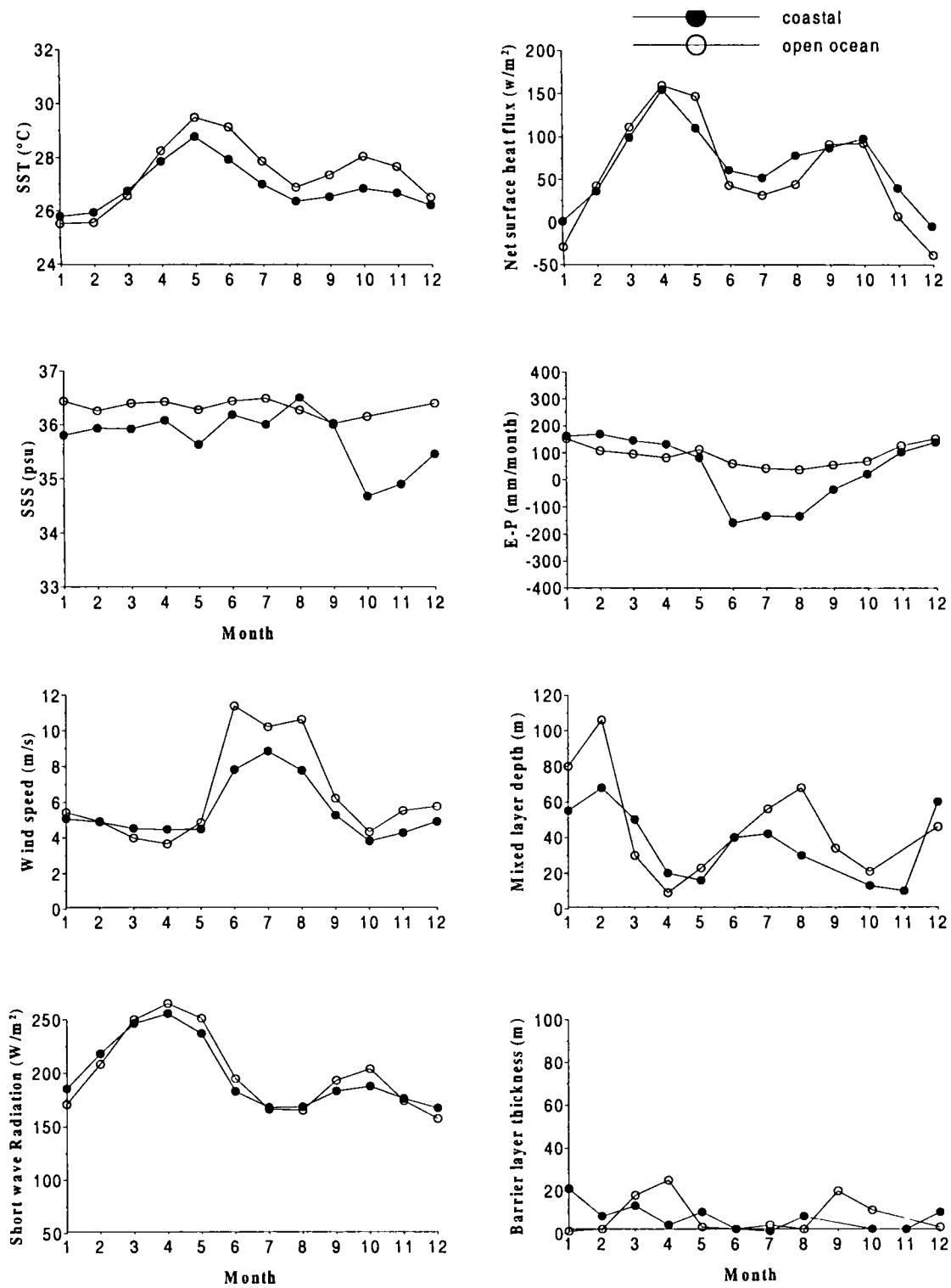


Figure 3.5. Monthly distribution of surface atmospheric and oceanographic parameters in Arabian Sea (16-18°N)

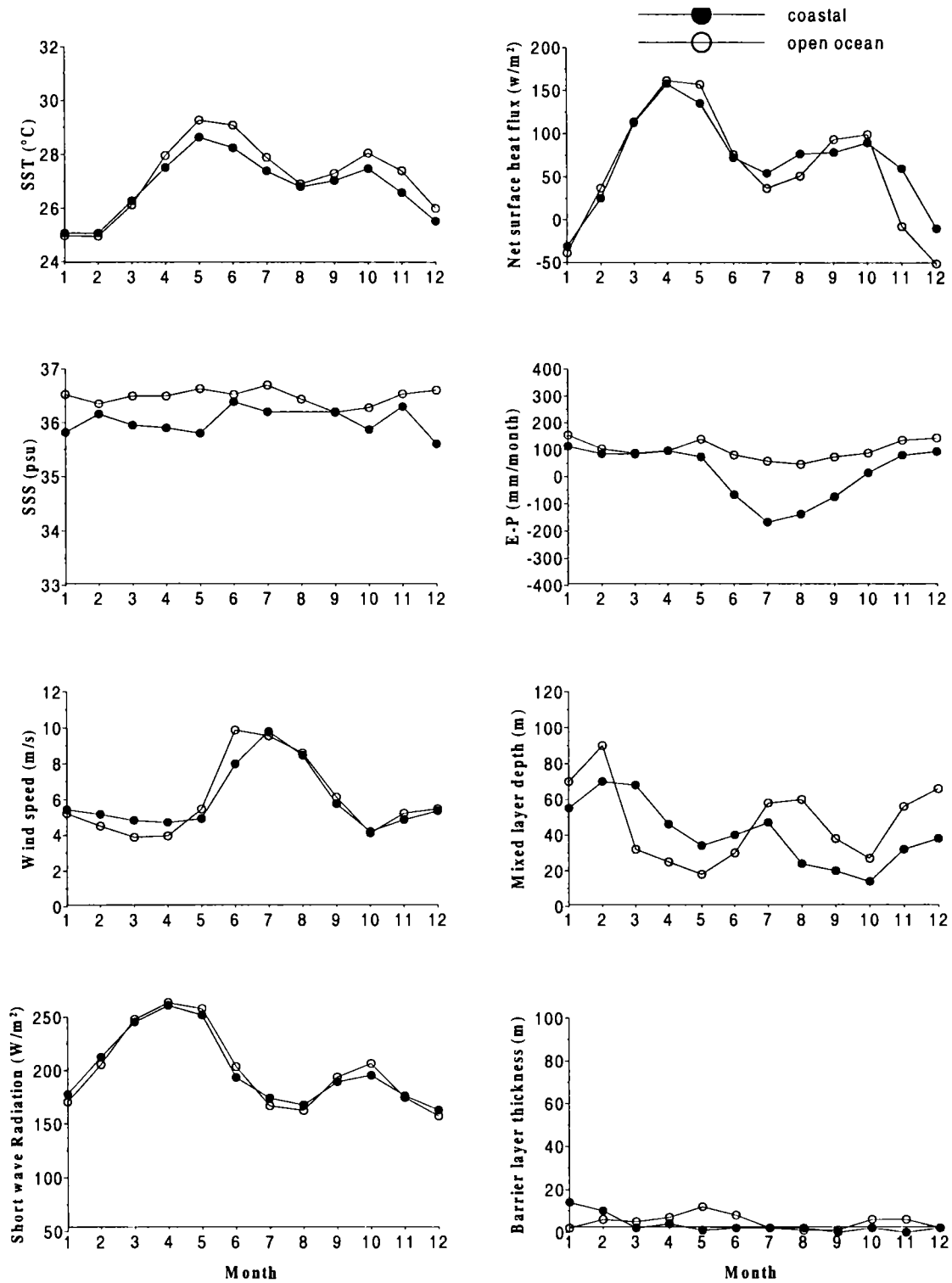


Figure 3.6. Monthly distribution of surface atmospheric and oceanographic parameters in Arabian Sea (18 -20°N)

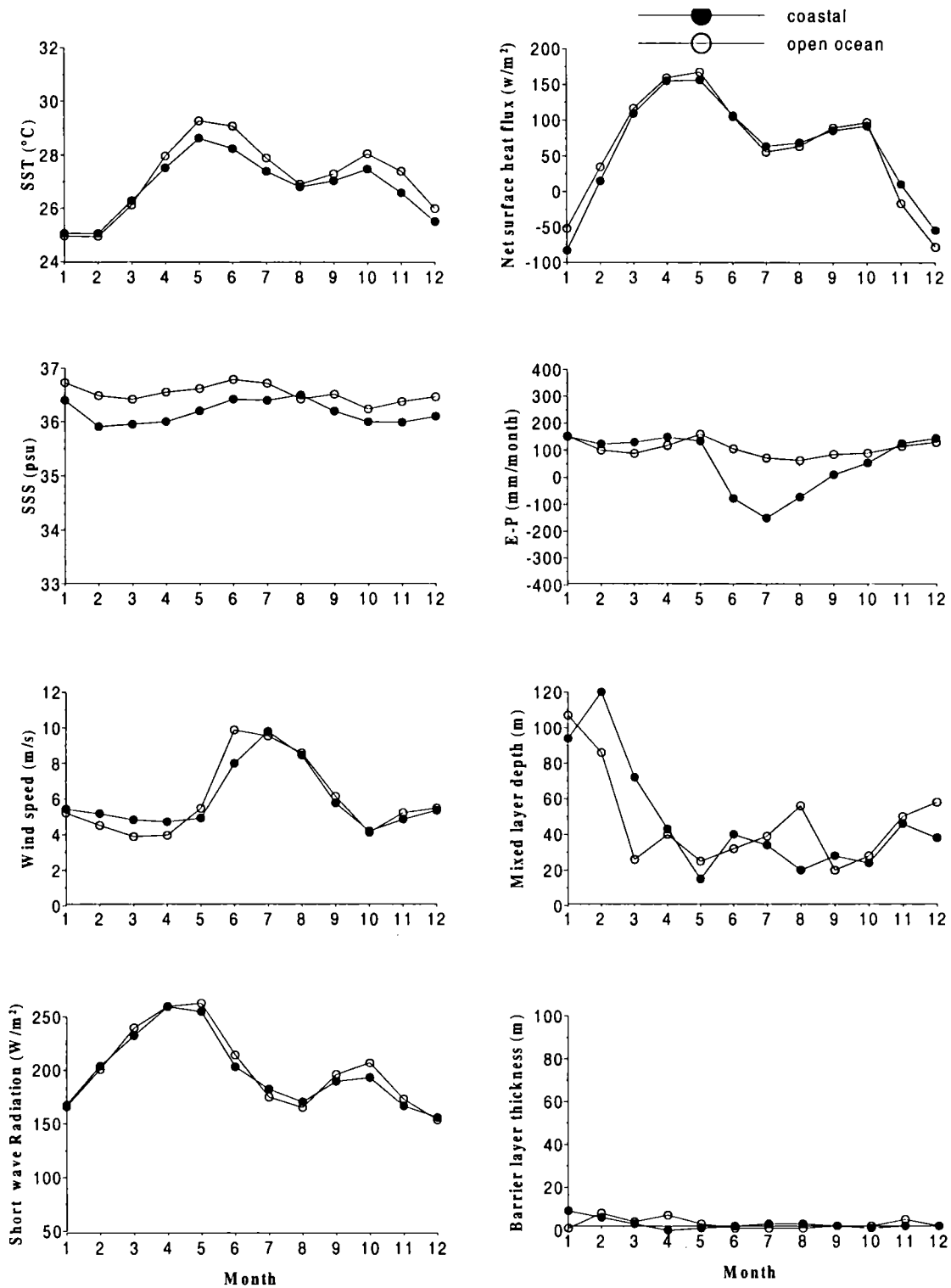


Figure 3.7. Monthly distribution of surface atmospheric and oceanographic parameters in Arabian Sea (20 -22°N)

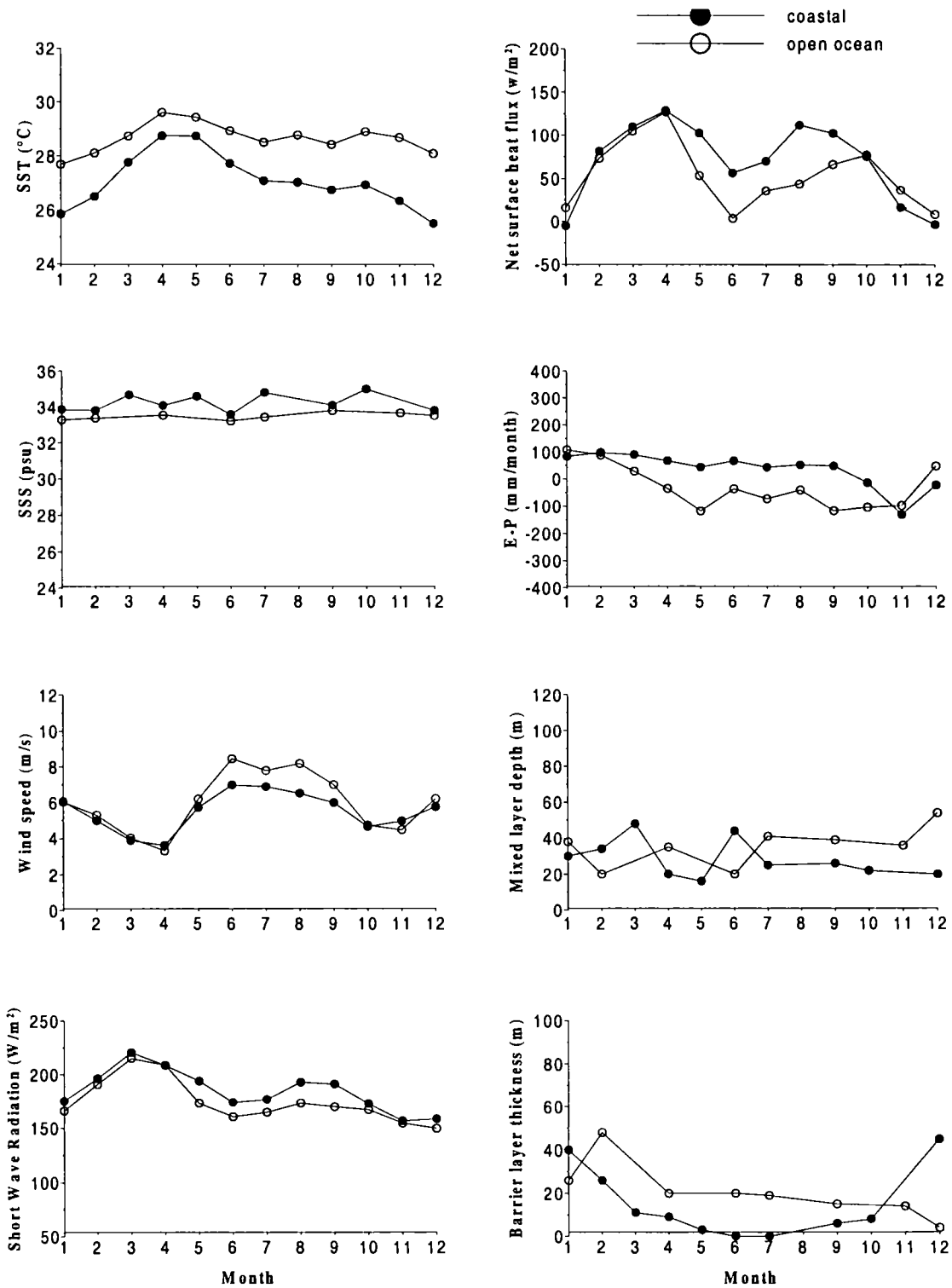


Figure 3.8. Monthly distribution of surface atmospheric and oceanographic parameters in Bay of Bengal (8 - 10°N)

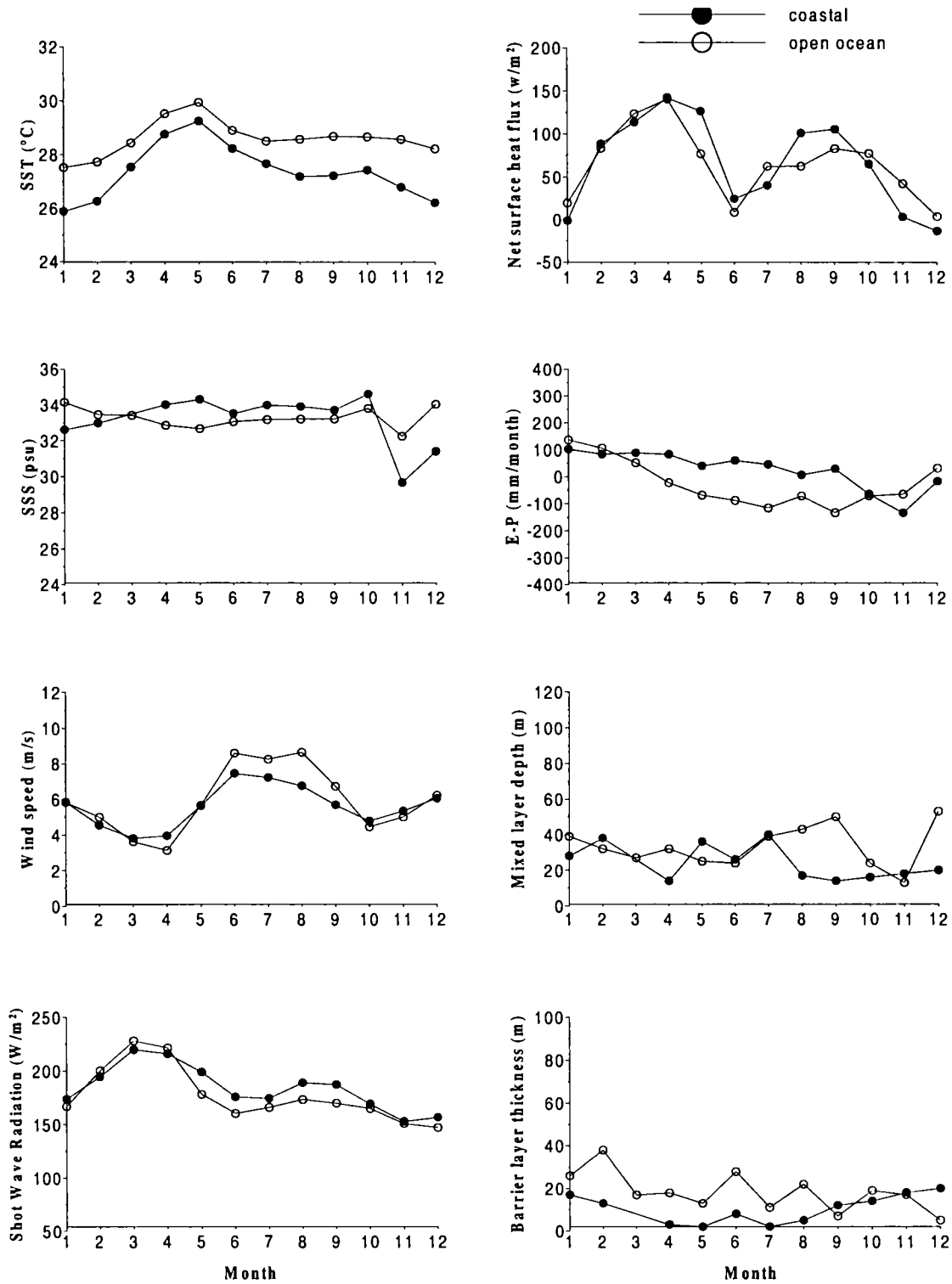


Figure 3.9. Monthly distribution of surface atmospheric and oceanographic parameters in Bay of Bengal (10 - 12°N)

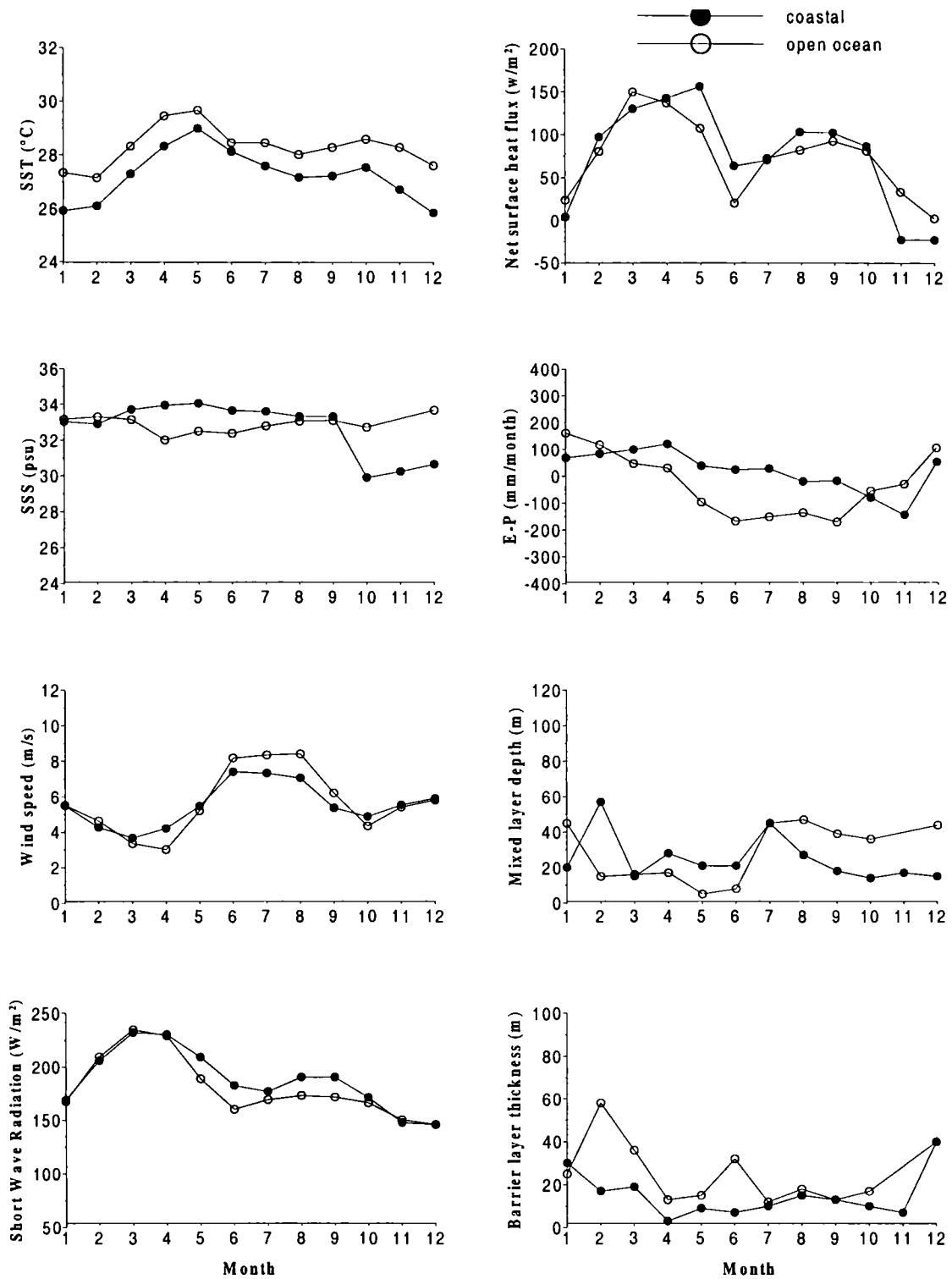


Figure 3.10. Monthly distribution of surface atmospheric and oceanographic parameters in Bay of Bengal (12 - 14°N)

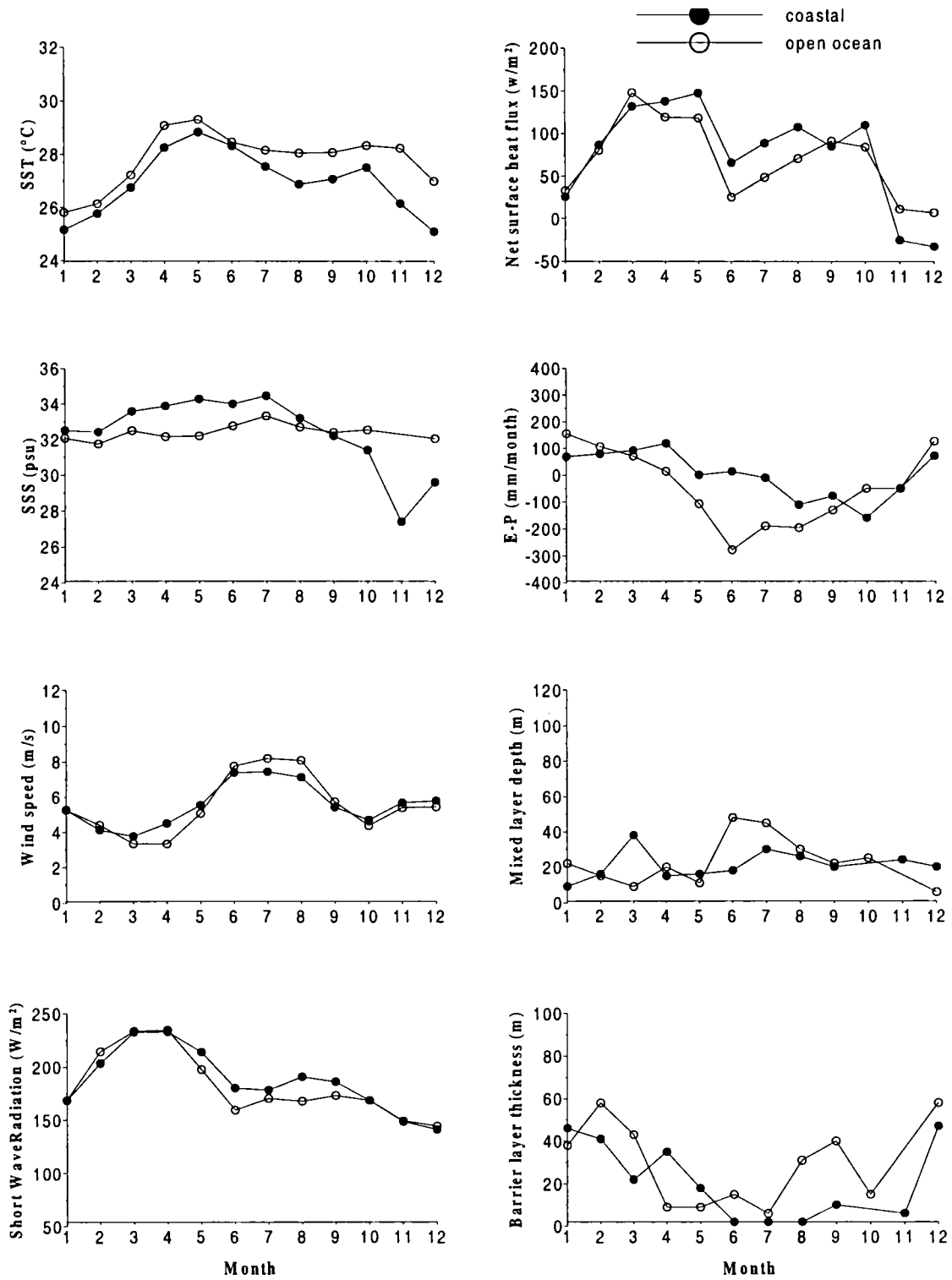


Figure 3.11. Monthly distribution of surface atmospheric and oceanographic parameters in Bay of Bengal (14 - 16 $^{\circ}\text{N}$)

G8968

Chapter 3 - Mixed Layer Characteristics

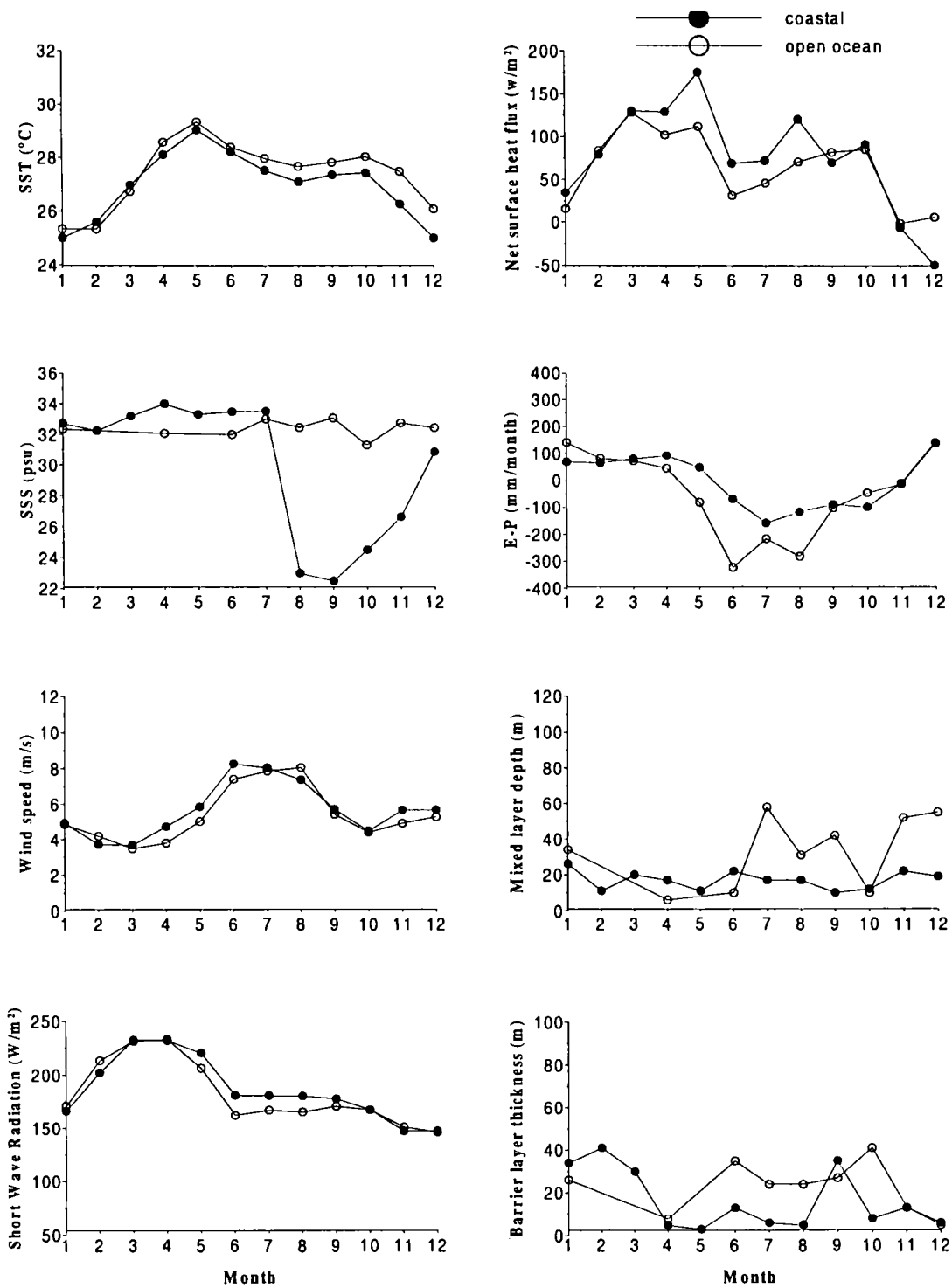
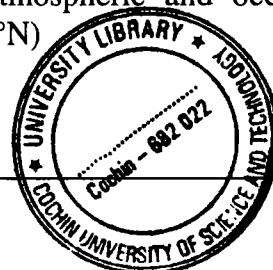


Figure 3.12. Monthly distribution of surface atmospheric and oceanographic parameters in Bay of Bengal (16 - 18 $^{\circ}\text{N}$)



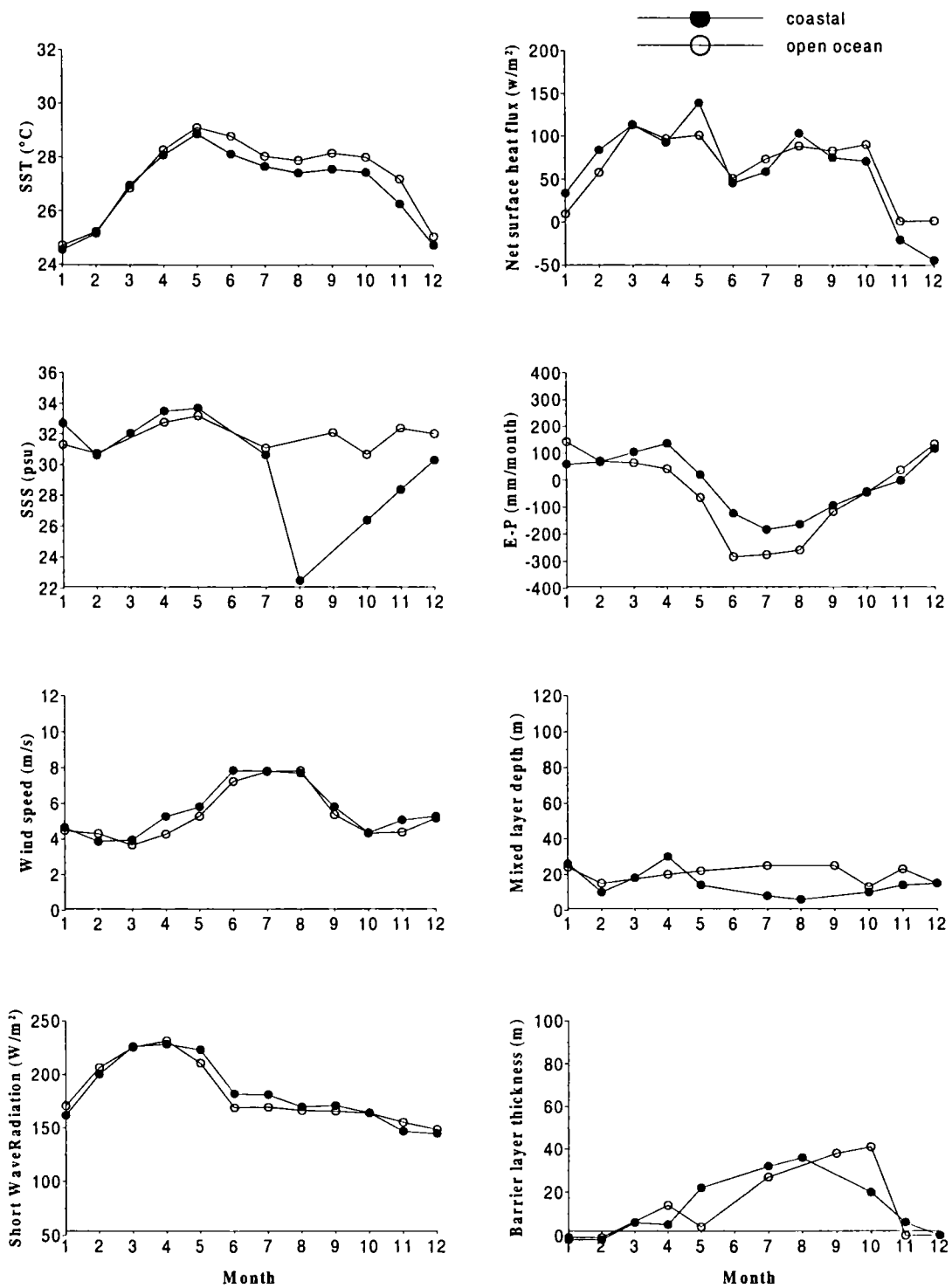


Figure 3.13. Monthly distribution of surface atmospheric and oceanographic parameters in Bay of Bengal (18 - 20°N)

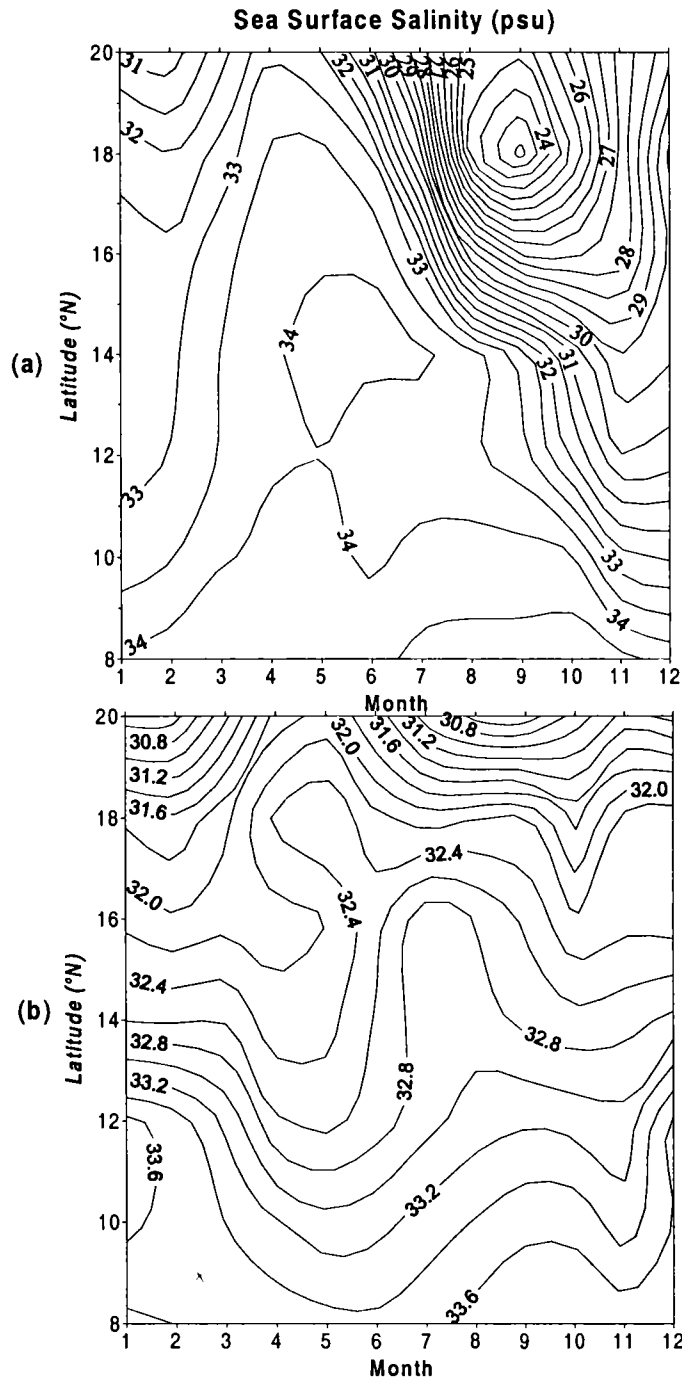


Figure 3.14. Monthly distribution of sea surface along a) the coastal region and b) open ocean region (along 91°E) in the BOB

Chapter 4

Hydrography off the eastern Arabian Sea

In this chapter, apart from the meteorological data over AS, the vertical profiles of temperature, salinity, density collected at 1m intervals as well as data on nitrate, primary productivity and oxygen under saturation collected at discrete standard depths are discussed. These data represent the hydrographic stations along 8°N, 10°N, 13°N, 15°N, 17°N, 19°N and 21°N transects (Fig.4.1). The thermohaline structure and the physical forcing (of the upper 300m) on biological production during different seasons are also included. The stations sampled in May along 8°N, 10°N and 13°N and those sampled in March along 17°N, 19°N and 21°N are included in the spring intermonsoon season. During summer monsoon season, the stations were covered in June for most of the areas of west coast of India. The station sampled in 6 transects from 8°N – 19°N during September – October are included in the fall intermonsoon season. The hydrographic stations along the west coast of India, sampled in December/January were included in the winter monsoon season.

4.1. Spring intermonsoon

4.1.1. Hydrography

During May, the winds along the southwest coast of India were predominantly northwesterly and the magnitude on an average was 5m/s; while relatively weak winds (<3m/s) were observed off the northwest coast of India during March with predominant northwesterlies.

The distribution of SST, SSS, MLD and depth of 1 μ M nitrate concentration are plotted in Figure 4.2. SST showed a steady decrease towards the coast along the southwest coast of India and the lowest value (27.6°C) was observed near the coast along 8°N. In general, SST showed an increasing trend northwards up to

15°N, beyond which it showed a decreasing trend and reached the lowest value (24.9°C) near the coast along 21°N. SSS ranged between 33.8 *psu* and 36.3*psu*, having minimum near the coast along 10°N and maximum along 21°N. MLDs along the eastern Arabian Sea ranged from 15 to 70m, having minimum near the coast along the southwest coast (8°N - 10°N) and deeper MLDs (>60m) were observed off the northwest coast. In general, the MLDs along the southwest coast (south of 15°N) decreases gradually towards the coast in each transect. North of 17°N, the MLDs deepened towards the coast. The barrier layer thickness during the season appears to be insignificant (<10m, not shown). The distribution of the isopleths of 1μM nitrate concentration follow a similar pattern of the MLD distribution along the southern transects. The upper limit of isopleths of 1μM nitrate concentration varied from 10 to 60m and surfaces (at ~15m) near the coast along 8°N and 10°N.

To decipher the signals of upwelling and the winter cooling, vertical sections of temperature, salinity and density are plotted for the different transects (Fig. 4.3). The vertical thermal structure along 8°N shows distinct upsloping of isotherms towards the coast leading to colder surface waters there (Fig. 4.3a). This upsloping extends up to 140m depth, below which the trend reversed and the isotherms were deepening towards coast, indicating the presence of an undercurrent (Antony, 1990, Shetye *et al.*, 1990). Surface salinities near the coast were almost 0.7 *psu* higher than the offshore values. Salinity in the upper 50m showed an isolated pocket of low salinity about 150km away. Protrusion of high saline water (>35.8 *psu*) towards the shore was seen at 40 to 90m depth. The thermohaline index of this high saline watermass is in agreement with the characteristics of ASHSW (Prasanna Kumar & Prasad, 1999) and it is interesting to note that the eastern extent of the ASHSW is confined to the west of 74°E. Relatively low saline waters (<35.2 *psu*), hugging the continental slope of the region in the subsurface layer is well discernible below 150m, where the isotherms showed the signatures of poleward undercurrent. Isopycnals showed a close

resemblance to the isotherms. Upsloping of isopycnals from 120m depth towards the shore indicated the presence of denser water along the shelf and lighter water offshore. Vertical sections of temperature along 10°N also indicated strong upwelling signals (Fig. 4.3b). Shoaling of isotherms towards the coast was prominent which started approximately from 200m depth. This was much deeper when considering the shoaling of isotherms observed off 8°N, indicating the deepening of undercurrent towards north. The remarkable shoaling of the thermocline towards the coast is again reflected in the density distribution indicating active upwelling. The surface salinity near the coast was almost 1.0 *psu* lesser than the offshore values. The protrusion of ASHSW towards the coast was well discernible in this transect and the core values were relatively higher than that of the previous transect. Relatively low saline waters (<35.2 *psu*) observed along the continental shelf in 150 to 200m depth can be linked to the poleward undercurrent (Shetye *et al.*, 1990), which is a typical feature of the wind driven eastern boundary upwelling regions (Mittlestaedt, 1986). Vertical section of temperature along 13°N also showed the distinct upsloping of isotherms on approaching the coast (Fig. 4.3c). The shoaling of isotherms starts from 300m depth and it is much deeper compared to the shoaling of isotherms observed off 8°N and 13°N. The isopycnals follow the isotherms in this section indicating upwelling. The vertical salinity structure showed the protrusion of ASHSW towards the coast and the core values are higher than that seen along 8° and 10°N transects, and it protrudes relatively nearer to the shore. The presence of low saline waters hugging the continental shelf at 150 to 200m depth suggested the presence of an undercurrent. On the contrary, along 17°N, 19°N and 21°N, the isolines generally showed a downsloping trend towards the coast (Figs. 4.3d, 4.3e, 4.3f). The temperature at the surface layer showed a decreasing trend, while the surface density showed an increasing trend, towards north. In general, the ASHSW were observed in the upper 50m in all the three transects. Vertical sections of sigma-t

along the three transect showed the downsloping of the isolines towards the coast and the surface density also increased northwards.

The integrated values of chlorophyll *a* and PP are presented in Table 4.1. High surface and integrated values of chlorophyll *a* and PP near the coast along 8°N and 10°N can be attributed to the upwelling. The depth integrated PP showed a wide range: 35 to 9144 mgC m⁻² d⁻¹; having highest value of 9144 mgC m⁻² d⁻¹ along the coastal region off 8°N. In general, the coastal stations along the SW coast of India recorded higher biological production. The northwest coast of India also showed particularly high PP (ave. 608 mgC m⁻² d⁻¹). The chlorophyll *a* concentration (depth integrated) also showed a wide range, 10 to 203 mg m⁻², the maximum being coastal transect off 8°N.

4.1.2. Discussion

Since the spring intermonsoon is represented by a set of observations during March and May, the period of coverage in the southern transects (8°-13°N) represents the onset of the SW monsoon (May), and that in north (17-21°N) represents the retreat of northeast monsoon (March). Distribution of SST showed warmer waters along the southern region (8°-13°N) as compared to the northern region (17-21°N). The upward tilting of isotherms and isopycnals on approaching the coast in the southern transects, were not seen in the northern transects. MLD in the southern transects showed a decreasing trend towards the coast, while in the northern transects, the MLDs deepen towards the coast. In general, winds in the southern transects during May were predominantly northwesterly. The wind steadiness over southwest coast of India during May-June is relatively high (>85%, Hastenrath and Lamb, 1979). Hence, the wind system along the southwest coast of India was favourable to the upwelling. The causative factors for the upwelling along the west coast of India, is a matter of controversy. Darbyshire (1967) observed cold surface waters (<22°C) along the coastal region off Kerala, but denied the role of wind driven upwelling. According to Banse (1959; 1968), the prevailing current system and not the wind is the main cause for initiating and

maintaining the upwelling. Studies made by Johannessen *et al* (1981) revealed that upwelling along the west coast of India is not only associated with the local wind, but also with more large-scale monsoonal conditions which drive the anticyclonic AS monsoonal gyre. Shetye and Shenoi (1988) compared the annual cycles of longshore component of wind stress with ship drift along the coast and interpreted that the local winds drive the surface circulation during SW monsoon. Shetye *et al.* (1990) after conducting a comprehensive survey along the west coast of India during June –August, concluded that the upwelling along the southwest coast of India is a typical eastern boundary wind driven upwelling system with equatorward surface current and poleward undercurrent. The appearance of distinct cold waters, shallow MLDs, nitracline and high productivity near the coast substantiate that the upwelled water reaches the surface in the month of May itself along the southwest coast of India. The present study also supports the earlier findings: the processes of upwelling begins as early as February/March, well before the upwelling favourable southwest monsoon winds, at the deeper levels (Longhurst and Wooster, 1995), possibly initiated by the northerly winds, which would transport the surface water away from the coast, and favouring a motion from below (Sharma, 1966; Pillai, 1983) for the upwelled water to gradually reach the surface by May. But, Shankar and Shteye (1997) suggested that the early upwelling signals along the southwest coast of India is a manifestation of remote forcing. The radiation of Rossby waves weakens the WICC off southwest coast of India and it eventually reverses as equatorward and by mid-January, the upwelling favorable current off southwest India, closing the circulation around a high. In the present study, strong upwelling was noticed off 8°N, relatively less at 10°N and weak off 13°N indicating the gradual propagation of the upwelling from south to north (Muraleedharan and Prasanna Kumar, 1996; Sanilkumar *et al.*, 2004).

The upwelling of subsurface waters brings nutrients to the euphotic zone and eventually results in the high biological production in the coastal region off 8°N and 10°N. In contrast, low SSTs, downsloping of isolines towards the coast

and deepening of MLD and the thermocline towards the coast, along 19°N and 21°N, ascertain that during March, the northwestern coasts of India are still under the grip of winter cooling. However, the high chlorophyll concentration (37 mgC m⁻²) and primary productivity (1192 mgC m⁻² d⁻¹) in the open ocean region along 17°N can be attributed to the post winter mechanism (phytoplankton bloom) as follows. After the winter mixing, the oceanic regions stabilize much faster than coastal regions in March. So in the open ocean region, under the improved light and weak wind conditions along with the availability of nutrients present in the euphotic zone are favorable for spring blooms. These spring blooms are short lived, because of the grazing of zooplankton and the rapid depletion of nutrients (McCreary *et al.*, 2001).

4.2. Summer monsoon

4.2.1. Hydrography

During the onset of the southwest monsoon, the winds are predominantly southwesterly with occasional northwesterlies near the coast between 8°N and 15°N. Strong winds (~8m/s) blow off the northern and southern transects, while relatively weak winds (<4m/s) were observed in the region between 15°N – 19°N.

The most important feature of the SST distribution is the monsoonal cooling (<26.4°C) along the southwest coast of India (Fig. 4.4). SST near the coast along 8°N are almost 2.7°C lower than that of the farthest open ocean station. The coastal station along 10°N exhibited colder waters nearshore (~26.1°C), which was about 3.4°C cooler than the open ocean waters. North of 13°N, SST showed minimum spatial variability (<0.5°C) and the SST increased further northwards. The SSS ranged from 34.6 to 36.8 *psu* with a gradual increase towards north and exhibited minimum variability. SSS near the coast along 8°N was almost 0.6 *psu* higher than that seen in the farthest station, which can be indicative of the upwelling process, where the cool high saline waters replaces warm, less saline waters towards offshore. However, along 10°N, the coastal waters are about 0.7 *psu* lower than the open ocean waters, probably due to the

monsoonal rainfall and associated runoff from the Vembanad lake. During the season, MLD varied between 10 and 50m and the lowest value was observed near the coast along 10°N. In general, MLD along the southwest coast decreases gradually towards the coast, while along the northwest coast of India, MLD ranged from 20 to 40m, and the thickness of the barrier layer appears to be insignificant (<15m). The top of the nitracline ranged from 10 to 90m and in the south it follows the mixed layer pattern. The nitracline was seen well below 60m in the open ocean region and surfaces near the coast along 8°N and 10°N (at around 10-15m depth). However, along the northwest coast, the nitracline was observed below the mixed layer.

Vertical section of temperature along 8°N showed the distinct upsloping of isotherms towards the coast resulting in colder waters near the coast (Fig. 4.5a). It can be seen that the waters from 70m reached the surface near the coast in the beginning of the southwest monsoon. The upsloping extends up to 180m, below which the trend was seen to reverse. Salinity structure clearly showed relatively high saline surface waters (<35.2 *psu*) nearshore and low saline waters (<34.8 *psu*) offshore. The ASHSW was observed in a narrow width (50 – 70m) along the open ocean region with the core having a salinity of around 36.0 *psu*. The spreading of ASHSW towards the coast was not evident. Isopycnals showed almost close resemblance to the temperature section. It could be seen that denser waters from 60m depth reached the surface near the coast. Vertical section of temperature along 10°N also showed the distinct upsloping of isotherms towards the coast (Fig. 4.5b). Colder waters (<27°C) were observed near the coast and extend offshore to 100km. Below 160m depth, the isotherms were deepening towards the coast indicating the presence of a poleward undercurrent. Salinity structure along this transect showed low saline surface waters nearshore and high saline waters offshore. Below the surface low saline waters, the ASHSW was evident between 40 and 90m depth, the core of which (salinity > 36.2 *psu*) shallowed often towards

the coast. Isopycnals also showed the distinct upsloping and exhibited relatively denser waters nearshore.

Vertical section along 13°N showed the upsloping of isolines towards the coast and the upwelled waters were confined below the warmer surface waters (Fig. 4.5c). The warm surface water (>30°C) was found to spread in the upper 50m, below which the isolines showed gentle upsloping towards the coast. Salinity structure clearly showed the presence of ASHSW, which was observed below the surface low saline waters with the core salinity of 36.2 *psu* between 40 – 100m depth. The distribution of density indicate that salinity dominates over temperature in the upper 300m, below which, isopycnals showed almost close resemblance to the temperature profile indicating the dominance of temperature on density.

Along 15°N, the upsloping of isotherms were confined below the warm surface waters as in the previous transect (Fig. 4.5d). The upsloping of isolines towards the coast was clearly seen below 100m. Salinity structure showed relatively low saline surface waters nearshore (<35.2 *psu*) and the values increased towards the offshore region. The ASHSW was seen below 30m. Isopycnals showed close resemblance to the temperature sections below 40m depth, above which the density was mainly controlled by the salinity.

Vertical thermal structure along 17°N indicated that warm waters (>30°C) are present in the upper 30m (Fig. 4.5e). The upsloping of isolines was clearly seen below 100m depth. ASHSW was seen below 30m and core salinity values increased from those seen in the previous transects. Isopycnal patterns showed an exact resemblance to the isotherms in this transect.

In the vertical sections of temperature along 19°N, the upsloping of isotherms were seen below 100m depth near the coastal region (Fig. 4.5f). The ASHSW was observed below the surface, extending from 10 to 60m with a core value of ~36.4 *psu*. Below 30m, isopycnals followed the isothermal distributions. Thermal structure along 21°N showed the upsloping towards the coast in the upper

50m (Fig. 4.5g), below which the isolines do not show any distinct pattern. ASHSW was clearly seen in the upper 60m depth having a core value of 36.7 *psu*.

Surface and column chlorophyll *a* values showed high biological production near the coast (along 8°N and 10°N). The depth integrated PP ranged from 179 to 1629 mgC m⁻² d⁻¹ (average 503 mgC m⁻² d⁻¹) and the chlorophyll *a* concentration varied from 8.7 to 44.7 mg m⁻² (average 23.2 mg m⁻²). An increase in biological production was noticed in the coastal region along the southwest coast and the highest PP and chlorophyll *a* concentration were observed off 8°N, suggesting active upwelling (Table 4.1).

4.2.2. Discussion

The period of coverage (May/June) in the eastern AS represented the onset of the southwest monsoon. The hydrographic data confirmed that the upwelling processes is initiated in the south along with the onset of the southwest monsoon and slowly propagates towards north with time. Analyses of hydrographic characteristics (along 8°N) revealed that the cold upwelled waters replace the warm low saline surface waters towards offshore by the month of June. Strong upwelling was also evident off 10°N, but the upwelling band was found restricted to the coastal region. North of 10°N, the upwelling was confined below the warm surface waters. The presence of cold waters near the coast and SST gradient between the coastal and open ocean stations were in contrast to earlier reports (Shetye *et al.*, 1990; Sanilkumar *et al.*, 2004). The reason must be the difference in the survey periods; the present observation was in phase with the onset of monsoon, while others have captured the signals during the peak of southwest monsoon season. However, the biological production indicated that the production is enhanced at the initial phase of upwelling itself. The shallow mixed layer in north was associated with the warm surface conditions in May/June, the primary heating season in the AS. The warm sea surface (>30°C) provides the strong thermal stratification, which prevents the entrainment of nutrients to the

mixed layer. Hence, the nitracline was observed well below the mixed layer and this leads the poor production in the north.

4.3. Fall Intermonsoon

4.3.1. Hydrography

During September – October, variable surface winds with predominant south westerlies were observed along the west coast of India. Strong southwesterlies (4-7 m/s) and weak westerlies (<3 m/s) were observed along 8°N, 10°N and 13°N. Along 15°N and 17°N, the winds were predominantly southeasterlies (> 5m/s); relatively strong northerlies (> 6m/s) were observed off 19°N.

SST ranged from 27.5°C to 30.2°C and colder waters were observed near the coast along the southwest coast and warmer SSTs in north (Fig. 4.6). SST near the coast along 8°N and 10°N were almost 1°C lower than the open ocean waters. SSS ranged between 33.9 to 36.8 *psu* and showed that the low saline waters spread along the entire west coast was due to the monsoonal runoff. MLDs near the shore was observed to be shallow (15-20m), while in the open ocean region, relatively deeper (~55m) MLDs were observed. Along 17°N and 19°N, MLD was observed to be shallow and had a narrow range (15–25m). The nitracline was observed between 15 and 80m, surfacing near the coast. In general, the nitracline shallows towards the coast in all transects (south of 17°N), while along 19°N, deep nitracline was observed.

Vertical thermal structure along 8°N showed the gentle upsloping of isotherms towards the coast between 50m and 130m depth (Fig. 4.7a). The vertical structure of salinity along this transect showed the presence of ASHSW as a protrusion of high saline waters towards the coast in the surface layer. ASHSW occurs in the surface at 70°E and is seen up to 73°E at about 50m. Isopycnals below 150m deep resembled the isotherms. There were indications of downwelling below a depth of about 100m in the temperature and density sections.

Vertical sections of temperature along 10°N, 13°N and 15°N are presented in Figs. 4.7b-4.7d. The upsloping of isotherms towards the coast was seen to be relatively weak at 13°N and 15°N, as compared to 10°N. Salinity structure at 10°N, 13°N and 15°N showed the presence of ASHSW as a protrusion, which extends towards the coast. Density structure showed the dominance of salinity effects in the upper 50m, below which the temperature was found to play a major role in the density distribution. Signatures of poleward undercurrent is clearly seen in all the three transects. A distinct feature of the thermal structure along 17°N and 19°N is the presence of warmer waters (>30°C) at the surface (Figs. 4.7e, 4.7f). However, below 40m, the isotherms were upsloping towards the coast. ASHSW was clearly seen in the salinity structure, but the low saline waters and the coastal currents prevent the water mass to move towards the coast. Isopycnals below 50m showed a distribution pattern, which almost resembles the isothermals. The downsloping of isotherms and isopycnals along 17°N starts at depth below 150m, and is characterized by low saline waters hugging the continental shelf. A general increase in biological production in the coastal region and a decrease in the open ocean region was evident in October. The depth integrated PP and chlorophyll a along the open ocean are 316 mgC m⁻² d⁻¹ and 5.6 mg m⁻², while in the coastal region it increased to 550 mgC m⁻² d⁻¹ and 24 mg m⁻², respectively (Table 4.1).

4.3.2. Discussion

The period of coverage (September – October) in the eastern AS represented the retreating phase of southwest monsoon characterized by comparatively higher wind velocities with predominant westerlies. The hydrography during the period is marked by the following: in the near coastal region, upsloping of isotherms and isopycnals are clearly seen up to around 75m deep along the southern transects (8°-13°N). Moreover, depth of the nitracline and mixed layer shallows on approaching the coast and hence the biological production near the coast was relatively high near the coast (820 mgC/m²/d at 8°N

and 935 mgC/m²/d at 10°N). Along the open ocean region, the convergence of surface waters is evident. This happens, when the coastal upwelling intensifies as the monsoon progresses, which eventually transport the surface waters offshore and by September it might converge in the open ocean region, leading to a deep nutrient depleted mixed layer and transform the region into an oligotrophic condition. North of 13°N, the upsloping of isolines are confined below the warm surface water and is seen between 25 and 100m, implying that upwelling was in the retrieval stage in north, while it was still active along the southwest coast of India. This supports the views of Banse (1959; 1968), that the upwelling along the southwest coast of India starts with the onset of southwest monsoon and reaches the maximum intensity during July – August, and ends by mid-October. Johannessen *et al.*(1981) found that the upwelling lasts throughout the southwest monsoon period until September – October.

The occurrence of an undercurrent was suggested by the presence of low salinity water hugging the continental slope (Antony, 1990; Shetye, *et al.*, 1990), along the west coast of India. It is inferred that the downsloping of isotherms and the presence of low saline waters in the shelf, seen at all transects could be the signatures of a poleward undercurrent. This signature was relatively well discernible than that seen in May/June. The reason might be, in an active upwelling system, the undercurrent feeds the surface current by vertical transport of subsurface water to the surface and in the process it loses water as well as momentum and gets weaker (Muraleedharan *et al.*, 1995). During the period the surface current were weak (Cutler and Swallow, 1984; Shenoi and Shetye, 1988), hence the vertical transport becomes weaker which leading to a strong undercurrent.

4.4. Winter monsoon

4.4.1. Hydrography

In December, the winds are predominantly northeasterly with occasional westerlies. The magnitude of the winds on an average was around 5m/s and relatively strong winds (>6m/s) blow along 17°N and 21°N.

The distribution of SST, SSS, MLD and nitracline are presented in Figure 4.8, for the various transects. The SST in the study region varied between 25.5 and 29.2°C, having colder water along the northeastern and warmer water in the southeastern Arabian Sea. SST was 29.2°C at 8°N and showed a steady decrease northwards to a value of 25.2°C at 21°N. During the season, the coastal and open ocean variability of SST appeared to be a minimum. The most conspicuous feature in the SSS distribution is the occurrence of low saline waters (<33psu) along the southwest coast of India, the lowest value (32 psu) was observed along 8°N, while the open ocean waters recorded relatively high salinity (>36.2 psu). In general, the SSS increased northwards and the maximum (~36.7 psu) was observed along 21°N. MLDs along the eastern Arabian Sea ranged from 15m at 8°N to 75m at 21°N and shallow MLDs were observed in the region where the SSSs are quite low. In general, MLDs were moderately deeper (>50m) except at a few coastal stations and the deeper MLDs were observed along 17°N and 21°N. Unlike the previous seasons for which the barrier layers were not significant, the barrier layer was thick in the regions of low saline waters along the southwest coast, while north of 15°N the layer thickness was negligible. The nitracline was observed well below 60m in the region of low saline BOB waters. However, shallow nitracline (~40m) was observed along the northwest coast.

Vertical thermal structure along 8°N and 10°N showed warm (>29°C), and relatively deeper (>60m) isothermal layer (Figs 4.9a, 4.9b). High surface salinity waters in the offshore and low saline surface waters near the coastal region were characteristic of the salinity structure. The low saline waters from the BOB, spreads near the coast in the surface layer (~20m) and below which, the salinity showed maximum gradients. In general, the offshore spreading of low saline BOB waters narrows towards north. Along 8°N, the offshore spreading of low saline

waters can be seen to be about 500km from the shore, whereas along 10°N, it is limited offshore by about 120 km from the shore. The vertical density distribution showed the occurrence of lighter waters along the shelf and denser waters offshore. The density structure mainly reflects the effects of salinity in the surface layer and stratification near the coastal region. Below 50m, density structure exhibited combined thermohaline effects.

Vertical sections of temperature along 13°N and 15°N could also indicate the downwelling process (Figs. 4.9c, 4.9d). Gentle downsloping of isolines towards the coast was clearly seen in the upper 200m. It is interesting to note that the low saline waters near the coast showed marked increment from the previous transect (10°N). Along 13°N, low salinity waters (35.2 *psu*) was observed almost close to the shore, while along 15°N, low saline waters are hardly visible and the salinity low of 35.8 *psu* was observed near the coast. The horizontal and vertical gradients in the upper 50m appeared to be relatively minimum in the two transects, suggesting the absence of low saline BOB waters in these transects, as compared to the previous transects. The high salinity tongue towards the coast suggested the protrusion of ASHSW and was modified in the coastal region by the low saline waters. In general, the density structure indicated the dominance of temperature over salinity in the density field, except in the upper 50m depth near the coast. The density distribution showed a deeper mixed layer with lighter waters nearshore and denser waters offshore. The vertical thermal structure along 17°N, showed relatively deeper isothermal layer (>60m) (Fig. 4.9e). ASHSW was well discernible from the salinity structure as a protrusion of high salinity towards the coast. Another high salinity pocket (~36.2 *psu*) was observed immediately below the ASHSW in the depth range of 80 to 120m. The sigma-t structure mainly reflects the combined effects of thermohaline structure in the upper 75m depth, below which the temperature controls the density. The isopycnals in the upper 120m showed downsloping towards the coast, which indicates the downwelling process.

Unlike the previous transects, thermal structure along 19°N showed the upsloping of isolines towards the coast in the upper 100m, below which the trend is reversed (Fig. 4.9f). The salinity structure also showed the presence of ASHSW as a high salinity tongue, but its extension is limited to the offshore region. Sigma-t structure in the upper 50m reflects the combined effects of temperature and salinity, below which the isopycnals followed the isothermal pattern.

Thermal structure along 21°N showed colder deep isothermal layer (Fig. 4.9g). The isolines in the upper layer did not show any significant features. Salinity structure showed the presence of ASHSW near the surface. The sigma-t distribution showed a weakly stratified mixed layer extending up to 70m, below which the isopycnals resembled the isothermal distribution.

The biological production showed remarkable difference between northwest and southwest coast (Table 4.1). The integrated PP ranged from 141 to 1854 mgC m⁻² d⁻¹, having an average value of 238 mgC m⁻² d⁻¹ in the southwest and 1262 mgC m⁻² d⁻¹ in the northwest coasts. Similarly, the chlorophyll *a* values ranged from 4.1 to 82.4 mg m⁻², having average values of 10.1 (southwest coast) and 53.4 mg m⁻² (northwest coast). Highest PP and chlorophyll *a* were recorded at 21°N: 69°E (open ocean waters off Veraval), which was about 7-8 folds higher than that of the respective values in south.

4.4.2. Discussion

During the season, the northwest and southwest coasts of India exhibited two contrasting scenarios. Along the southern transects, sea surface exhibited comparatively warm and low saline features, but the surface waters in the northern transects exhibited cool and high saline nature. The observed low saline waters along the southwest coast of India could be attributed to the intrusion of Bay of Bengal waters. During winter, the coastal current along the east coast, the (East India Coastal Current) EICC flows equatorward and carries low saline Bay of Bengal waters, which turns around Sri Lanka and continue to flow as west India coastal current (WICC) in AS towards north.

Vertical structure of temperature and density along the west coast of India showed the downsloping of isotherm and isopycnals towards the coast indicating the poleward coastal current and downwelling processes. The dynamic topography of 10db surface with reference to 500db inferred from the hydrography also suggesting the poleward coastal current along the west coast of India (Fig. 4.10). The dynamic topography showed a high in the southeastern AS which is the well-known Laccadive high. This anticyclonic circulation around the Laccadive high spreads the low saline BOB waters along 8°N and is clearly seen about west of 72.5°E from the shore. Many have been reported the dynamics and flow pattern of this Laccadive high (Bruce *et al.*, 1994, Shankar and Shetye, 1997). The presence of coastal current along the southwest coast of India can also be inferred from the intrusion of low saline waters from the BOB. The existences of the downwelling process and the poleward flowing coastal current have been reported earlier. Darbyshire (1967) observed that along the continental shelf off Kerala coast, the northward flowing current sets after the withdrawal of the southwest monsoon and also she called November – January, the season of sinking because the isotherms sink on approaching the coast. Banse (1968) pointed out that the mean sea level along the coast rises sharply from October to November during the change from southward to northward flow. Johannessen *et al.* (1981) pointed out that in November and December the coastal flow reverses from a narrow, shallow southward current to wide, deep northward flow having larger transport. Shetye *et al.* (1991) observed the poleward coastal current along the west coast of India, to be wide along the southwest coast and narrow towards north. They concluded that the driving mechanism for this current is the alongshore pressure gradient, which overwhelms the winds during the northeast monsoon. But the investigation over the last few years discussed the role of remote forcings (by way of Kelvin and Rossby wave propagation) on the dynamics of the processes in the southwest coast of India (Yu *et al.*, 1991; McCreary *et al.*, 1993; Bruce *et al.*, 1994; Shankar and Shetye, 1997). They found

that the Kelvin waves propagate along the perimeter of the BOB contributing the dynamics of EICC, WICC and Lakshdweep high. From the analysis of hydrography along each transect off the west coast of India, it was found that the presence of low saline waters from the BOB waters was hardly visible north of 13°N. According to Hareesh Kumar and Mathew (1997), the maximum of northward extension of the low saline BOB water is about 12°N in January. The low saline BOB waters are well discernible in the two transects along 8°N and 10°N. This provides the strong stratification near the surface along the southwest coast of India, which overwhelms the expected deeper MLD owing to the downwelling processes. However, along 13°N and 15°N, where the appearance of BOB waters is hardly seen, signatures of the downwelling process occurred, as deep and warm nutrient depleted mixed layer. But in the northern transects, the hydrographic fields indicated the active winter cooling processes. The ASHSW, the PGW and the RSW make the northern AS high saline. The cool and dry continental air brought by the prevailing northeast trade winds enhance the evaporation in the northern AS which leads to the surface cooling and initiates the convective overturning. This was clearly seen along 17°N and 21°N as a weakly stratified cold and deep mixed layer. The deepening of mixed layer from south to northern latitudes coincided with the intensification of winter except at the coastal station along 19°N where shallow MLD (~30 m) was observed and this could be due to the low winds (~4 ms⁻¹) prevailed in that region. Similarly, comparatively low MLD was observed at 17°N:70°E where wind speed was low (<4 ms⁻¹). These observations indicate that at the initial phase of winter, the entrainment was mainly initiated by the surface cooling and the wind stirring. In the northern AS, in general, the presence of nitracline in the upper 50m water column is a clear indication of convective mixing mechanism operating in the region. The resultant high chlorophyll *a* (average- 47.5 mg m⁻²) in the northern AS is attributed to high nutrient concentration by convective mixing. Highest column PP (1854 mg C m⁻² d⁻¹) and chlorophyll *a* (82.4 mg m⁻²) observed at the station in the northernmost

latitude (21°N:69°E) coincided with the deepest MLD (~80 m). Relatively low integrated chlorophyll *a* and PP (average-chlorophyll *a* 22 mg m⁻², average- PP 551 mg C m⁻² d⁻¹) observed along 19 °N in AS correspond with the low MLD in that transect.

Deepening of the mixed layer as a result of cooling and sinking of surface waters under winter conditions is common in temperate and polar waters. However, nutrient input to the upper water column arising from these processes does not translate into production in high latitudes, until spring when light becomes available. Since light is not a limiting factor in the upper layers of the AS, it immediately results in higher primary productivity. Many workers have reported winter convection and associated enhanced production in the northern AS (Banse, 1987; Bauer *et al.*, 1991; Madhupratap *et al.*, 1996; Prasanna Kumar *et al.*, 2001b).

4.5. Summary

Along the west coast of India, a surface salinity gradient occurs throughout the year and was particularly high in southern transects. This gradient was apparently high immediately after the southwest monsoon, which brings most of the freshwater influx into the region. During northeast monsoon the hydrography was by the low saline water intrusion from BOB and the eastern equatorial region into the southwest coast of India. The ASHSW was evident along the west coast of India, throughout the region, but its onshore spreading was always restricted by the prevailing low saline waters and the along shore coastal current. In general, along the southern transects (south of 13°N) from May to October, ASHSW was found at 50 to 100m depth, and after the retreat of southwest monsoon, this watermass is seen at the surface. North of 13°N, the ASHSW was always observed in the upper 100m, except during summer, when it moved into the subsurface levels of 50 to 100m. The upwelling along the southwest coast starts even as early as February – March in deeper layers and upwelled water gradually reaches the surface by May/June. The upwelling ceases along the northwest coast

of India by September, while it persists even in October along the southwest coast of India and by December, the downwelling/sinking occurs all along the west coast of India. Relatively weak poleward undercurrent during May/June and strong poleward undercurrent during September/October can be linked to the strong and weak upwelling processes. It should be noted that the season covered in the present study do not represent the peak of southwest monsoon. However, the PP and chlorophyll *a* values obtained in the present study are apparently higher than that obtained during the peak of southwest monsoon. The PP and chlorophyll *a* values obtained from the intense upwelling region (coastal region off 8°N) during the two upwelling periods (May and June) are respectively 9144 mg C m⁻² d⁻¹; 203 mg m⁻² and 1629 mg C m⁻² d⁻¹; 44.7 mg m⁻². Whereas during the peak of southwest monsoon (July-August), the Indian JGOFS reported active upwelling off Mangalore and the corresponding PP and chlorophyll *a* values 1760 mgC m⁻² d⁻¹ and 88 mg m⁻², respectively. Similarly, the present study made during the winter represents the initial phase of the northeast monsoon period (29 November - 5 January 2000). However, the comparison between the average integrated chlorophyll *a* and PP obtained during the present study (chlorophyll *a* 47.5 mg m⁻² and PP 1114 mgC m⁻² d⁻¹) with Indian JGOFS (chlorophyll *a* 34.4 mg m⁻² and PP 870 mgC m⁻² d⁻¹) showed that the former average is much higher than the latter. The Indian JGOFS was conducted during late winter monsoon (3 February - 4 March 1994). Hence, the present study showed that, since light is not a limiting factor in AS for primary production, the high primary productivity occurred at the initial phase of upwelling and winter cooling itself. Moreover, it can be seen that, winter cooling generated PP values as high as 1854 mgC m⁻² d⁻¹ at the northernmost latitude, which is higher than the production (1629 mgC m⁻² d⁻¹) of southwest coast of India, during southwest monsoon (upwelling period) and suggest that winter production in the northern AS is roughly of the same magnitude as the summer production in the south.

Shallow mixed layer can evolve in two ways. Under warm and light wind conditions (spring intermonsoon and fall intermonsoon), the surface layer becomes more stable which inhibits the vertical mixing and thins the mixed layer. As a result, the entrainment of nutrients to the surface is not possible and makes deep nutrient depleted surface layer and eventually poor biological production. The intense forcing during the southwest monsoon drives the upwelling along the southwest coast resulting in a shallow MLD. But the effect of offshore Ekman transport and associated Ekman pumping brings the nutrients in to the surface and the region becomes highly productive. Deeper MLDs also evolves in two ways. During winter, along the northwestern Arabian Sea, the high rate of evaporation leads to surface cooling and densification; its subsequent sinking initiates the turbulence and the development of deep mixed layer. The entrainment of nutrient rich thermocline waters during mixed layer deepening drives high biological production. On the contrary, the wind-induced downwelling along the southwest coast drives the surface waters to converge near the coast, which results in a deep mixed layer, often devoid of nutrients and consequently the region becomes less productive. It is thus found that the mechanisms for the development of MLD may also play an important role in the biological production.

4.6. Hydrological structure

It is well known that light and nutrients are important for the primary production in the ocean. In the tropical situation, the nitracline divides the euphotic layer into two layers; the upper layer, which is nutrient limited and the lower layer with light as the limiting factors. In such situations the subsurface chlorophyll maxima were observed at a depth, where the light and nutrients are optimum. Herbland and Voituriez (1979) have identified a typical tropical structure (TTS) of an ecosystem in the euphotic layer in the tropical Atlantic Ocean. They found that TTS has the characteristic of statistically same depths of the nitracline, oxycline and chlorophyll maximum. Besides, there was a relationship between the depth of the nitracline and the depth of the maximum

thermal gradient. Usha and Muraleedharan (2000) have identified the TTS in the tropical Indian Ocean for certain seasons and regions. In this section, an investigation is made to examine whether a TTS exists or not in the Arabian Sea. The inter-relationships between MLD, the maximum thermal gradient, nitracline, oxycline and chlorophyll maxima are examined.

Figure 4.11a presents the relationship between MLD and SST, for all the seasons. In general, MLD and SST have an inverse relationship. Shallow mixed layers were often associated with warmer surface waters, which was evident during intermonsoon (spring and fall) and summer monsoon seasons. Surface warming stabilizes the surfaces and the momentum transfer from atmosphere to ocean becomes less significant for providing the degradation of the mixed layer. During winter the surface cooling ($<27^{\circ}\text{C}$) in northern AS destabilizes the surface layer, which initiates the turbulence for the convective mixing and eventually builds up a deeper mixed layer. But there were few exceptions during which the SST was found to decrease with shallow MLD during upwelling in the summer and an inverse relationship during downwelling in the winter, in the coastal regions. In general, the SST can be taken as the surface expression of MLD. It is interesting to note that high thermal gradients were characterized by shallow mixed layer and vice versa (Fig. 4.11b). Scatter plots of the depths of the nitracline against the depths of the maximal thermal gradient are plotted in figure 4.11c, with a linear regression equation: $D_{\text{NO}_3} = 0.85 * D_{\text{GTmax}} + 9$. The correlation coefficient was found to be positive and significant ($r = 0.82$, $p = 0.99$). From the above equation, it was determined that when the depth of maximal thermal gradient was less than 60m, the level of nitracline is statistically below the level of the maximum thermal gradient. When it is greater than 60m the nitrate crosses the barrier of stability. Figure 4.11d reveals that the top of the nitracline is coinciding with the first level of under saturation in oxygen (D_{ox}), with a linear regression equation: $D_{\text{ox}} = 0.64 D_{\text{NO}_3} + 8.1$. The correlation coefficient was found to be positive and significant with a very high coefficient of correlation ($r = 0.87$,

$p = 0.99$). Since the samples were collected at discrete depths, it was difficult to determine the exact depth of the chlorophyll *a* maxima. However, it was observed that the subsurface chlorophyll *a* maxima displayed a positive relationship with the nitracline (Fig. 4.11e). An inverse relationship was seen between the depth of the chlorophyll maximum and the integrated chlorophyll value (Fig. 4.11f). Since the chlorophyll *a* maxima and the nitracline are statistically at the same depth, the chlorophyll *a* values are expected to decrease when the nitracline deepens because of the lack of optimum illumination.

When the thermal gradient is high, a barrier of stability forms and NO_3 is not able to cross this barrier. In contrast, when the MLD is deeper, the thermal gradient decreases and NO_3 crosses the weak barrier and produces a shallow nitracline. Exceptions to the above pattern can occur. During winter, along the southwest coast, the low saline waters from the BOB leads to the formation of a thick barrier layer below the pycnocline, and nutrients are restricted to the deeper layer (below 60m). It can thus be concluded that the AS follows a TTS of the ecosystem in the euphotic layer, when the vertical advection is negligible, excluding upwelling and active convergence.

Table 4.1. Biological production (primary) in the eastern Arabian Sea during different seasons

Season	Primary productivity ($\text{mgC m}^{-2} \text{d}^{-1}$)			Chlorophyll <i>a</i> (mg m^{-2})		
	Range	station observed maximum	Physical processes	Range	Maximum	Physical processes
Spring intermonsoon	35-9144	8°N:77°E	upwelling	10-203	8°N:77°E	upwelling
Summer	179-1629	8°N:77°E	upwelling	8.7-44.7	8°N:77°E	upwelling
Fall intermonsoon	149-820	8°N:77°E	upwelling	8.8-39.1	19°N:70°E	-
Winter monsoon	141-1854	21°N:69°E	Winter cooling	4.1-82.4	21°N:69°E	Winter cooling

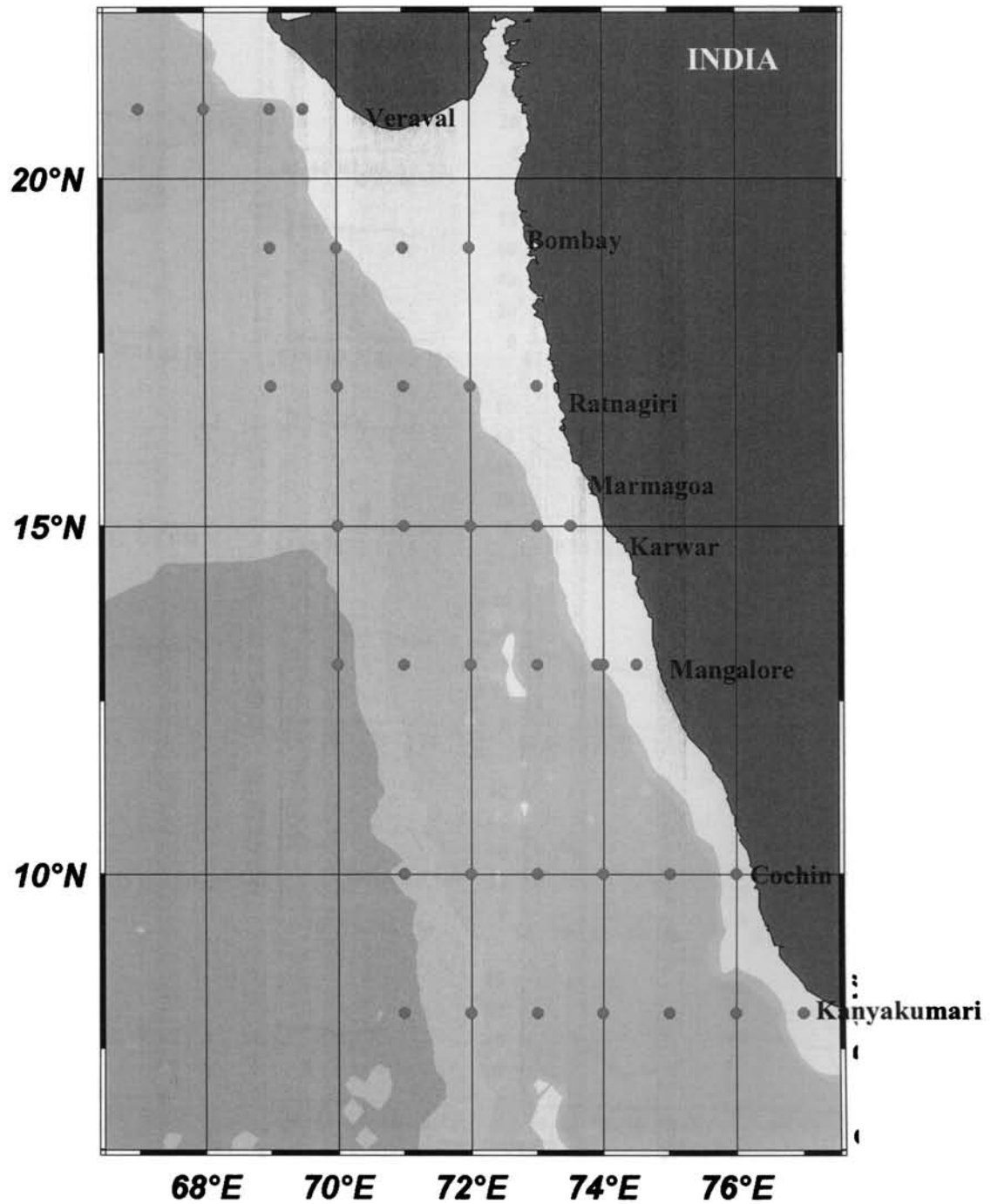


Figure 4.1. Hydrographic stations along the eastern Arabian Sea during the MR-LR programme

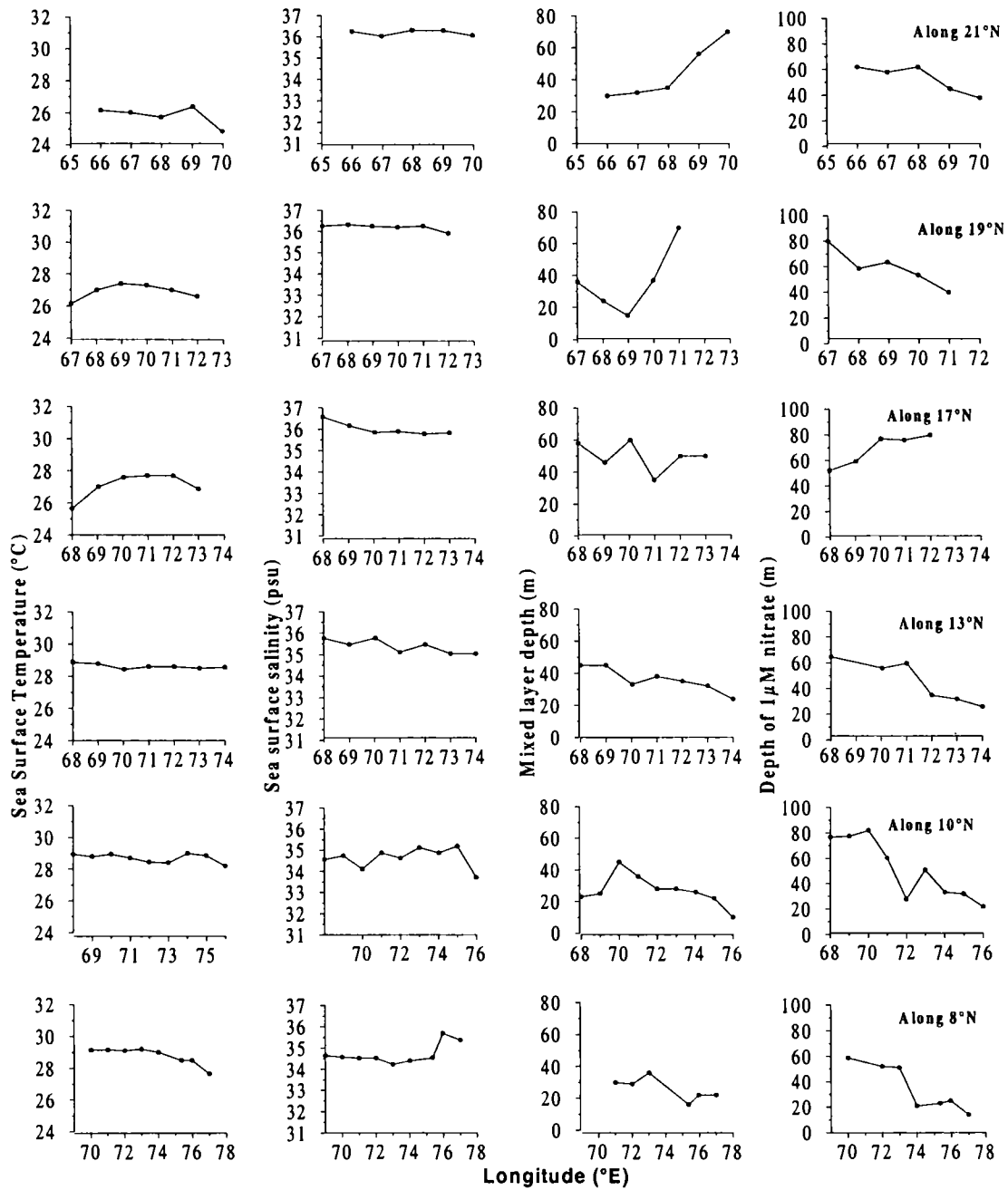


Figure 4.2. Latitude wise distribution of SST, SSS, MLD and the nitracline during spring intermonsoon in the eastern Arabian Sea

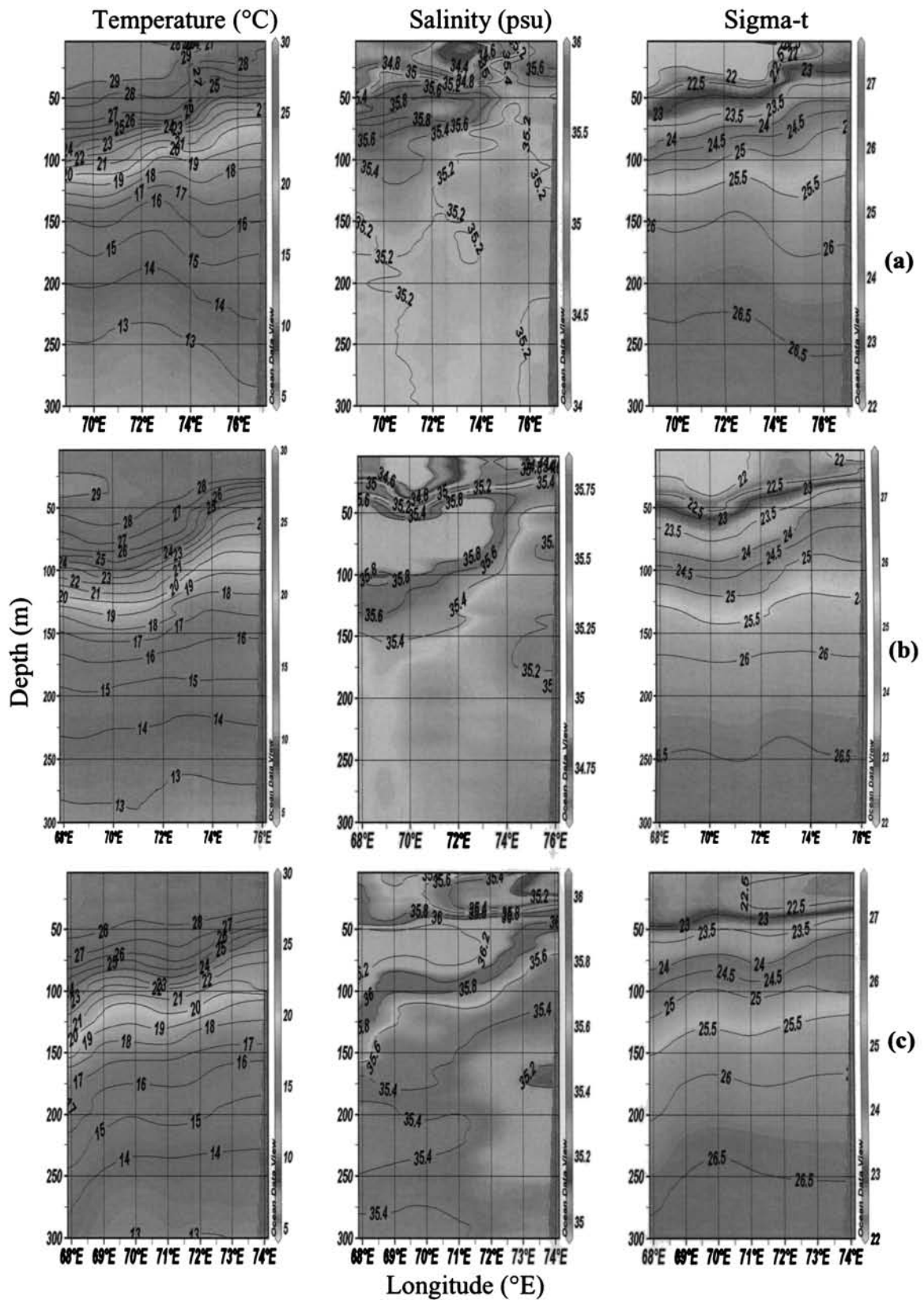


Figure 4.3. Vertical distribution of temperature, salinity and sigma-t along (a) 8°N, (b) 10°N, (c) 13°N, (d) 17°N, (e) 19°N and (f) 21°N during spring inter monsoon in the eastern Arabian Sea

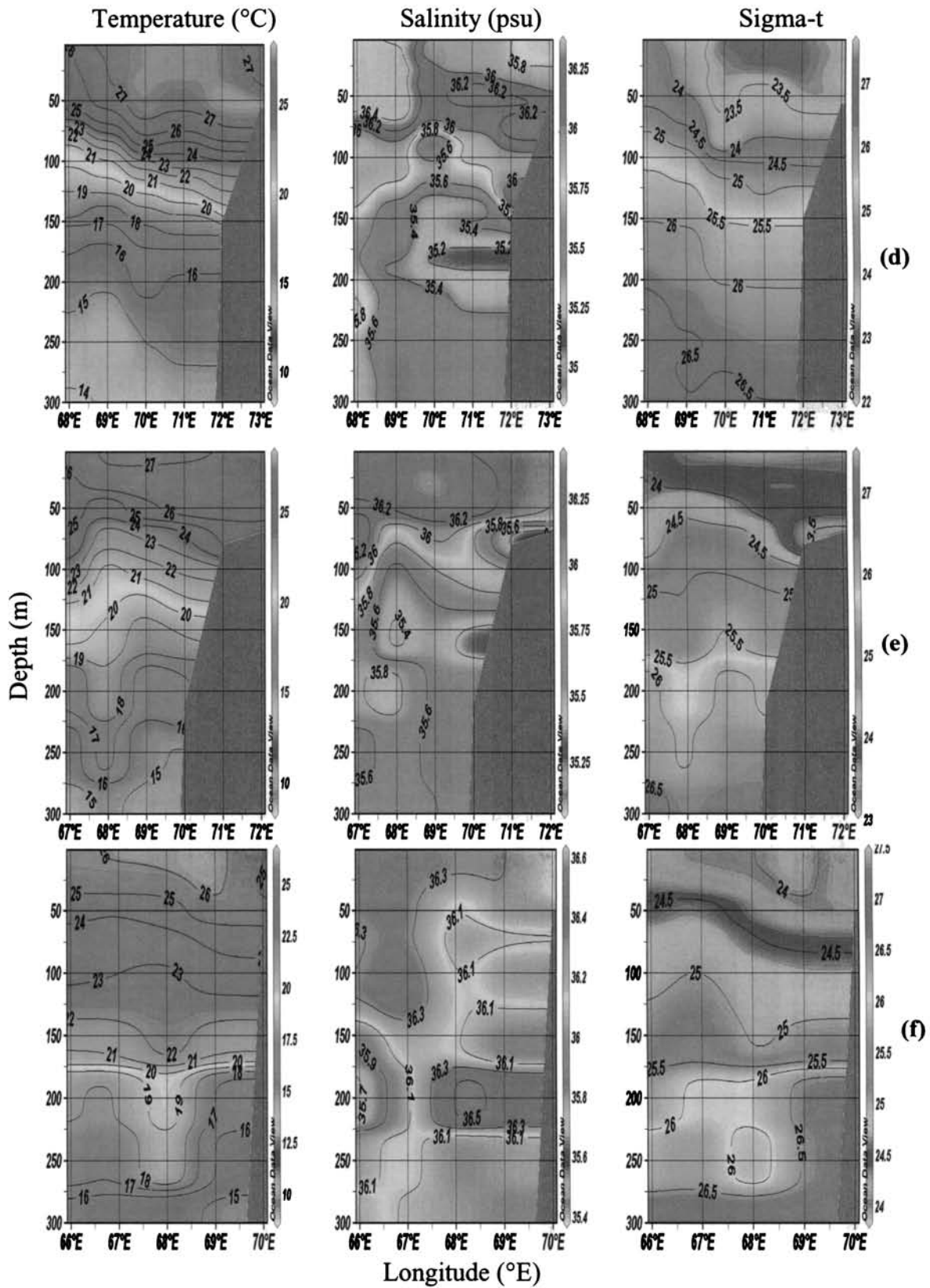


Figure 4.3. (continued)

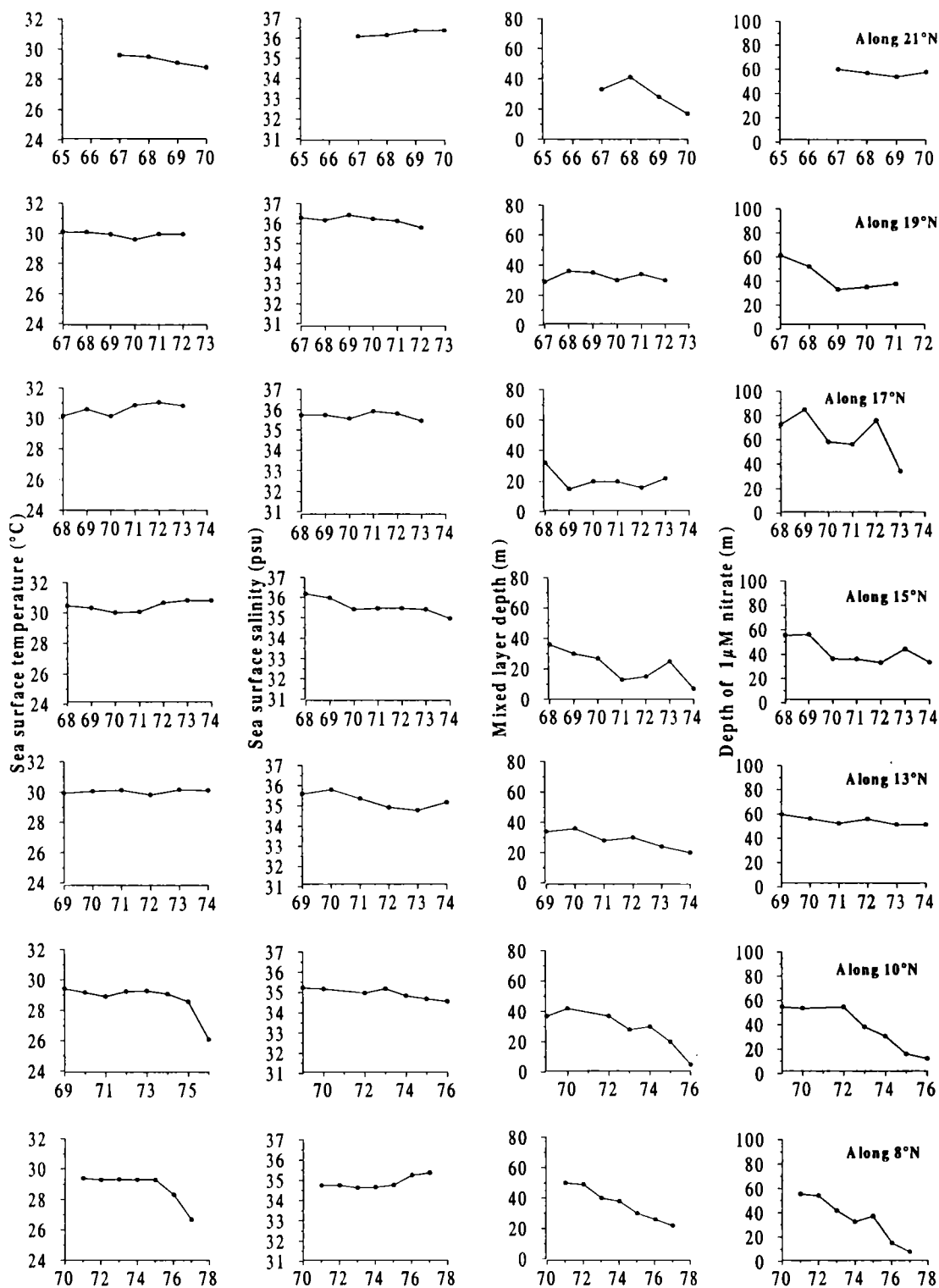


Figure 4.4. Latitude wise distribution of SST, SSS, MLD and the nitracline in the eastern Arabian Sea during summer monsoon

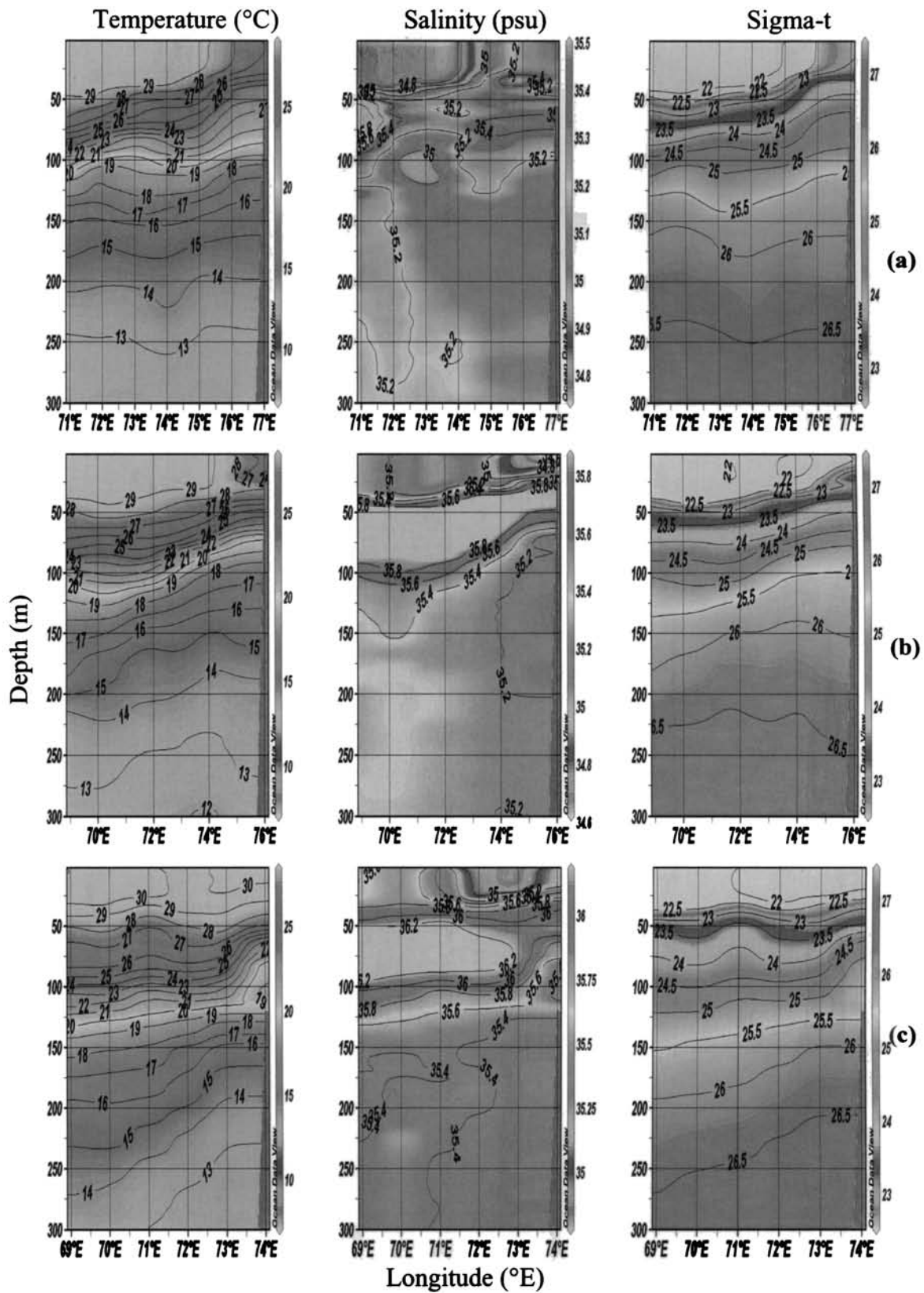


Figure 4.5. Vertical distribution of temperature, salinity and sigma-t along (a) 8°N, (b) 10°N (c) 13°N (d) 15°N, (e) 17°N (f) 19°N and (g) 21°N during summer monsoon in the eastern Arabian Sea

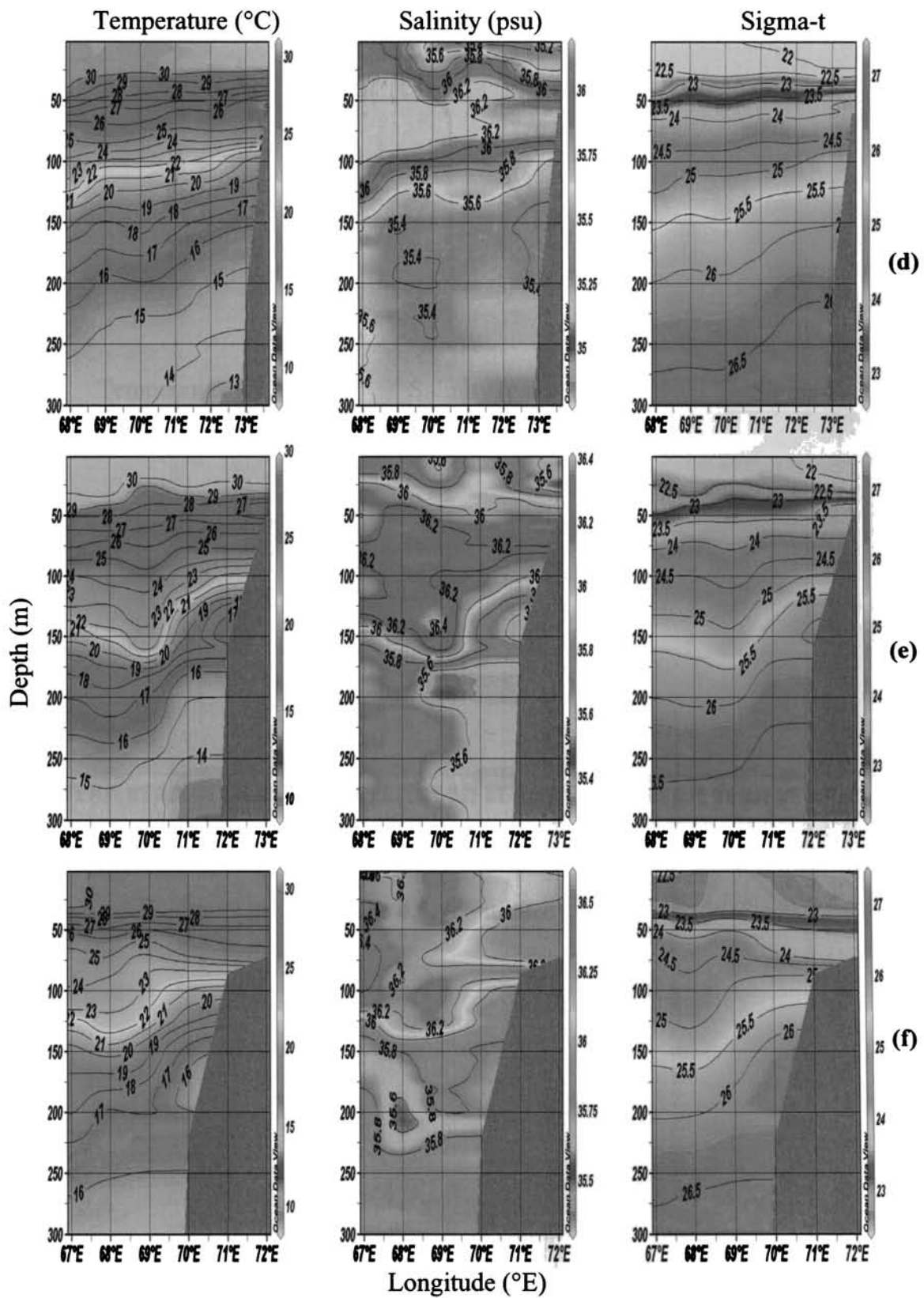


Figure 4.5. (continued)

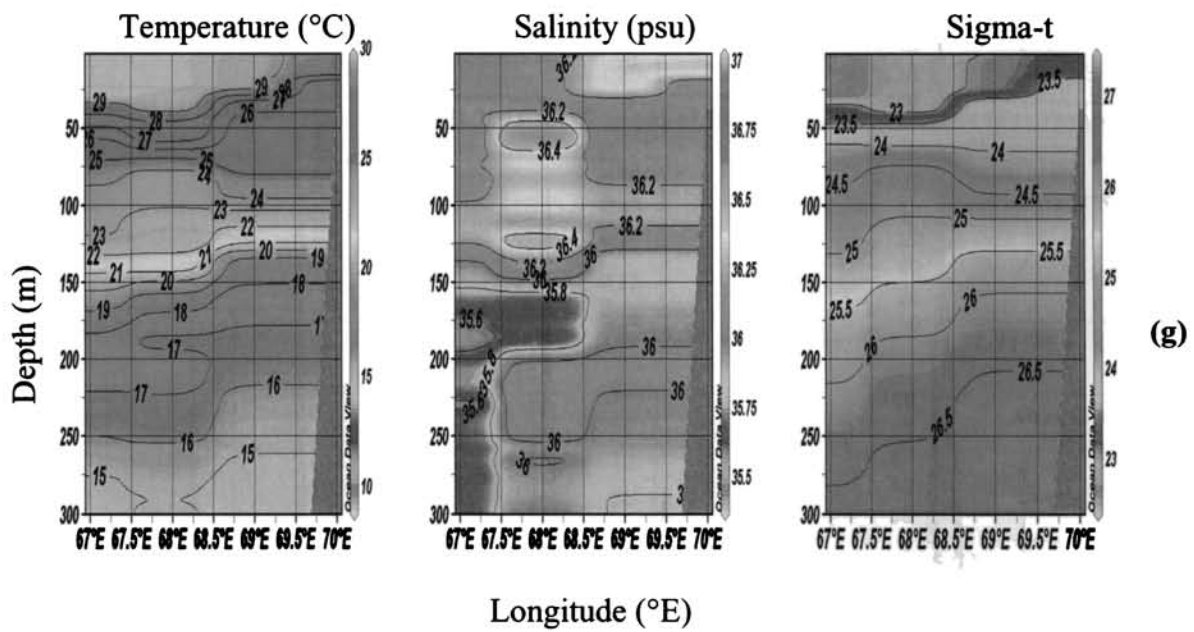


Figure 4.5. (continued)

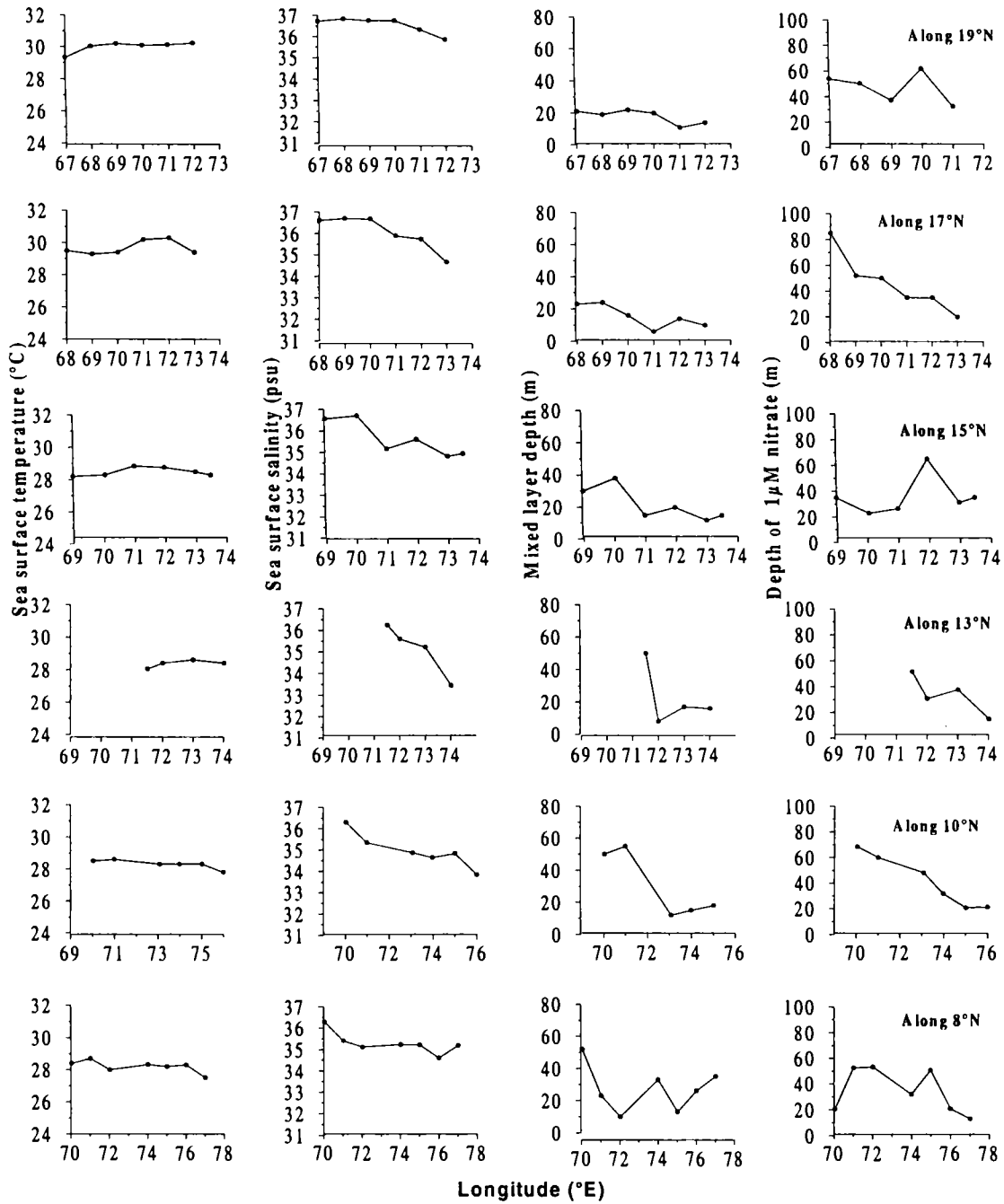


Figure 4.6. Latitude wise distribution of SST, SSS, MLD and the nitracline in the eastern Arabian Sea during fall intermonsoon

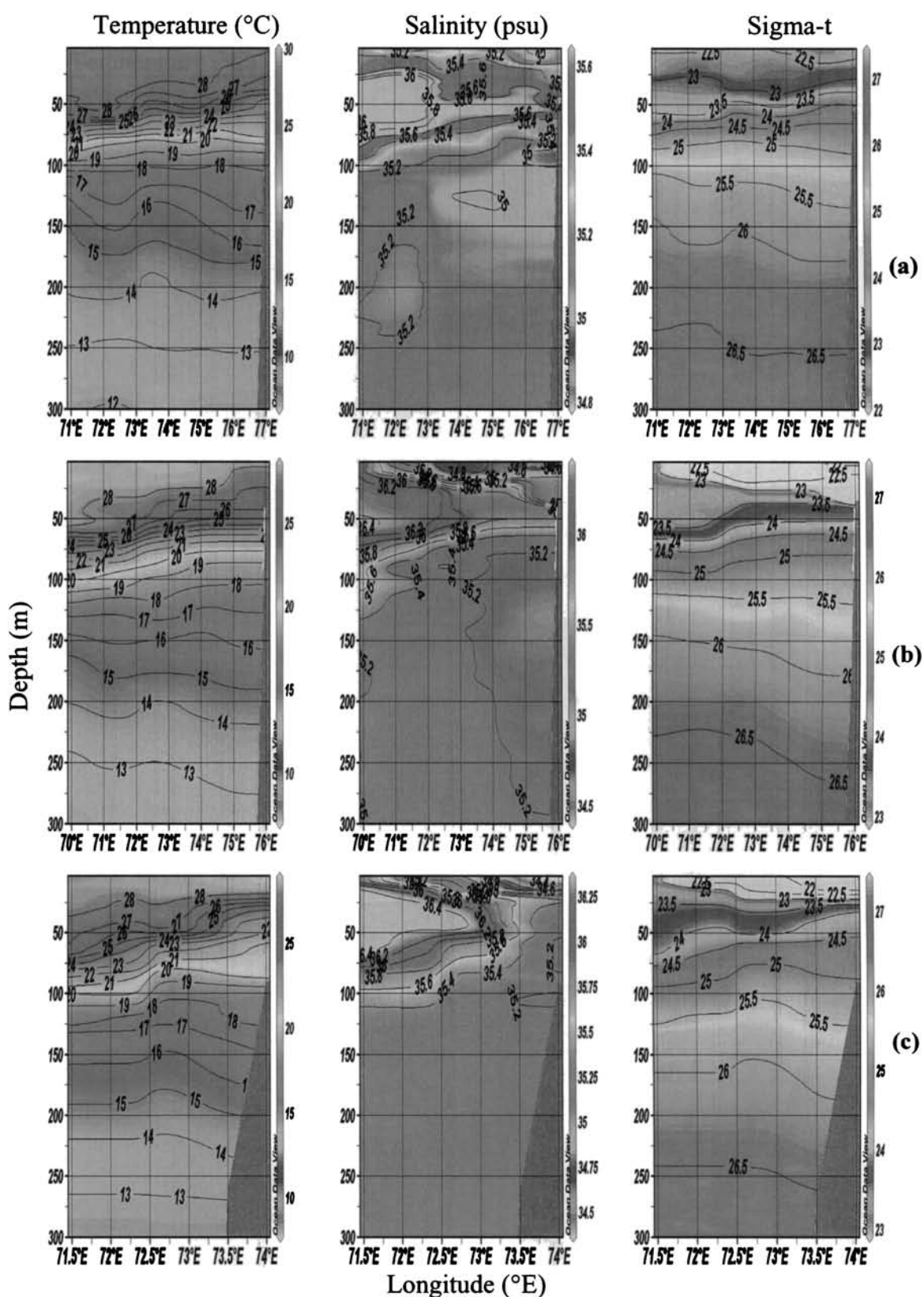


Figure 4.7. Vertical distribution of temperature, salinity and sigma-t along (a) 8°N, (b) 10°N (c) 13°N, (d) 15°N, (e) 17°N and (f) 19°N during fall intermonsoon in the eastern Arabian Sea

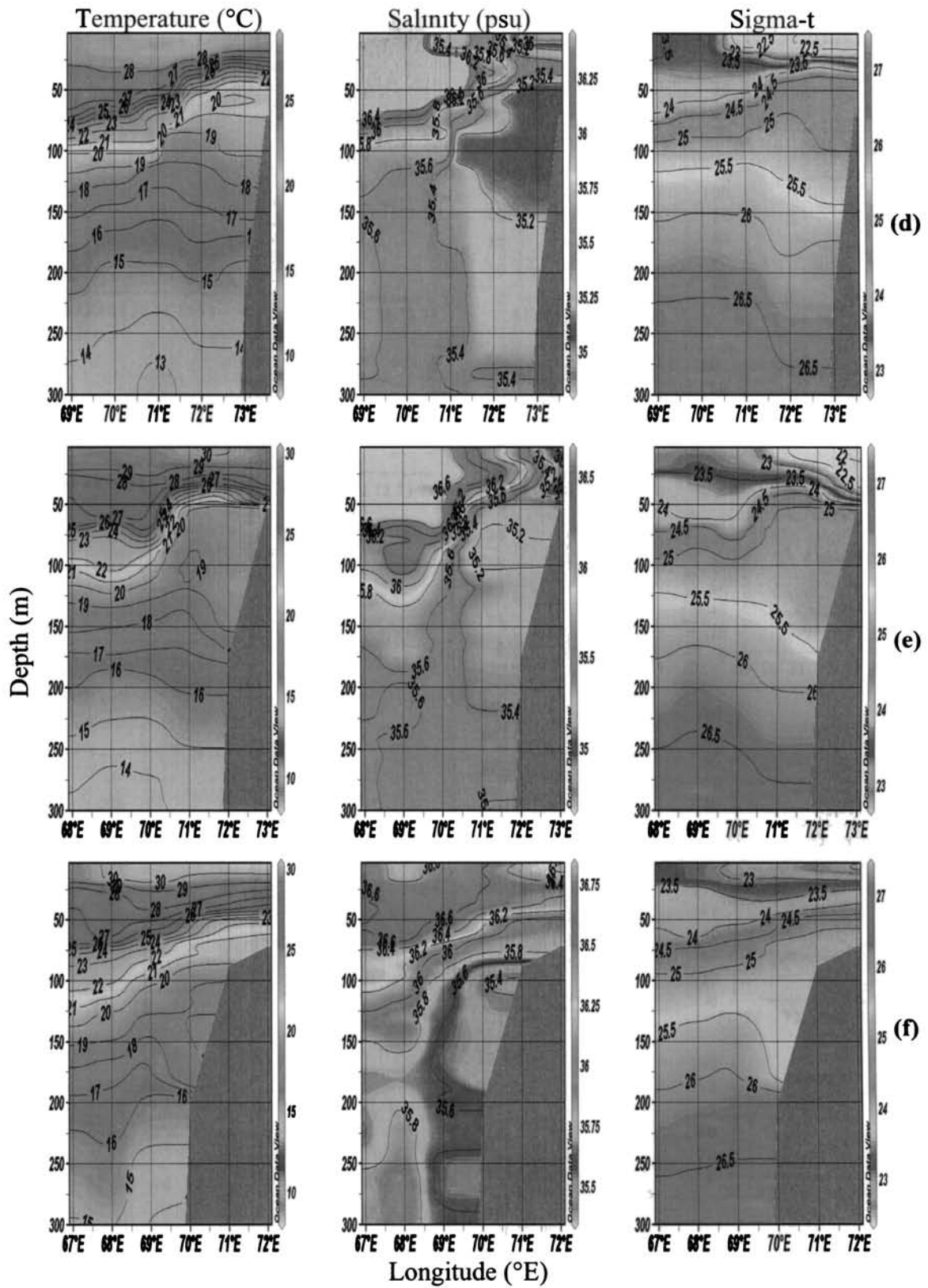


Figure 4.7. (continued)

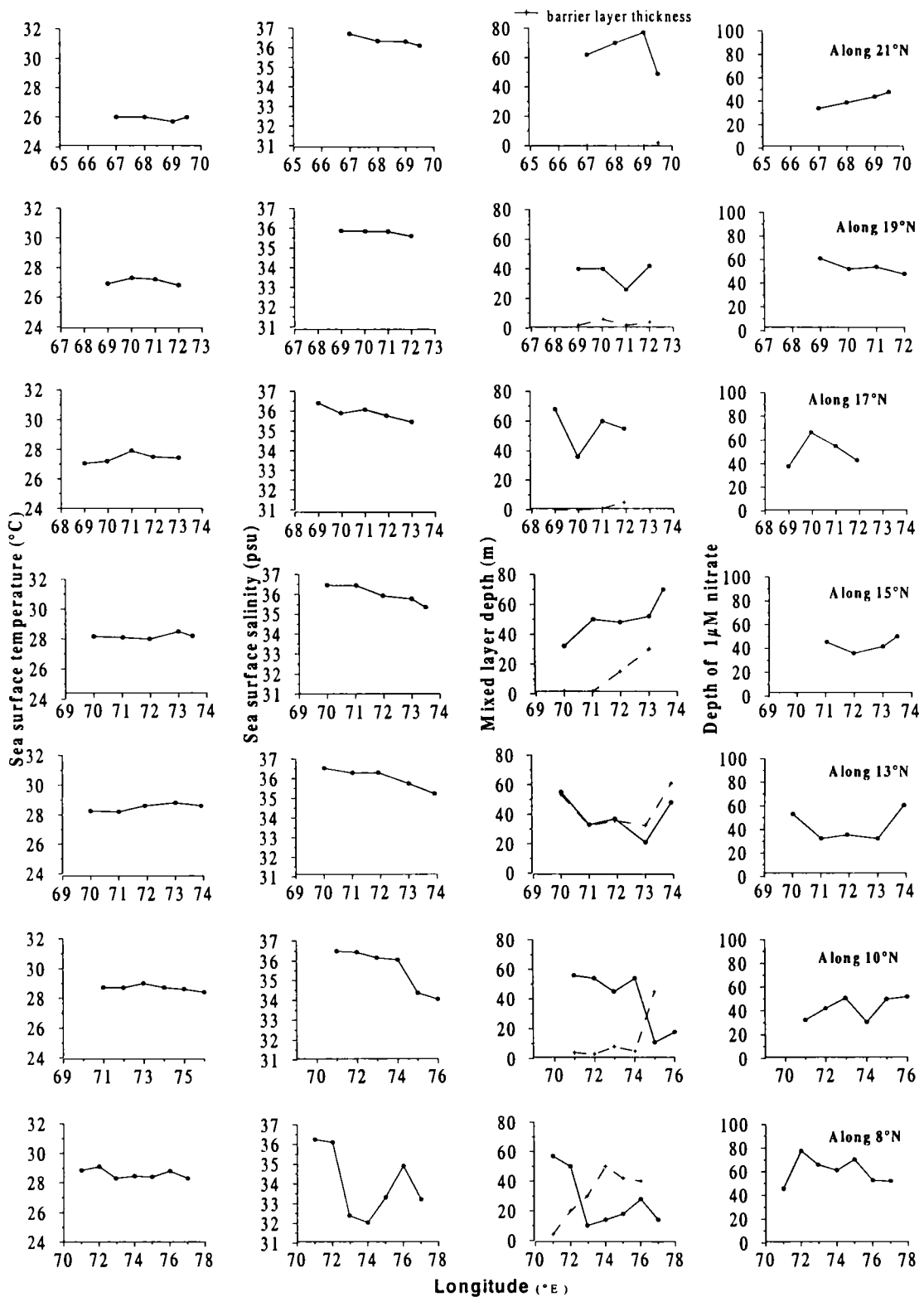


Figure 4.8. Latitude wise distribution of SST, SSS, MLD, barrier layer thickness and the nitracline in the eastern Arabian Sea during winter monsoon

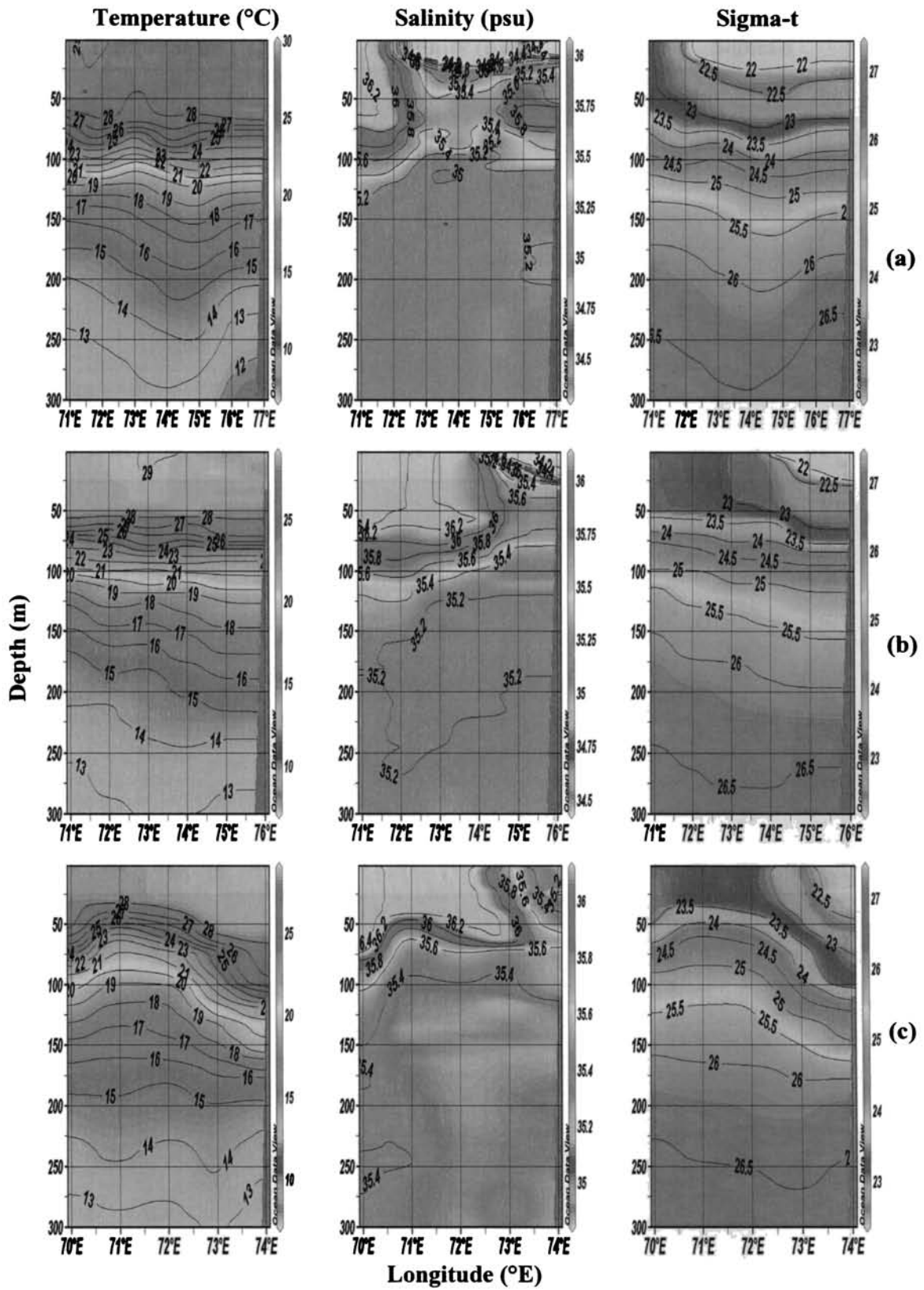


Figure 4.9. Vertical distribution of temperature, salinity and sigma-t along (a) 8°N, (b) 10°N (c) 13°N (d) 15°N, (e) 17°N (f) 19°N and (g) 21°N during winter monsoon in the eastern Arabian Sea

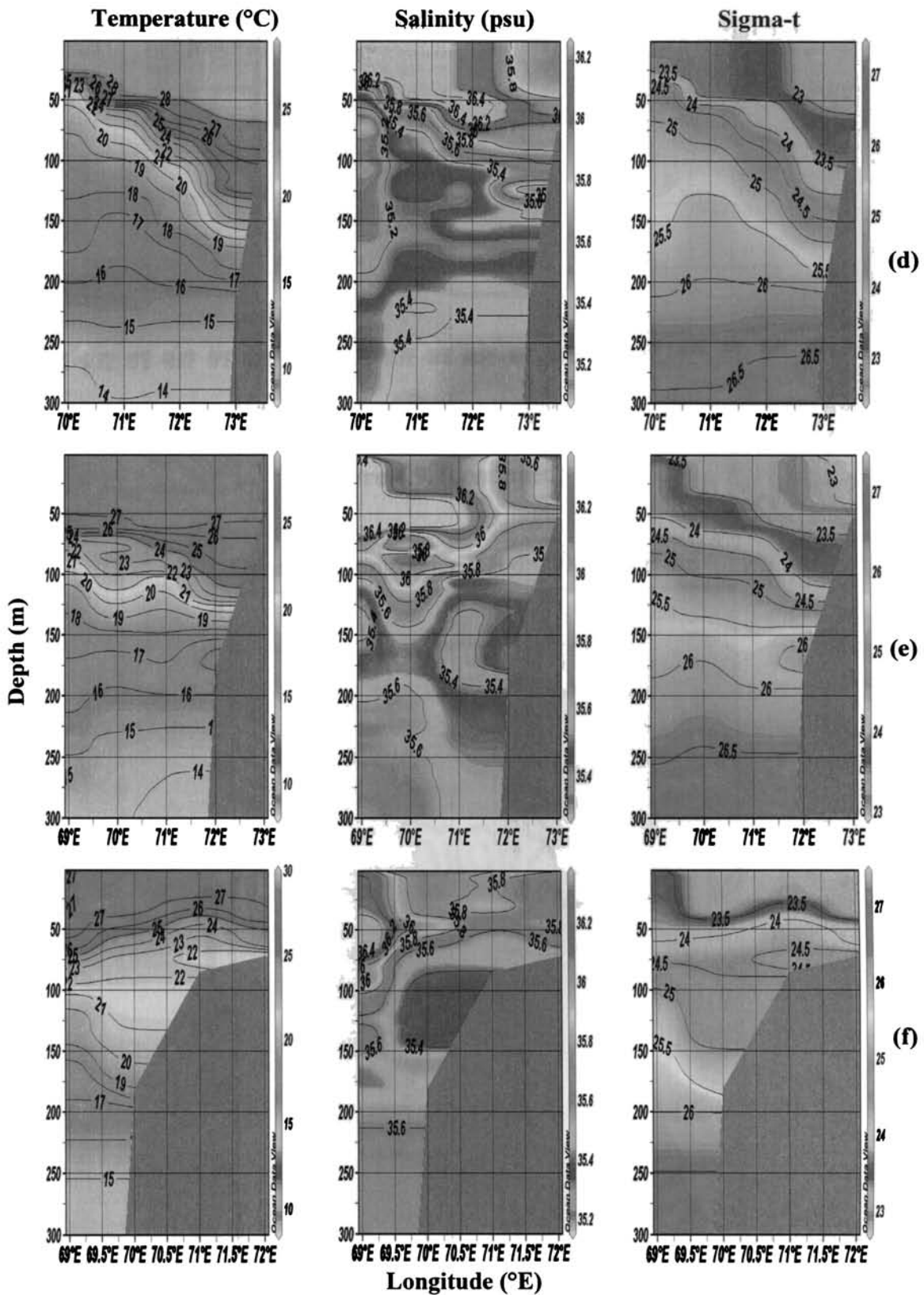


Figure 4.9. (continued)

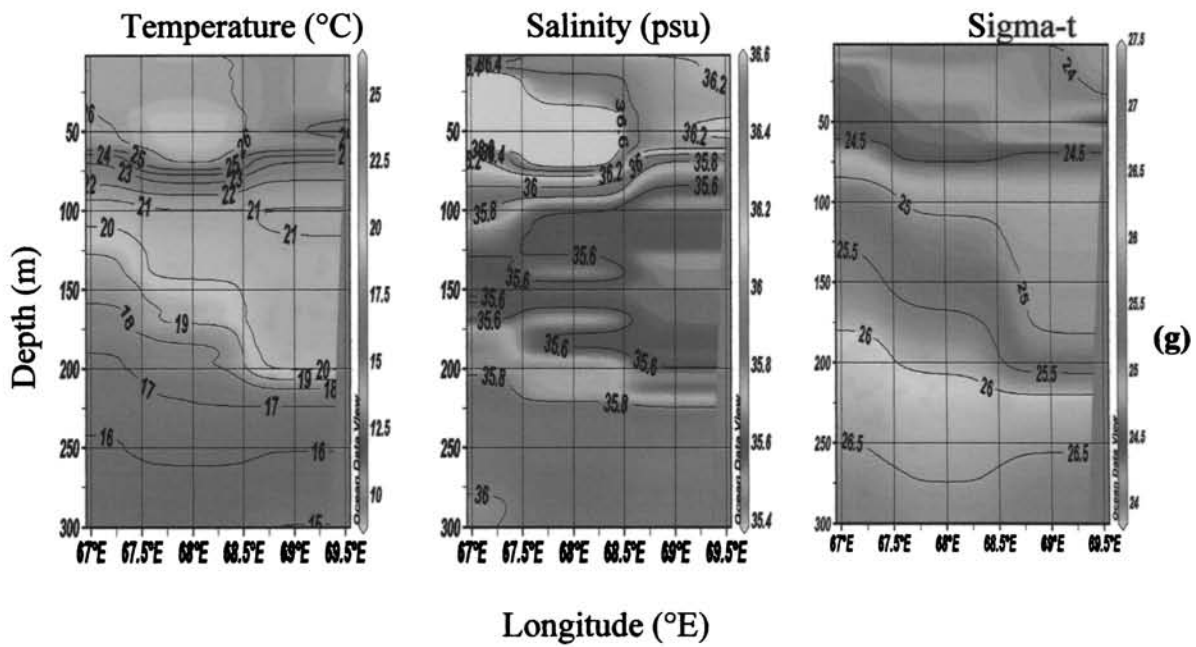


Figure 4.9. (continued)

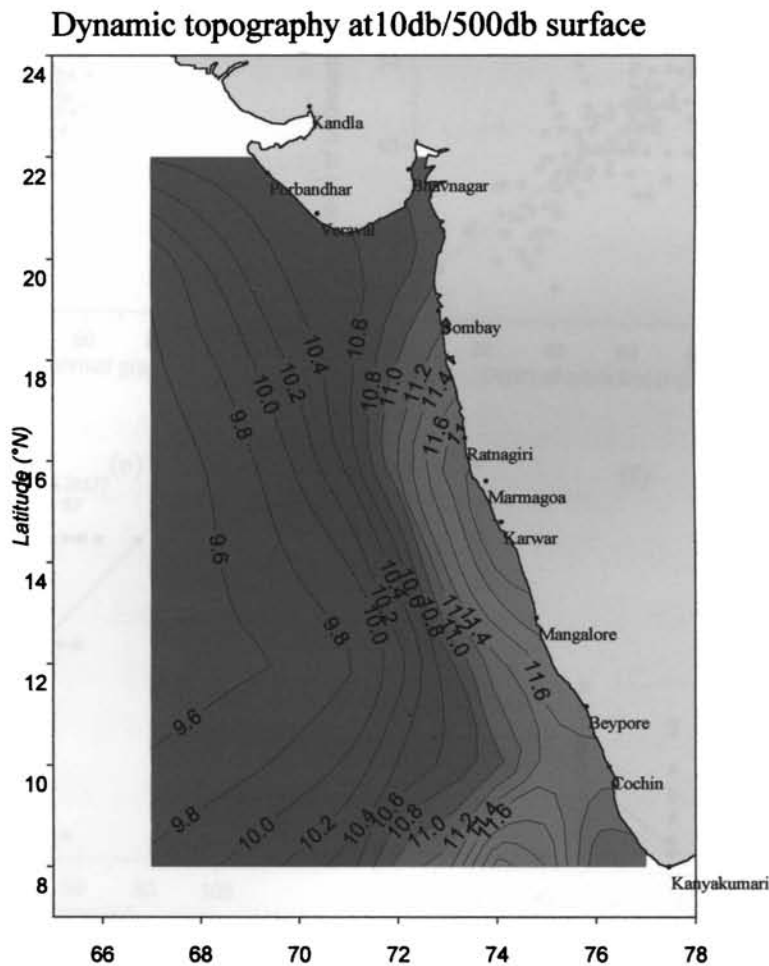


Figure 4.10. Dynamic topography at 10db surface with respect to 500db along the eastern Arabian Sea during winter

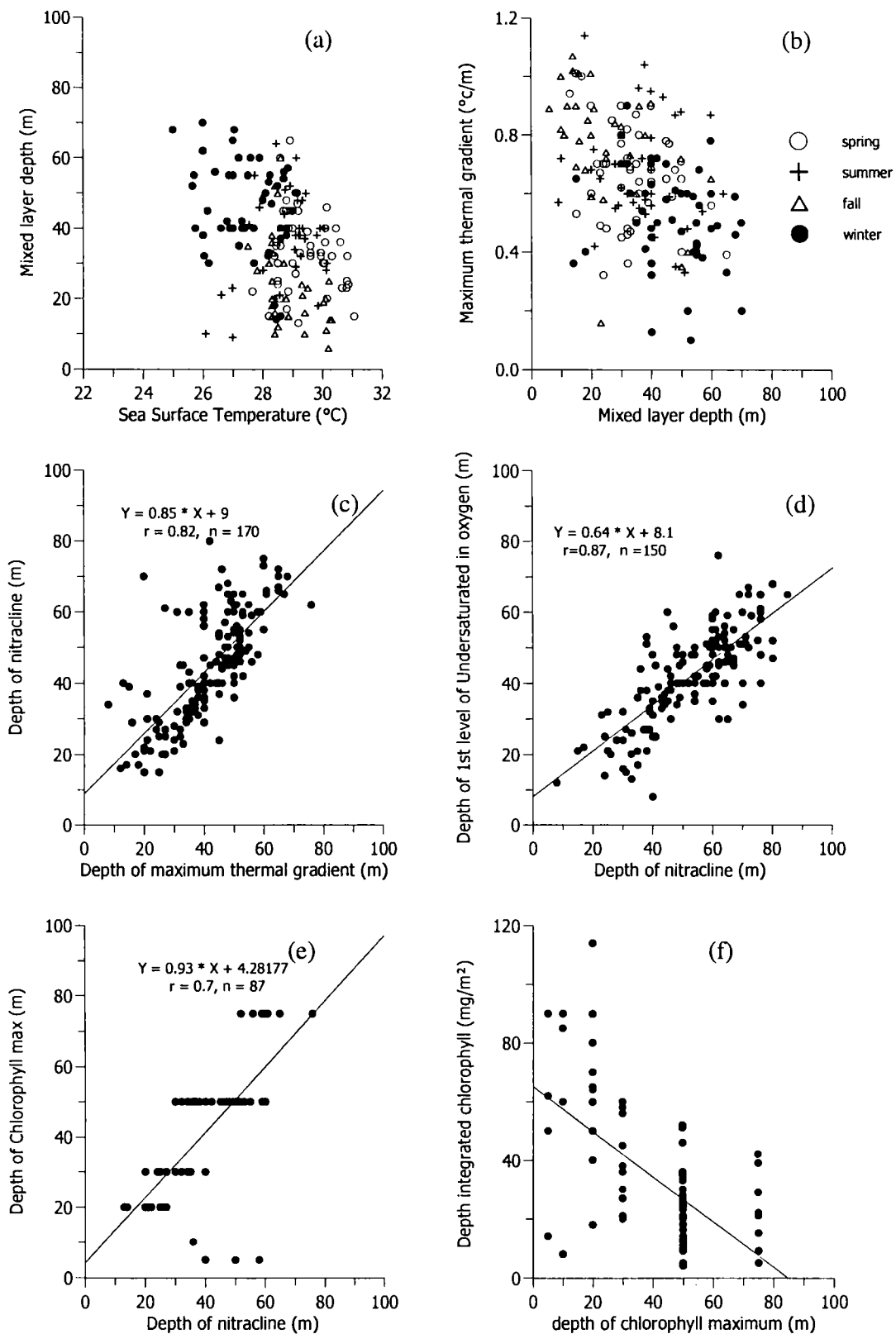


Figure 4.11. Relationship between the mixed layer depth and a) SST, b) maximal thermal gradient. Linear regression between the depth of the nitracline and c) depth of maximal thermal gradient, d) depth of first level of under saturation in oxygen e) depth of chlorophyll maxima. f) Relation between the depth of the chlorophyll maxima and the depth integrated chlorophyll

Chapter - 5

Hydrography off the western Bay of Bengal

In this chapter, the thermohaline characteristics of the upper 300m along the western Bay of Bengal and the physical forcings on biological production are addressed. The stations occupied during different seasons along 6 transects in the western Bay of Bengal are shown in Fig. 5.1.

5.1. Spring intermonsoon

The stations occupied in April along 6 transects, viz., 11°N, 13°N, 15°N, 17°N, 19°N and 20.5°N in the western Bay of Bengal are included in this season. The surface winds during April showed a steady flow from the southwest and the magnitude increases towards north. Strong south westerlies (>7m/s) were seen along 19°N and 20.5 °N.

5.1.1. Hydrography

The distribution of SST showed minimum spatial variability and ranged from 28.6°C to 30.3°C, having minimum near the coast off 15°N and maximum in the open ocean waters off 13°N (Fig. 5.2). SSS ranged from 32.8 to 34.3 psu and the minimum was observed along 15°N and maximum near the coast off 11°N. In general, low saline waters were observed between 100 –300km, away from the shore. The warm and less saline water provides stratified surface layer and hence the mixed layer was observed to be shallow (<30m). However, along 17°N, between 84°E and 86°E, comparatively deeper MLDs were observed (~40m). During the season, the barrier layer thickness was insignificant (<20m), except at a few stations. Thick barrier layer (>40m) was observed along 15°N and, in general, thick barrier layer was observed in the region of low saline plumes. The top of the nitracline was observed in 35 – 90m depths showing shallow nutrient depleted surface layer in north (along 20.5°N). In general, the upper 60m of the

western BOB was devoid of nitrate and the deepest nitracline (90m) was observed between 84 – 86°E along 17°N. Similarly along 19°N, between 86°E – 89°E, deeper nitracline (~75m) were observed.

The vertical section of temperature, salinity and sigma-t along the 6 transects are presented in Fig. 5.3. The vertical thermal structure and along 11°N and 13°N showed a warm surface layer (>30°C) (Figs. 5.3a, 5.3b). The low salinity pockets were observed in the surface layer about 220 to 400km away from the shore. In general, the salinity showed a steady increase with depth in the upper 120m, below which the salinity showed little variation. The isopycnals in the surface layer resembled the isohaline pattern, below which the isopycnals followed the isothermal pattern. The near shore values of SST along 15°N were relatively lesser (<29°C) than that of the offshore values (~30°C) (Fig. 5.3c). Compared to the previous transect, the pools of low salinity were observed much far from the coastal region (~400km from the shore). The salinity structure showed sharp gradients in the upper 120m, below which the gradients were minimum. The density distribution showed strong stratification at the surface and consequently a reduced MLD is seen. Occurrence of relatively denser water (~20.5) near shore and lighter waters offshore (~19.5) in the surface was seen. Isopycnals showed the dominance of salinity over the temperature in the upper 50m, below which temperature field dominates in the density.

The vertical thermal structure along 17°N exhibited warm surface isothermal layer, below which topography of isotherms showed a depression centred around 85°E (Fig. 5.3d). This feature was more conspicuous at 150m depth. Below the surface layer, salinity structure also showed the downsloping of isohalines towards 85°E. The low saline patches at the surface layer were observed about 300km from the shore. The isopycnals at the surface layer followed the same trend as the salinity, below which the density reflects the thermohaline effects and showed the downsloping of isolines towards the 85°E.

Though the downsloping was not as intense as seen along the 17°N transect, the temperature, salinity and sigma-t structure along 19°N also exhibited the downsloping of isolines towards 87°E (Fig. 5.3e). However, along 20.5°N, temperature, salinity and density profiles did not show any conspicuous feature (Fig. 5.3f).

In order to decipher eddy structures, the horizontal sections of temperature, salinity, dynamic topography, dissolved oxygen and nitrate at 100m were separately plotted (Fig. 5.4 & Fig. 5.5). The thermohaline distribution at 100m showed significant features. Relatively cold (~17°C) and high saline waters (~34.8 psu) were observed in the head of the Bay (Figs. 5.4a, 5.4b). The notable feature is the appearance of a warm and less saline pool of water centred around 17°N; 85°E. The temperature showed a value of 27°C, which was about 4°C higher from the ambient waters, while the salinity showed a decrease of nearly 0.5 psu from the surrounding water and was 34.2 psu. Similarly, relatively small pools were observed centred at 15°N;83°E and 13°N;83°E. The most conspicuous feature of 10db surface is a large area of high dynamic topography (>15.0 dyn.m), which represents the core of the anticyclonic eddy centred at 17°N; 85°E. The dynamic topography along the east coast of India showed the signatures of the northward flowing EICC (Fig. 5.4c). However, the dynamic topography at 100db showed the meandering of EICC along the southeast coast of India, but the anticyclonic cell was well evident (Fig. 5.4d).

5.1.1.1. Chemical and biological characteristics

The chemical and biological parameters also show eddy signatures as was seen in the horizontal section of temperature and salinity. Dissolved oxygen at 100m, ranged from 20 –140 μM , having high value of 140 μM at the core of the eddy (Fig. 5.5a). Similarly nitrate at 100m ranged between 18 and 31 μM and the minimum (which is about 7 μM lesser than the surrounding waters) was observed at the core of the anticyclonic eddy (Fig. 5.5b). Over the western BOB, the column chlorophyll *a* in the euphotic zone (0-120m) ranged between 8.5-22.3

mgm^{-2} (average 14.9 mg m^{-2}) and the corresponding integrated primary production were $139\text{-}394 \text{ mgC m}^{-2} \text{ d}^{-1}$ with an average of $262 \text{ mg C m}^{-2} \text{ d}^{-1}$ (Table 5.1). The depth integrated chlorophyll *a* and primary production at the core of anticyclonic eddy was relatively low (8.5 mg m^{-2} : $144 \text{ mgC m}^{-2} \text{ d}^{-1}$).

5.1.2. Discussion

The anticyclonic circulation pattern with the pole ward flowing EICC during spring intermonsoon is a well-known feature in the western Bay. This feature was reported in the hydrographic (Shetye *et al.*, 1993; Murty *et al.*, 1993; Sanil Kumar *et al.*, 1997) as well as satellite observations (Legeckis, 1987) and successfully simulated in modeling studies too (Vinayachandran *et al.*, 1996; McCreary *et al.*, 1993, Shankar *et al.*, 1996). Shetye *et al.* (1993) observed the warm water recirculation zone in the offshore region of the EICC and cold core eddy structure in the coastward direction of this boundary current and Gomes *et al.* (2000) reported highest biomass of phytoplankton inside the cold core eddy region between 13°N and 16°N in the same survey. The generating mechanism of this anticyclonic gyre and the poleward western boundary current is the net effect of local forcing and the remote forcing. But the modelling study by McCreary *et al.* (1993) showed that the remote forcing from the equatorial wave-guide by Rossby waves was not an important factor in the formation of western boundary current, while coastally trapped upwelling favourable Kelvin waves along the eastern periphery is an important factor. The pole ward flowing EICC appears first in the northern part of the Bay and extends towards south, all along the coast within a few months and by March, negative wind stress curl within the Bay will also reinforce the processes. But, the local forcing - the negative wind stress curl, alone is sufficient to drive anticyclonic gyral circulation in the Bay and strengthens the western boundary current by March (Shetye *et al.*, 1993; Vinayachandran *et al.*, 1996). During February, the northeasterly winds are weak and by March the wind pattern along the western Bay reverses, replacing the northeasterlies with south/southwesterlies and forming a well defined anticyclonic

wind filed by April (Babu *et al.*, 2003). Based on the above and the dynamic topography distribution suggested that during the present study, the flow eventually builds up in to a well developed anticyclonic circulation with pole ward western boundary current. But in the subsurface layers (~100m) along the southeast coast of India, the meandering of pole ward current indicates the formative stage of the full-developed EICC. This meandering of EICC develops the subsurface cyclonic cells along the coastward direction of the EICC in the southeast coast and is well evident in the horizontal distribution of nitrate and dissolved oxygen.

5.2. Summer monsoon

The stations covered in July/August along the western Bay of Bengal are included in the summer monsoon season. During this season, the surface winds are predominantly south westerlies with occasional north westerlies and the magnitude was often exceeding 6 m/s.

5.2.1. Hydrography

In general, warm sea surface ($>29.2^{\circ}\text{C}$) was observed in July/August except near the coast off 15°N where the SST dropped to 27.9°C (Fig. 5.6). The most important feature of the SSS is the north – south gradients of salinity along the western BOB. Relatively high saline waters (>33.5 psu) was observed along the southeast coast, whereas in the northeast coast the SSS was marginally small and the lowest value of 25 psu was observed near the coast off 20.5°N . Similar to the SSS distribution, MLD also showed the differences between the northeast and southeast coast. Along the southeast coast, mixed layer, in general, was comparatively deeper and ranged from 30 to 60m, while along the northern transects (19°N and 20.5°N) mixed layer was shallow ($<20\text{m}$). However, in the open ocean region off 17°N , comparatively deeper MLDs were noticed. Further, there exists a thin mixed layer near the coast along 15°N . In general, barrier layers have fairly large thickness in the region of low saline waters. It is interesting to note that the barrier layer has inverse relation to the mixed layer and salinity.

Thicker barrier layer was observed in the region of low salinity and shallow mixed layer. The upper limit of the nitracline ranged from 20 to 70m, except near the coast along 15°N, where the nitracline shoals to the surface (~5m).

The vertical section of temperature, salinity and sigma-t along the 6 transects are presented in Fig. 5.7. The thermal structure along 11°N showed a relatively deep isothermal surface layer (>50m), below which a dome shape of isolines are distinct and the maximum ascent observed at 82°E (Fig.5.7a). This feature was more conspicuous at 175m. Comparatively high surface salinity was observed in the coastal region. The sigma-t structure also showed relatively deep mixed layer along this transect, except near the coast. In general, the isopycnals followed the same trend of the isotherms indicating the dominance of temperature effect over salinity in the density field. The doming of isopycnals at 82°E was more prominent at 175m. Vertical structures of temperature, salinity and density along 13°N showed relatively deeper MLD and ranged between 40 and 50m depth (Fig. 5.7b). Below 75m, the isotherms, isohalines and isopycnals showed an upsloping trend towards the coast indicating the subsurface upwelling. Another notable feature is the appearance of a high salinity core (>35.2 psu) between 75 and 150m, centred around at 82.5°E, where the corresponding thermal structure also showed a diffused thermocline. The vertical thermal structure along 15°N exhibits the distinct upsloping of isotherms towards the coast and relatively cold surface waters (<28°C) were observed near the coast. The upsloping of isotherms are conspicuous in the upper 100m (Fig. 5.7c). The isohalines and isopycnals also showed the upsloping trend towards the coast in the upper 75m and indicating upwelling signals. Distribution of temperature, salinity and density along 17°N showed the fine upsloping of isolines from the offshore region (Fig. 5.7d). Unfortunately the observations towards the coast could not be carried out due to technical problems and so the upwelling signals as reported earlier (Murty and Varadachary, 1968; Rao *et al.*, 1989; Shetye *et al.*, 1993; Rao, 2002) could not be delineated.

Sections of temperature, salinity and density along 19°N and 20.5°N showed an appreciable isothermal surface layer (Fig. 5.7e, 5.7f), but the low saline waters in the surface layers dominate over the temperature in the density field and provide stratification in the surface and reduce the thickness of the mixed layer.

The thermohaline structure at 100m along the western BOB showed a noteworthy feature. Relatively warm (26°C) and high saline (35.2psu) water was observed between 11°N – 14°N and 82 – 84°E (Figs. 5.8a, 5.8b). In the rest of the region, the temperature and salinity varied from 20 to 23°C and 34.6 to 34.7psu, respectively. Geostrophic computations with reference to 500db surface indicate that EICC is not fully developed during summer (Figs. 5.8c, 5.8d). Dynamic topography at 10db and 100 db surface exhibited a high at 13°N; 84°E and two cyclonic cellular structures centred around 15°N;84°E and 11°N; 82°E.

5.2.1.1. Chemical and biological characteristics

The horizontal sections of dissolved oxygen and nitrate at 100m depth are presented in the Fig. 5.9. Concurrent to the warm and high saline pools observed in the horizontal distribution at 100m, relatively high dissolved oxygen (~100μM) and low nitrate (<10μM) were observed (Figs. 5.9a, 5.9b). Comparatively low dissolved oxygen and high nutrients along the shelf waters of the southeast coast of India could be linked to the subsurface upwelling. High biological production was recorded at the coastal station along 15°N, where the upwelling was evident. Column chlorophyll *a* and primary production ranged from 4.6 to 42.8 mg m⁻² and 107 to 548 mgC m⁻² d⁻¹ respectively, having high value at the upwelling site (Table 5.1). Maximum surface chlorophyll *a* (0.88 mg m⁻³) and primary production (46 mgC m⁻³ d⁻¹) was also coinciding in the station near the coast off 15°N.

5.2.2. Discussion

The prevailing southwesterly winds give rise to southeastward Ekman transport at the surface. In addition to the cold waters near the coast, shallow mixed layer and nitracline and the upsloping of isotherms, isohalines and isopycnals towards the coast, the high surface as well as column chlorophyll *a* and

primary production suggest that the upwelled water reaches the surface near the coast along 15°N. But the cold waters are observed in a narrow band, which confirm the earlier studies (Shetye *et al.*, 1991). However, along the southeast coast of India, the upwelled waters were confined below 75m. Based on the forcing mechanism, western BOB can be divided into three divisions, northern (freshwater influenced), central (wind influenced) and southern (thermohaline driven) region (Murty *et al.*, 1992b). They stated that, over the central region, the southwesterly winds lead to the divergence (and hence upwelling) at subsurface depths (50-100m) giving rise to cold waters along the axis of the positive curl and leads to cyclonic circulation in this region. The cyclonic eddy observed along 11°N does not benefit the biological production. The reason is that the cyclonic eddies are more pronounced below 100m. Similar pattern of cyclonic cell was observed in the central BOB during summer monsoon (Babu *et al.*, 1991, Prasanna Kumar *et al.*, 2004). But, Prasanna Kumar *et al.* (2004) found that the cyclonic eddy, observed around 17°N:83.5°E was capable of pumping the nutrients to the surface layers (~20m) and thereby enhances the biological production. The high salinity pockets (~35.2 psu) observed in the section along 11°N and 13°N between 50 and 120m was thought to be advected from the AS through the Indian monsoon current. Similar observation was also reported (Murty *et al.*, 1992b), but the pathways are marginally east of the present observation. But the depth at which it seen (50 to 120m) and the northward intrusion (south of 14°N) of the AS watermass was comparable in both observation. This leads to the point that, even though the cyclonic circulation and intrusion of monsoon current in the BOB is a seasonal feature, it undergoes spatial variability.

5.3. Winter monsoon

The stations investigated in November/December along the western Bay of Bengal are included in the winter season. During this season, the surface winds were predominantly north easterlies and the magnitude on an average was greater than 5m/s.

5.3.1. Hydrography

The Fig. 5.10 represents the distribution of SST, SSS, MLD, barrier layer thickness and the upper limit of the nitracline along 6 transects in the western BOB. During the season SST ranged from 25.5° to 29.2°C (Fig. 5.10). SST, in general, showed a steady decrease towards the coast along 11°N and 13°N. Along 15°N, SST ranged between 27.7°C to 28.4°C and the minimum was observed at 83°E. North of 15°N, SST decreases towards north and showed the lowest value of 25.5°C along 20.5°N. SSS ranged from 25.3 – 33.8 psu and showed high saline waters in the open ocean region along the southeast coast and the low saline waters along the entire east coast. Very low saline waters were observed near the coast along 19°N and 20.5°N, which could be linked to the Ganges – Mahanadi river system, where as that along 15°N was due to the Krishna river influx. Unlike the previous seasons, the southeast coast of India exhibited low salinity values (<30 psu). MLD ranged from 5 to 50m and very shallow MLD was found in the regions where SSS are quite low and deeper mixed layer was observed in the region of high surface salinity. In general, the MLD increased towards offshore along 11°N – 17°N, except along 15°N, where the MLD shallowed towards 83°E and reached a value of 10m. Further, MLD in the northern transects were observed to be very shallow (<10m). In the nearshore region, thicker barrier layer was observed whereas in the offshore region the layer was much shallower. In general, relatively thicker barrier layer (>40m) was observed in the regions of low surface salinity, except in the northern transects. The nitracline distribution did not show any noticeable zonal variation south of 17°N and ranged between 45 – 65m, while north of 19°N, the nitracline showed little more variation and varied between 30 and 70m.

The vertical section of temperature, salinity and sigma-t along the 6 transects are presented in Fig. 5.11. Vertical thermal structure along 11°N showed relatively deep isothermal surface layer in the open ocean region (Fig. 5.11a). In the coastal areas, thermal structure showed an inversion below 30m. Another

conspicuous feature observed in the thermal structure was the doming of isotherms, which can be clearly seen below 50m, centered around 82°E. This feature was more conspicuous at 200m depth. Salinity structure in the upper 50m showed the frontal pattern towards the coast indicating freshwater influx from the continent. Isopycnals in the upper 50m resembled the isohaline pattern, below which the temperature dominates over salinity in the density field. The vertical profiles along 13°N also resembled the above pattern along 11°N (Fig. 5.11b). But the eddy like signals were not so prominent as seen in the 11°N transect. However, the profiles of temperature, salinity and density along 15°N showed the dome like structure of isotherms between 82°E and 85°E, indicating the presence of cold waters (Fig. 5.11c). This feature was more conspicuous at 75m. The vertical sections along 17°N and 19°N exhibited the dome like structure, but the doming of isolines are not so conspicuous as that along 15°N (Fig. 5.11d, 5.11e). Salinity structure in the upper 40m along 17°N showed a frontal pattern with low saline waters near the coast, which indicated the freshwater influx from the continent and showed a gradient of almost 2 psu in the upper 50m. But along 19°N, the low salinity pools were observed about 200km from the shore and showed the gradient of almost 5 psu in the upper 50m. Salinity structure along 20.5°N also showed a frontal pattern, which indicated the fresh water influx from the continent and showed a sharp gradient of 8 psu in the upper 50m (Fig. 5.11f). The most important feature in the thermal structure along the northern transects was the presence of cold surface waters lying over the warm subsurface waters. The vertical sections of temperature, salinity and density along 20.5°N did not show any noticeable feature, but strong thermal inversion and low saline surface waters were evident.

To examine the degree of inversion in the thermal structure, the vertical profiles of temperature at selected stations along each transect are plotted (Fig. 5.12). The magnitude of the thermal inversion increased northward and the

maximum ($>3^{\circ}\text{C}$) was observed in the northern transects (19°N & 20.5°N), while in the southern region small scale inversion ($<0.5^{\circ}\text{C}$) was noticed.

Horizontal distribution of temperature at 100m showed the presence of cold waters ($<17^{\circ}\text{C}$) centred at 15°N ; 83°E and with a decrease of about $4\text{-}5^{\circ}\text{C}$ from the ambient water, indicating the signature of a cold core eddy (Fig. 5.13a). Similar structure of relatively high saline waters (>34.8 psu) was noticed in the salinity structure (Fig. 5.13b). The dynamic topography at 10db surface showed an equatorward flow of EICC along the western BOB and having cyclonic cellular structure around 15°N ; 83°E (Fig. 5.13c). The cyclonic structure was also noticed at the dynamic topography distribution at 100db (Fig. 5.13d).

5.3.1.1. Chemical and biological characteristics

The dissolved oxygen at 100m showed a value of $10\mu\text{M}$ at the core of the eddy, which was about $20\mu\text{M}$ drop from the adjacent waters (Fig. 5.14a). Nitrate distribution at 100m showed a value of $19\mu\text{M}$ at the core of the eddy, which was about $2\text{-}4\mu\text{M}$ rise from the ambient values (Fig. 5.14b). The high values of chlorophyll *a* and primary productivity values reflected the cyclonic eddy characteristics. Along the western BOB, column chlorophyll *a* and primary production values showed a patchy distribution and ranged from 5.6 to 16.5 mg m^{-2} (average 10.4) and 28 to 487 $\text{mgC m}^{-2} \text{d}^{-1}$ (average 217 $\text{mgC m}^{-2} \text{d}^{-1}$), respectively. The open ocean regions between 15°N and 17°N showed the maximum chlorophyll *a* (>11 mg m^{-2}) and primary production (>230 $\text{mgC m}^{-2} \text{d}^{-1}$) during this season. The depth integrated chlorophyll *a* and primary production values were comparatively high (16.5 mg m^{-2} , 444 $\text{mgC m}^{-2} \text{d}^{-1}$) in the region of cold core eddy (Table 5.1). Very low chlorophyll *a* concentration and primary production in the northern transects (19°N and 20.5°N) could be linked to the low saline surface waters, which inhibit the vertical mixing.

5.3.2. Discussion

Atmospheric forcing and the response on BOB from summer to winter were abrupt. In the northwestern Bay, conditions are favorable for the winter

cooling processes. The cold dry air (humidity <45%) from the continents blows over northwestern Bay. But the heat loss caused by the winter cooling process does not trigger convective overturning in the Bay. This is prevented by low saline surface waters, which stay stagnant in surface layers. As compared to Arabian Sea (Madhupratap *et al.*, 1996), winter cooling process in the Bay does not enhance biological production but it leads to strong thermal inversion in the surface layers. A significant feature observed along the western Bay was the presence of cold core eddy with high salinity centred at 15°N; 83°E observed below 40m depth. Under the influence of the subsurface cyclonic eddy, the nutrients are pumped in to the upper layer, consequently relatively high production is seen in this region. The generating mechanism of the cyclonic eddy is thought to be the circulation pattern. In November, *i.e.*, during the onset of northeast monsoon, the BOB has a basin wide cyclonic circulation pattern (Eigenheer and Quadfasel, 2000). The geostrophic estimates based on the hydrographic data collected during the season shows the cyclonic circulation pattern with equatorward EICC. In addition to the thermohaline distribution, and dynamic topography, nitrate, dissolved oxygen, chlorophyll *a* and primary productivity pattern gives the confirmative evidence of eddies.

5.4. Hydrological structure

In general, based on the observations during the various season, the SST and MLD did not show any relationship (Fig. 5.15a). Most of the time, MLD was observed to be shallow (<40m). The low SST during winter were associated with winter cooling, but the corresponding shallow mixed layer gives the nature of the winter cooling in the northwestern BOB, *i.e.*, the winter cooling does not cause the convective overturning. Surface warming and relatively less saline waters during spring intermonsoon, very low saline waters during summer and winter, also reduces the mixed layer thickness. Similarly, the maximum thermal gradient and the mixed layer, not showed any relationship (Fig. 5.15b). During winter, wide ranges of thermal gradients were observed. On an annual scale, the figure

representing the relationship between the thermal gradient and nitracline (Fig. 5.15c) did not show any conspicuous relationship. However, the depth of the 1st level of oxygen undersaturation and the depth of the nitracline showed fairly good relation. The relation between the depth of the nitracline and chlorophyll *a* maxima showed that the chlorophyll maximum was observed mostly in the surface layers (<30m), except during spring intermonsoon. During spring intermonsoon, it can be seen that the depth of thermal gradient and nitracline are statistically at same depth and the equation of linear regression is

$$Y = 0.88 * X + 5.3$$

and having significantly high correlation coefficient ($r = 0.87$, $p = 0.99$). Similarly, a very good relation between the depth of 1st level of oxygen undersaturation and the nitracline are observed at approximately same depths. The equation of linear regression is

$$Y = 0.92 * X + 13.3 \quad (r = 0.88, p = 0.99)$$

The deep chlorophyll maxima was also observed in spring intermonsoon and observed in general between 50 –75m. Since the sampling were done at discrete depths, the precise depth of the chlorophyll maxima was difficult to find out. The scatter plot of the depth of the chlorophyll maxima and the depth integrated chlorophyll concentration did not show any distinct relationship. It can be seen that, irrespective of the seasons, the BOB is less productive and often showed values less than 40 mg m⁻². Highest chlorophyll concentration (depth integrated) was observed during the upwelling time with the chlorophyll maxima occurring at the surface.

The analyses of hydrological structure suggest that, during spring intermonsoon, the depths of the thermal gradient maxima, nitracline and 1st level of oxygen undersaturation are statistically same. Further, there exist deep chlorophyll maxima, which is a feature of the TTS. Hence during spring intermonsoon the BOB is behaves as a typical tropical structure, while rest of the season, the features of TTS are hardly visible. The reason must be, during spring

intermonsoon the BOB receives maximum solar insolation and least freshwater influx and hence the particle flux was minimum, which permits the light into the deeper layers and possibly makes the production at the top of nitracline.

5.5. Differential response of Arabian Sea and Bay of Bengal to the atmospheric forcing

Although the AS and BOB are located in the same latitude band, both exhibited very contrasting oceanographic response to the monsoons. Despite the upwelling that was evident in the west and east coast of India, they show large variation in its intensity. Compared to the AS, the winds along the western BOB are more favourable to the upwelling processes, however, the AS experience the more intense upwelling. Accordingly, the biological productions of the two basins show remarkable variation in the upwelling region. The AS, having the highest PP and chlorophyll *a* (integrated over 120m) were recorded at the upwelling site and the values are $9144 \text{ mgC m}^{-2} \text{ d}^{-1}$ and 203 mg m^{-2} respectively. In contrast, the BOB having the highest PP and chlorophyll *a* values of $548 \text{ mgC m}^{-2} \text{ d}^{-1}$ and 43 mg m^{-2} respectively at the peak of upwelling. Along the southwest coast, the upwelling processes begin in the deeper layer during the intermonsoon spring and the upwelled water reaches the surface by May. This upwelling band spreads slowly towards north with the progress of monsoon and persists till the retreat of southwest monsoon (September). The cold upwelled waters spread about 200 km width from the shore. But along the east coast of India, the upwelling was evident at few locations and is often noticed as subsurface upwelling. This upwelling band is confined very close to the coast (within 50 km). In general, there are three reasons for the lack of intense upwelling along the east coast. The river discharge in the northwestern BOB is responsible for an equatorward flow along the east coast during southwest monsoon, which would overwhelm the upwelling processes (Gopalakrishna and Sastry, 1985). Another reason for the subdued upwelling along the east coast is believed to be the remote forcing. The westward propagating Rossby waves radiated from the eastern periphery suppresses the

offshore Ekman transport in the east coast (Usha and Muraleedharan, 2000). It is believed that the narrow shelf width along the east coast of India may also be the one of the reason for the weak upwelling.

The winter response to the two basins gives the two contrasting scenario. The ASHSW, the PGW and the RSW make the AS highly saline. The heat loss by the winter cooling caused the densification of surface waters, which initiates the turbulence at the surface and finally the convective overturning of subsurface waters. The deepening of mixed layer from south to northern latitudes coincided with the intensification of winter. The atmospheric conditions in the BOB were more favourable to the winter cooling processes. Relatively colder dry air (humidity < 60%) blown over the BOB as compared to the northeastern AS (humidity > 65%). The climatological atlas of evaporation and latent heat flux corroborate the heat loss of the sea surface to the atmosphere by the winter cooling (Hastenrath and Lamb, 1979). In addition, the fresh water influx due to precipitation and run off freshens the surface layers in the northern BOB. As a result, the cold fresh water in the surface layers stay stagnant, below which the temperature increases with depth resulting in thermal inversion. The low saline waters compensate the static stability loss by the thermal inversion. Many authors have reported earlier on the BOB inversions (Varkey *et al.*, 1996; Shetye *et al.*, 1996; Han *et al.*, 2001; Pankajakshan *et al.*, 2002). The thermal inversion mostly dominates during winter. Shetye *et al* (1996) suggested that the process of formation of inversion in the bay starts in the north during the southwest monsoon and accelerates with the onset of the northeast monsoon, when cold continental winds cool the surface waters of the bay, particularly its northern part. During winter, due to atmospheric cooling, the surface layers attains low temperature but fails to transfer it to the deeper waters owing to the lack of sinking and convective mixing.

The distribution of nitracline in the northern transects along the AS and the BOB showed marked variations. In the AS, the upper 50m water column

possessed 1 μM nitrate, which is a clear indication of convective mixing mechanism occurring in the region. Interestingly, in the BOB the upper 50 m water was devoid of nitrate, which point out the low efficiencies of vertical mixing mechanisms in that region. The absence of nitrate in the upper water column of BOB during winter monsoon has been reported earlier also (Rao *et al.*, 1994). High chlorophyll *a* (Avg. 47.5 mg m^{-2}) in the AS is attributed to high nutrient concentration by convective mixing. Highest average PP (1854 $\text{mg C m}^{-2} \text{d}^{-1}$) obtained at the coastal station of the northernmost latitude coincided with the highest mixed layer depth (~ 80 m). Relatively low integrated Chl *a* and PP (Average chlorophyll *a* 22 mgm^{-2} , Average PP 551 $\text{mg C m}^{-2} \text{d}^{-1}$) observed along 19 °N in AS correspond with the low mixed layer depth in that transect.

In the BOB, PP and chlorophyll *a* was very low (Average 117 $\text{mg m}^{-2}\text{d}^{-1}$, Average 10.3 mg m^{-2} respectively) and the low PP was due to the absence of nitrate and phosphate in the water column. In the AS, the northernmost latitude (21 °N) sustained high phytoplankton biomass and production (Average chlorophyll *a* 69 mg m^{-2} , Average PP 1608 $\text{mg C m}^{-2} \text{d}^{-1}$) but in the BOB, northernmost latitude had the least (Average 69 $\text{mgC m}^{-2} \text{d}^{-1}$. Average chlorophyll 9 mg m^{-2}). Higher PP in the northern most latitude of AS could be due to the intensification of winter towards north, which increased the mixed layer, but the northernmost latitudes of the BOB receive maximum influence from fresh water, which lead to strong stratification of the upper waters.

Climatological data (Conkright *et al.*, 1998) suggest that combined effect of rainfall and river discharge reduces the salinity in the northern BOB from May to July by as much as 5psu. During August – September 1990, Murty *et al* (1996) observed a decrease of 3 psu in the surface salinity. The introduction of fresh water forms a new halocline within the isothermal layer. The formation of the barrier layer in the BOB restricts the ocean – atmosphere interaction to the thin mixed layer and hence restricts the upward transport of nutrients. The barrier formation was more pronounced in the northwestern BOB during summer, the

maximum was observed along the western BOB during winter, except along the northwestern BOB. However, along the northwestern BOB during winter, the strong thermal inversion restricted the isothermal layer into the thin surface layer. Therefore, the isothermal layer and mixed layer appeared to be shallow and hence their difference, i.e. the barrier layer thickness, was observed to be insignificant. During spring intermonsoon, the barrier layer was not so pronounced in the western BOB. In the AS, the barrier layer thickness was less significant, however, along the southwest coast during winter, the entry of low saline waters through EICC leads to the formation of thick barrier layer. Rao and Sivakumar (2003) showed the similar pattern of barrier layer distribution in the eastern AS and western BOB, but the discrepancies occurred in the northwestern BOB during northeast monsoon

A comparison of the static stability parameter E showed large differences between the two basins. Profiles of the stability parameter showed larger values in the BOB than that in AS. Along the northern transects in the AS, the stability parameter showed highest value during spring intermonsoon and was observed at about 40m (Figs. 5.17a, 5.17b). During winter, it showed little variation in the upper 100m indicating the convective mixing in the water column. In BOB, the stability maximum was observed in the upper 20m for the whole year, but during summer and winter, the stability was much higher, because of the large freshwater influx. Stability profiles in the southern transects (Figs. 5.17 c-f) in the AS showed relatively small values and the maxima were observed in shallower depths (25-40m) in spring intermonsoon as compared to the summer and winter monsoon. Little variation in the stability profile during summer monsoon can be linked to the wind mixing. However, in the BOB, the stability maxima remained at shallower depths. The freshwater influx in the southeast coast of India during winter provides relatively high values of stability maxima.

The AS, in general, shows the characteristics of the TTS during the whole year, whereas in the BOB, the feature of TTS was obscure, except during spring

intermonsoon. During the spring intermonsoon, most of the region in the BOB showed the sub surface chlorophyll maxima. But the resulting biological production (depth integrated – 120m) was remarkably lower than the AS, suggesting the particle flux in the water column also plays a major role in the less productive Bay.

Table. 5.1. Average depth integrated chlorophyll *a* (Chl *a*) and primary productivity (PP) for three seasons in the Bay of Bengal

Season	Average-primary production		Production at the core of the eddy/upwelling site		
	Chl <i>a</i> (mg m ⁻²)	PP (mg C m ⁻² d ¹)	Chl <i>a</i> (mg m ⁻²)	PP (mg C m ⁻² d ¹)	Nature of physical process
Spring intermonsoon	14.9 ± 4.6	262 ± 94.5	8.5	144	warm, less saline (warm core)
Summer Monsoon	17.1 ± 10.9	277 ± 163	42.8	470	upwelling
Winter monsoon	10.4 ± 3.6	217 ± 163	16.5	444	cold, high saline (cold core)

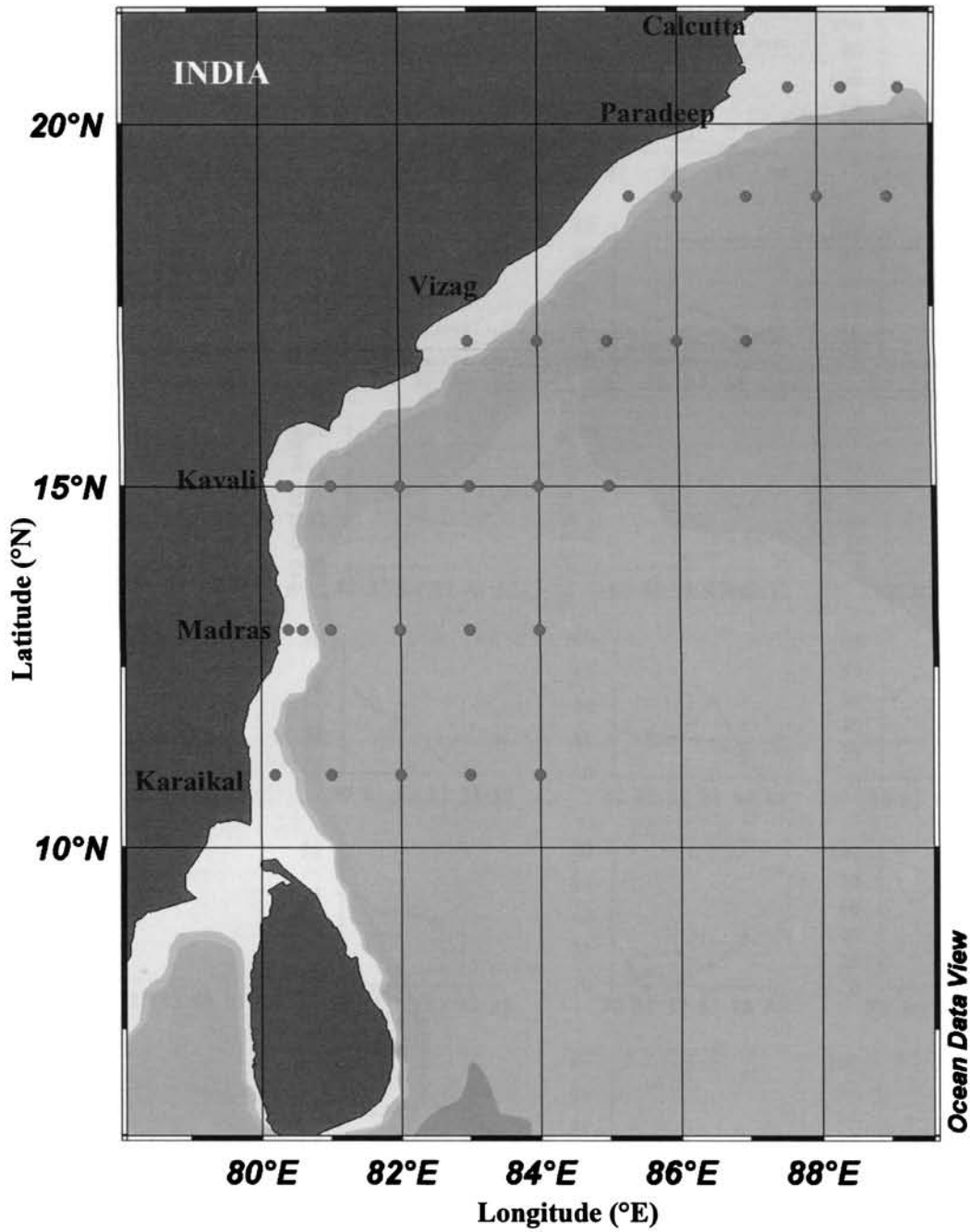


Figure 5.1. Hydrographic stations along the western Bay of Bengal during the MR-LR programme

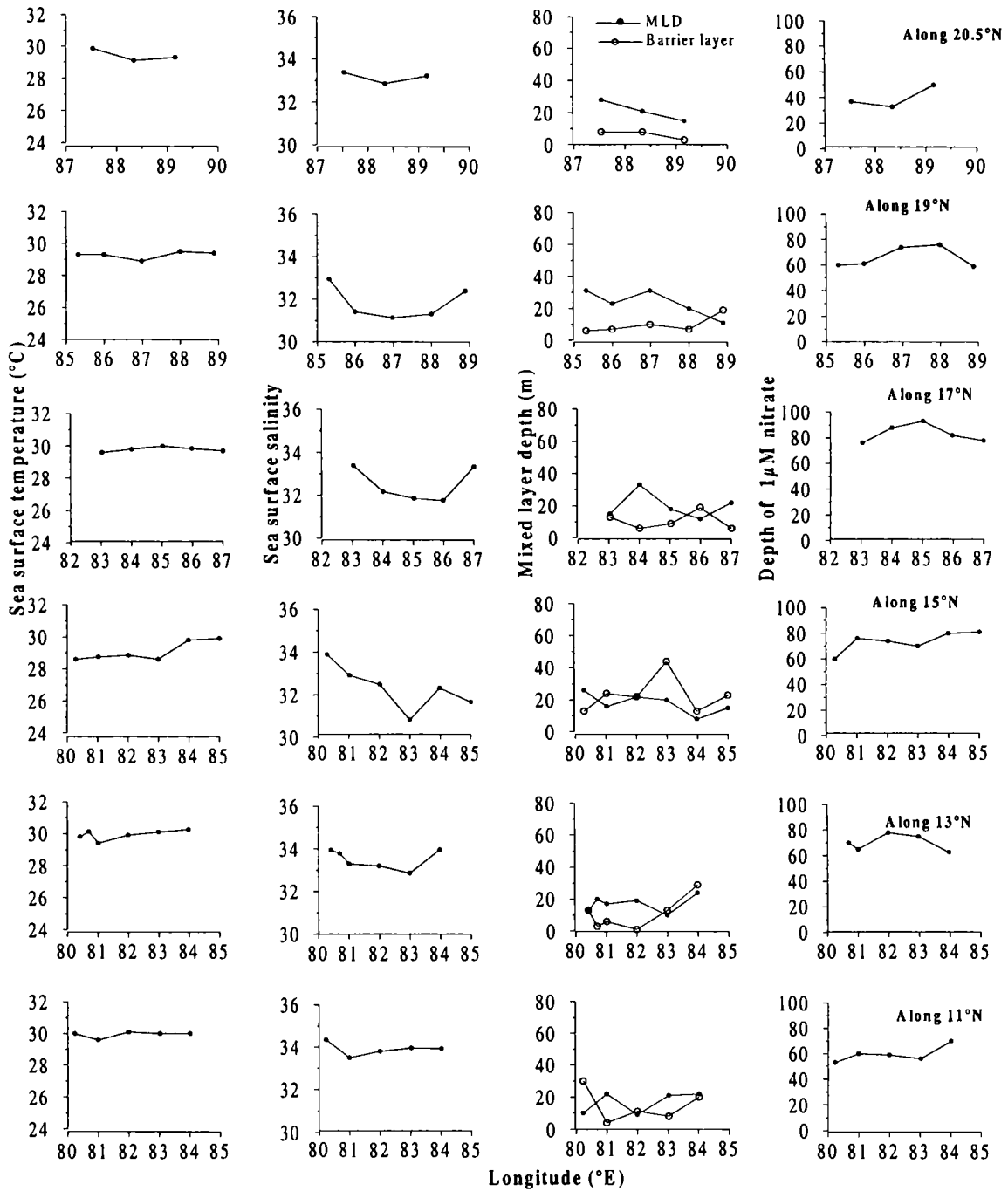


Figure 5.2. Latitude wise distribution of SST, SSS, MLD, barrier layer thickness and nitracline along the western Bay of Bengal during spring intermonsoon

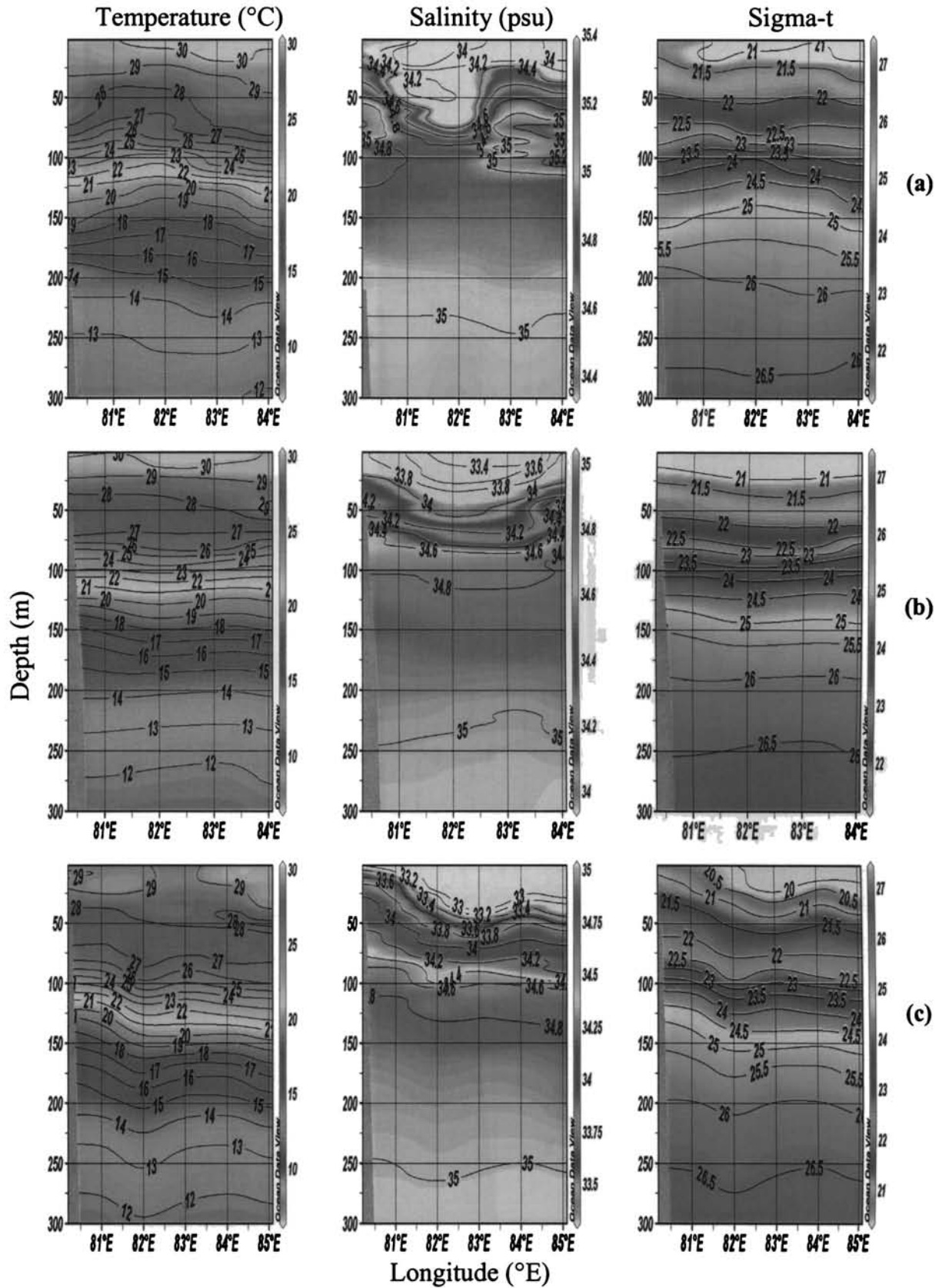


Figure 5.3. Vertical distribution of temperature, salinity and sigma-t along (a) 11°N, (b) 13°N (c) 15°N (d) 17°N, (e) 19°N and (f) 20.5°N during spring intermonsoon in the western Bay of Bengal

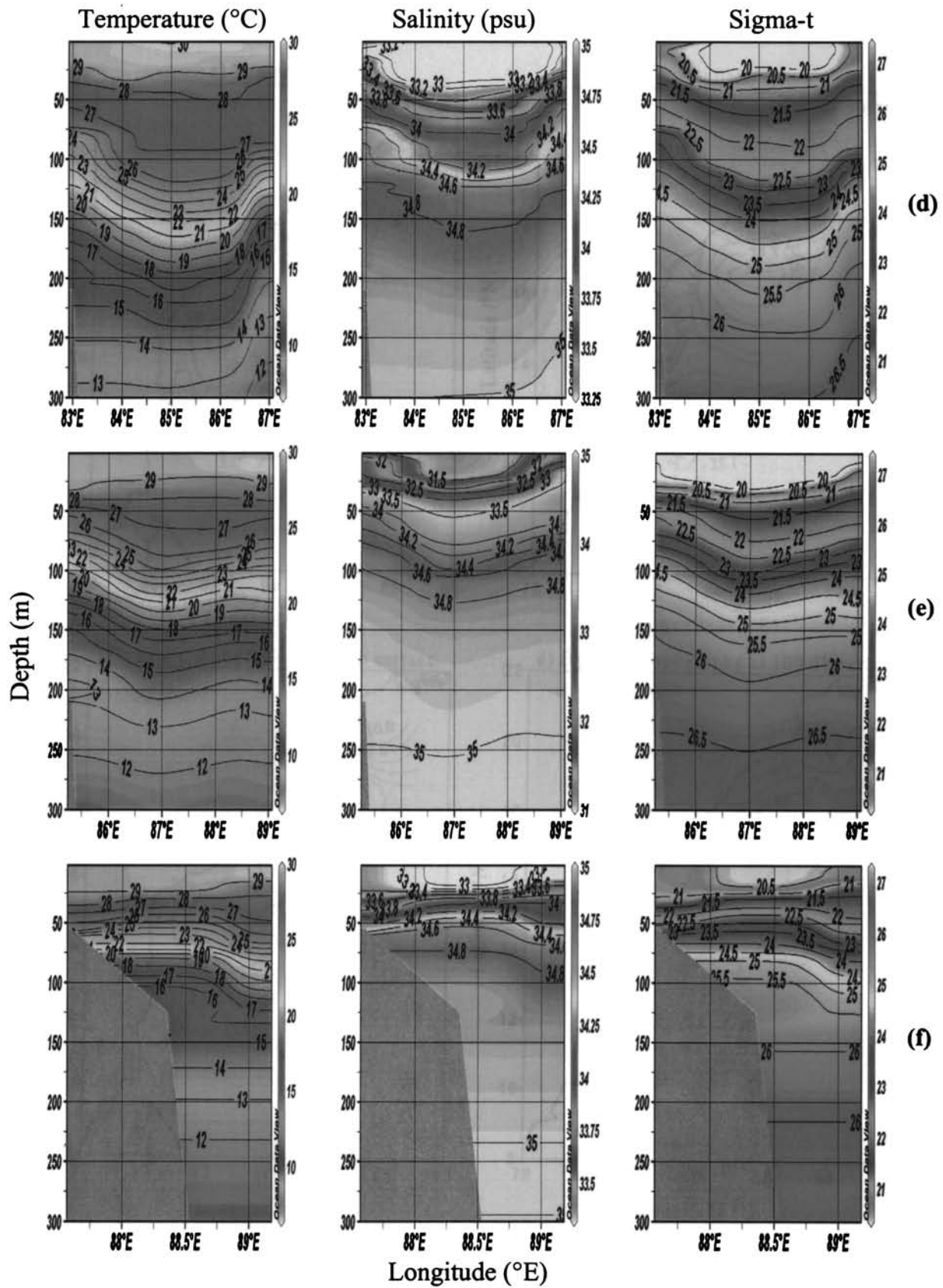


Figure 5.3. (continued)

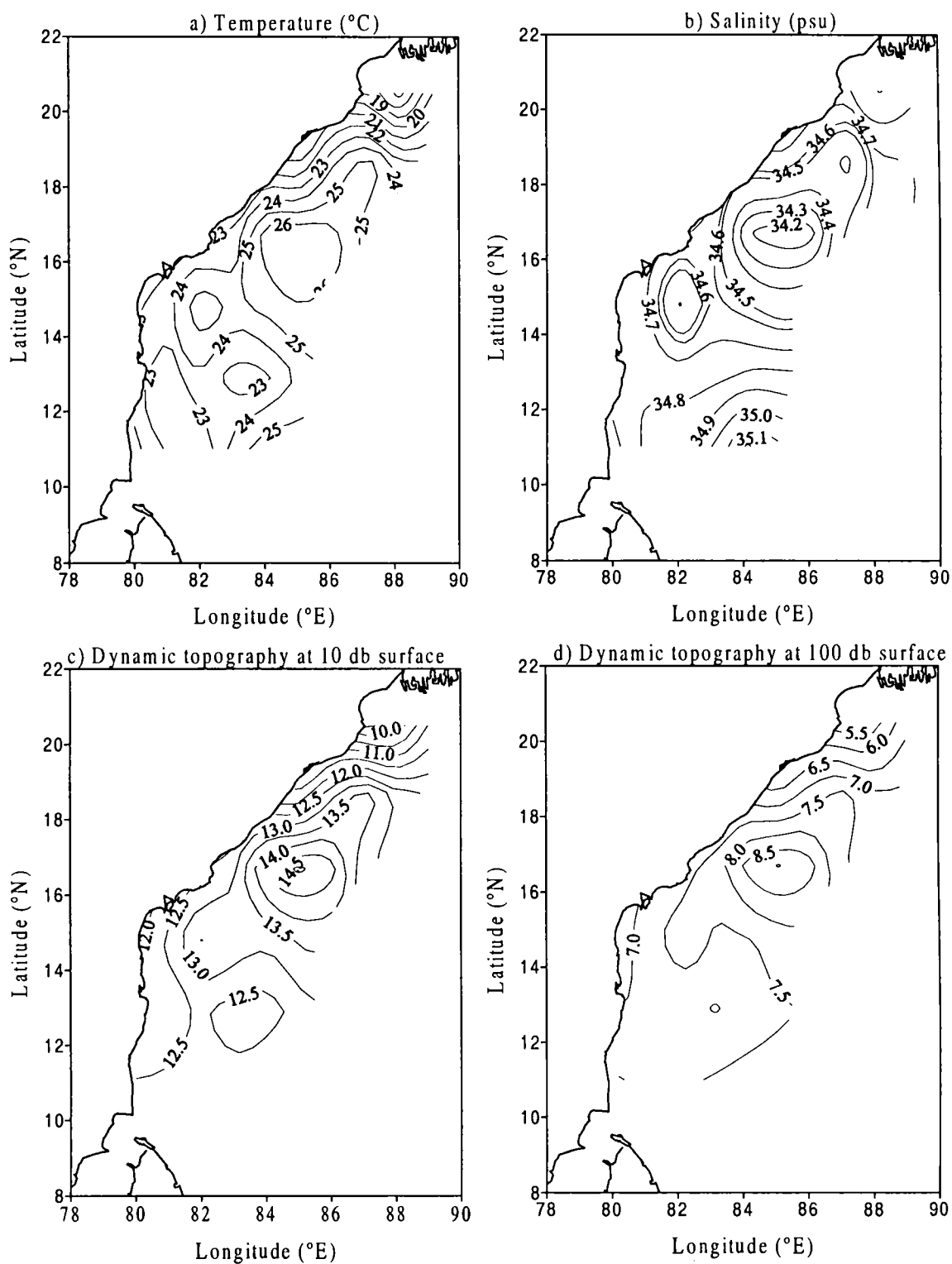


Figure 5.4. Distributions of: a) temperature and b) salinity at 100m, dynamic topography with reference to 500 db at c) 10 db and d) 100 db surfaces along the western BOB during spring intermonsoon

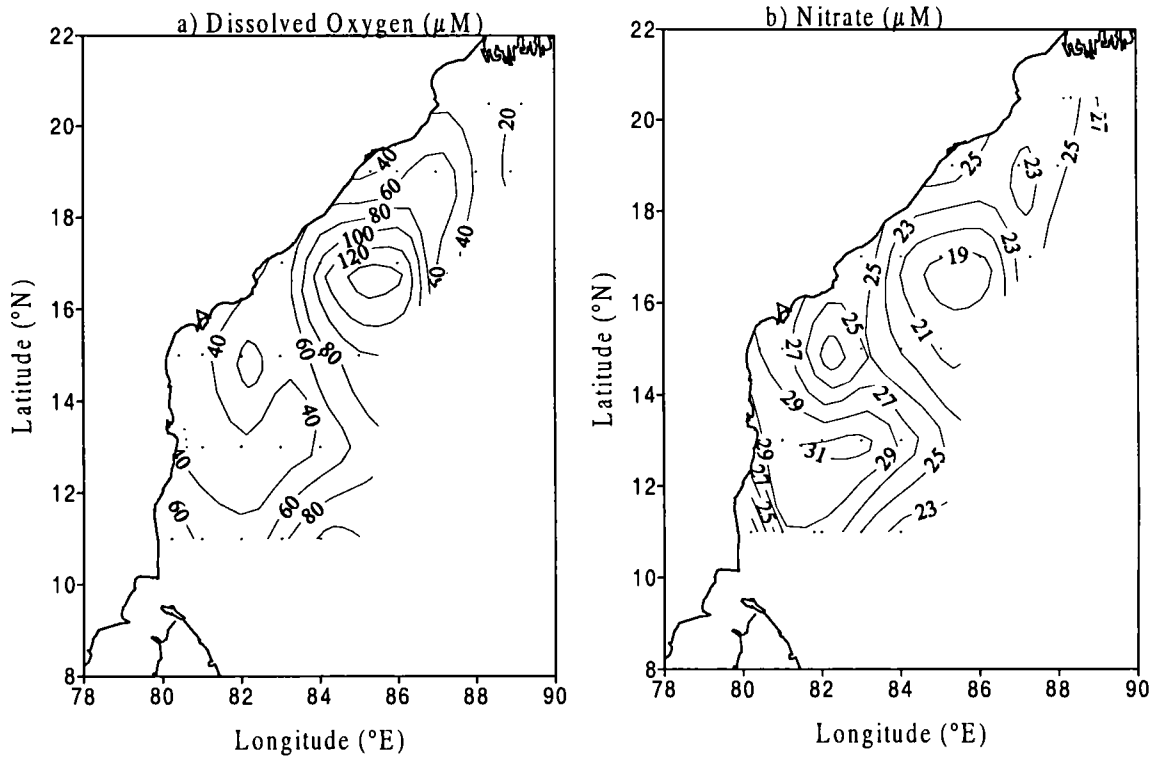


Figure 5.5. Distribution of dissolved oxygen and nitrate at 100m in the western BOB during spring intermonsoon

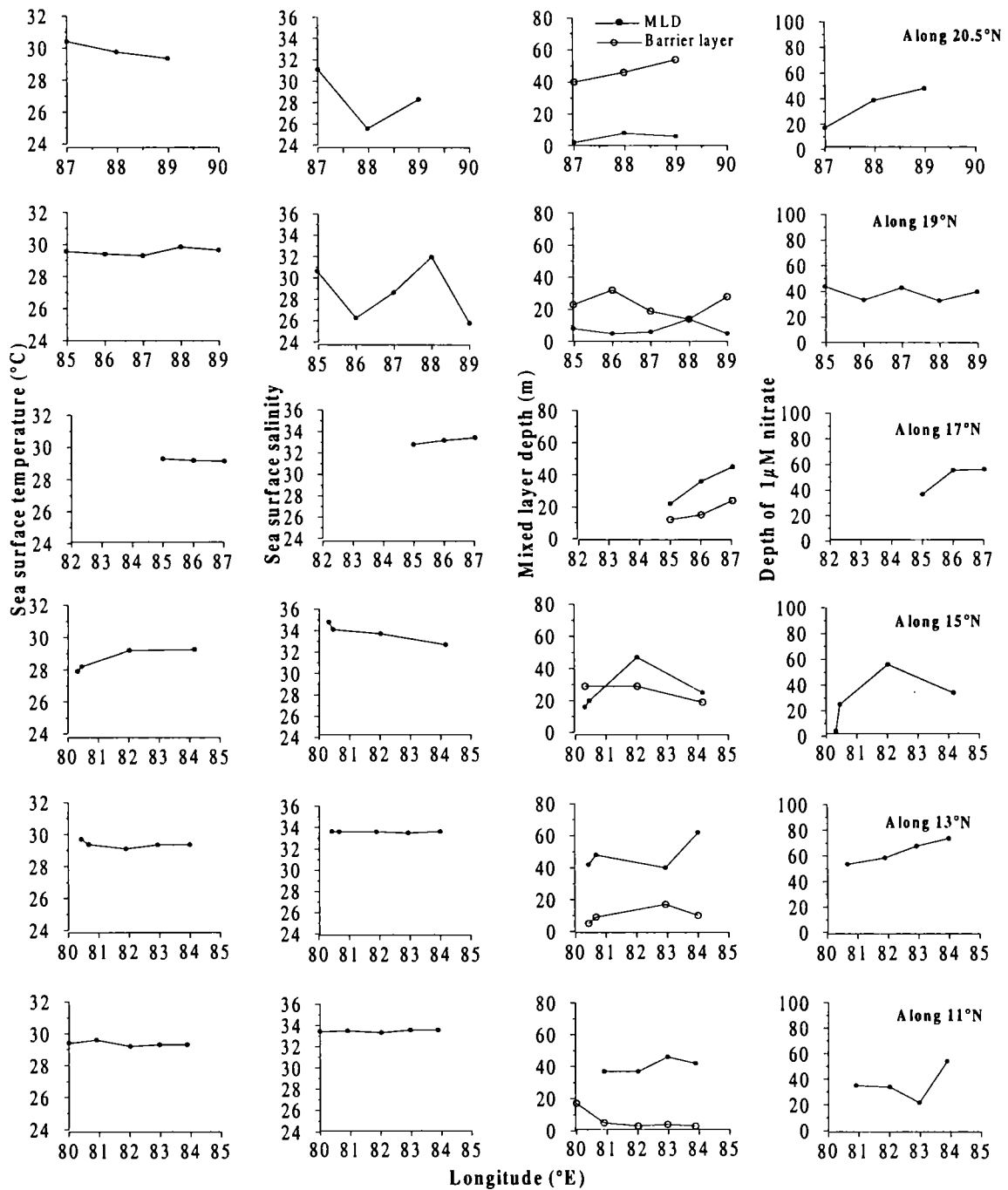


Figure 5.6. Latitude wise distribution of SST, SSS, MLD, barrier layer thickness and nitracline along the western Bay of Bengal during summer monsoon

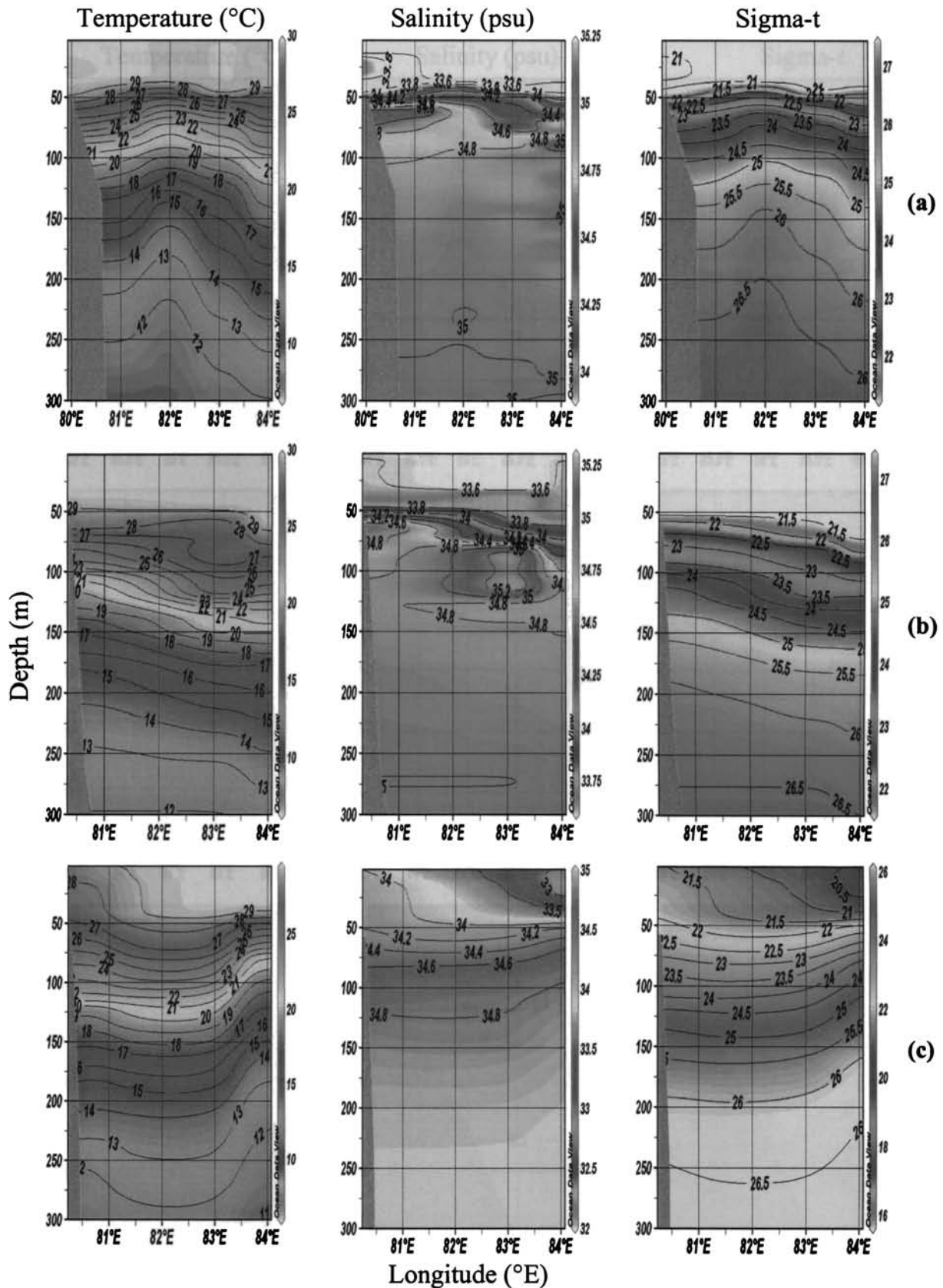


Figure 5.7. Vertical distribution of temperature, salinity and sigma-t along (a) 11°N, (b) 13°N, (c) 15°N, (d) 17°N, (e) 19°N and (e) 20.5°N during summer monsoon along the western Bay of Bengal

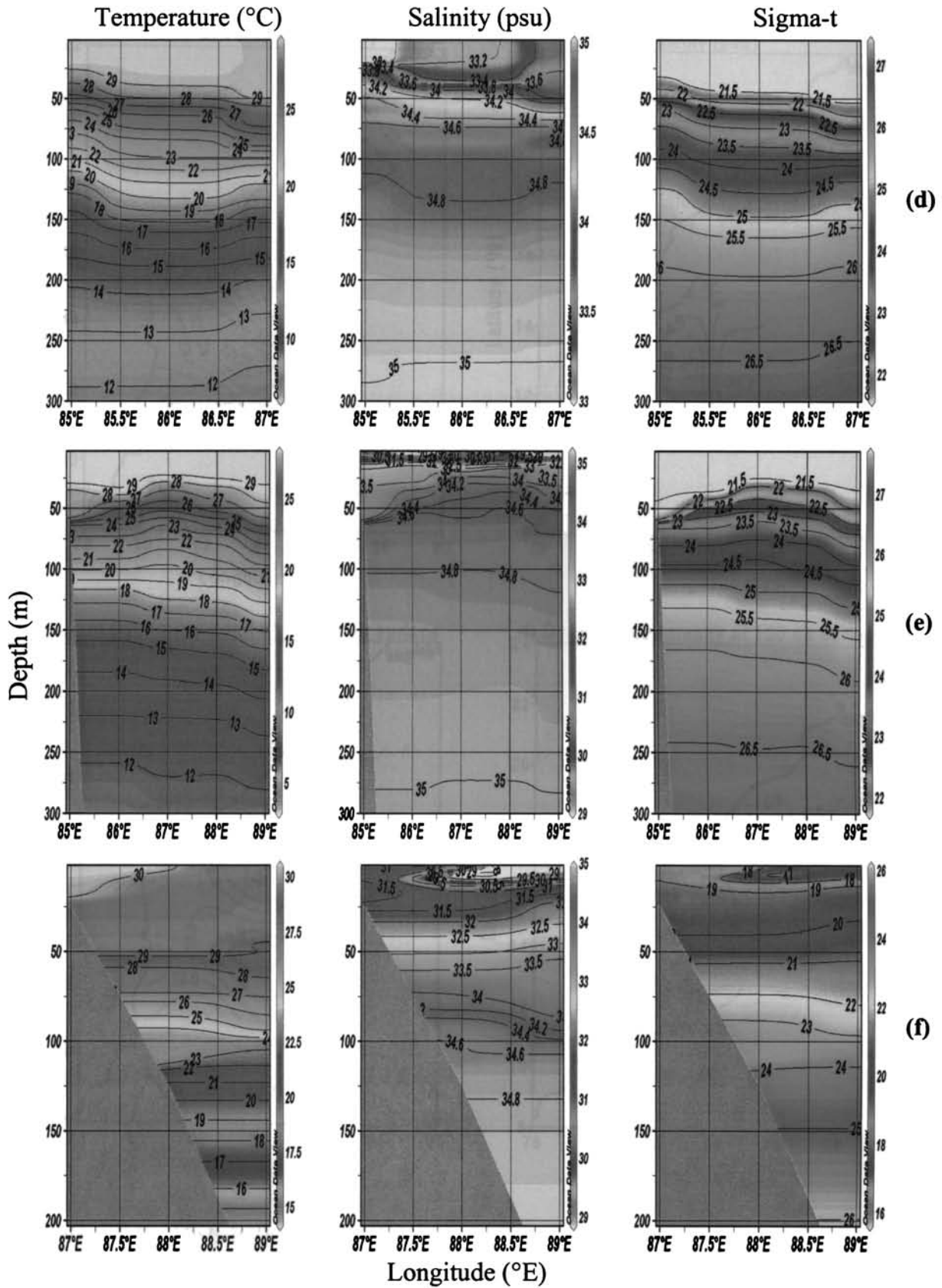


Figure 5.7. (continued)

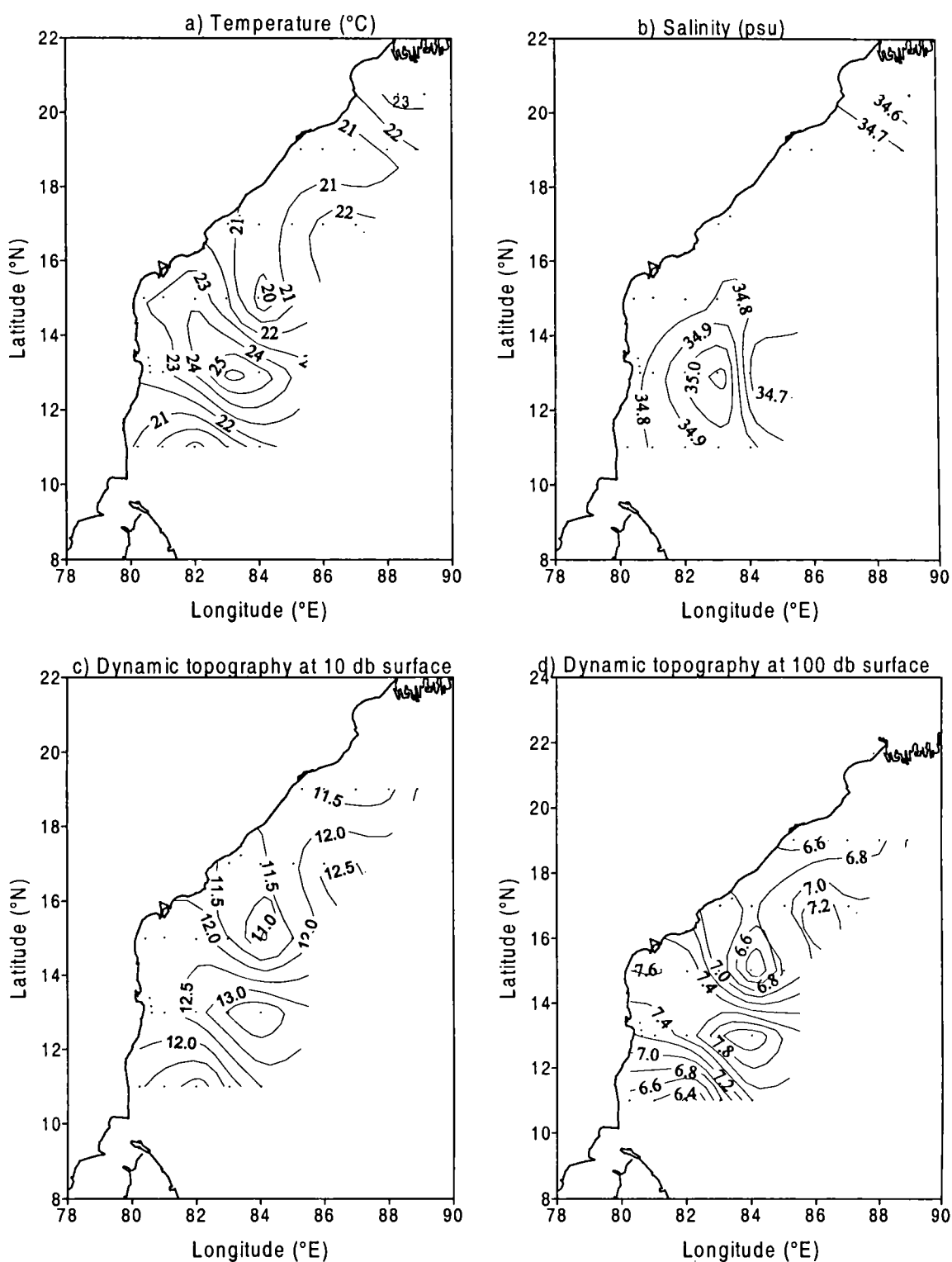


Figure 5.8. Distributions of: a) temperature and b) salinity at 100m depth. Distribution of dynamic topography at: c) 10 db and d) 100 db surfaces with reference to the 500 db along the western BOB during summer monsoon

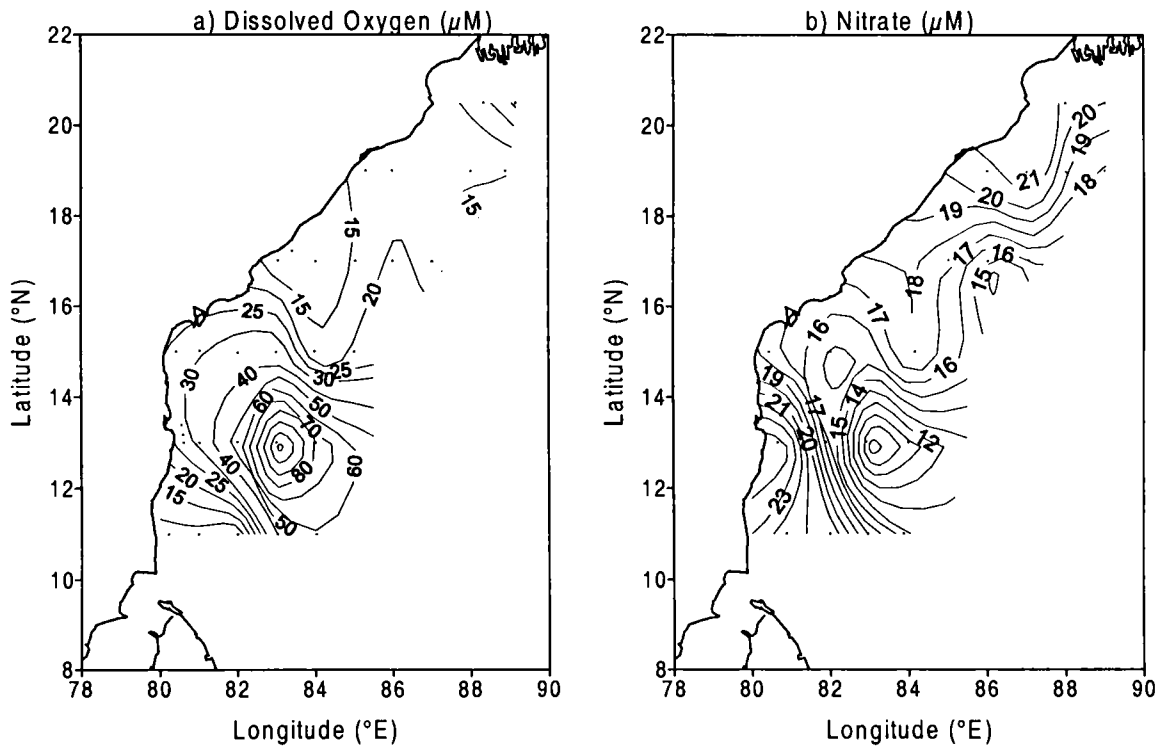


Figure 5.9. Distribution of: a) dissolved oxygen and b) nitrate at 100m along the western BOB during summer monsoon

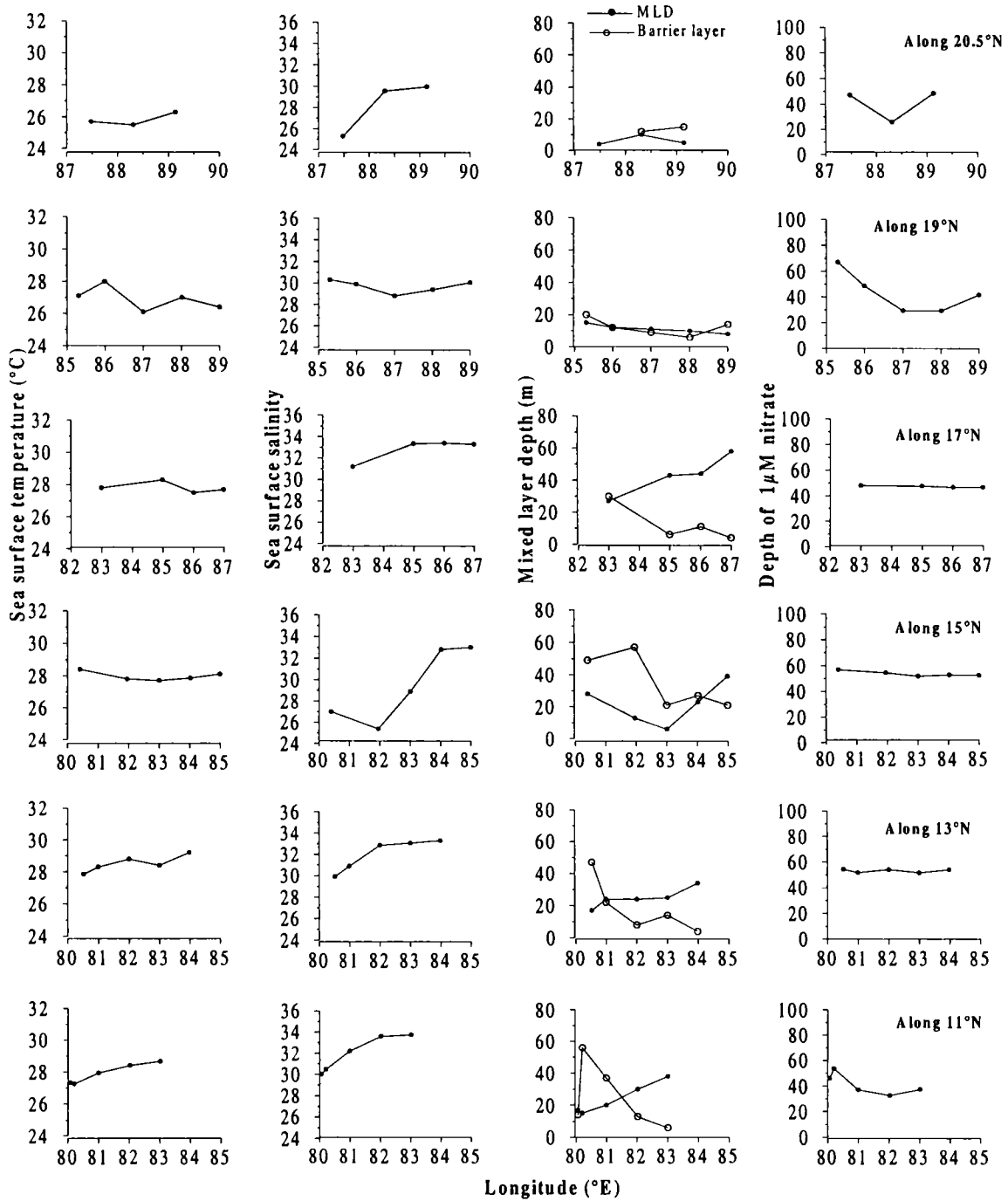


Figure 5.10. Latitude wise distribution of SST, SSS, MLD, barrier layer thickness and nitracline along the western Bay of Bengal during winter monsoon

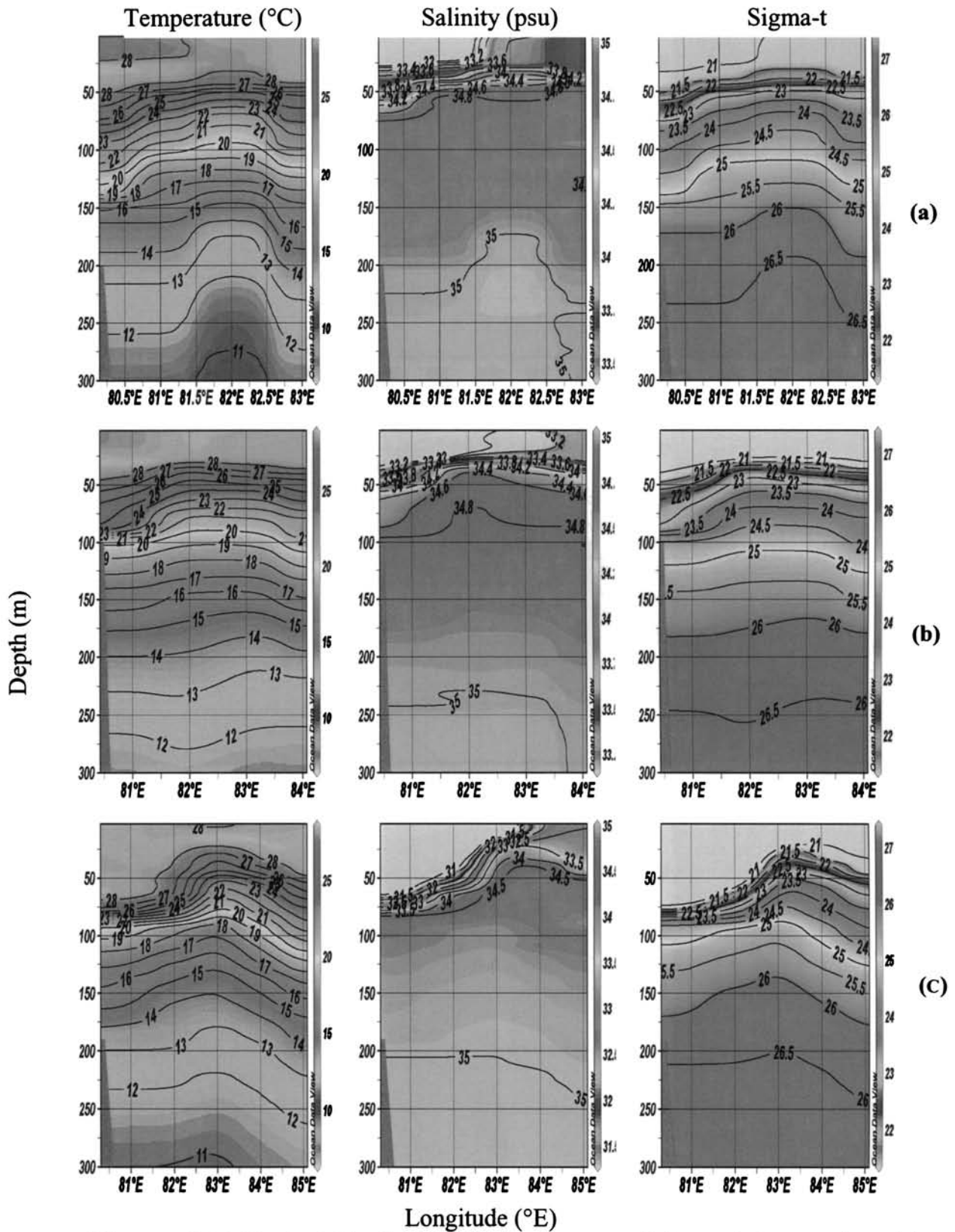


Figure. 5.11. Vertical distribution of temperature, salinity and sigma-t along (a) 11°N, (b) 13°N, (c) 15°N, (d) 17°N, (e) 19°N and (e) 20.5°N during winter monsoon in the western Bay of Bengal

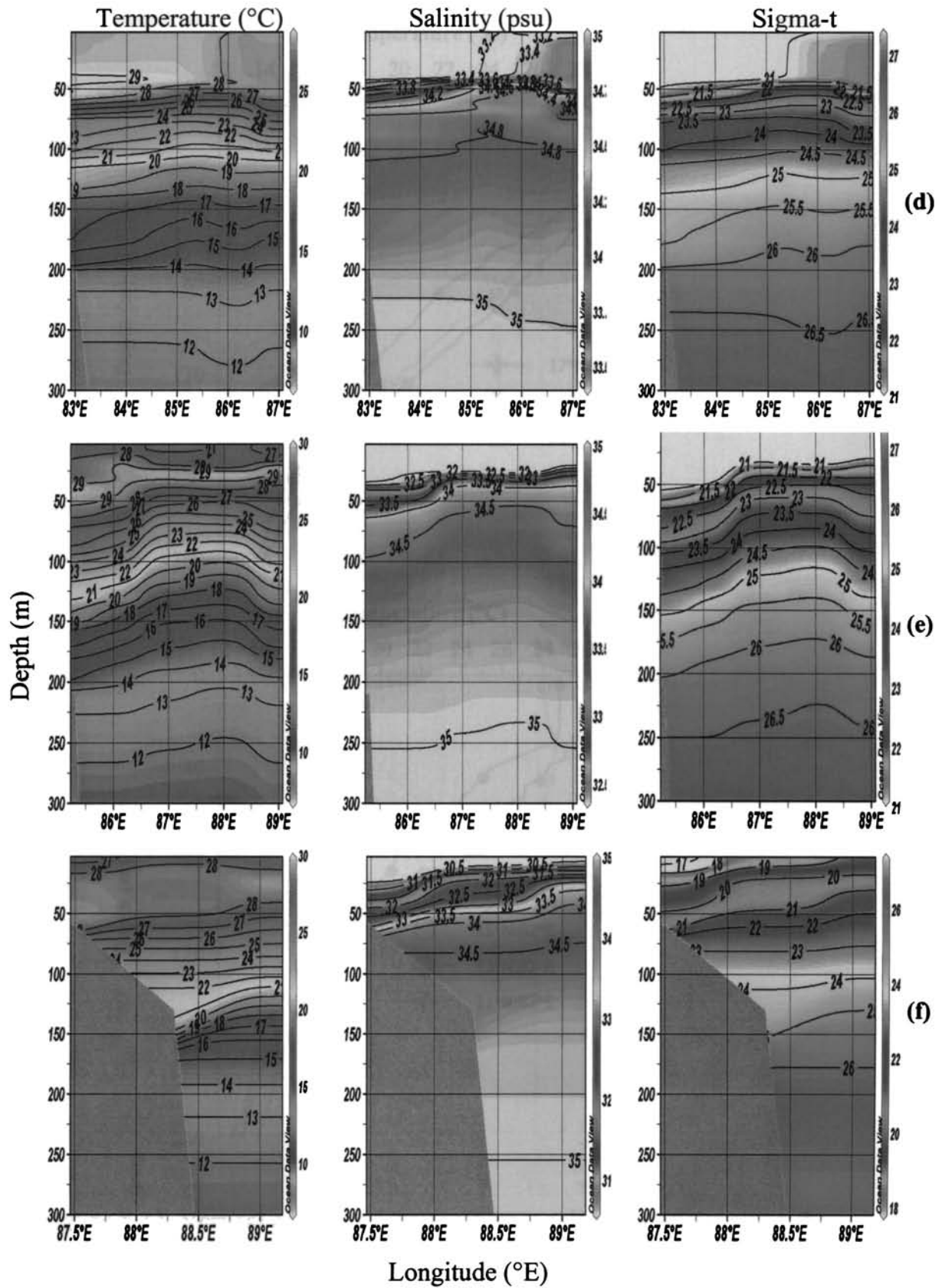


Figure 5.11. (continued)

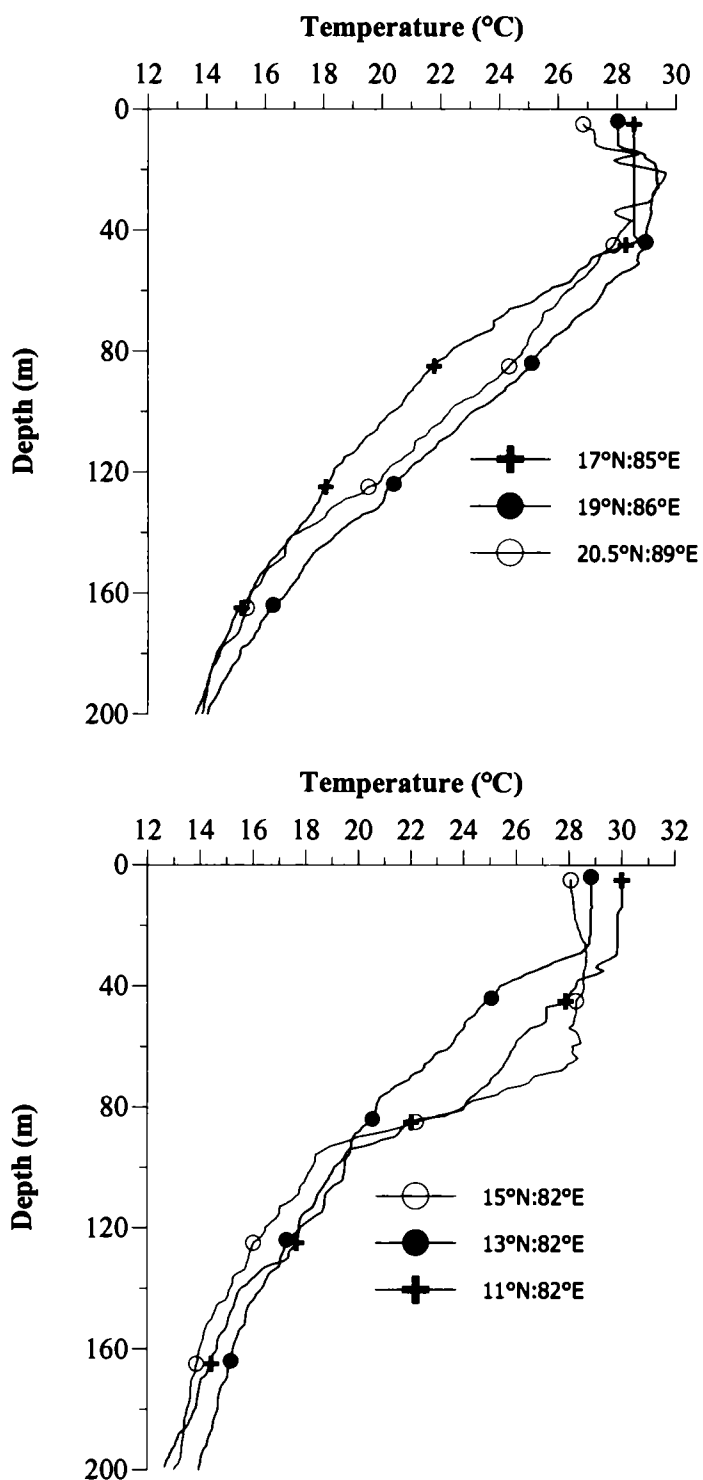


Figure 5.12. Vertical profiles of temperature at selected stations along the western BOB during winter

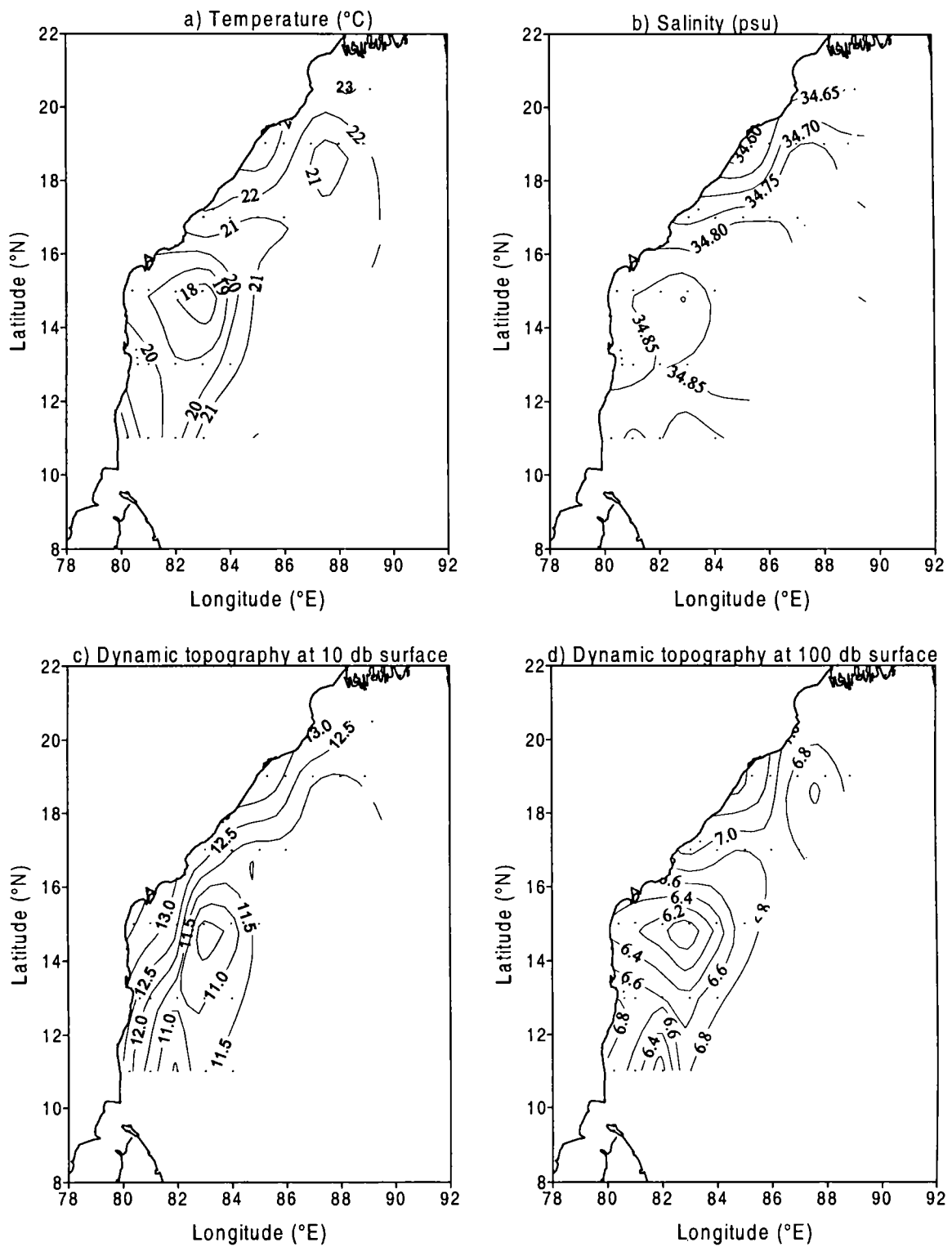


Figure 5.13. Distributions of: a) temperature and b) salinity at 100m depth. Distribution of dynamic topography at: c) 10 db and d) 100 db surfaces with reference to the 500 db along the western BOB during winter monsoon

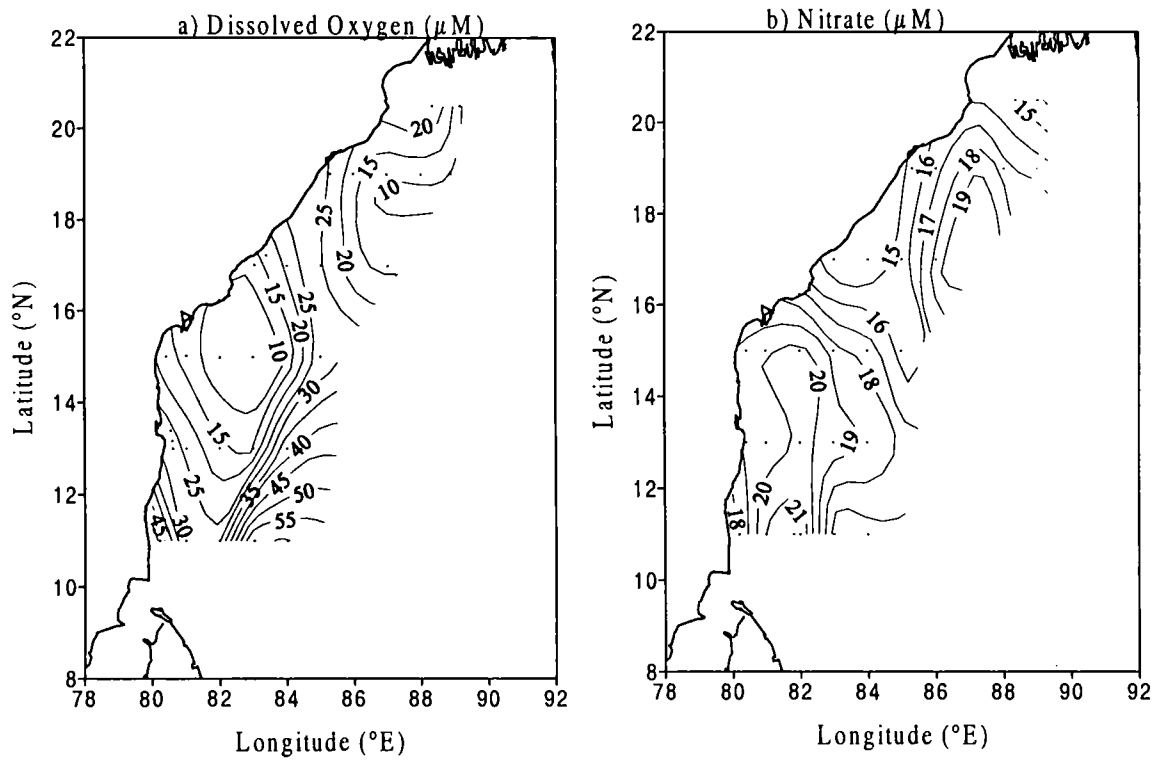


Figure 5.14. Distribution of: a) dissolved oxygen and b) nitrate at 100m along the western BOB during winter monsoon

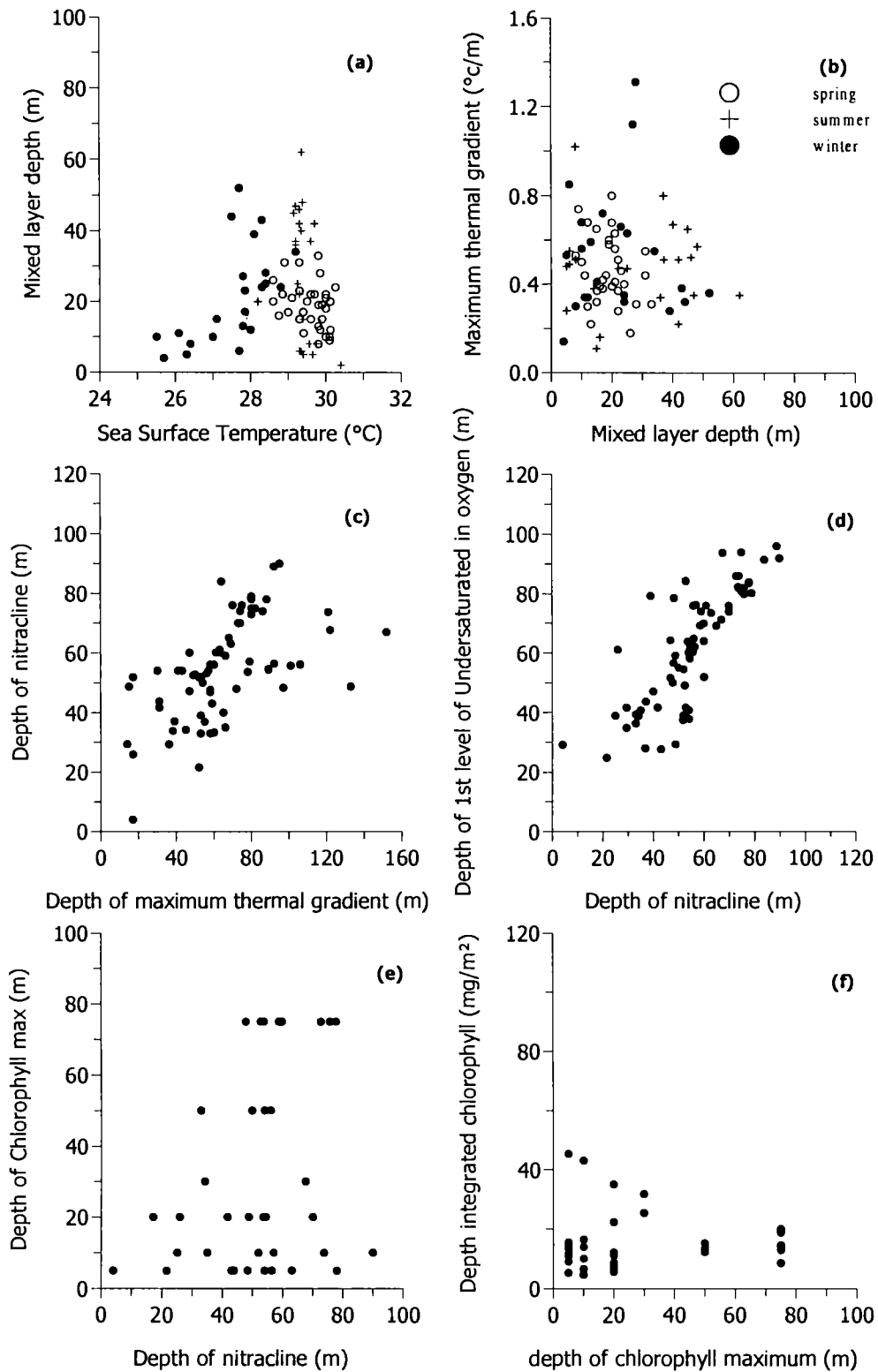


Figure 5.15. Relationship between the mixed layer depth and a) SST, b) maximal thermal gradient. Linear regression between the depth of the nitracline and c) depth of maximal thermal gradient, d) depth of first level of under saturation in oxygen e) depth of chlorophyll maxima. f) Relation between the depth of the chlorophyll maxima and the depth integrated chlorophyll along the western BOB

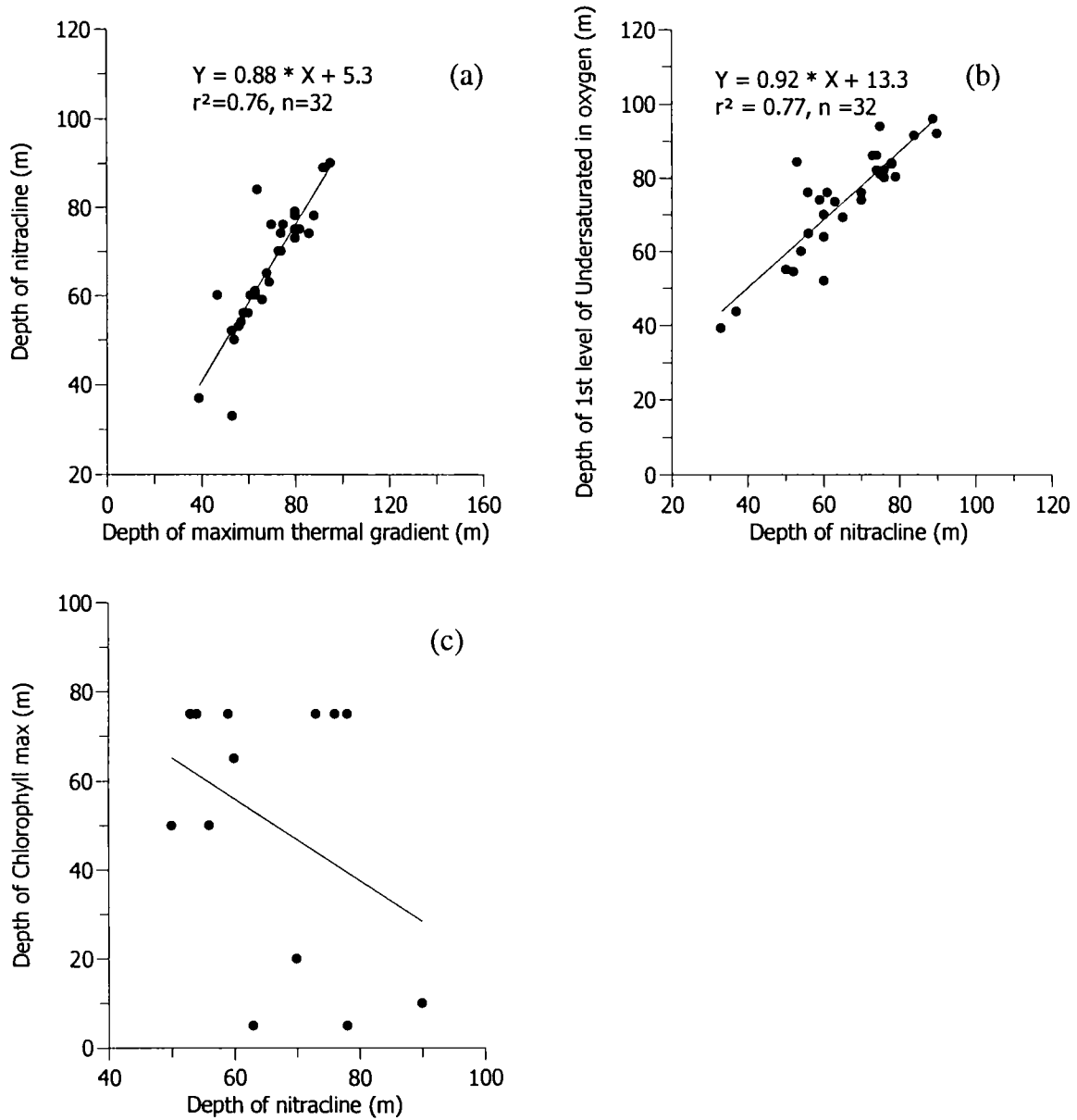


Figure 5.16. Linear regression between the depth of the nitracline and a) depth of the maximal thermal gradient, b) depth of first level of under saturation in oxygen and c) depth of chlorophyll maxima along the western BOB during spring intermonsoon

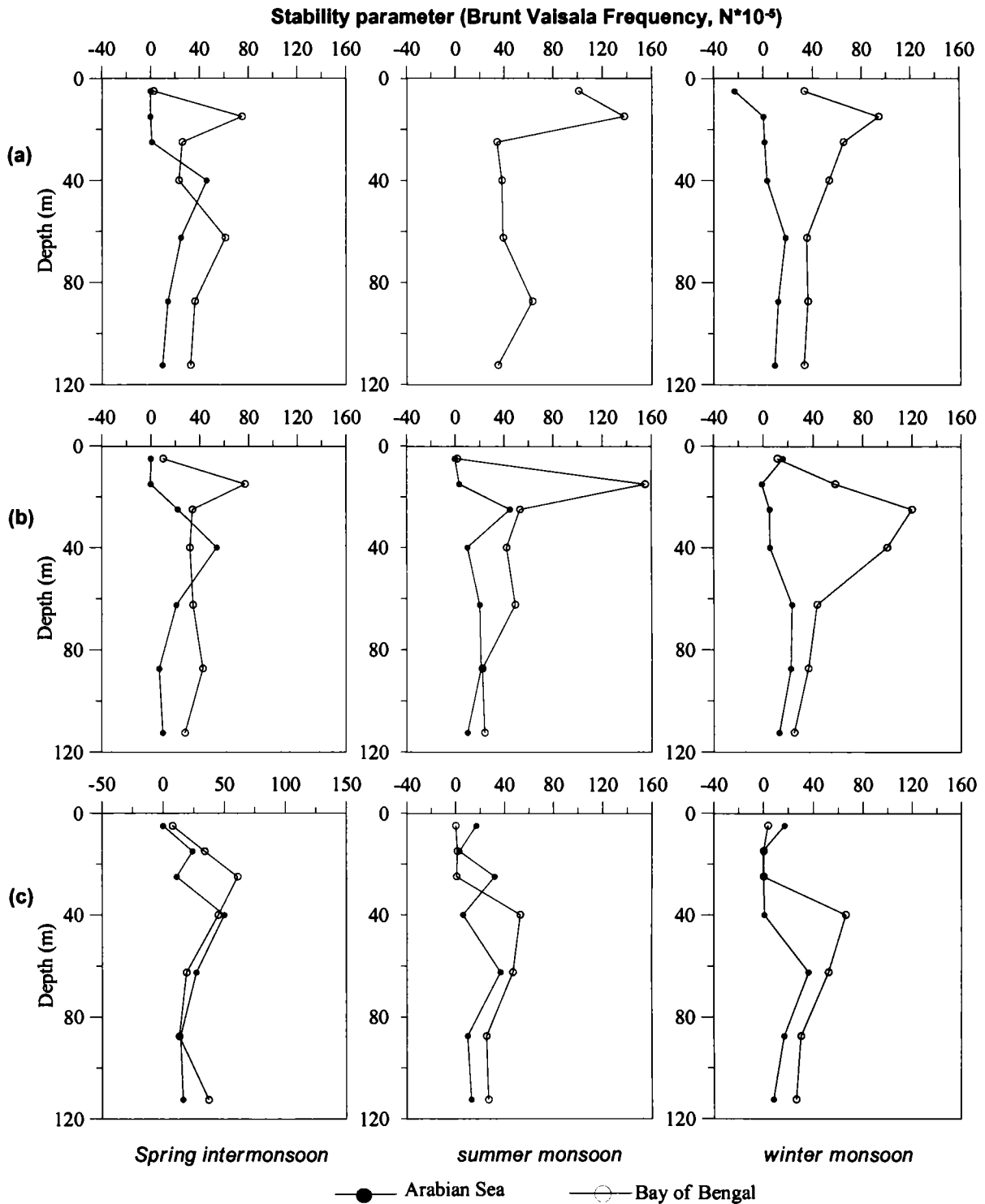


Figure 5. 17. Profiles of upper ocean stability parameter in the AS and BOB at selected stations along a) 21°N; 20.5°N (in BOB) b) 19°N, c) 17°N, d) 15°N, e) 13°N, f) 10°N; 11°N (in BOB) during different seasons

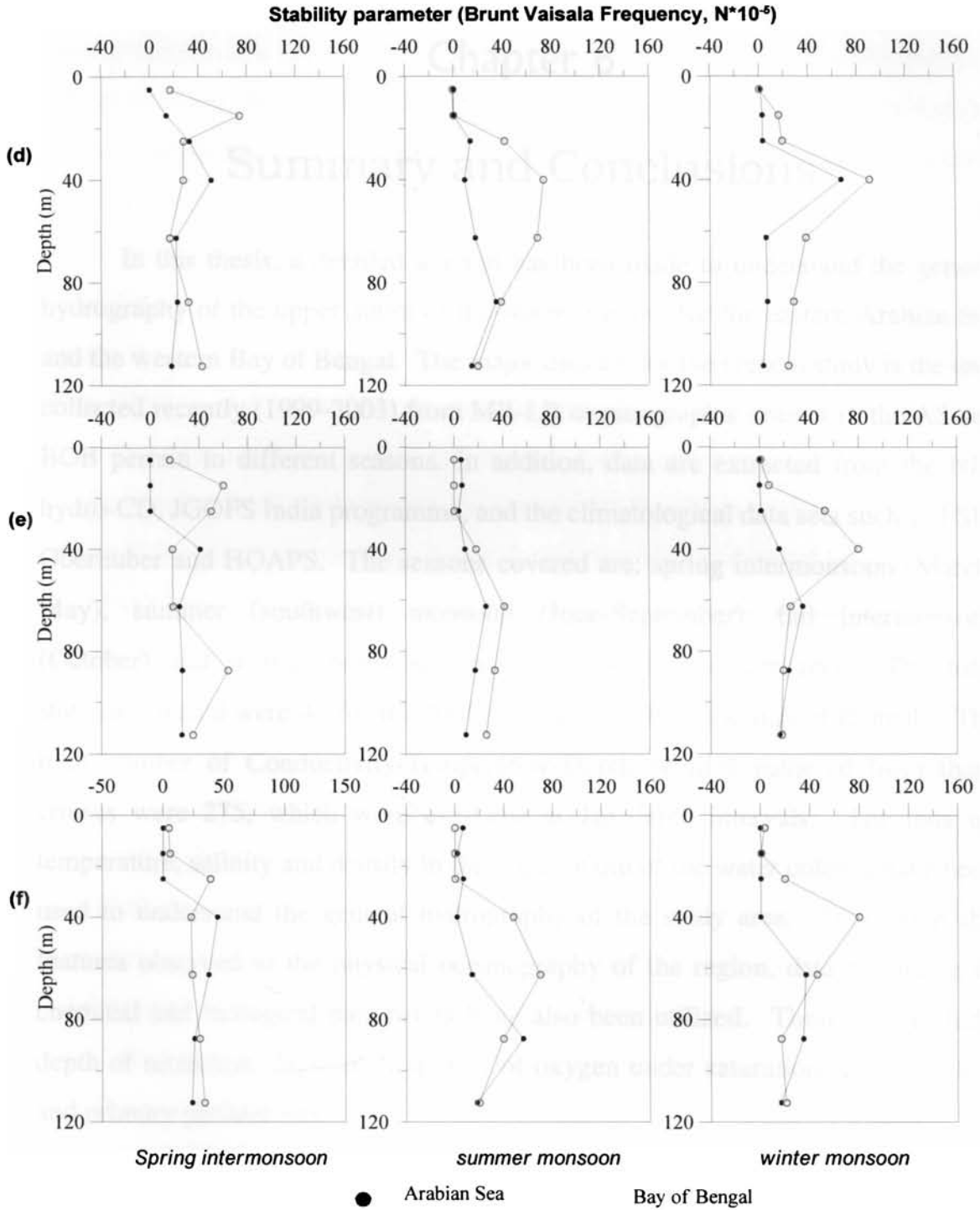


Figure 5.17. (continued)

Chapter 6

Summary and Conclusions

In this thesis, a detailed attempt has been made to understand the general hydrography of the upper 300m of the water column, for the eastern Arabian Sea and the western Bay of Bengal. The major data set for the present study is the data collected recently (1999-2003) from MR-LR oceanographic cruises in the AS and BOB pertain to different seasons. In addition, data are extracted from the NIO hydro-CD, JGOFS India programme, and the climatological data sets such as FSU, Oberhuber and HOAPS. The seasons covered are: spring intermonsoon (March-May), summer (southwest) monsoon (June-September), fall intermonsoon (October) and winter (northeast) monsoon (November-February). The total stations covered were 41 for the Arabian Sea and 29 for the Bay of Bengal. The total number of Conductivity-Temperature-Depth profiles gathered from these cruises were 275, which were available at 1m depth intervals. The data on temperature, salinity and density in the upper 300m of the water column have been used to understand the general hydrography of the study area. To support the features observed in the physical oceanography of the region, data pertaining to chemical and biological parameters have also been utilized. These data include depth of nitracline, depth of first level of oxygen under saturation, chlorophyll *a* and primary productivity.

In Chapter 1, introduction to general hydrography off the west and east coasts of India are covered, in the context of ML processes.

In Chapter 2, the materials and methods of the present study are covered. In the past, many MLD criteria have been used in the literature, and the differences in the criteria can lead to considerable differences in the MLD, which in turn, influence the findings of the study. No studies have been reported for the AS and BOB, justifying a particular temperature change (for example, 1.0, 0.5 or 0.2° C

drop of temperature from the sea surface) or density change (for example, 0.125 or 0.2 kg/m³ rise of density from the sea surface) as the most appropriate criterion, by quantitative analysis. To compare the hydrography of the AS and BOB, a unique MLD definition is essential, for which the 275 CTD profiles were used. In the BOB, thermal inversions usually exceed 1°C, and hence the conventional definition of the isothermal layer depth (defined as a drop of 1°C temperature from the sea surface) may not hold true. Therefore, in the present study, the isothermal layer depth is defined as an absolute change of temperature by 1°C from an approximately uniform region of temperature just below the surface. A comparison has been made among the various MLD criteria with the actual MLD (obtained by visual inspection). It was found that MLDs defined by the density rise of 0.2 units from the approximately uniform region of density, just below the surface (Z=5m), coincides most closely to the actual MLD.

In Chapter 3, the monthly evolution of SST, SSS, wind speed, short wave radiation, net surface heat flux, evaporation minus precipitation, MLD and barrier layer thickness were studied. The role of atmospheric forcing on the dynamics of the mixed layer in the AS and BOB were discussed. For understanding this, and the variability in the coastal and open ocean regions, the above mentioned data pertaining to 7 open ocean and 7 coastal grids (2°X2° latitude-longitude) in the AS and 6 open ocean and 6 coastal grids in the BOB were examined.

SST distribution in the AS showed a distinct bimodal pattern, a warming phase during spring and fall intermonsoons and cooling phase during summer and winter monsoons. However, in the BOB, the bimodal pattern is not well discernible. This is because the summer cooling phase in the BOB is not significant as that seen in AS. The prevailing low saline waters, which overwhelm the wind stirring and relatively weak upwelling, hamper the summer cooling in BOB.

In the central AS, mixed layer is chiefly controlled by heating and cooling as well as by wind stirring. In the coastal regions, the advection (for example, that

of low saline waters from the BOB) and vertical motion (upwelling/downwelling) controls the evolution of MLD. But in the Bay of Bengal, though wind speed and surface heat flux are comparable to AS, the two basins showed notable variation in the MLD (~60m). Though the winds in the AS and BOB are similar, these winds drives deep mixed layers in AS by wind driven and convective mixing. While in BOB, similar winds are insufficient to break the strong stratification.

Along the western BOB, the surface is stratification is more influenced by salinity rather than temperature, which reduce the mixed layer and often forms a primary barrier layer above the thermocline. This barrier layer prevents the turbulent entrainment of cool thermocline waters into the surface mixed layer. It can be found that the fresher and warmer waters in the BOB increase the surface buoyancy flux, which inhibits the turbulent mixing. It was seen that the salinity is the important physical property of seawater in BOB, which controls the dynamics of the mixed layer.

Along the SW coast, the intrusion of low saline waters from the BOB and equatorial region, creates a salinity stratified halocline within the isothermal layer and consequently limits the surface mixing to the shallow mixed layer and maintains a thick barrier layer. The formation of barrier layer starts even as early as December along the southwest coast of India, and spreads towards north with time, and north of 16°N it was hardly seen. The barrier layer was best developed during the December - February period and then begins to decrease. In general, in the BOB, the barrier layer has significant thickness during summer and winter, except along the southeast coast in summer and northeast coast in winter. The absence of the barrier layer along the northeast coast of India, during winter, is in contradiction to the earlier observations. The strong thermal inversion (>2.5°C) during winter along the northeast coast of India causes the isothermal layer to thin and consequently wipes out the barrier layer. The salinity structure along the coastal region off the east coast of India showed the flow characteristics of East India Coastal Current. Its poleward phase was best developed during spring

intermonsoon, and its equatorward phase during winter monsoon, all along the coast. During southwest monsoon, the East India Coastal Current is poleward off most of the east coast of India, while it is equatorward along the northeast coast only.

Another result that emanated from the present study is that a time lag exists between the coastal and open ocean MLDs (coastal region showed nearly one-month lag), even when the atmospheric conditions are similar at both the regimes in the AS. This lag was clearly discernible in the northern grids during winter monsoon season. In general, the open ocean showed deepest MLDs during January-February, whereas coastal region showed the maximum in February-March. In the open ocean, the drastic decrease of MLD during the final phase of winter was seen to be much faster than that observed in the coastal region.

Frequent cyclonic and anticyclonic eddies are observed in BOB, which regulate the MLDs significantly. Hence, in addition to the atmospheric parameters and SSS, surface currents and eddies are needed to explain the MLD variability. The formation of the barrier layer though to a large extent was regulated by the E-P and surface salinity, except in certain regions in the central BOB.

In Chapter 4, the general hydrography off the west coast of India is described. It was evident that upwelling along the southwest coast starts even as early as February – March in deeper layers and the upwelled water gradually reaches the surface by May/June, and propagates towards the north with the progress of the summer monsoon. The upwelling ceases along the northwest coast of India by September, while it persists even in October along the southwest coast of India and by December, the downwelling/sinking occurs all along the west coast of India. The equatorward coastal current and poleward undercurrent associated with the upwelling along the west coast of India indicates the signals of a typical wind driven eastern boundary upwelling system. Relatively weak poleward undercurrent during May/June and strong undercurrent during September/October can be linked to the strong and weak upwelling processes.

The hydrography along the southwest coast of India showed the signature of Laccadive High, in winter.

In the AS, it was found that the mechanisms for the development of mixed layer play an important role in the biological production. Shallow mixed layer can be formed in two ways. Under warm and light wind conditions (spring and fall), the surface layer becomes more stable, which inhibits the vertical mixing and results in a shallow mixed layer. As a result, the entrainment of nutrients to the surface is not possible and makes a deep nutrient depleted surface layer and eventually poor biological production. The intense wind forcing during the SW monsoon drives the upwelling along the southwest coast, which results in a more stratified surface layer having shallow mixed layer. But the effect of offshore Ekman transport and associated Ekman pumping bring the nutrients in to the surface and the region becomes highly productive. Deeper mixed layer also forms in two ways. During winter, along the northwestern Arabian Sea, the high rate of evaporation leads to surface cooling and initiates turbulence and drives the deep mixed layer. The entrainment of thermocline nutrient rich waters during mixed layer deepening drives high biological production. On the contrary, the downwelling along the southwest coast drives the surface waters to converge near the coast resulting in a deep mixed layer, often devoid of nutrients and results in poor productivity. So it is therefore, the mechanism of the evolution of mixed layer gives an idea about the productivity pattern of the region.

Since light is not a limiting factor in the AS for primary production, whenever the nutrient is available at the euphotic layer, it immediately result in high primary production. The present study showed that, high primary productivity occurred at the initial phase of upwelling and winter cooling itself.

In Chapter 5, the general hydrography of the Bay of Bengal is covered. The most striking feature during spring intermonsoon observed in the hydrography is the warm core eddy centered around 17°N and 85°E. Relatively large diameter of the eddy (more than 400 km) and the poleward East India Coastal Current

points that it is an integral part of the subtropical gyre reported by earlier workers. The chemical and biological parameters also showed eddy signatures as was seen in the horizontal sections of temperature, salinity and dynamic topography. Relatively high concentration of dissolved oxygen, low nitrate concentration sustains less productivity in the core of the eddy.

In the present study, during the summer monsoon season, intrusion of southwest monsoon current (bringing in AS water mass- ASHSW) into the BOB, at 100-150 m depth range, south of 13°N and to the west (82°E - 84E), was seen. This feature undergoes spatial variability as earlier it was reported by a few workers that the intrusion occurs more to the east (Murty *et al.*, 1992b) than that reported here.

A significant feature observed along the western Bay during winter monsoon was the presence of a cyclonic cold core eddy (high salinity, nutrient rich and oxygen poor) centered at 15°N; 83°E observed below 40m depth. Under the influence of this subsurface eddy, the nutrients are pumped in to the upper layer, consequently relatively higher production is seen in this region. However, this pumping is not an efficient process as the nutrient rich subsurface waters are capped by prevalent low saline water and prevent the surfacing of nutrients. The generating mechanism of the eddy is thought to be the circulation pattern. The geostrophic estimates based on the hydrographic data collected during the season shows the cyclonic circulation pattern with equatorward EICC

Along the southwest coast, upwelled water reaches the surface by May. This upwelling band spreads slowly towards north with the progress of monsoon and persists till the retreat of southwest monsoon (September). The cold upwelled water spreads about 200 km width from the shore. The BOB does not experience intense upwelling as compared to AS. In fact, winds along the western BOB are more favourable to the process of upwelling, as compared to the eastern AS. But along the east coast of India, the upwelling was evident at few locations and is often noticed as subsurface upwelling during southwest monsoon. Upwelling

during the summer monsoon was restricted to a narrow band (<50km) along the most of the east coast, while in the north it is overwhelmed by the substantial freshwater influx that occurs during the season. Accordingly, the biological productions of the two basins show remarkable variation in the upwelling region. The AS, having the highest PP and chlorophyll a (integrated over 120m) were recorded at the upwelling site and the values are $9144 \text{ mgC m}^{-2} \text{ d}^{-1}$ and 203 mg m^{-2} respectively.

The winter response of the two basins are also contrasting. The atmospheric conditions in winter along both the northeastern AS and northwestern BOB are favourable to cooling. In the AS, the heat loss by the winter cooling and the ambient high surface salinity leads the densification of surface waters, which initiates the turbulence at the surface and finally the convective overturning of subsurface waters. As a result the mixed layer deepens and the nutrients are pumped in the euphotic zone, which enhance the primary production. While in the northwestern BOB, the cooling at the surface does not lead to the densification and associated convective mixing. This is prevented by low saline surface waters, which stay stagnant in surface layers. As a result, the cold fresh water in the surface layers stay inactive, below which the temperature increases with depth resulting in thermal inversion (the amplitude of inversion exceeds 2.5°C in the northwestern Bay).

In general, in the BOB, processes like upwelling, cyclonic eddy formation and winter cooling do not benefit biological productivity, as compared to the eastern AS. Static stability computation showed that stratification is strong in the upper 20 m of the water column in the BOB whereas in the AS it is seen at a depth of around 50 m, on an average.

The investigation of the TTS of the tropical ecosystem in the euphotic layer in the AS, the depth of the maximum thermal gradient, nitracline and the first depth of the oxygen under saturation are statistically at same depth and the existence of deep chlorophyll maxima follows the TTS characteristics. Which

implies that the mixed layer is nitrate depleted and has the important biological significance. At the nitracline, the light and nutrients are optimal and hence the chlorophyll maxima stand at this level, below this layer oxygen is under saturated. Whereas in the BOB, the feature of TTS was obscure, except during spring intermonsoon. During spring intermonsoon, most of the region in the BOB showed the sub surface chlorophyll maxima. But the resulting biological production (depth integrated – 120m) was remarkably lower than the AS, suggesting the particle flux in the water column also plays a major role in the less productive Bay.

The present study has clearly revealed the important role MLD plays in the physical, chemical and biological processes in the AS and BOB. Salinity plays a dominant role in these processes in the BOB as compared to the AS. Arabian Sea behaved as a TTS throughout the year whereas BOB does during the spring intermonsoon only. However, our current understanding on the hydrography of the 300m of the water column would significantly improve when adequate high quality data by ARGO profiling floats and moored buoys become routinely available. The routine hydrographic data collected from ships are also to be shorter space and time intervals. These data sets can be used in conjunction with data available from oceanographic and meteorological satellites.

References

- Antony, M.K., 1990. Northward under current along west coast of India during upwelling - some inferences. *Indian Journal of Marine Science*, **19**, 95-101.
- Babu, M.T., Prasanna Kumar, S. and Rao, D.P., 1991. A subsurface cyclonic eddy in the Bay of Bengal. *Journal of Marine Research*, **49**, 403-410.
- Babu, M.T., Sarma, Y.V.B., Murthy, V.S.N. and Vethamony, P., 2003. On the circulation in the Bay of Bengal during northern spring inter-monsoon (March-April 1987), *Deep-Sea Research, II*, **50**, 855-865.
- Banse, K., 1959. On upwelling and bottom-trawling off the southwest coast of India. *Journal of Marine Biological Association of India*, **1**, 33-49.
- Banse, K., 1968. Hydrography of the Arabian Sea shelf of India and Pakistan and effects on demersal fishes. *Deep-Sea Research*, **15**, 45-79.
- Banse, K., 1987. Seasonality of phytoplankton division chlorophyll in the central and northern Arabian Sea. *Deep-Sea Research*, **34**, 713-723.
- Banse, K. and McClain, C.R., 1986. Winter blooms of phytoplankton in the Arabian Sea as observed by the coastal zone color scanner. *Marine Ecology Progress Series*, **34**, 201-211.
- Barber, R.T., Marra, J., Bidigare, R.C., Codispoti, L.A., Halpern, D., Johnson, Z., Latasa, M., Goericke, R. and Smith, S.L., 2001. Primary productivity and its regulation in the Arabian Sea during 1995. *Deep-Sea Research, II*, **48**, 1127-1172.
- Bathen, K.H., 1972. On the seasonal changes in the depth of the mixed layer in the North Pacific Ocean. *Journal of Geophysical Research*, **77**, 7138-7150.
- Bauer, S., Hitchcock, G.L. and Olson, D.B., 1991. Influence of monsoonally forced Ekman dynamics of upper surface layer depth and phytoplankton biomass distribution in the Arabian Sea. *Deep-Sea Research*, **38**, 531-553.
- Brainerd, K.E. and Gregg, M.C., 1995. Surface mixed and mixing layer depths. *Deep-Sea Research*, **42**, 1521-1543.
- Brock, J.C., McClain, C.R. and Hay, W.W., 1992. A Southwest monsoon hydrographic climatology for the Northwestern Arabian Sea. *Journal of Geophysical Research*, **97**, 9455-9465.

- Brock, J.C., McClain, C.R., Hay, W.W., 1999. The Phytoplankton bloom in the north western Arabian Sea during the south west monsoon of 1979. *Deep-Sea Research*, II, **46**, 1746-1768.
- Brown, J., Colling, A., Park, D., Philips, J., Rothery, D. and Wright, J., 1989. In: *Ocean Circulation: Gerry bearman (eds)*, Pergamon Press, Oxford.
- Brown, S.L., Landry, M.R., Barber, R.T., Campell, L., Garison, D.L. and Gowing, M.M., 1999. Picophytoplankton dynamics and production in the Arabian Sea during the 1995 southwest monsoon. *Deep- Sea Research*, II, **46**, 1745-1768.
- Bruce, J.G., Johnson, D.R. and Kindle, J.C., 1994. Evidence for eddy formation in the eastern Arabian Sea during the northeast monsoon. *Journal of Geophysical Research*, **99**, 7651-7664.
- Chen, D., Busalacchi, A.J. and Rosthtein, L.M., 1994. The roles of vertical mixing, solar radiation, and wind stress in a model simulation of the sea surface temperature seasonal cycle in the tropical Pacific Ocean. *Journal of Geophysical Research*, **99**, 20, 345- 359.
- Colborn, J.G., 1975. The thermal structure of the Indian Ocean, IIOE Oceanography Monographs, 2, University Press of Hawaii, Honolulu.
- Conkright, M., Levitus, S., O'Brien, T., Boyer, T., Antonov, J. and Stephen, C., 1998. World Ocean Atlas 1998 CD-ROM Data set Documentaion. *Technical Report, 15*, and National oceanographic Data Centre, Silver Spring, Md.
- Cronin, M.F. and McPhaden, J.M., 2002. Barrier layer formation during westerly wind bursts. *Journal Geophysical Research*, **107**, 8020, doi:10.1029/2001JC001171
- Cutler, A.N. and Swallow, S.C., 1984. Surface currents of the Indian Ocean (to 25°S, 100°E): Compiled from historical data archived by Meteorological Office, Bracknell, U.K., *Report. 187*, 8 pp., 36 charts, Inst. of Oceanogr. Sci., Godalming, England.
- Darbyshire, M., 1967. The surface waters off the coast of Kerala, southwest India. *Deep-Sea Research*, **14**, 295-320.
- Denman, K.L., 1973. A time-dependent model of the upper ocean. *Journal of Physical Oceanography*, **3**, 173-184.

- Eigenheer, A. and Quadfasel, D., 2000. Seasonal variability of the Bay of Bengal circulation inferred from TOPEX/Poseidon altimetry. *Journal of Geophysical Research*, **105**, 3243-3252.
- Fairall, C.W., Bradley, E.F., Godfrey, J.S., Wick, G.A., Edson, J.B., and Young, G.S., 1996. Cool skin and warm layer effects on sea surface temperature, *Journal of Geophysical Research*, **101**, 1295-1308.
- Findlater, J., 1969. A major low-level air current near the Indian Ocean during the northern summer. *Quarterly Journal of Royal Meteorological Society* ., **95**, 362-380.
- Fomin, L.M., 1964. The Dynamic method in Oceanography, London, Elsevier, pp 212.
- Gadgil, S., Joseph, P.V. and Joshi, N.V., 1984. Ocean-atmosphere coupling over monsoon regions. *Nature*, **312**, 141-143.
- Gardner, W.D., Gunderson, J.S., Richardson, M.J. and Walsh, I.D., 1999. The role of seasonal and diel changes in mixed layer depth on carbon and chlorophyll distributions in the Arabian Sea, *Deep-Sea Research, part II*, **46**, 1833 – 1858.
- Gardner, W.D., Chung, S. P., Richardson, M.J. and Walsh, I.D., 2001. The oceanic mixed layer pump, *Deep- Sea Research, II*, **42**, 757 – 775.
- ✓ Garwood, R.W., 1977. An oceanic mixed-layer model capable of simulating cyclic states. *Journal of Physical Oceanography*, **7**, 455-468.
- Gaspar, P., 1988. Modeling the seasonal cycle of the upper ocean. *Journal Physical Oceanography*, **18**, 161-180.
- ✓ Gill, A.E., 1982. Atmosphere – Ocean Dynamics. *Academic Press, New York* 662pp.
- ✓ Godfrey, J.S., and Lindstorm, E., 1989. The heat budget of the equatorial western Pacific surface mixed layer, *Journal of Geophysical Research*, **94**, 8007-8017.
- ✓ Gomes, H.R., Goes, J.I. and Saino, T., 2000. Influence of physical processes and freshwater discharge on the seasonality of phytoplankton regime in the Bay of Bengal. *Continental Shelf Research*, **20**, 313-330.

- Gopalakrishna, V.V. and Sastry, J. S., 1985. Surface circulation over the shelf off the east coast of India during southwest monsoon. *Indian Journal of Marine Science*, **14**, 62-65.
- Gopalakrishna, V.V., Sadhuram, Y. and Ramesh Babu, V., 1988. Variability of mixed layer depth in the northern Indian Ocean during 1977 and 1979 summer monsoon seasons. *Indian Journal of Marine Science*, **17**, 258–264.
- Gopalakrishna, V.V., Murty, V.S.N., Sengupta, D., Shenoi, S.S.C. and Nilesh Araligidat, 2002. Upper ocean stratification and circulation in the northern Bay of Bengal during southwest monsoon of 1991, *Continental Shelf Research*, **22**, 791-802 .
- Gopalakrishna, V.V., Pednekar, S.M. and Murty, V.S.N., 1996. T-S variability and volume transport in the central Bay of Bengal during southwest monsoon. *Indian Journal of Marine Science*, **25**, 50–55.
- Grassl, H., Jost, V., Kumar, R., Schulz, J., Bauer, P. and Schluessel, P., 2000: *The Hamburg Ocean-Atmosphere Parameters and Fluxes from Satellite Data (HOAPS): A Climatological Atlas of Satellite-Derived Air-Sea-Interaction Parameters over the Oceans*. Report No. 312, ISSN 0937-1060, Max Plank Institute for Meteorology, Hamburg.
- Halpern, D. and Woiceshyn, P. M., 2001. Onset of the Somali Jet in the Arabian Sea, during 1997. *Journal of Geophysical Research*, **104**,18041-18046.
- Han, W., 1999. Influence of salinity on dynamics, thermodynamics and mixed layer physics on the Indian Ocean, Ph.D.thesis, 147 pp., Nova South eastern Univ., Fort Lauderdale, Fala.
- Han, W., and McCreary, J. P., 2001. Modeling salinity distribution in the Indian Ocean, *Journal of Geophysical Research*, **106**, 859-877.
- Han, W., McCreary, J.P. and Kohler, K., 2001. Influence of precipitation minus evaporation and Bay of Bengal rivers on dynamics, thermodynamics, and mixed layer physics in the upper Indian Ocean, *Journal of Geophysical Research*, **106**, 6895–6916.
- Hareeshkumar, P.V. and Mathew, B., 1997. Salinity distribution in the Arabian Sea. *Indian Journal of Marine Science*, **26**, 271-277.

- Hastenrath, S. and Lamb, P., 1979. Climatic Atlas of the Indian Ocean, Part 1: Surface climate and Atmospheric circulation, 273 pp., Univ. of Wisc. Press, Madison.
- Hastenrath, S. and Greischar, L.L., 1989. *Climatic Atlas of the Indian Ocean, Part 3: Upper ocean structure*, 273 pp., Univ. of Wisc. Press, Madison.
- Hellerman, S. and Rosenstein, M., 1983. Normal wind stress over the world ocean with error estimates, *Journal of Physical Oceanography*, **13**, 1093-1104.
- Herbland, A. and Voituriez, B., 1979. Hydrological structure analysis for estimating the primary production in the tropical Atlantic Ocean. *Journal of Marine Research*, **37**, 87-101.
- Howden, S.D. and Murtugudde, R., 2001. The effects of river input in the Bay of Bengal. *Journal of Geophysical Research*, **106**, 19,825-19,843.
- Huang, R.X. and Russell, S., 1994. Ventilation of the subtropical North Pacific. *Journal of Physical Oceanography*, **24**, 2589-2605.
- Johannessen, O.M., Subbaraju, G. and Blindheim, J., 1981. Seasonal variation of the Oceanographic condition off the Southwest coast of India during 1971-75. *Fisk. Dir. Skr. Ser. HavUnders.*, **18**, 247-261.
- Joint Global Ocean Flux Studies, 1996. *Current Science*, Special Section: JGOFS (INDIA).
- Joseph, P.V., 1990. Warm pool over the Indian Ocean and monsoon onset. *Trop.Ocean Global Atmos.Newsl.*, **53**, 1-5
- Jyothibabu, R., Maheswaran P.A., Madhu N.V., Mohamed Asharaf, Vijay, J.G., Venugopal, P., Revichandran, C., Balasubramaniam, T., Gopalakrishnan T.C. and Nair, K.K.C. Differential response of winter cooling on biological production in the northeastern Arabian Sea and northwestern Bay of Bengal. *Current Science* (Accepted).
- Kara, A.B., Rochford, P.A. and Hurlburt, H.E., 2000. An optimal definition for ocean mixed layer depth. *Journal of Geophysical Research*, **105**, 16,803-16,821.
- Kraus, E.B. and Turner, J.S., 1967. A one-dimensional model of the seasonal thermocline. II. The general theory and its consequences. *Tellus*, **19**, 98-105.

- ✓ Kraus, E.B., 1977. Modelling and prediction of the upper layers of the Ocean, Pergamon Press, Oxford, England.
- La Fond E.C., 1957. Oceanographic studies in the Bay of Bengal. *Proceedings of the Indian Academy of Science*, **46B**, 1-46.
- ✓ Laevastu, T. and Hela, I., 1970. In: *Fisheries Oceanography*, Fishing News (Books) Ltd, 110 Fleet street, London.
- ✓ Lee, C.M., Jones, B.H., Brink, K.H. and Fischer, A.S., 2000. The upper ocean response to monsoonal forcing in the Arabian Sea: Seasonal and spatial variability. *Deep- Sea Research, II*, **47**, 1177-1226.
- Legickis, R., 1987. Satellite observation of a western boundary current in the Bay of Bengal. *Journal of Geophysical Research*, **92**, 1325-1342.
- Levitus, S., 1982: *Climatological Atlas of the World Ocean*. NOAA Prof. Paper 13, U.S. Govt. Printing Office, Washington DC, 173pp.
- ✓ Levitus S, Booyer, T.P., M.E., Conkright, T., Brien, J., Antonov, C., Stephens, L., Stathoplos, D., Johnson, R. and Gelfeld. 1998. NOAA Atlas NESDIS 18, Washington D.C., U.S.A.
- ✓ Lewis, M.R., Carr, M., Feldman, G., Esaias, W. and McClain, C., 1990. Influence of penetrating solar radiation on the heat budget of the equatorial Pacific Ocean. *Nature*, **347**, 543-544.
- Longhurst, A.R. and Wooster, W.S., 1995. Abundance of oil sardine (*Sardinella longiceps*) and upwelling on the southwest coast of India, *Can. J. Fish. Aquat. Sci.*, **47**, 2407-2419.
- ✓ Lukas, R. and Lindstorm, E., 1991. The mixed layer of the western equatorial Pacific Ocean. *Journal of Geophysical Research*, **96**, 343-357.
- Luther, M.E., 1987. Indian Ocean modeling. In: Katz, E., Whitte, J.(Eds), *Further Progress in Equatorial Oceanography*. Nova University Press, Dania, FL, pp. 303-316.
- ✓ Madhu, N.V., Maheswaran, P.A., Jyothibabu, R., Sunil, V., Revichandran, C., Balasubramaniam, T., Gopalakrishnan, T.C and Nair, K.K.C., 2001. Enhanced biological production Off Chennai triggered by October super cyclone (Orissa), *Current Science*, **82**, 1472-1479.

Madhupratap, M., Prasanna Kumar, S., Bhattathiri, P.M.A., Dileep Kumar, M., Reghukumar, S., Nair, K.K.C. and Ramaiah, N., 1996. Mechanism of the biological response to winter cooling in the northeastern Arabian Sea. *Nature*, **384**, 549-552.

Madhupratap, M., Mangesh Gauns, Ramaiah, N., Prasanna Kumar, S., Muraleedharan, P.M., de Sousa, S. N., Sardesai, S. and Usha Muraleedharan., 2003. Biogeochemistry of the Bay of Bengal: Physical, chemical and primary productivity characteristics of the central and western Bay of Bengal during summer monsoon 2001, *Deep-Sea Research*, II, **50**, 881-896.

Maheswaran, P.A., Rajesh, G., Revichandran, C. and Nair, K.K.C., 2000. Upwelling and associated hydrography along the west coast of India during south west monsoon, 1999. *Prosec, Proceedings*, vol.II:873-878.

Martin, P.J., 1985. Simulation of the mixed layer at OWS November and Papa with several models. *Journal of Geophysical Research*, **90**, 903-916.

McCreary, J.P., Kundu, P.K. and Molinari, R.L., 1993. A numerical investigation of dynamics, thermodynamics and mixed layer process in the Indian Ocean. *Progress in Oceanography*, **31**, 181-244.

McCreary, J.P., Han, W., Shankar, D. and Shetye, S.R., 1996. Dynamics of the East India Coastal Current: 2. Numerical solutions. *Journal of Geophysical Research*, **101**, 13993–14010.

McCreary, J.P., Kohler, K.E., Hood, R.R., Smith, S., Kindle, J., Fischer, A.S. and Weller, R. A., 2001. Influence of diurnal and intra seasonal forcing on mixed-layer and biological variability in the central Arabian Sea. *Journal of Geophysical Research*, **106**, 7139 – 7155.

Miller, J.R., 1976. The salinity effect in a mixed layer ocean model. *Journal of Physical Oceanography*, **6**, 29-35.

Mittelstaedt, E., 1986. Upwelling regions. *Landolt Bornstein, Group V*, Vol.3, Sub volume, C,J. Sundermann, ed., Springer- Verlag, **349**.

Mohan, M. and Ali, M.M., 1995. Estimation of wind stress induced offshore upwelling, *Continental shelf Research*, **15**, 757-762.

Monterey, G. and Levitus, S., 1997. Seasonal variability of mixed layer depth for the World Ocean, NOAA Atlas NESDIS, **14**, 100pp, U.S. Govt. Print. Off., Washington, D.C.

- ✓ Munk, W.H. and Anderson, E.H., 1948. Notes on a theory of the thermocline. *Journal of Marine Research*, **7**, 276-295.
- ✓ Muraleedharan, P.M., Ramesh Kumar, M.R., Rao, L.V.G., 1995. A note on poleward undercurrent along the southwest coast of India. *Continental Shelf Research*, **15**, 165-184.
- Muraleedharan, P.M. and Prasanna Kumar, S., 1996. Arabian Sea upwelling - A comparison between coastal and open ocean regions. *Current Science*, **71**, 842-846.
- ✓ Murty C.S. and Varadhachary, V.V.R. 1968. Upwelling along the east coast of India. *Bulletin of National Institute of Sciences India*, **36** (1), 80-86.
- ✓ Murty V.S.N., Sarma, Y.V.B., Babu, M.T. and Rao, D.P., 1992a. Hydrography and circulation in the northwestern Bay of Bengal during the retreat of southwest monsoon. *Proceedings of Indian Academy of Sciences, (Earth and Planetary)*, **101**, 67-75.
- ✓ Murty, V.S.N., Sarma, Y.V.B., Rao, D.P. and Murty, C.S., 1992b. Water characteristics, mixing and circulation in the Bay of Bengal during southwest monsoon. *Journal of Marine Research*, **50**, 207-228.
- ✓ Murty, V.S.N., Suryanarayana, A. and Rao, D.P., 1993. Current structure and volume transport across 12°N in the Bay of Bengal, *Indian Journal of Marine Science*, **22**, 12-16.
- ✓ Murty, V.S.N., Gupta, G.V.M., Sarma, V.V., Rao, B.P., Jyothi, D., Shastri, P.N.M. and Supraveena, Y., 2000. Effect of vertical stability and circulation on the depth of the chlorophyll maximum in the Bay of Bengal during May-June, 1996. *Deep-Sea Research I*, **47**, 859-873.
- ✓ Naidu, S.V., 1993. Mixed layer depth of the North Indian Ocean during May and September, *Mahsagar*, **26**, 87-93.
- ✓ Naidu, D.P., Ramesh Kumar, M.R. and Ramesh Babu, V., 1999. Time and space variations of monsoonal upwelling along the west and east coasts of India. *Continental Shelf Research*, **19**, 559-572.
- ✓ Nakamoto, S., Prasanna Kumar, S., Oberhuber, J.M., Muneyamma, K. and Frouin, R., 2000. Chlorophyll modulation of sea surface temperature in the Arabian Sea in

a mixed layer isopycnal general circulation model. *Geophysical Research Letters*, **27**, 747-750.

Niiler, P.P. and Kraus, E.B., 1977. One-dimensional models of the upper ocean. *Modelling and Prediction of the Upper layers of the Ocean*, E.B. Kraus, Ed. Pergamon, 143-172.

Obata, A., Ishizaka, J. and Endoh, M., 1996. Global verification of critical depth theory for phytoplankton bloom with climatological in situ temperature and satellite ocean color data. *Journal of Geophysical Research*, **101**, 20,657-20,667.

Oberhuber, J.M., 1988. An atlas based on COADS data set, Tech, Rep. **15**, 182 pp, *Max-Planck-Inst. Fur Meteorol.*, Hamburg, Germany.

Ohlmann, J.C., Siegel, D.A. and Gautier, C., 1996. Ocean mixed layer radiant heating and solar penetration: A global analysis. *Journal of Climate*, **9**, 2265-2280.

Pankajakshan T, Gopalakrishna, V.V., Muraleedharan, P.M., Reddy, G.V., Nilesh Araligidad, and Shenoi, S., 2002. Surface layer temperature inversion in the Bay of Bengal, *Deep - Sea Research*, **49**, 1801-1818.

Pant, A., 1992. Primary productivity in coastal and off-shore waters of India during two southwest monsoons, 1987 and 1989. In: *Oceanography of the Indian Ocean*. Desai, B.N. Editor, Oxford and IBH, New Delhi, pp. 81-90.

Philips, O. M., 1958. On the equilibrium range in the spectrum of wind generated waves, *Journal of Fluid Mechanics*, **4**, 426-434.

Pickard, G.L and Emery, W.J., 1982. *Descriptive Physical Oceanography: An Introduction*, 4th Edition, Pergamon Press Ltd, Headington Hill Hall, Oxford, England, 249.

Pillai, V. N., 1983. Physical characteristics of the coastal waters off the south west coast of India with an attempt to study the possible relationship with sardine, mackerel and anchovy fisheries. Ph. D Thesis, Cochin university of Science and technology.

Pond, S. and Pickard, G.L., 1983. *Introductory dynamical oceanography* (2nd ed.), Pergamon Press, Oxford.

Potemra, J. T., Luther, M.E. and O'Brien, J.J., 1991. The seasonal circulation of the upper ocean in the Bay of Bengal. *Journal of Geophysical Research*, **96**, 12667-12683.

- Prasad T.G. and Bahulayan, N., 1995. Mixed layer depth and thermocline climatology atlas of the Arabian Sea and Western Indian Ocean, NIO/TR-1/95, 11 pp. and 44 figures.
- ✓ Prasad T.G., 2004. A comparison of mixed layer dynamics between the Arabian Sea and Bay of Bengal: one dimensional model results. *Journal of Geophysical Research*, **109**, C03035, doi:10.1029/2003JC002000
- ✓ Prasannakumar, S. and Prasad, T.G., 1996. Winter cooling in the northern Arabian Sea. *Current science*, **71**, 11.
- ✓ Prasanna Kumar, S. and Prasad, T.G., 1999. Formation and spreading of Arabian Sea high-salinity water mass. *Journal of Geophysical Research*, **104**, 1455-1464.
- Prasanna Kumar, S., Madhupratap, M., Dileep Kumar, M., Muraleedharan, P.M., de Souza, S.N., Gauns, M. and Sarma, V.V.S.S., 2001a. High biological productivity in the central Arabian Sea during summer monsoon driven by Ekman pumping and lateral advection, *Current Science*, **81**, 1633 – 1638.
- Prasanna Kumar, S., Gauns, M., Sarma, V.V.S.S., Muraleedharan, P.M., Raghukumar, S., Dileep Kumar, M. and Madhupratap, M., 2001b. Physical forcing of biological productivity in the Northern Arabian Sea during the Northeast monsoon. *Deep-Sea Research*, **48**, 115-1126.
- ✓ Prasanna Kumar, S., Muraleedharan, P.M., Prasad, T.G., Gauns, M., Ramaiah, N., de Souza, S.N., Sardesai, S. and Madhupratap, M., 2002. Why is the Bay of Bengal less productive during summer monsoon compared to the Arabian Sea?, *Geophysical Research Letters*, **29**, X1-X5.
- ✓ Prasanna Kumar, S., Nuncio, M., Jayu, N., Ajoy Kumar, Sardesai, S., de Souza, S.N., Gauns, M., Ramaiah, N. and Madhupratap, M., 2004. Are eddies nature's trigger to enhance biological productivity in the Bay of Bengal? *Geophysical Research Letters*, **31**, L07309, doi:10.1029/2003GL019274.
- ✓ Price, J.F., Weller, R.A. and Pinkel, R., 1986. Diurnal cycling: Observations and models of the upper ocean response diurnal heating, cooling and wind mixing. *Journal of Geophysical Research*, **91**, 8411-8427.
- Qazim, S.Z., 1982. Oceanography of the northern Arabian Sea. *Deep-Sea Research*, **29**, 1041-1068.

Qazim, S.Z., 1977. Biological productivity of the Indian Ocean. *Indian Journal of Marine Science*, **6**, 122-137.

Radhakrishna, K., Bhattathiri, P.M A. and Devassy, V P., 1978. Primary productivity of Bay of Bengal during August-September 1976, *Indian Journal of Marine Science*, **7**, 94-98.

Ramasastriy, A.A. and Myrland, P., 1959. Distribution of temperature, salinity and density in the Arabian Sea along the south Malabar coast (South India) during the post monsoon season. *Indian Journal of Fisheries*, **6**, 223-255.

Rao, C.K, Naqvi, S.W.A., Kumar, M.D., Varaprasad, S.J.D., Jayakumar, D.A., George, M.D. and Singbal, S.Y.S., 1994. Hydrochemistry of the Bay of Bengal: Possible reasons for a different water-column cycling of carbon and nitrogen from the Arabian Sea. *Marine Chemistry*, **47**, 279 - 290.

Rao, D.S. and Rao. R.R., 1986. A case study of the genesis of a monsoon low and the thermal structure of the upper NBB during MONEX-79, *Mahasagar*, **19**(1), 1-9.

Rao, K.N., 1981. Tropical cyclones of the Indian seas. In: world Survey of Climatology, Vol.9: Climates of southern and western Asia, K Takahashi and H. Arakawa (eds). Amsterdam: *Elsevier Scientific*, 257-281.

Rao, R.R. and Sanil Kumar, K.V., 1991. Evolution of salinity field in the upper layers of the east central Arabian Sea and northern Bay of Bengal during summer monsoon experiments. *Proceedings of Indian Academy of Science*, **100**, 69-78.

Rao, R.R. and Sivakumar, R., 2000. Seasonal variability of the heat budget of the mixed layer and the near-surface layer thermal structure of the tropical Indian Ocean from a new global ocean temperature climatology. *Journal of Geophysical Research*, **105**, 995-1015.

Rao, R.R. and Sivakumar, R., 2003. Seasonal variability of sea surface salinity and salt budget of the mixed layer of the north Indian Ocean, *Journal of Geophysical Research*, **108**, C1,3009, doi:10.1029/2001JC000907.

Rao, R.R., 1984. A case Study on the influence of summer Monsoonal vortex on the thermal structure of upper central Arabian Sea during the onset phase of MONEX-79. *Deep-Sea Research*, **31**, 1511-1521.

- Rao, R.R., 1986. Cooling and deepening of the mixed layer in the central Arabian Sea during Monsoon -77: observations and simulations. *Deep-Sea Research*, **33**, 1413-1424.
- Rao, R.R., Molinari, R.L. and Festa, J.F., 1991. Surface meteorological and near - surface oceanographic atlas of the tropical Indian Ocean, *NOAA Tech. Memo. ERL AOML-69*, National Oceanic and Atmospheric Administration, Silver Spring , Md.
- Rao, R.R., Sivakumar, R., 2000: Seasonal variability of near-surface thermal structure and heat budget of the mixed layer of the Indian Ocean from new global ocean temperature climatology. *Journal of Geophysical Research*, **105**(C1), 995-1015.
- Rao, R.R., and Sivakumar, R., 1999. On the possible mechanism of the evolution of a mini - warm pool during the pre - summer monsoon season and the onset vortex in the southeastern Arabian Sea, *Quarterly Journal of Royal Meteorological Society* , **125**, 787-809.
- Rao, R.R., Molinari, R.L. and Festa, J.F., 1989. Evolution of the climatological near-surface thermal structure of the tropical Indian Ocean, 1: Description of mean monthly mixed layer depth, sea surface temperature, surface current and surface meteorological fields. *Journal of Geophysical Research*, **94**, 10,801-10,815.
- Rao, T.V.N., 2002. Spatial Distribution of Upwelling off the Central East Coast of India. *Estuarine, Coastal and Shelf Science*, **54**, 141- 156.
- Rao, T.V.N., Rao, B.P., Rao, D.P. and Raju, V.S., 1986. Upwelling and sinking along Visakhapatnam coast. *Indian Journal of Marine Science*, **15**, 84-87.
- Richards, K.J., Inall, M.E and Wells, N.C., 1995. The diurnal mixed layer and upper ocean heat budget in the western equatorial Pacific. *Journal of Geophysical Research*, **100**, 6865-6879.
- Robinson, M.K., Bauer, R.A. and Schroeder, E.H., 1979. Atlas of North Atlantic-Indian Ocean monthly mean temperatures and mean salinities of the surface layer. *Ref. Publ.*, **18**, 213pp, Nav. Oceanogr. Off, Washington, D.C.
- Ryther, J. and Menzel, D.W., 1965. On the production, composition, and distribution of organic matter in the Western Arabian Sea. *Deep-Sea Research*, **12**, 199-209.

Sanilkumar, K.V., Sarma, K.D., Joseph, M.X., Viswambharan, N.K., 1988. Variability in current and thermohaline structure off Visakhapatnam during late June 1986. *Indian Journal of Marine Science*. 17, 135-145.

Sanil Kumar, K.V., Kuruvilla, T.V., Jogendranath, D. and Rao, R.R., 1997. Observation of the western boundary current of the Bay of Bengal from a hydrographic survey during March 1993. *Deep-Sea Research I*, **44**, 135-145.

Sanilkumar, K.V., Unni, V.K. and James, V.V., 2004. Upwelling characteristics off the southwest coast of India during 2003. *METOC, Proceedings of National symposium on emerging trends in the fields of Meteorology and Oceanography*, pp 137-143.

Sanilkumar, K.V., Hareesh Kumar, P.V., Jossia Joseph and Panigrahi, J.K., 2004. Arabian Sea mini warm pool during May 2000. *Current Science*, **86**, 180-184.

Sarma, Y.V.B., Rama Rao, E.P., Saji, P.K and Sarma, V.V.S.S., 1999. Hydrography and Circulation of the Bay of Bengal during withdrawal phase of the southwest Monsoon, *Oceanologica Acta*, **22**.

Sathyendranath, S., Gouveia, A.D., Shetye S.R and Platt, T., 1991. Biological controls of surface temperature in the Arabian Sea, *Nature*, **349**, 54-56.

Schott, F., 1983. Monsoon response of the Somali current and associated upwelling. *Progress in Oceanography*, **12**, 357 – 382.

Sengupta, D., Ray, P.K. and Bhat, G.S., 2002. Spring warming of the eastern Arabian Sea and Bay of Bengal from buoy data. *Geophysical Research Letters*, **29**, 15340-15345.

Shankar, D., 2000. Seasonal cycle of sea level and currents along the coast of India. *Current Science*, **78**, 279–288.

Shankar, D. and Shetye, S.R., 1999. Are interdecadal sea level changes along the Indian coast influenced by variability of monsoon rainfall? *Journal of Geophysical Research*, **104**, 26031-26042.

Shankar, D. and Shetye, S.R., 1997. On the dynamics of the Lakshadweep high and low in the southeastern Arabian Sea. *Journal of Geophysical Research*, **102**, 12,551-12,562.

Shankar, D., McCreary, J.P., Han, W. and Shetye, S.R., 1996. Dynamics of the East India Coastal Current: 1. Analytic solutions forced by interior Ekman

pumping and local alongshore winds. *Journal of Geophysical Research*, **101**, 13975–13991.

Shankar, D., Vinayachandran, P.N., Unnikrishnan A.S., 2002. The monsoon currents in the north Indian Ocean. *Progress in Oceanography*, **52**, 63-120.

Sharma, G.S., 1966. Thermocline as an indicator of upwelling. *Journal of Marine Biological Association of India*, **8**, 8-19.

Sharma, G.S., 1978. Upwelling off the southwest coast of India. *Indian Journal of Marine Science*, **7**, 209-218.

Shenoi, S.S.C., Saji, P.K., Almeida, A.M., 1999. Near-surface circulation and kinetic energy in the tropical Indian Ocean derived from Lagrangian drifters. *Journal of Marine Research*, **57**(6), 885-907.

Shenoi, S.S.C., Shankar, D. and Shetye. S.R., 2002. Difference in heat budgets of the near surface Arabian Sea and Bay of Bengal: Implications for the summer monsoon. *Journal of Geophysical Research*, **107**, 3052,doi:10.1029/2001JC000679.

Shenoi, S.S.C., Shankar, D. and Shetye. S.R., 2004. Remote forcing annihilates barrier layer in southeastern Arabian Sea, *Geophysical Research Letters*, **31**, L05307, doi:10. 1029/2003GL019270.

Shetye, S.R. and Shenoi, S.S.C., 1988. The seasonal cycle of surface circulation in the coastal North Indian Ocean. *Proceedings of the Indian Academy of Sciences (Earth and Planetary Sciences)*, **97**, 53-62.

Shetye, S.R., 1984. Seasonal variability of the temperature field off the south west coast of India. *Proceedings of the Indian Academy of Sciences (Earth and Planetary Science)*, **93**, 399-411.

Shetye, S.R., 1986. A model study of the seasonal cycle of the Arabian Sea surface temperature. *Journal of Marine Research*, **44**, 521-542.

Shetye, S.R., Gouveia, A.D., Shenoi, S.S.C., Shankar, D., Vinayachandran, P.N., Sundar, D., Michael, G.S. and Nampoothiri, G., 1996. Hydrography and circulation in the western Bay of Bengal during the northeast monsoon. *Journal of Geophysical Research*, **101**, 14,011-14,025.

Shetye, S.R., Gouveia, A.D., Shenoi, S.S.C., Sundar, D., Michael, G.S., and Nampoothiri, G. 1993. The western boundary current of the seasonal sub-tropical gyre in the Bay of Bengal. *Journal of Geophysical Research* **98**, 945-954.

- Shetye, S.R., Gouveia, A.D., Shenoi, S.S.C., Michael, G.S., Sunder, D., Almeida, A.M. and Santanam, K., 1991a. The coastal current off western India during the northeast monsoon. *Deep-Sea Research*, **38**, 1517-1529.
- Shetye, S.R., Shenoi, S.S.C., Gouveia, A.D., Michael, G.S., Sundar, D. and Nampoothiri, G. 1991b. Wind-driven coastal upwelling along the western boundary of the Bay of Bengal during the southwest monsoon. *Continental Shelf Research*, **11**, 1397-408.
- Shetye, S.R., Gouveia, A.D., Shenoi, S.S.C., Michael, G.S., Sunder, D., Almeida, A.M. and Santanam, K., 1989. Hydrography and circulation off the west coast of India during north east monsoon 1987-1988. (Unpublished Manuscript).
- Shetye, S.R., Gouveia, A.D., Shenoi, S.S.C., Sunder, D., Michael, G.S., Almeida, A.M. and Santanam, K., 1990. Hydrography and circulation off the west coast of India during the Southwest Monsoon 1987. *Journal of Marine Research*, **48**, 1-20.
- Smith, S.L.(Ed.), 1998. 1994-1996 Arabian Sea Expedition: Oceanic response to Monsoonal Forcing, Part I. *Deep- Sea Research*, **45**, 1905-2501.
- Smith, S.L.(Ed.), 1999. 1994-1996 Arabian Sea Expedition: Oceanic response to Monsoonal Forcing, Part 2. *Deep- Sea Research*, **46**, 1531-1964.
- Smith, S.L.(Ed.), 2000. 1994-1996 Arabian Sea Expedition: Oceanic response to Monsoonal Forcing, Part 3. *Deep- Sea Research*, **47**, 1177-1677.
- Smith, S.L.(Ed.), 2001. 1994-1996 Arabian Sea Expedition: Oceanic Response to Monsoonal Forcing Part 4. *Deep-Sea Research II*, **48**, 1069-1402.
- Spall, M.A., 1991. A diagnostic study of the wind- and buoyancy-driven North Atlantic circulation. *Journal of Geophysical Research*, **96**, 18,509-18,518.
- Sprintall, J. and Tomczak, M., 1992. Evidence of barrier layer in the surface layer of the tropics. *Journal of Geophysical Research*, **97**, 7305-7316.
- Suryanarayana, A., Murty, V.S.N., Sarma, Y.V.B., Babu, M.T., Rao, D.P. and Sastry, J.S. 1991. Hydrographic features of the western Bay of Bengal in the upper 500m under the influence NE and SW monsoons. In *Oceanography of the Indian Ocean*, B.N. Desai (ed.) New Delhi: Oxford & IBH Publishing, 595-604.
- Swallow, J.C., 1984. Some aspects of the physical oceanography of the Indian Ocean, *Deep-Sea Research*, **31**, 639-650.

- Thompson, R.O.R.Y., 1976. Climatological models of the surface mixed layer of the ocean. *Journal of Physical Oceanography*, **6**, 496-503.
- Thomson, R.E. and Fine, I.V., 2003. Estimating mixed layer depth from oceanographic profile data. *Journal of Atmospheric and Oceanic Technology*, **20**, 319-329.
- UNESCO, 1981. *UNESCO Technical papers in Marine Science*, NO.38,pp.192.
- UNESCO, 1988. *River inputs to ocean systems: status and recommendations for research*. Unesco Technical Papers in Marine Science, No. 55. Final Report of SCOR Working Group 46, Paris, 25pp.
- Usha, D.M. and Muraleedharan, P.M., 2000. Hydrological structure and biological productivity of the tropical Indian Ocean. *PROSEC Proceedings*, Vol II, 853-857.
- Varadachari, V.V.R., Murty, C.S. and Das, P.K., 1968a. On the level of least motion and the circulation in the upper layers of the Bay of Bengal. *Bulletin of National Institute of Sciences of India*, **38**, 301-307.
- Varkey M.J., Murty, V.S.N., Suryanarayana, A., 1996. Physical Oceanography of the Bay of Bengal and Andaman Sea. In: *Oceanography and Marine Biology an Annual Review*, Ansell, A.D., Gibson, R.N., Barnes, M (Eds.), University College London Press, London, pp.1-70.
- Vinayachandran, P.N., Murty, V.S.N and Ramesh Babu, V. 2002. Observations of barrier of layer formation in the Bay of Bengal during summer monsoon, *Journal of Geophysical Research*, Vol.107, No.C12, doi: 10.1029/2001JC000831.
- Vinayachandran, P.N. and Yamagata, T., 1998. Monsoon response of the sea around Sri Lanka: generation of thermal domes and anticyclonic vortices. *Journal of Physical Oceanography*, **28**, 1946-1960.
- Vinayachandran, P.N., Masumoto, Y., Mikawa, T. and Yamagata, T., 1999. Intrusion of the Southwest Monsoon Current in to the Bay of Bengal, *Journal of Geophysical Research*, **104**, 11077-11085.
- Vinayachandran, P.N., Shetye, S.R., and Sengupta D., 1996. Forcing mechanisms of the Bay of Bengal circulation, *Current science*, **71**, 753-763.

Wagner, R.G., 1996. Decadal scale trends in mechanisms controlling meridional sea surface temperature gradients in the tropical Atlantic. *Journal of Geophysical Research*, **101**, 16,683-16,694.

Wyrtki, K., 1971. *Oceanographic Atlas of the International Indian Ocean Expedition*, 531pp., U.S. Govt. Print. Off. Washington D.C.

Wyrtki, K., 1973. Physical oceanography of the Indian Ocean, In: *The Biology of the Indian Ocean*, edited by B. Zeitzschel, pp. 18-36, Springer-Verlag, New York.

Yemagata, T., Mizuno, K. and Masumoto, Y., 1996. Seasonal variation in the equatorial Indian Ocean and their impact on the Lombok throughflow. *Journal of Geophysical Research*, **101**, 12,465-12,473.

You, Y., 1995. Salinity variability and its role in the barrier layer formation during TOGA-COARE. *Journal of Physical Oceanography*, **25**, 2778-2807.

Yu, L., O'Brien, J.J. and Yang, J., 1991. On the remote forcing of the circulation in the Bay of Bengal. *Journal of Geophysical Research*, **96**, 20449-20454.

List of Papers published/communicated

Maheswaran, P.A., Jyothibabu, R., Madhu, N.V., Vijay, J.G., Nuncio, M., Mohammed Ashraf, T.T., Haridas, P.C, Revichandran, C., Venugopal, P. and K.K.C. Nair. Hydrography of western Bay of Bengal: Physical controls on biological production, *Current Science*, (communicated)

Jyothibabu, R., **Maheswaran, P.A.**, Madhu, N.V., Mohammed Ashraf, T.T., Vijay, J.G., Haridas, P.C, Revichandran, C., T. Balasubramanian, K.K.C. Nair, Gopalakrishnan, T.C. and Venugopal, P. Differential response of winter cooling on biological production in the northeastern Arabian Sea and northwestern Bay of Bengal, *Current Science* (Accepted for publication)

Madhu, N.V, **Maheswaran, P.A.**, Jyothibabu, R., Revichandran, C., T. Balasubramanian, Gopalakrishnan, T.C and Nair, K.K.C (2001). Enhanced biological production off Chennai triggered by October 1999 super cyclone (Orissa). *Current Science*, 82 (12), 1472-1479.

Maheswaran, P.A, Rajesh, G., Revichandran, C. and Nair, K.K.C., (2000). Upwelling and associated hydrography along the west of India during southwest monsoon, 1999. PORSEC 2000 proceedings vol II, 873-876.

Jyothibabu, R., Madhu, N.V, **Maheswaran, P.A.**, Nair, K.K.C, P.Venugopal and T. Balasubramanian (2003). Dominance of dinoflagellates in microzooplankton community in the oceanic regions of Bay of Bengal and Andaman Sea. *Current Science*, 84 (9), 1247-1253.

Srinivas, K., Revichandran, C., **Maheswaran, P.A.**, Mohammed Ashraf, T.T., Nuncio, M., (2003). Propagation of tides in the Cochin estuarine system, southwest coast of India, *Indian journal of Marine Science*, 32 (1), 14-24.

Srinivas, K., Revichandran, C., Thottam, T.J., **Maheswaran, P.A.**, Mohammed Ashraf, T.T and Nuncio Murukesh (2003). Currents in the Cochin estuarine system [southwest coast of India] during March, 2000, *Indian Journal of Marine Sciences*, 32 (2), 123 – 132.

Srinivas K., Revichandran C., Mohamed Ashraf T.T., Thottam T.J., **Maheswaran P.A.** and Nuncio Murukesh (2004). Sea level and currents in the upper reaches of the Cochin estuarine system during October 2000, *Indian Journal of Marine Sciences*, 33 (Accepted for publication)

S.W.A. Naqvi, M.D. George, P.V. Narvekar, D.A. Jayakumar, M.S. Shailaja, S. Sardesai, V.V.S.S. Sarma, D.M. Shenoy, H. Naik, **P.A. Maheswaran**, K. Krishanakumari, G. Rajesh, A.K. Sudheer, and M.S.Binu, (1998). Severe fish

C18968

mortality associated with 'red tide' observed in the sea off Cochin: Current Science. 75, 543-544.

Maheswaran, P.A., Muraleedharan, G. and Rao, M.G.S,. (1997). Linear models for wave power potential along the island coasts, Proceedings of the second Indian National Conference on Harbour and Ocean Engineering (inchoe-97), Thiruvananthapuram, India, 215-220.

